Insights into the versatile metabolism of the Alphaproteobacterium *Paracoccus denitrificans*

Dissertation

„kumulativ“

zur Erlangung des Grades eines

Doktor der Naturwissenschaften

(Dr. rer. nat.)

des Fachbereichs Biologie der Philipps-Universität Marburg

Vorgelegt von

Katharina Kremer

aus Bad Nauheim

Marburg/Lahn, 2023

Die vorliegende Dissertation wurde von 12/2017 bis 01/2023 am Max-Planck-Institut für terrestrische Mikrobiologie unter Leitung von Prof. Dr. Tobias Erb angefertigt.

Vom Fachbereich Biologie der Philipps-Universität Marburg (Hochschulkennziffer 1180) als Dissertation angenommen am 04.01.2023.

Erstgutachter: Prof. Dr. Tobias Erb

Zweitgutachter: Prof. Dr. Martin Thanbichler

Weitere Mitglieder der Prüfungskommission:

Dr. Georg Hochberger

Prof. Dr. Michael Bölker

Tag der Disputation: 26.05.2023

Erklärung

Ich versichere, dass ich meine Dissertation mit dem Titel „Insights into the versatile metabolism of the Alphaproteobacterium *Paracoccus denitrificans*“ selbstständig ohne unerlaubte Hilfe angefertigt und mich dabei keiner anderen als der von mir ausdrücklich bezeichneten Quellen und Hilfsmittel bedient habe.

Diese Dissertation wurde in der jetzigen oder einer ähnlichen Form noch bei keiner anderen Hochschule eingereicht und hat noch keinen sonstigen Prüfungszwecken gedient.

Marburg, den 03.01.2023

Katharina Kremer

Kumulative Dissertation

Erklärung zum Eigenanteil der Doktorandin an den vorgelegten Publikationen/Manuskripten

Teile dieser Dissertation sind veröffentlicht oder zur Veröffentlichung einem biologischen Fachjournal eingereicht:

1) **Kremer K**, van Teeseling MCF, von Borzyskowski LS, Bernhardsgrütter I, van Spanning RJM, Gates AJ, Remus-Emsermann MNP, Thanbichler M, Erb TJ. 2019. Dynamic metabolic rewiring enables efficient acetyl Coenzyme A assimilation in *Paracoccus denitrificans*. mBio 10. https://doi.org/10.1128/mBio.00805-19

Meine wissenschaftlichen Anteile an der Veröffentlichung gestalten sich wie folgt:

Autorenschaft	Beitrag im Einzelnen	Unterschrift der Doktorandin
Katharina Kremer	Problemherstellung, Planung und Durchführung aller Experimente, Datenauswertung, Erstellung und Überarbeitung des Manuskriptes	

2) **Kremer K,** Meier D, Theis L, Miller S, Rost-Nasshan A, Naing YT, Zarzycki J, Paczia N, Serrania J, Blumenkamp P, Goesmann A, Becker A, Thanbichler M, Hochberg GKA, Carter MS, Erb TJ. 2022. Functional degeneracy in *Paracoccus denitrificans* Pd1222 is coordinated via RamB, linking expression of the glyoxylate cycle to activity of the ethylmalonyl-CoA pathway. *Manuscript submitted.*

Meine wissenschaftlichen Anteile an der Veröffentlichung gestalten sich wie folgt:

Autorenschaft	Beitrag im Einzelnen	Unterschrift der Doktorandin
Katharina Kremer	Problemherstellung, Planung und Durchführung der Experimente, Datenauswertung, Erstellung und Überarbeitung des Manuskriptes	

Die unter 1) und 2) genannten Publikationen sollen im Rahmen dieser kumulativen Dissertation verwendet werden. Sie sind kein Bestandteil einer weiteren wissenschaftlichen Qualifikationsarbeit.

Ich, Prof. Dr. Tobias Erb, bin mit der Abfassung der Dissertation als kumulative Dissertation einverstanden und bestätige die vorstehenden Angaben.

_____ _____

Ort, Datum Prof. Dr. Tobias Erb

TABLE OF CONTENTS

I ZUSAMMENFASSUNG

Zwei unterschiedliche Stoffwechselmodi versorgen Bakterien mit Energie (Katabolismus) und Zellbausteinen (Anabolismus). An der Schnittstelle zwischen Katabolismus und Anabolismus liegen der zentrale Metabolit Acetyl-CoA, sowie der amphibole Citratzyklus. Das katabole Schicksal von Acetyl-CoA ist seine Oxidation im Citratzyklus zur Gewinnung von Reduktionsäquivalenten und Energie, wobei sein Kohlenstoffgerüst vollständig als CO_2 abgespalten wird und damit verloren geht. Um zu anabolen Zwecken stattdessen den Kohlenstoff aus Acetyl-CoA in Biomasse einzubauen, benötigt der Citratzyklus die Unterstützung von sogenannten Auffüllreaktionen (Anaplerose). Diese Reaktionen umgehen die oxidativen, CO_2-produzierenden Schritte des Citratzyklus, erlauben den Einbau von Kohlenstoff aus Acetyl-CoA in Biomasse und ermöglichen so letztendlich bakterielles Wachstum auf kleinen Kohlenstoffverbindungen wie Acetat.

Obwohl nach dem ursprünglichen Verständnis von Stoffwechsel angenommen wurde, dass jeder Organismus die gleiche spezialisierte Route zur Umsetzung eines bestimmten Substrates besitzt, sind bis zum heutigen Tage bereits mehrere verschiedene Auffüllreaktionen des Citratzyklus in Bakterien bekannt. Darunter befinden sich der Glyoxylatzyklus (GC) und der Ethylmalonyl-CoA Weg (EMCP). Die meisten Bakterienspezies besitzen nur einen der beiden Acetyl-CoA Assimilationswege als alleinstehende Route. Das Alphaproteobakterium *Paracoccus denitrificans* zeigt hingegen, wie nur wenige andere Vertreter seiner Domäne, die genetische Ausstattung für beide Wege. Dies wirft die Fragen auf, was der biologische Zweck dieser vermeintlich funktionellen Redundanz im bakteriellen Stoffwechsel ist und wie diese innerhalb der Zelle koordiniert wird.

Die vorliegende Arbeit zeigt, dass sowohl der GC als auch der EMCP in *P. denitrificans* während verschiedenen Stadien des Wachstums auf Acetat genutzt werden. Während der EMCP auf mehreren Substraten konstitutiv exprimiert und nach einem Wechsel zu Acetat zusätzlich hochreguliert wird, ist der GC ein spezialisierter Weg, der ausschließlich der Assimilierung von Acetyl-CoA, während des Wachstums auf Acetat oder anderen Verbindungen, die über Acetyl-CoA assimiliert werden, dient. Beide Stoffwechselwege allein bergen unterschiedliche Vorteile für ihren Wirt. Während der EMCP auf Acetat zu hohen

Wachstumserträgen bei moderater Teilungsrate führt, ermöglicht der GC ein schnelles exponentielles Wachstum von *P. denitrificans* auf Acetat mit jedoch niedrigerer Gesamtbiomasseausbeute.

Eine präzise abgestimmte genetische Regulation kontrolliert die Expression beider Stoffwechselwege in *P. denitrificans* und vermittelt durch das gezielte Umschalten zwischen beiden Wegen eine Plastizität im zentralen Stoffwechsel dieses Organismus. Diese ermöglicht dem Bakterium dynamisch auf sich ändernde Umweltbedingungen zu reagieren, um seinen jeweiligen physiologischen Ansprüchen gerecht zu werden.

Mit einer Kombination von genetischen, molekularbiologischen und biochemischen Methoden zeigt diese Arbeit, dass RamB, ein Transkriptionsfaktor der ScfR Familie, CoA-Ester Intermediate des EMCP detektiert und in Antwort darauf die Expression des GC aktiviert. Dies demonstriert ein neues Phänomen in bakteriellem Stoffwechsel, bei dem ein vermeintlich redundanter Stoffwechselweg die Expression eines anderen stimuliert.

In Summe erweitert diese Arbeit unser Verständnis von mikrobiellem Stoffwechsel und präsentiert die molekulare Basis von metabolischer Plastizität. Die vollständige Aufklärung der daran beteiligten Mechanismen in der Zukunft könnte die Möglichkeit eröffnen, neue regulatorische Module für den Einsatz in der synthetischen Biologie, sowie im *metabolic engineering* zu entwickeln.

II SUMMARY

Two distinct metabolic modes provide bacteria with energy (*i.e.*, catabolism) and cellular building blocks (*i.e.*, anabolism). At the interface between both lie the central metabolite acetyl-CoA, as well as the amphibolic tricarboxylic acid (TCA) cycle. The fate of acetyl-CoA in catabolism is its complete oxidation in the TCA cycle for the generation of reducing equivalents and energy, whereby the carbon backbone of the metabolite is fully lost to CO_2. To assimilate acetyl-CoA into biomass in anabolism, instead, additional help of so-called replenishment (*i.e.,* anaplerotic) pathways is therefore needed. These pathways circumvent the oxidative, CO_2-producing steps of the TCA cycle, thereby allow the incorporation of acetyl-CoA into biomass, and ultimately enable bacterial growth on small carbon compounds such as acetate.

While the old picture of metabolism has assumed a biochemical unity, according to which each organism possesses the same dedicated metabolic route for the conversion of a certain substrate, multiple distinct replenishment routes have been discovered in bacteria by today. Amongst them are the glyoxylate cycle (GC) and the ethylmalonyl-CoA pathway (EMCP). Most bacterial species possess only one of the two acetyl-CoA assimilation pathways as standalone route. However, the Alphaproteobacterium *Paracoccus denitrificans,* like only few others, has the genetic potential for both. This raised the questions what the biological purpose behind this apparent functional degeneracy in the metabolism of this organism is and how it is coordinated in the cell.

This work shows that both routes the GC and the EMCP are employed by *P. denitrificans* during different stages of growth on acetate. While the EMCP is constitutively expressed on various substrates and additionally upregulated in the lag phase after growth switch to acetate, the GC is specifically induced on this substrate and only few others that are solely assimilated via acetyl-CoA as well. Each acetyl-CoA assimilation strategy alone confers distinct advantages on the cell. The EMCP allows metabolization of a great variety of carbon substrates and its action results in high growth yields of *P. denitrificans* on acetate. The GC, in contrast, is specialized for the rapid metabolization of acetyl-CoA and enables fast exponential growth of the bacterium on the carbon source.

A fine-tuned genetic regulation controls expression of both pathways in *P. denitrificans* and thereby mediates dynamic metabolic rewiring between the two acetyl-CoA assimilation routes. This metabolic plasticity provides the organism with the ability to respond to changes in the nature and availability of carbon sources in a highly flexible manner to meet its physiological requirements.

Using a combination of genetic, molecular biological, and biochemical methods, this work shows that RamB, a transcription factor of the ScfR family, senses CoA-ester intermediates of the EMCP to activate expression of the GC. This demonstrates a so-far undescribed phenomenon in bacterial metabolism, in which one seemingly degenerate metabolic pathway directly drives expression of the other.

In all, this work expands our understanding of microbial metabolism and presents the molecular basis of plasticity in the central carbon metabolism of bacterial cells. Complete elucidation of the underlying mechanisms hereafter may open possibilities to develop new regulatory modules for application in synthetic pathways and metabolic engineering in the future.

1 Introduction

1.1 Bacterial metabolism

Metabolism is defined as the minimal set of chemical processes that occurs within in a living cell in order to maintain life. It is composed of two functionally distinct modes of action that are termed catabolism and anabolism. In catabolism, the break-down of complex multi-carbon compounds into smaller units yields energy in form of reducing equivalents and adenosine triphosphate (ATP). This energy, in turn, is invested in anabolism to fuel the assembly of small carbon units into larger building blocks, ultimately facilitating the generation of biomass and, hence, cellular growth (1). At the heart of catabolism lie conserved metabolic pathways that are widespread throughout all domains of life, among them glycolysis and β-oxidation. Glycolysis in the narrow sense, the Embden-Meyerhoff-Parnas pathway (EMPP; (2)), but also related routes like the Entner-Doudoroff pathway (EDP; (3, 4)), as well as the Pentose Phosphate pathway (PPP; (5)) in combination with the subsequent reaction of the pyruvate dehydrogenase complex (PDH) serve the oxidation of glucose (1–5). β-oxidation, instead, is committed to the degradation of fatty acids (6). Despite different structures and the conversion of different substrates, the action of these pathways results in the generation of a common product metabolite: the energy-rich molecule acetyl-CoA, which also derives from the degradation of several amino acids (1). Further oxidation of acetyl-CoA occurs in the tricarboxylic acid (TCA) cycle (7). This cycle can be considered an amphibolic pathway with catabolic as well as anabolic features and represents a linking point in metabolism. Serving catabolism, complete oxidation of acetyl-CoA in the TCA cycle results in the generation of reducing power and energy (7), but also leads to the complete loss of the acetate carbon backbone as CO_2. Alternatively, deduction of intermediates from the TCA cycle for the purpose of anabolism provides the cell with building blocks for biosynthetic processes ((8); Figure 1). The latter especially occurs at the levels of α-ketoglutarate and oxaloacetate, which constitute precursors of amino acids of the glutamate and aspartate family, as well as purine and pyrimidine bases, respectively (9). Besides this, oxaloacetate is also withdrawn under gluconeogenic conditions for the regeneration of pyruvate. Beyond oxaloacetate and α-ketoglutarate, intermediates are also withdrawn from the TCA cycle at other positions. For example, pyruvate can also be regenerated from malate (10, 11), citrate can serve the regeneration

of acetyl-CoA as precursor for fatty acid synthesis (12, 13), and succinyl-CoA functions as precursor for tetrapyrrole synthesis (14). In any case, the withdrawal of intermediates for biosynthetic or gluconeogenic purposes will require the replacement of these intermediates in order to avoid stalling of the cycle. For this reason, bacteria have evolved so-called anaplerotic or replenishment pathways.

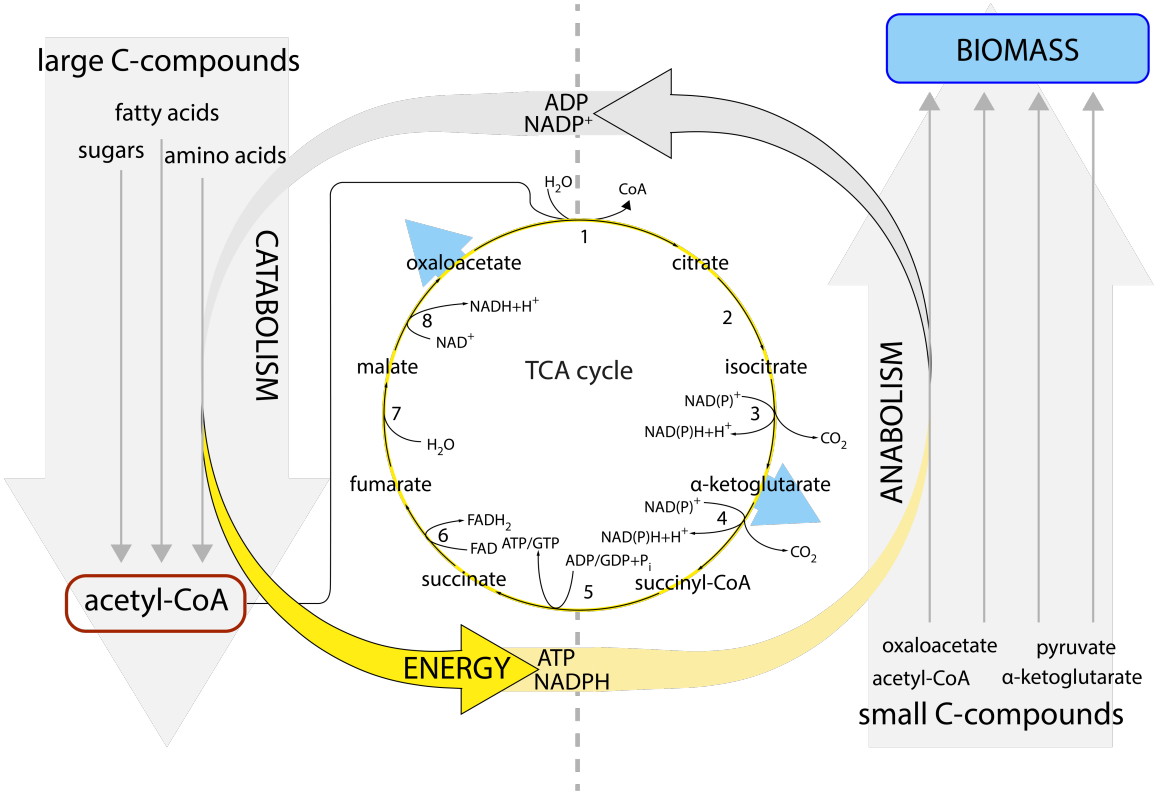

Figure 1: Principles of bacterial metabolism. Two different modes function in metabolism. Degradation of complex multi-carbon compounds into smaller units in catabolism provides bacteria with energy and reducing equivalents. These are invested in anabolism to fuel the assembly of small carbon compounds into biomass. The TCA cycle lies at the interface between both modes. It yields reducing equivalents and energy, and provides precursors for biosynthetic processes. The latter are especially withdrawn at the levels of α-ketoglutarate and oxaloacetate. See text for detailed descripton. 1: citrate synthase; 2: cis-aconitase; 3: isocitrate dehydrogenase (Idh); 4: α-ketoglutarate dehydrogenase (Kdh); 5: succinyl-CoA synthetase; 6: succinate dehydrogenase; 7: fumarase; 8: malate dehydrogenase.

1.2 Anaplerosis

The term anaplerosis was first introduced by the biochemist Sir Hans Kornberg in 1966 (15). Composed of the Greek words ‘ἀνά’ (ανά; up) and ‘plēróō’ (πληρόω; to fill), he used the word to describe pathways that refill a metabolic cycle, in this case

the TCA cycle, with intermediates. Since then, a vast variety of different anaplerotic reaction sequences has been proposed by various scientists over the years. For numerous of them, a biological function could never be confirmed. Others are today recognized as conserved pathways of cellular core metabolism (16, 17). Some, like the reaction steps of gluconeogenesis, are well conserved among all domains of life. Others are solely present in (some) microorganisms, whilst they are missing in (higher) eukaryotes. This contributes to the phenomenon that despite their small size, microorganisms, and bacteria in particular, constitute the group of life that holds the greatest metabolic diversity on earth. This enables them to use numerous compounds as substrates for growth and survive in countless environmental niches (18, 19). Thereby, replenishment pathways are not only crucial for the replacement of the TCA cycle with intermediates that are withdrawn for biosynthetic purposes. They, notably, also allow bacteria to utilize small carbon compounds ranging from C_1 to C_3 as sole source of carbon for growth. Naturally occurring examples for such routes are: (i) the serine cycle, the ribulose monophosphate cycle (RuMP), or the Calvin-Benson-Bassham cycle (CBB) for the assimilation of methanol via CO_2 (20–22) , (ii) the β-hydroxyaspartate pathway (BHAP; (23, 24)) for the assimilation of glycolate (C_2) via glyoxylate (C_2), (iii) the citramalate cycle (25, 26) involved in the assimilation of acetate (C_2) and pyruvate (C_3), or (iv) the methylmalonyl-CoA pathway (MMCP; (27, 28)) and the methylcitrate cycle (MCC; (29, 30)) for the assimilation of propionate.

This work specifically focuses on the natural assimilation of acetyl-CoA during microbial growth on acetate as sole source of carbon. For this, four dedicated pathways are described in literature to this day: (i) the glyoxylate cycle (8, 31), (ii) the ethylmalonyl-CoA pathway (32, 33), (iii) the pyruvate synthase route (13, 34, 35), and (iv) the methylaspartate cycle (36, 37). The former two are of specific interest to this study and will be explained in more detail below. The pyruvate synthase route is only found in anaerobic, anoxygenic bacteria (13, 34, 35) and the methylaspartate cycle has by now only been found in haloarchea (36, 37). Therefore, these routes will not be further addressed here.

1.2.1 The glyoxylate cycle (GC)

Identified and described by Kornberg and Krebs in 1957, the glyoxylate cycle (GC; Figure 2) was the first replenishment pathway discovered (8, 31). It is found in bacteria, fungi, and protists, but not in human or animal cells (38). The GC can be considered as a variation of the TCA cycle, as it comprises only two additional enzymes (8). These, isocitrate lyase (Icl) and malate synthase (Ms), establish a short cut in the TCA cycle that allows circumvention of its decarboxylating steps (Figure 2B). For this reason, the GC is also referred to as glyoxylate shunt or bypass (31).

In more detail, condensation of acetyl-CoA (C_2) with oxaloacetate (C_4) by the enzyme citrate synthase yields citrate (C_6) in the TCA cycle (see Figure 1, step 1). Dehydration and subsequent re-hydration of this product by cis-aconitase leads to the formation of D-isocitrate (C_6; see Figure 1, step 2). In the following course of the TCA cycle, this intermediate is oxidized and decarboxylated into α-ketoglutarate (C_5) by the enzyme isocitrate dehydrogenase (Idh; Figure 1, step 3) followed by oxidative decarboxylation and activation into succinyl-CoA by α-ketoglutarate dehydrogenase (Kdh; see Figure 1, step 4). Both reaction steps result in the formation of reducing equivalents in form of one molecule of NAD(P)H per reaction. Succinyl-CoA synthetase then converts succinyl-CoA into succinate (C_4) and free CoA (see Figure 1, step 5), conserving energy in GTP or ATP via substrate level phosphorylation (7). As mentioned before, due to the decarboxylation steps, this gain of energy comes at the loss of all carbon (C_2) initially present in acetyl-CoA. However, carbon loss can be prevented by the action of Icl. Like Idh, Icl accepts isocitrate but cleaves it into succinate (C_4) and glyoxylate (C_2) instead of oxidizing it. Followingly, the Icl reaction does not lead to reducing equivalents or ATP, but conserves the two carbon atoms of isocitrate derived from acetyl-CoA ((8); Figure 2B, step 1). In the following, Ms catalyzes the condensation of glyoxylate with another molecule of acetyl-CoA, which results in the formation of malate ((C_4); Figure 2B, step 2). In sum, the combined action of Icl and Ms in the GC allows the assimilation of four carbon atoms from two molecules of acetyl-CoA, replenishing the TCA cycle with intermediates that enter the cycle at the levels of succinate and malate (8, 31).

As typical for genes of metabolic pathways, the genes of the GC are usually organized in a metabolic operon under joint transcriptional control, which is termed the *aceBAK*-operon in *Escherichia coli* (39) and will be referred to as GC operon in the following.

1.2.2 Discovery of the ethylmalonyl-CoA pathway (EMCP)

Icl is the key enzyme of the GC. Its presence is considered a prerequisite for the operation of the cycle. For many years, the GC was the only acetyl-CoA assimilation route known. Yet, it was recognized that organisms like the Alphaproteobacterium *Methylobacterium extorquens* (now reclassified as *Methylorubrum extorquens* (40)), the purple non-sulfur bacterium *Rhodobacter sphaeroides* (41), the actinomycete *Streptomyces collinus* (42), and others existed that were able to utilize acetate as sole source of carbon for growth despite the lack of a functional Icl enzyme (43–49). This pointed to the presence of an alternative acetyl-CoA assimilation route. It was first suggested that this route in Icl-negative organisms involved the formation of the intermediates mesaconyl-CoA, β-methylmalyl-CoA, propionyl-CoA, and methylmalonyl-CoA. Later it was shown that the process also required the activity of MeaA, a then novel vitamin B_{12}-dependent methylmalonyl-CoA mutase (46, 50), the activitiy of a propionyl-CoA carboxylase (PccA; (46, 51)), and that it additionally involved the formation of crotonyl-CoA and butyryl-CoA as further intermediates, as well as the activity of a reductase capable of transforming the latter two into each other (42, 51). This putative reductase was Ccr, at that time believed to solely catalyze the reduction of crotonyl-CoA into butyryl-CoA (42). It was then also proposed that a β-ketothiolase that condenses two molecules of acetyl-CoA into acetoacetyl-CoA is involved in the initial steps of acetyl-CoA assimilation in Icl-negative organisms (48, 49). In 2006, Birgit Alber and colleagues combined and extended the existent knowledge and proposed for the first time the operation of a stringent pathway for acetyl-CoA assimilation alternate to the GC in *Rhodobacter sphaeroides* (41). The authors presented first, but preliminary, evidence that this pathway, in addition to the already suggested intermediates, contained the later eponymous intermediate ethylmalonyl-CoA that would arise through carboxylation of a yet unknown precursor molecule. Also, it was still unclear which enzymes were responsible for

catalyzing the underlying reaction steps. It was the work of Tobias Erb and co-workers in 2007 that finally elucidated the key step of the alternate acetyl-CoA assimilation route by showing that the initially believed crotonyl-CoA reductase was, in fact, a combined crotonyl-CoA carboxylase/reductase (Ccr) that catalyzes the unique reaction of reductive carboxylation of crotonyl-CoA (C_4-CoA) into ethylmalonyl-CoA (C_5-CoA) (32, 52). Together with the discovery of a (*2S*)-methylsuccinyl-CoA dehydrogenase (Mcd), this finding closed the gap in the mysterious alternative acetyl-CoA assimilation route and, fifty years after the discovery of the GC, gave rise to the ethylmalonyl-CoA pathway (EMCP; (32, 33, 52)) as well as to a new class of highly effective CO_2-fixing enzymes: carboxylating enoyl-thioester reductases (Ecr; (52)).

1.2.3 Biochemistry of the EMCP

The EMCP gives rise to the same products as the GC, namely succinyl-CoA (that is further converted to succinate in the TCA cycle) and malate. Yet, consisting of at least twelve enzymes (32, 33) that require in total five different co-factors (32, 33, 52, 53), it is a much longer and more complex route for assimilation of acetyl-CoA than the GC. It uses in total three molecules of acetyl-CoA and additionally fixes two molecules of CO_2 or HCO_3^-, respectively. Moreover, it consumes two molecules of NADPH and one molecule of ATP. Unlike the genes of the GC and many other metabolic pathways, the genes encoding the enzymes of the EMCP are usually located dispersed over the genome of the respective host organisms (33). Accordingly, the EMCP is composed of several individual reaction sequences that are committed to diverse biological functions on their own but act together for the assimilation of acetyl-CoA under anaplerotic conditions.

Overall, the pathway can be divided into an upper and a lower part (Figure 2A). The former starts with condensation of two molecules of acetyl-CoA into acetoacetyl-CoA catalyzed by a β-ketothiolase (PhaA) as known from polyhydroxybutyrate synthesis (41) and ends with cleavage of the C_5-CoA-ester intermediate β-methylmalyl-CoA into glyoxylate (C_2) and propionyl-CoA (C_3-CoA) by β-methylmalyl-CoA lyase (Mcl-1). The signature step in the upper part of the EMCP is the reductive carboxylation of crotonyl-CoA into ethylmalonyl-CoA catalyzed by the EMCP's key enzyme Ccr (52). This step follows the NADPH-

consuming reduction of acetoacetyl-CoA to β-hydroxybutyryl-CoA through an acetoacetyl-CoA reductase (PhaB) and subsequent dehydratation of the latter, yielding crotonyl-CoA. The product of the Ccr reaction, ethylmalonyl-CoA, is further converted to mesaconyl-CoA. This occurs through the combined action of an epimerase reaction (Epi) and the vitamin B_{12}-dependent transformation into methylsuccinyl-CoA by ethylmalonyl-CoA mutase (Ecm) (53), and subsequent oxidation of the latter by methylsuccinyl-CoA dehydrogenase (Mcd). Mesaconyl-CoA is then hydrated by mesaconyl-CoA hydratase (Mch) to form β-methylmalyl-CoA (C_5-CoA), which is finally split into glyoxylate (C_2) and propionyl-CoA (C_3-CoA) by Mcl-1.

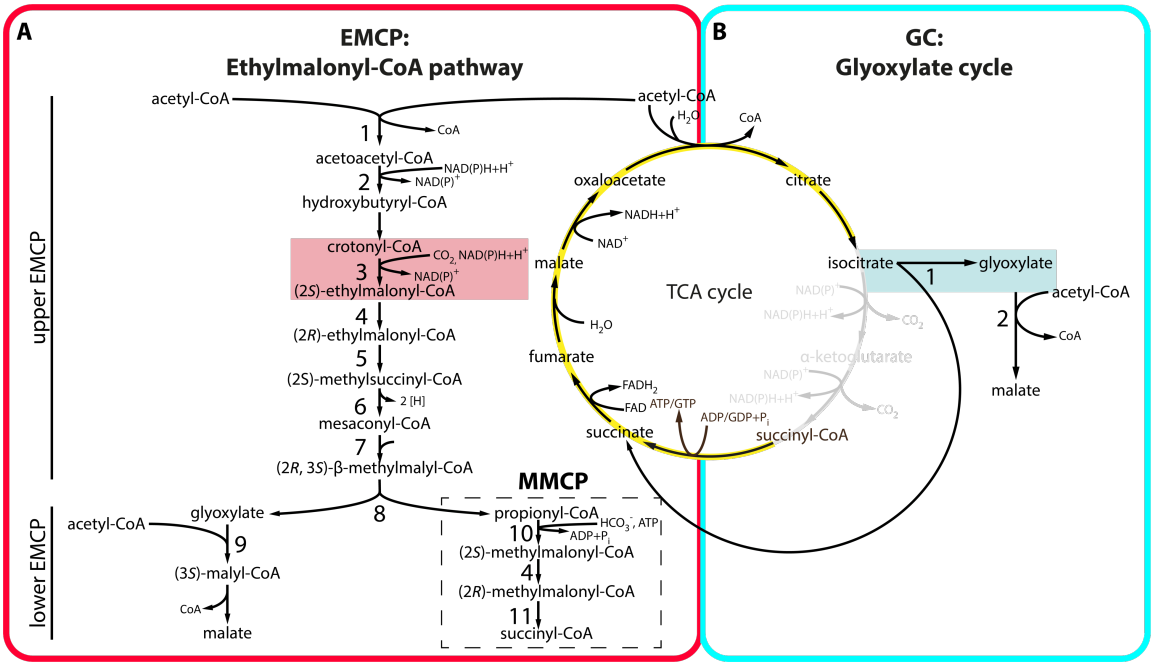

Figure 2: Bacterial acetyl-CoA and propionyl-CoA assimilation pathways. Key reations of the EMCP and GC are highlighted in red and cyan background, respectively. (A) 1: β-ketothiolase (PhaA); 2: acetoacetyl-CoA reductase (PhaB); 3: crotonyl-CoA carboxylase/reductase (Ccr; key enzyme of the EMCP); 4: ethylmalonyl-CoA/methylmalonyl-CoA epimerase (Epi); 5: ethylmalonyl-CoA mutase (Ecm); 6: methylsuccinyl-CoA dehydrogenase (Mcd); 7: mesaconyl-CoA hydratase (Mch); 8: β-methylmalyl-CoA/L-malyl-CoA lyase (Mcl-1); 9: malyl-CoA thioesterase (Mcl-2); 10: propionyl-CoA carboxylase (PccAB); 11: methylmalonyl-CoA mutase (Mcm). MMCP: Methylmalyl-CoA pathway. (B) 1: isocitrate lyase (Icl/AceA); 2: malate synthase (Ms/AceB). Figure modified from (55).

The lower part of the EMCP is divided into two branches. One is responsible for the condensation of glyoxylate with another acetyl-CoA into malate catalyzed by

β-methylmalyl-CoA/malyl-CoA thioesterase (Mcl-2), the activity of which results in an apparent malate synthase activity in Icl-negative organisms (54). The other branch is committed to the conversion of propionyl-CoA into succinate via the known reaction steps of the methylmalonyl-CoA pathway (MMCP), consisting of biotin-dependent carboxylation of propionyl-CoA by propionyl-CoA carboxylase (PccAB; (27)) and subsequent vitamin B_{12}-dependent transformation of the resulting methylmalonyl-CoA into succinyl-CoA by methylmalonyl-CoA mutase (Mcm; (28)).

1.2.4 The methylcitrate cycle (MCC)

The lower part of the EMCP yields the intermediate propionyl-CoA. While the MMCP is considered the dedicated route for further metabolization of propionyl-CoA in the EMCP, other routes for conversion of propionyl-CoA distinct to the MMCP generally exist in bacterial cells (see above in section 1.2). To this date, none of them have been described as part of the EMCP (56–58). However, in the scope of this work, a significant contribution of the methylcitrate cycle (MCC; (29, 30, 59)) to acetate assimilation in the model organism of this study will be shown, which is why the pathway is shortly described in the following.

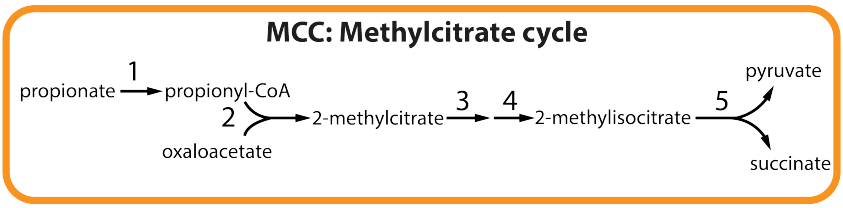

Figure 3: The methylcitrate cycle (MCC). 1: propionyl-CoA synthase (PrpE); 2: methylcitrate synthase (PrpC); 3: methylcitrate dehydratase/hydratase (PrpD); 4: aconitase (AcnB); 5: methylisocitrate lyase (PrpB).

The genes of the MCC are usually organized in the *prp*-operon where they encode (i) propionyl-CoA synthase (PrpE) responsible for activating propionate into propionyl-CoA, (ii) methylcitrate synthase (PrpC) that catalyzes the aldol condensation of propionyl-CoA with oxaloacetate into 2-methylcitrate, (iii) methylcitrate dehydratase/hydratase (PrpD) and (iv) aconitase (AcnB) that isomerize 2-methylcitrate into 2-methylisocitrate, and (v) methylisocitrate lyase

(PrpB) that catalyzes the cleavage of 2-methylisocitrate into the final products pyruvate and succinate ((60, 61); Figure 3).

1.3 Functional degeneracy in central carbon metabolism

The ancient picture of metabolism was influenced by the Dutch microbiologist Albert Jan Kluyver in the 19th century. Kluyver assumed the existence of a biochemical unity, according to which central metabolism is always composed of the same conserved biochemical routes between all domains of life, 'from *E. coli* to an elephant' (62, 63). More than a century of microbiological, biochemical, and genetic research since then has contributed to the elucidation of numerous different metabolic pathways and variations thereof. This has allowed the emergence of a more modern picture of metabolism that recognizes the occurrence of genetic redundancy and functional degeneracy in the metabolism of microorganisms. The term 'genetic redundancy' thereby refers to the existence of paralogs of a gene that code for enzymes with distinct functions. 'Functional degeneracy', on the other hand, describes the phenomenon that different biochemical routes can serve the same metabolic purpose (17). Functional degeneracy mainly exists between organisms that contain distinct specialized routes for the conversion of a certain substrate. In some cases, however, functional degeneracy is also found in a single organism (16, 52, 64). The GC and the EMCP pose an example for this. The EMCP was originally discovered as an alternative pathway for C_2-assimilation present in bacteria that lacked the strategy commonly used by other bacterial species, namely the GC. Then, it was recognized that the EMCP does not only exist in Icl negative organisms, but also occurs in some bacteria that additionally possess the genetic potential for the GC (52). This unusual co-occurrence of two metabolic pathways with seemingly degenerate function in one organism raised the questions (i) which purpose this degeneracy fulfills, and (ii) how it is coordinated in the cell. Amongst the organisms found to encode both the GC as well as the EMCP is the Alphaproteobacterium *Paracoccus denitrificans* (52), which represents the model organism used in this study.

1.4 *Paracoccus denitrificans* – a member of the Alphaproteobacteria

Alphaproteobacteria are an ancient and versatile class in the domain of bacteria. Not only are they thought to be ancestral to the eukaryotic mitochondrion (65, 66), but they also inhabit a vast range of environments from ocean to land, where they often comprise the most abundant class of bacteria present (67–69). This characteristic is reflective of the diverse metabolic traits contained in the members of this group. Next to *P. denitrificans*, prominent examples of Alphaproteobacteria are the oligotrophic *Caulobacter crescentus*, the methylotrophic *Methylorubrum extroquens*, and the purple non-sulfur bacteria *Rhodobacter sphaeroides* and *Rhodobacter capsulatus*. All these bacterial species represent model organisms for different microbiological fields. While *C. crescentus* serves as model in cellular microbiology to study the bacterial cell cycle, cellular differentiation as well as asymmetric cell division (70, 71), *M. extorquens* as well as *R. sphaeroides* and *R. capsulatus* possess biotechnological potential for metabolic engineering and usage as microbial cell factories (72–74). *P. denitrificans,* in contrast, is mainly used as a model to study denitrification (75, 76) as well as the (alphaproteobacterial) respiratory chain (66, 77, 78). The interest in *P. denitrificans* in this study, however, lies in its versatile metabolism and the simultaneous coexistence of the GC and the EMCP.

The bacterium was first isolated as *Micrococcus denitrificans* from garden floor by the Dutch microbiologist Martinus Beijerinck in 1908 (79) and later reclassified as *P. denitrificans* by Davis and co-workers (80). Its multipartite genome is composed of two chromosomes and a megaplasmid (ch1: 2.8 Mbp; ch2: 1.7 Mbp, plasmid: 0.7 Mbp). Potentially due to the presence of a strong restriction/modification system, initial attempts of the scientific community to genetically modify *P. denitrificans* proved unsuccessful. Finally, random mutagenesis with N-methyl-N'-nitro-N-nitrosoguanidine allowed the isolation of a *P. denitrificans* mutant (Pd1222) with increased conjugation efficiency, which ultimately enabled the genetic manipulation of the bacterium and therefore opened the gate to extensive molecular biological and biochemical research on *P. denitrificans* as model organism (81).

1.5 Regulation of replenishment pathways

The activity of a replenishment pathway that assimilates carbon into biomass instead of oxidizing it for energy generation shifts the metabolic program of the cell from catabolism to anabolism. For balanced growth (*i.e.,* the steady state condition of a bacterial culture, in which the concentration of all cell components increases at the same rate in a constant environment (82)), bacteria must distribute fluxes at this branching point of metabolism in a highly coordinated fashion (83). This makes a strict regulation of the above individually introduced replenishment pathways (see section 1.2) inevitable. The simultaneous presence of two seemingly degenerate pathways of this nature (*i.e.*, the GC and the EMCP as is the case in *P. denitrificans* according to genome sequencing data (52)) increases the complexity of the metabolic node between catabolism and anabolism even further and, hence, adds to the complexity of the regulatory strategy behind it.

Generally, several fundamental layers of regulation in bacterial metabolism are recognized today. These involve control of enzyme abundance through transcriptional and post-transcriptional/translational mechanisms, as well as control of enzyme activity through post-translational modifications and allostery. Decades of research in different organisms have discovered the occurrence of various of these strategies especially for control of the GC (summarized in (38)) but also the EMCP. This knowledge will be briefly summarized in the following.

1.5.1 Regulation of the GC in *Escherichia coli*

The branching point between flux through the TCA cycle and the GC lies at the level of isocitrate, the substrate for which the TCA cycle enzyme isocitrate dehydrogenase (Idh) and the GC key enzyme isocitrate lyase (Icl) compete with each other. This metabolic node is most extensively studied in the Gammaproteobacterium *Escherichia coli* (Figure 4A). Here, one layer of control is reflected by differing affinities of the individual enzymes to their substrate with Idh showing an up to almost 100-fold higher affinity to isocitrate than Icl (84, 85). Activity of the Icl reaction, and, hence, metabolic flux through the GC in this organism depends on the accumulation of drastically elevated concentrations of isocitrate in the cell that is only achieved upon inactivation of Idh (86). The latter is

facilitated by a post-translational modification of the enzyme, namely the phosphorylation of a conserved serine residue in Idh through the kinase activity of the dedicated regulator AceK (87). This regulator is a bifunctional enzyme, possessing not only kinase but also phosphatase activity (88). The phosphatase activity of AceK allows reversion of the inactivation of Idh by dephosphorylation of the protein. The switch between kinase and phosphatase activity of AceK is thought to be regulated allosterically by a number of different metabolites, such as ATP (89–92), isocitrate (93), NADPH (92), and phosphoenolpyruvate (94). Additionally, the enzymes of the GC, including AceK, are controlled on genetic level. Thereby the transcriptional repressor IclR (repressor of isocitrate lyase), itself under control of another transcriptional regulator involved in fatty acid metabolism, FadR (fatty acid metabolism regulator (95)), inhibits expression of the *aceBAK*-operon (GC operon in *E. coli*) under non-anaplerotic conditions (96, 97).

1.5.2 Regulation of the GC in *Mycobacterium tuberculosis*

Different strategies to those found in *E. coli* have been identified in other bacteria. Amongst them the pathogenic *Mycobacterium tuberculosis*, where the GC represents a crucial target point for medical treatment of infections caused by the bacterium and is therefore studied thoroughly (57, 98–108). Two isoforms of Icl, Icl1 and Icl2, exist in this organism (106, 107). Both are involved not only in the function of the GC, but also substitute the function of a lacking methylisocitrate lyase enzyme (PrpB) of the MCC (57, 102). The two *M. tuberculosis* isoforms of Icl are subject to different regulatory mechanisms. While native Icl1 constitutively exhibits a catalytic function as isocitrate lyase of the GC, and as methylisocitrate lyase of the MCC (100), Icl2 does not show catalytic activity *in vitro* in the absence of allosteric activators. To enable Icl and PrpB acitivity of this protein, it requires binding of acetyl-CoA or propionyl-CoA (101). For this reason, the *M. tuberculosis* Icl2 enzyme is considered a gatekeeper that shifts metabolic flux from oxidation in the TCA cycle towards carbon assimilation through the GC and MCC in the presence of the metabolites acetyl-CoA and propionyl-CoA (101). Activity of Icl1, in turn, is regulated on the post-transcriptional level by acetylation (*i.e.*, activity of Icl1 is increased by acetylation of lysine residue K392, while decreased by acetylation of lysine residue K322 (108)). The enzyme is additionally controlled in

abundance on the transcriptional level through the antagonistic action of three regulatory players, namely PrpR, RamB, and GlnR. Here, the dedicated propionate metabolism regulator PrpR (regulator of the *prp*-operon/MCC) activates expression of *icl1* (104, 105), while RamB and the global response regulator GlnR, in turn, block PrpR-mediated expression of the *icl1* gene under nitrogen-limiting conditions ((103); Figure 4B).

1.5.3 Regulation of the GC in *Corynebacterium glutamicum*

RamB is also employed for transcriptional control of the GC together with another regulator of acetate metabolism (Ram), RamA, in the Gram-positive soil bacterium *Corynebacterium glutamicum* (109). This organism represents the bacterium in which RamB was originally discovered. Here, RamB was shown to function as a transcriptional repressor of the GC and other acetate-metabolism-derived genes (109, 110), while RamA is considered a more superordinate regulator that for one functions as activator of the genes involved in acetate metabolism and additionally positively controls expression of *ramB* ((109, 111); Figure 4C).

1.5.4 The family of short chain fatty acid metabolism regulators (ScfR)

M. tuberculosis PrpR and *C. glutamicum* RamB are members of the family of short chain fatty acid metabolism regulators (ScfR). The protein family was previously defined following the characterization of a transcriptional regulator for propionyl-CoA carboxylase, PccR, from *R. sphaeroides* (112). It is spread throughout various bacteria and holds transcriptional regulators for different metabolic pathways, such as the MMCP (dedicated regulators named PccR for regulator of propionyl-CoA carboxylase (PccAB)), the methylcitrate cycle (MCC; dedicated regulators named MccR for regulator of the MCC or PrpR for regulator of the MCC-encoding *prp*-operon), the GC (dedicated regulators named RamB) and metabolism for isobutyryl-CoA assimilation (IBC; dedicated regulators named IbcR) (7).

1.5.5 Regulation of the EMCP

While knowledge from different organisms has contributed to a broader picture of how regulation of the GC occurs, only few reports on the regulation of the EMCP exist in literature to-date (112, 113). Hu and Lidstrom have reported the presence

of CcrR, a transcriptional regulator of the TetR family, which was shown to stimulate expression of *ccr* during growth of *M. extorquens* AM1 on methanol or acetate ((113); Figure 4D). Additionally, a contribution of PccR as transcriptional activator of the gene encoding propionyl-CoA carboxylase of the MMCP (part of the lower EMCP) has been discovered in *R. sphaeroides* (112). Beyond that, how exactly the EMCP is regulated remains enigmatic.

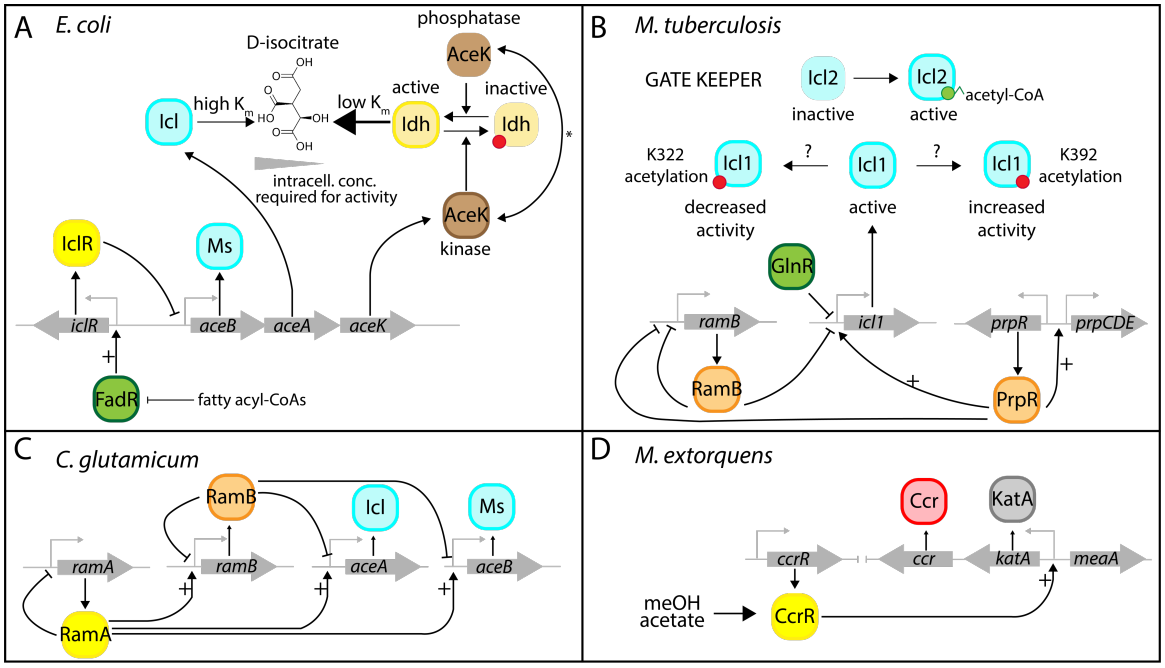

Figure 4: Regulation of the GC or EMCP in organisms that possess one of the alternative pathways as standalone replenishment route. Except coloring of Icl, Ccr and RamB, color code is not standardized between individual panels. (A) Regulation of the GC in *E. coli*. (B) Regulation of the GC in *M. tuberculosis*. (C) Regulation of the GC in *C. glutamicum*. (D) Regulation of the EMCP in *M. extorquens*.

1.6 Aims of this work

The GC and the EMCP are two distinct anaplerotic pathways that seem to serve a functionally degenerate purpose. By circumvention of the decarboxylating steps of the TCA cycle to produce the intermediates succinate (or succinyl-CoA, respectively) and malate, they shift the metabolic program of the cell from catabolism (*i.e.*, acetyl-CoA oxidation) to anabolism (*i.e.*, acetyl-CoA assimilation). Balanced bacterial growth requires a fine-tuned regulation of this metabolic shift.

Various studies from the last decades of research have revealed many aspects of the regulation of either the GC or the EMCP in model organisms that possess only one of the pathways as standalone route. However, beyond these well-studied models several other organisms exist that could potentially employ the GC and the EMCP at the same time. While for these organisms, genome sequencing data display the simultaneous presence of genes for the GC and the EMCP, it remains largely unknown what the biological function of this apparent metabolic degeneracy is. Furthermore, the strategies underlying the regulation of both pathways in these organisms are not understood.

A representative of a GC and EMCP double-positive organism is the Alphaproteobacterium *P. denitrificans*. Using this bacterium as a model, this work seeks to shed light on the nature and regulation behind the coexistence of the GC and EMCP in bacterial cells.

Therefore, Chapter 2 will address the question if and under which conditions both pathways operate in *P. denitrificans* Pd1222 and Chapter 3 aims at elucidating the regulatory mechanisms that control the employment of both pathways in the Alphaproteobacterium.

1.7 References

1. Chubukov V, Gerosa L, Kochanowski K, Sauer U. 2014. Coordination of microbial metabolism. Nature Reviews Microbiology 12:327–340.

2. Fothergill-Gilmore LA. 1986. The evolution of the glycolytic pathway. Trends Biochem Sci 11:47–51.

3. Conway T. 1992. The Entner-Doudoroff pathway: history, physiology and molecular biology. FEMS Microbiol Rev 9:1–27.

4. Nathan Entner B, Doudoroff M. 1952. Glucose and gluconic acid oxidation of *Pseudomonas saccharophila*. J Biol Chem 196:853–62.

5. Meléndez-Hevia E, Isidoro A. 1985. The game of the pentose phosphate cycle. J Theor Biol 117:251–263.

6. Ghisla S. 2004. β-Oxidation of fatty acids. Eur J Biochem 271:459–461.

7. Krebs HA. 1940. The citric acid cycle: A reply to the criticisms of F. L. Breusch and of J. Thomas. Biochemical Journal 34:460.

8. Kornberg HL, Krebs HA. 1957. Synthesis of cell constituents from c2-units by a modified tricarboxylic acid cycle. Nature 179:988–991.

9. Stephanopoulos GN, Aristidou AA, Nielsen J. 1998. Review of cellular metabolism. Metab Eng 21–79.

10. Hansen EJ, Juni E. 1974. Two routes for synthesis of phosphoenolpyruvate from C4-dicarboxylic acids in *Escherichia coli*. Biochem Biophys Res Commun 59:1204–1210.

11. Sauer U, Eikmanns BJ. 2005. The PEP—pyruvate—oxaloacetate node as the switch point for carbon flux distribution in bacteria. FEMS Microbiol Rev 29:765–794.

12. Watson JA, Fang M, Lowenstein JM. 1969. Tricarballylate and hydroxycitrate: Substrate and inhibitor of ATP:citrate oxaloacetate lyase. Arch Biochem Biophys 135:209–217.

13. Evans MC, Buchanan BB, Arnon DI. 1966. A new ferredoxin-dependent carbon reduction cycle in a photosynthetic bacterium. Proc Natl Acad Sci U S A 55:928–934.

14. Shemin D, Rittenberg D. 1946. The biological utilization of glycine for the synthesis of the protoporphyrin of hemoglobin. Journal of Biological Chemistry 166:621–625.

15. Kornberg HL. 1966. The role and control of the glyoxylate cycle in *Escherichia coli*. Biochemical Journal 99:1–11.

16. Petushkova E, Mayorova E, Tsygankov A. 2021. TCA cycle replenishing pathways in photosynthetic purple non-sulfur bacteria growing with acetate. Life 11.

17. Schada Von Borzyskowski L, Bernhardsgrütter I, Erb TJ. 2020. Biochemical unity revisited: Microbial central carbon metabolism holds new discoveries, multi-tasking pathways, and redundancies with a reason. Biol Chem 401:1429–1441.

18. Bergey DH, Buchanan RE, Gibbons NE. 2015. Bergey's manual of systematics of archaea and bacteria.

19. Torsvik V, Øvreås L, Thingstad TF. 2002. Prokaryotic diversity--magnitude, dynamics, and controlling factors. Science 296:1064–1066.

20. Šmejkalová H, Erb TJ, Fuchs G. 2010. Methanol Assimilation in *Methylobacterium extorquens* AM1: Demonstration of all enzymes and their regulation. PLoS One 5:e13001.

21. Dziewit L, Czarnecki J, Prochwicz E, Wibberg D, Schüter A, Pühler A, Bartosik D. 2015. Genome-guided insight into the methylotrophy of *Paracoccus aminophilus* JCM 7686. Front Microbiol 6:852.

22. Chistoserdova L. 2011. Modularity of methylotrophy, revisited. Environ Microbiol 13:2603–2622.

23. Kornberg HL, Morris JG. 1965. The utilization of glycollate by *Micrococcus denitrificans*: the beta-hydroxyaspartate pathway. Biochem J 95:577–586.

24. Schada von Borzyskowski L, Severi F, Krüger K, Hermann L, Gilardet A, Sippel F, Pommerenke B, Claus P, Cortina NS, Glatter T, Zauner S, Zarzycki J, Fuchs BM, Bremer E, Maier UG, Amann RI, Erb TJ. 2019. Marine Proteobacteria metabolize glycolate via the β-hydroxyaspartate cycle. Nature 575:500–504.

25. Berg IA, Ivanovsky RN. 2009. Enzymes of the citramalate cycle in *Rhodospirillum rubrum*. Microbiology 78:16–24.

26. Ivanovsky RN, Krasilnikova EN, Berg IA. 1997. A proposed citramalate cycle for acetate assimilation in the purple non-sulfur bacterium *Rhodospirillum rubrum*. FEMS Microbiol Lett 153:399–404.

27. Mazumder R, Sasakawa T, Kaziro Y, Ochoa S. 1961. A new enzyme in the conversion of propionyl coenzyme A to succinyl coenzyme A. J Biol Chem 236:53–55.

28. Mancia F, Evans PR. 1998. Conformational changes on substrate binding to methylmalonyl CoA mutase and new insights into the free radical mechanism. Structure 6:711–720.

29. Tabuchi T, Uchiyama H. 1975. methylcitrate condensing and methylisocitrate cleaving enzymes; evidence for the pathway of oxidation of propionyl-coA to pyruvate via C7-tricarboxylic acids. Agric Biol Chem 39:2035–2042.

30. Tabuchi T, Hara S. 1974. Production of 2-methylisocitric acid from n-paraffins by mutants of *Candida lipolytica*. Agric Biol Chem 38:1105–1106.

31. Kornberg HL, Madsen NB. 1957. Synthesis of C4-dicarboxylic acids from acetate by a "glyoxylate bypass" of the tricarboxylic acid cycle. Biochim Biophys Acta 24:651–653.

32. Erb TJ, Berg IA, Brecht V, Müller M, Fuchs G, Alber BE. 2007. Synthesis of C5-dicarboxylic acids from C2-units involving crotonyl-CoA carboxylase/reductase: The ethylmalonyl-CoA pathway. Proc Natl Acad Sci U S A 104:10631–10636.

33. Erb TJ, Fuchs G, Alber BE. 2009. (2S)-Methylsuccinyl-CoA dehydrogenase closes the ethylmalonyl-CoA pathway for acetyl-CoA assimilation. Mol Microbiol 73:992–1008.

34. Feng X, Tang KH, Blankenship RE, Tang YJ. 2010. Metabolic flux analysis of the mixotrophic metabolisms in the green sulfur bacterium *Chlorobaculum tepidum*. J Biol Chem 285:39544–39550.

35. Tang KH, Blankenship RE. 2010. Both forward and reverse TCA cycles operate in green sulfur bacteria. J Biol Chem 285:35848.

36. Khomyakova M, Bükmez Ö, Thomas LK, Erb TJ, Berg IA. 2011. A methylaspartate cycle in haloarchaea. Science 331:334–337.

37. Borjian F, Han J, Hou J, Xiang H, Berg IA. 2015. The methylaspartate cycle in haloarchaea and its possible role in carbon metabolism. The ISME Journal 10:546–557.

38. Dolan SK, Welch M. 2018. The Glyoxylate Shunt, 60 Years On. Annu Rev Microbiol 72:309-330.

39. Chung T, Klumpp DJ, LaPorte DC. 1988. Glyoxylate bypass operon of *Escherichia coli*: cloning and determination of the functional map. J Bacteriol 170:386.

40. Green PN, Ardley JK. 2018. Review of the genus *Methylobacterium* and closely related organisms: a proposal that some *Methylobacterium* species be reclassified into a new genus, *Methylorubrum* gen. nov. Int J Syst Evol Microbiol 68:2727–2748.

41. Alber BE, Spanheimer R, Ebenau-Jehle C, Fuchs G. 2006. Study of an alternate glyoxylate cycle for acetate assimilation by *Rhodobacter sphaeroides*. Mol Microbiol 61:297–309.

42. Han L, Reynolds KA. 1997. A novel alternate anaplerotic pathway to the glyoxylate cycle in Streptomycetes. J Bacteriol 179:5157–5164.

43. Anthony C, York Paris N, Diego S, Francisco S. 1975. the biochemistry of methylotrophs. Sci Prog 62:167–206.

44. Ehrensvärd G, Reio L, Saluste E, Stjernholm R. 1951. Acetic acid metabolism in *Torulopsis utilis*: III. metabolic connection between acetic acid and various amino acids. J Biol Chem 189:93–108.

45. Gottschal JC, Kuenen JG. 1980. Mixotrophic growth of *Thiobacillus* A2 on acetate and thiosulfate as growth limiting substrates in the chemostat. Archives of Microbiology 126:33–42.

46. Olsen' And I, Merrick JM. 1968. Identification of propionate as an endogenous CO2 acceptor in *Rhodospirillum rubrum* and properties of purified propionyl-coenzyme A carboxylase. J Bacteriol 1774–1778.

47. Albers H, Gottschalk G. 1976. Acetate metabolism in *Rhodopseudomonas* gelatinosa and several other *Rhodospirillaceae.* Arch Microbiol 111:45–49.

48. Chistoserdova L, Chen SW, Lapidus A, Lidstrom ME. 2003. Methylotrophy in *Methylobacterium extorquens* AM1 from a genomic point of view. J Bacteriol 185:2980–2987.

49. Korotkova N, Chistoserdova L, Kuksa V, Lidstrom ME. 2002. Glyoxylate regeneration pathway in the methylotroph *Methylobacterium extorquens* AM1. J Bacteriol 184:1750.

50. Smith LM, Meijer WG, Dijkhuizen L, Goodwin PM. 1996. A protein having similarity with methylmalonyl-CoA mutase is required for the assimilation of methanol and ethanol by *Methylobacterium extorquens* AM1. Microbiology (Reading) 142:675–684.

51. Chistoserdova L v., Lidstrom ME. 1996. Molecular characterization of a chromosomal region involved in the oxidation of acetyl-CoA to glyoxylate in the isocitrate-lyase-negative methylotroph *Methylobacterium extorquens* AM1. Microbiology (Reading) 142:1459–1468.

52. Erb TJ, Brecht V, Fuchs G, Müller M, Alber BE. 2009. Carboxylation mechanism and stereochemistry of crotonyl-CoA carboxylase/reductase, a carboxylating enoyl-thioester reductase. Proc Natl Acad Sci U S A 106:8871–8876.

53. Erb TJ, Rétey J, Fuchs G, Alber BE. 2008. Ethylmalonyl-CoA mutase from *Rhodobacter sphaeroides* defines a new subclade of coenzyme B12-dependent acyl-CoA mutases. J Biol Chem 283:32283–32293.

54. Erb TJ, Frerichs-Revermann L, Fuchs G, Alber BE. 2010. The apparent malate synthase activity of *Rhodobacter sphaeroides* is due to two paralogous enzymes, (3S)-malyl-coenzyme A (CoA)/β-methylmalyl-CoA lyase and (3S)-malyl-CoA thioesterase. J Bacteriol 192:1249–1258.

55. Kremer K, van Teeseling MCF, von Borzyskowski LS, Bernhardsgrütter I, van Spanning RJM, Gates AJ, Remus-Emsermann MNP, Thanbichler M, Erb TJ. 2019. Dynamic metabolic rewiring enables efficient acetyl coenzyme A assimilation in *Paracoccus denitrificans*. mBio 10.

56. Dolan SK, Wijaya A, Geddis SM, Spring DR, Silva-Rocha R, Welch M. 2018. Loving the poison: The methylcitrate cycle and bacterial pathogenesis. Microbiology (Reading) 164:251–259.

57. Eoh H, Rhee KY. 2014. Methylcitrate cycle defines the bactericidal essentiality of isocitrate lyase for survival of *Mycobacterium tuberculosis* on fatty acids. Proc Natl Acad Sci U S A 111:4976–4981.

58. Textor S, Wendisch VF, de Graaf AA, Müller U, Linder MI, Linder D, Buckel W. 1997. Propionate oxidation in *Escherichia coli*: evidence for operation of a methylcitrate cycle in bacteria. Archives of Microbiology 168:428–436.

59. Uchiyama H, Tabuchi T. 1976. Properties of methylcitrate synthase from *Candida lipolytica*. Agric Biol Chem 40:1411–1418.

60. Horswill AR, Escalante-Semerena JC. 1997. Propionate catabolism in *Salmonella typhimurium* LT2: two divergently transcribed units comprise the prp locus at 8.5 centisomes, prpR encodes a member of the sigma-54 family of activators, and the prpBCDE genes constitute an operon. J Bacteriol 179:928–940.

61. Horswill AR, Escalante-Semerena JC. 1999. *Salmonella typhimurium* LT2 catabolizes propionate via the 2-methylcitric acid cycle. J Bacteriol 181:5615–5623.

62. Singleton R, Singleton DR. 2017. Remembering our forebears: Albert Jan Kluyver and the unity of life. J Hist Biol 50:169–218.

63. Allen GE. 2005. Mechanism, vitalism and organicism in late nineteenth and twentieth-century biology: the importance of historical context. Stud Hist Philos Biol Biomed Sci 36:261–283.

64. Nayak DD, Marx CJ. 2014. Methylamine utilization via the N-methylglutamate pathway in *Methylobacterium extorquens* PA1 involves a novel flow of carbon through C1 assimilation and dissimilation pathways. J Bacteriol 196:4130–4139.

65. Yang D, Oyaizu Y, Oyaizu H, Olsen GJ, Woese CR. 1985. Mitochondrial origins. Proc Natl Acad Sci U S A 82:4443–4447.

66. Hutton JT, Gorham E, Junge CE, Werby RT, Meteorology ; S Cauer J, Rossby H, Egner C-G, Eriksson H, Harley E. 1975. *Paracoccus denitrificans* and the evolutionary origin of the mitochondrion. Nature 254:495–498.

67. Wang S, Luo H. 2021. Dating Alphaproteobacteria evolution with eukaryotic fossils. Nature Communications 2021 12:1 12:1–9.

68. Ettema TJG, Andersson SGE. 2009. The α-proteobacteria: the Darwin finches of the bacterial world. Biol Lett 5:429.

69. Dutilh BE, Snel B, Ettema TJG, Huynen MA. 2008. signature genes as a phylogenomic tool. Mol Biol Evol 25:1659–1667.

70. Thanbichler M. 2009. Spatial regulation in *Caulobacter crescentus*. Curr Opin Microbiol 12:715–721.

71. Skerker JM, Laub MT. 2004. Cell-cycle progression and the generation of asymmetry in *Caulobacter crescentus*. Nature Reviews Microbiology 2:325–337.

72. Alber BE. 2011. Biotechnological potential of the ethylmalonyl-CoA pathway. Appl Microbiol Biotechnol 89:17–25.

73. Orsi E, Beekwilder J, Eggink G, Kengen SWM, Weusthuis RA. 2021. The transition of *Rhodobacter sphaeroides* into a microbial cell factory. Biotechnol Bioeng 118:531–541.

74. Ochsner AM, Sonntag F, Buchhaupt M, Schrader J, Vorholt JA. 2014. *Methylobacterium extorquens*: methylotrophy and biotechnological applications. Applied Microbiology and Biotechnology 99:517–534.

75. Gaimster H, Alston M, Richardson DJ, Gates AJ, Rowley G. 2018. Transcriptional and environmental control of bacterial denitrification and N2O emissions. FEMS Microbiol Lett 365:277.

76. Olaya-Abril A, Hidalgo-Carrillo J, Luque-Almagro VM, Fuentes-Almagro C, Urbano FJ, Moreno-Vivián C, Richardson DJ, Roldán MD. 2018. Exploring the denitrification proteome of *Paracoccus denitrificans* Pd1222. Front Microbiol 9:1137.

77. Jarman OD, Biner O, Wright JJ, Hirst J. 2021. *Paracoccus denitrificans*: a genetically tractable model system for studying respiratory complex I. Scientific Reports 11:1–14.

78. de Gier JL, Lübben M, Reijnders WNM, Tipker CA, Slotboom D -J, van Spanning RJM, Stouthamer AH, van der Oost J. 1994. The terminal oxidases of *Paracoccus denitrificans*. Mol Microbiol 13:183–196.

79. Beijerinck M, Minkman D. 1910. Bildung und Verbrauch von Stickoxydul durch Bakterien. Zentbl Bakteriol Parasitenkd Infektionskr Hyg Abt II.

80. Davis DH, Doudoroff M, Stanier RY, Mandel M. 1969. Proposal to reject the genus *Hydrogenomonas*: Taxonomic implications. International Journal of Systematic and Evolutionary Microbiology 19:375–390.

81. de Vries GE, Harms N, Hoogendijk J, Stouthamer AH. 1989. Isolation and characterization of *Paracoccus denitrificans* mutants with increased conjugation frequencies and pleiotropic loss of a (nGATCn) DNA-modifying property. Archives of Microbiology 152:52–57.

82. Herbert D, Elsworth R, Telling RC. 1956. The continuous culture of bacteria; a theoretical and experimental study. J Gen Microbiol 14:601–622.

83. Thomas E. 2015. Microbial growth and physiology: a call for better craftsmanship. Front Microbiol 6.

84. MacKintosh C, Nimmo HG. 1988. Purification and regulatory properties of isocitrate lyase from *Escherichia coli* ML308. Biochemical Journal 250:25.

85. Laportes DC, Walsh K, Koshland DE. 1984. The branch point effect. Ultrasensitivity and subsensitivity to metabolic control. J Biol Chem 259:14068–14075.

86. Laportes DC, Thorsness PE, Koshland DE. 1985. Compensatory phosphorylation of isocitrate dehydrogenase. A mechanism for adaptation to the intracellular environment. J Biol Chem 260:10563–10568.

87. Garnak M, Reeves HC. 1979. Phosphorylation of Isocitrate dehydrogenase of *Escherichia coli*. Science 203:1111–1112.

88. Laporte DC, Koshland DE. 1982. A protein with kinase and phosphatase activities involved in regulation of tricarboxylic acid cycle. Nature 300:458–460.

89. Zheng J, Jia Z. 2010. Structure of the bifunctional isocitrate dehydrogenase kinase/phosphatase. Nature 465:961–965.

90. Nimmo GA, Nimmo HG. 1984. The regulatory properties of isocitrate dehydrogenase kinase and isocitrate dehydrogenase phosphatase from *Escherichia coli* ML308 and the roles of these activities in the control of isocitrate dehydrogenase. Eur J Biochem 141:409–414.

91. Laporte DC, Koshland DE. 1983. Phosphorylation of isocitrate dehydrogenase as a demonstration of enhanced sensitivity in covalent regulation. Nature 305:286–290.

92. Miller SP, Chen R, Karschnia EJ, Romfo C, Dean A, LaPorte DC. 2000. Locations of the regulatory sites for isocitrate dehydrogenase kinase/phosphatase. J Biol Chem 275:833–839.

93. Laporte DC. 1993. The isocitrate dehydrogenase phosphorylation cycle: regulation and enzymology. J Cell Biochem 51:14–18.

94. Ogawa T, Murakami K, Mori H, Ishii N, Tomita M, Yoshin M. 2007. Role of phosphoenolpyruvate in the NADP-isocitrate dehydrogenase and isocitrate lyase reaction in *Escherichia coli*. J Bacteriol 189:1176.

95. Gui L, Sunnarborg A, Laporte DC. 1996. Regulated expression of a repressor protein: FadR activates *iclR*. J Bacteriol 178:4704–4709.

96. Cortay JC, Negre D, Galinier A, Duclos B, Perriere G, Cozzone AJ. 1991. Regulation of the acetate operon in *Escherichia coli*: purification and functional characterization of the IclR repressor. EMBO J 10:675–679.

97. Lorca GL, Ezersky A, Lunin V v., Walker JR, Altamentova S, Evdokimova E, Vedadi M, Bochkarev A, Savchenko A. 2007. Glyoxylate and pyruvate are antagonistic effectors of the *Escherichia coli* IclR transcriptional regulator. J Biol Chem 282:16476–16491.

98. Eoh H, Rhee KY. 2013. Multifunctional essentiality of succinate metabolism in adaptation to hypoxia in *Mycobacterium tuberculosis*. Proc Natl Acad Sci U S A 110:6554–6559.

99. Serafini A, Tan L, Horswell S, Howell S, Greenwood DJ, Hunt DM, Phan MD, Schembri M, Monteleone M, Montague CR, Britton W, Garza-Garcia A, Snijders AP, VanderVen B, Gutierrez MG, West NP, de Carvalho LPS. 2019. *Mycobacterium tuberculosis* requires glyoxylate shunt and reverse methylcitrate cycle for lactate and pyruvate metabolism. Mol Microbiol 112:1284.

100. Gould TA, van de Langemheen H, Muñoz-Elías EJ, McKinney JD, Sacchettini JC. 2006. Dual role of isocitrate lyase 1 in the glyoxylate and methylcitrate cycles in *Mycobacterium tuberculosis*. Mol Microbiol 61:940–947.

101. Bhusal RP, Jiao W, Kwai BXC, Reynisson J, Collins AJ, Sperry J, Bashiri G, Leung IKH. 2019. Acetyl-CoA-mediated activation of *Mycobacterium tuberculosis* isocitrate lyase 2. Nature Communications 10:1–7.

102. Muñoz-Elías EJ, McKinney JD. 2005. *Mycobacterium tuberculosis* isocitrate lyases 1 and 2 are jointly required for *in vivo* growth and virulence. Nat Med 11:638.

103. Antelmann H, Bashiri G, Wang J, Serafini A, Qi N, She G-L, Du W, Ye B-C. 2021. *Mycobacterium smegmatis* GlnR regulates the glyoxylate cycle and the methylcitrate cycle on fatty acid metabolism by repressing *icl* transcription. Front Microbiol.

104. Tang S, Hicks ND, Cheng YS, Silva A, Fortune SM, Sacchettini JC. 2019. Structural and functional insight into the *Mycobacterium tuberculosis* protein PrpR reveals a novel type of transcription factor. Nucleic Acids Res 47:9934–9949.

105. Masiewicz P, Brzostek A, Wolański M, Dziadek J, Zakrzewska-Czerwińska J. 2012. A novel role of the PrpR as a transcription factor involved in the regulation of methylcitrate pathway in *Mycobacterium tuberculosis*. PLoS One 7.

106. Cole ST, Brosch R, Parkhill J, Garnier T, Churcher C, Harris D, Gordon S v., Eiglmeier K, Gas S, Barry CE, Tekaia F, Badcock K, Basham D, Brown D, Chillingworth T, Connor R, Davies R, Devlin K, Feltwell T, Gentles S, Hamlin N, Holroyd S, Hornsby T, Jagels K, Krogh A, McLean J, Moule S, Murphy L, Oliver K, Osborne J, Quail MA, Rajahdream MA, Rogers J, Rutter S, Seeger K, Skelton J, Squares R, Squares S, Sulsten JE, Taylor K, Whitehead S, Bartell BG. 1998. Deciphering the biology of *Mycobacterium tuberculosis* from the complete genome sequence. Nature 396:190–190.

107. Fleischmann RD, Alland D, Eisen JA, Carpenter L, White O, Peterson J, DeBoy R, Dodson R, Gwinn M, Haft D, Hickey E, Kolonay JF, Nelson WC, Umayam LA, Ermolaeva M, Salzberg SL, Delcher A, Utterback T, Weidman J, Khouri H, Gill J, Mikula A, Bishai W, Jacobs WR, Venter JC, Fraser CM. 2002. Whole-genome comparison of *Mycobacterium tuberculosis* clinical and laboratory strains. J Bacteriol 184:5479–5490.

108. Bi J, Wang Y, Yu H, Qian X, Wang H, Liu J, Zhang X. 2017. Modulation of central carbon metabolism by acetylation of isocitrate lyase in *Mycobacterium tuberculosis*. Scientific Reports 7:1–11.

109. Auchter M, Cramer A, Hüser A, Rückert C, Emer D, Schwarz P, Arndt A, Lange C, Kalinowski J, Wendisch VF, Eikmanns BJ. 2011. RamA and RamB are global transcriptional regulators in *Corynebacterium glutamicum* and control genes for enzymes of the central metabolism. J Biotechnol 154:126–139.

110. Gerstmeir R, Cramer A, Dangel P, Schaffer S, Eikmanns BJ. 2004. RamB, a novel transcriptional regulator of genes involved in acetate metabolism of *Corynebacterium glutamicum*. J Bacteriol 186:2798–2809.

111. Cramer A, Auchter M, Frunzke J, Bott M, Eikmanns BJ. 2007. RamB, the transcriptional regulator of acetate metabolism in *Corynebacterium glutamicum*, is subject to regulation by RamA and RamB. J Bacteriol 189:1145–1149.

112. Carter MS, Alber BE. 2015. Transcriptional regulation by the short-chain fatty acyl coenzyme A regulator (ScfR) PccR controls propionyl coenzyme A assimilation by *Rhodobacter sphaeroides*. J Bacteriol 197:3048–3056.

113. Hu B, Lidstrom M. 2012. CcrR, a TetR family transcriptional regulator, activates the transcription of a gene of the ethylmalonyl coenzyme a pathway in *Methylobacterium extorquens* AM1. J Bacteriol 194:2802–2808.

2 Metabolic rewiring in *P. denitrificans*

Dynamic metabolic rewiring enables efficient acetyl-CoA assimilation in *Paracoccus denitrificans*

Authors: Katharina Kremer[a], Muriel C.F. van Teeseling[b], Lennart Schada von Borzyskowski[a], Iria Bernhardsgrütter[a], Rob J. M. van Spanning[c], Andrew J. Gates[d], Mitja N.P. Remus-Emsermann[e,f], Martin Thanbichler[a,b,g], and Tobias J. Erb[a,b,g] (*)

Affiliations: [a] Max Planck Institute for Terrestrial Microbiology, Marburg, 35043, Germany; [b] Faculty of Biology, Philipps-Universität, Marburg, 35043, Germany; [c] Department of Molecular Cell Biology, Vrije Universiteit, HV Amsterdam, 1081, The Netherlands; [d] School of Biological Sciences, University of East Anglia, Norwich Research Park, Norwich, NR4 7TJ, U.K.; [e] School of Biological Sciences, University of Canterbury, Christchurch, 8140, New Zealand; [f] Biomolecular Interaction Centre, University of Canterbury, Christchurch, 8140, New Zealand; [g] LOEWE Center for Synthetic Microbiology, Marburg, 35043, Germany

Published in:
mBio 10.4 (2019): e00805-19.
https://doi.org/10.1128/mBio.00805-19

Author contributions:

K.K., I.B., L.S.v.B., and T.J.E. conceptualized the project. R.v.S. and A.J.G. contributed by giving fundamental advice in molecular biology and training in genetic manipulation of *Paracoccus denitrificans*. K.K and T.J.E. designed the study. K.K. performed all genetic and biochemical experiments and analyses. K.K., M.C.F.v.T. and M.T. planned and performed all microscopic analyses. K.K. and M.N.P.R.E. analysed the microscopic images of the time-lapse experiments. K.K. and L.S.v.B. performed homology and phylogenetic analyses. K.K. and T.J.E. wrote the manuscript.

2.1 Abstract

During growth, microorganisms have to balance metabolic flux between energy and biosynthesis. One of the key intermediates in central carbon metabolism is acetyl-CoA, which can be either oxidized in the citric acid cycle or assimilated into biomass through dedicated pathways. Two acetyl-CoA assimilation strategies have been described in bacteria so far, the ethylmalonyl-CoA pathway (EMCP) and the glyoxylate cycle (GC). Here, we show that *Paracoccus denitrificans* uses both strategies for acetyl-CoA assimilation during different growth stages, revealing an unexpected metabolic complexity in the organism's central carbon metabolism. The EMCP is constitutively expressed on various substrates and leads to high biomass yields on substrates requiring acetyl-CoA assimilation, such as acetate, while the GC is specifically induced on these substrates, enabling fast growth rates. Even though each acetyl-CoA assimilation strategy alone confers a distinct growth advantage, *P. denitrificans* recruits both to adapt to changing environmental conditions, such as a switch from succinate to acetate. Time-resolved single-cell experiments show that during this switch, expression of the EMCP and GC is highly coordinated, indicating fine-tuned genetic programming. The dynamic metabolic rewiring of acetyl-CoA assimilation is an evolutionary innovation by *P. denitrificans* that allows this organism to respond in a highly flexible manner to changes in the nature and availability of the carbon source to meet the physiological needs of the cell, representing a new phenomenon in central carbon metabolism.

2.2 Importance

Central carbon metabolism provides organisms with energy and cellular building blocks during growth and is considered as the invariable 'operating system' of the cell. Here we describe a new phenomenon in bacterial central carbon metabolism. In contrast to many other bacteria, that employ only one pathway for the conversion of the central metabolite acetyl-CoA, *Paracoccus denitrificans* possesses two different acetyl-CoA assimilation pathways. These two pathways are dynamically recruited during different stages of growth, which allows *P. denitrificans* to achieve both high biomass yield and fast growth rates under changing environmental conditions. Overall this dynamic rewiring of central carbon metabolism in

P. denitrificans represents a new strategy compared to other organisms employing only one acetyl-CoA assimilation pathway.

2.3 Introduction

During growth, bacteria have to distribute metabolic flux between catabolism and anabolism. An important central metabolic pathway is the tricarboxylic acid (TCA) cycle, which interfaces anabolism and catabolism. In the TCA cycle, the C2-unit acetyl coenzyme A (acetyl-CoA) is catabolized into CO_2, generating reducing equivalents and ATP for the cell. At the same time, the TCA cycle produces several intermediates that are committed to biosynthesis.

Note that the TCA cycle poses a special challenge for many compounds that are exclusively metabolized via acetyl-CoA, such as acetate, alcohols, short and long chain-fatty acids, esters and waxes. Because all carbon of acetyl-CoA is lost to CO_2, this allows energy conservation, but not carbon assimilation through the TCA cycle. Consequently, dedicated pathways for the assimilation of acetyl-CoA are required to allow growth on these ubiquitous substrates.

Two different acetyl-CoA assimilation pathways have been described in bacteria: the glyoxylate cycle (GC) (1, 2) and the ethylmalonyl-CoA pathway (EMCP) (3, 4). The GC uses two enzymes in addition to the enzymes of the TCA cycle. The first enzyme of the GC, isocitrate lyase (Icl), cleaves isocitrate into succinate and glyoxylate. This step is followed by the condensation of glyoxylate with a second molecule of acetyl-CoA to form malate and free CoA in a reaction catalyzed by the second enzyme of the GC, malate synthase (1, 2).

The EMCP also forms malate and succinate. However, unlike the GC, the EMCP is a linear pathway that employs 13 different enzymes that collectively convert a total of three acetyl-CoA and two CO_2 molecules into the TCA cycle intermediates malate and succinate. The key enzyme of the EMCP is crotonyl-CoA carboxylase/reductase (Ccr), which catalyzes the reductive carboxylation of crotonyl-CoA to ethylmalonyl-CoA (3-5).

Overall, the GC and the EMCP differ substantially in terms of co-factor and carbon requirements. The GC requires four ATP and generates reducing equivalents on

the level of two nicotinamides as well as two quinols per four acetates converted into malate (estimated $\Delta_rG'^0$ = -129 kJ/mol). To generate two malate from acetate in the EMCP, three molecules of acetate and two CO_2 are converted at the expense of three ATP and two reduced nioctinamides, while two quinols are generated (estimated $\Delta_rG'^0$ = -142 kJ/mol). When acetate is used to generate the CO_2 and fuel the cycle, this changes the stoichiometry to three consumed ATP, and one reduced nicotinamide, as well as three quinols generated (estimated $\Delta_rG'^0$ = -190 kJ/mol). While the EMCP requires more enzymatic steps (and likely more cellular resources), it enables the fixation of inorganic carbon into biomass, as well as the co-assimilation of different C5- and C3-carbonic acids compared to the GC, indicating that the two pathways provide different physiological advantages. In most bacteria, only one of the two acetyl-CoA assimilation pathways is present. Importantly, the Alphaproteobacterium *Paracoccus denitrificans* encodes the enzymes for both acetyl-CoA assimilation pathways (Figure 1), raising the question of which role each individual pathway would play in the cell.

In this work, we show that *P. denitrificans* uses both the GC and the EMCP. The EMCP serves as default acetyl-CoA assimilation pathway that is always present with low activity in the cell during growth on various substrates, including carbon sources that do not require acetyl-CoA assimilation. By contrast, the GC is specifically induced after switching to carbon sources that depend on acetyl-CoA assimilation, such as acetate or crotonate. We further demonstrate that the two acetyl-CoA assimilation pathways confer distinct physiological advantages. Growth with the EMCP results in increased biomass yield in *P. denitrificans*, while the GC allows for higher growth rates, suggestive for a rate-yield trade-off between the two pathways. Phylogenetic analysis indicates that *P. denitrificans* and several other Alphaproteobacteria acquired the GC through lateral gene transfer, consisting with a specific adaptation of the central carbon metabolism of these organisms during evolution. Collectively, our experiments show a surprising flexibility in central carbon metabolism of Alphaproteobacteria that allows the complete rewiring of metabolic flux depending on the type and availability of the carbon and free energy source according to the physiological needs of the cell.

2.4 Results

2.4.1 *P. denitrificans* uses the EMCP and the GC for acetyl-CoA assimilation

Earlier studies suggested that *Paracoccus* might use the EMCP as well as the GC for acetyl-CoA assimilation (4, 6, 7). We therefore searched the genome of the fully sequenced strain *P. denitrificans* Pd1222 for homologs of genes involved in the EMCP and the GC from *Rhodobacter sphaeroides* 2.4.1 and *Escherichia coli* K-12, respectively. Our analysis verified that *P. denitrificans* has the genetic potential for both, the GC as well as the EMCP (Figure 1, Table 1; (4)).

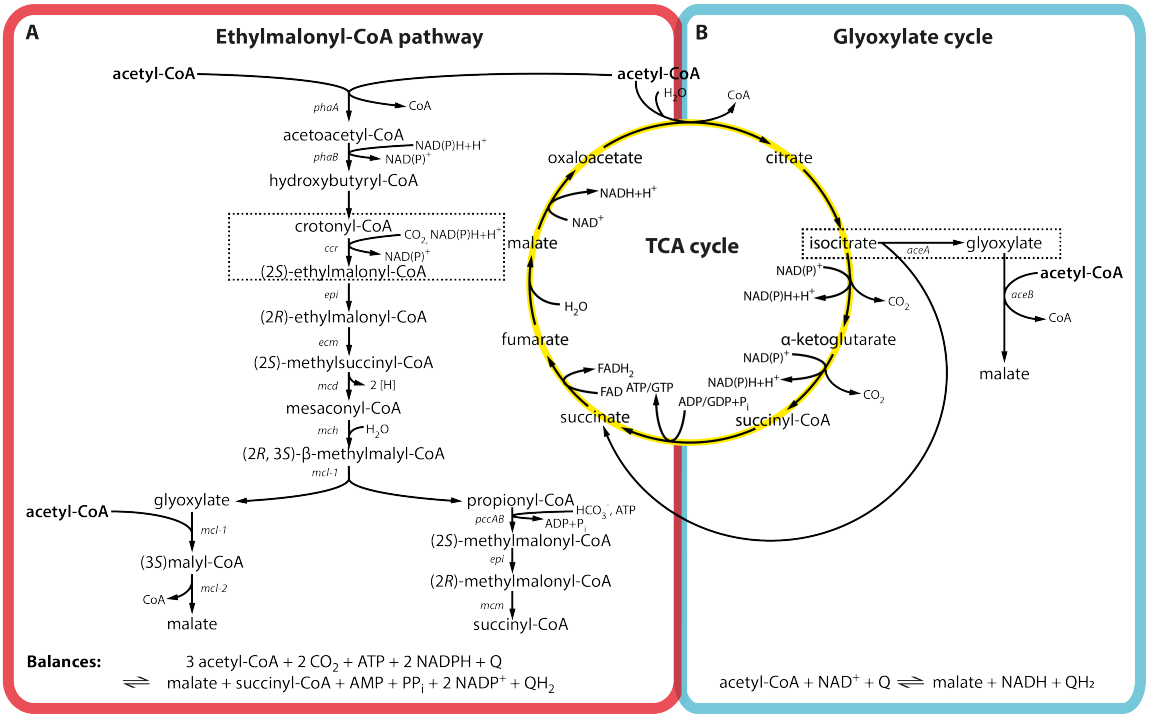

Figure 1: The fate of acetyl-CoA in anabolism and catabolism. Acetyl-CoA is either oxidized to CO_2 in the tricarboxylic acid cycle (TCA) to generate reducing equivalents and ATP/GTP, or assimilated into biomass. Two acetyl-CoA assimilation pathways are present in bacteria, the ethylmalonyl-CoA pathway (A) and the glyoxylate cycle (B). Reaction balances of the individual pathways are shown on the bottom. Note that the activation of acetate to acetyl-CoA requires the hydrolysis of one ATP into AMP and PP_i (not included in balance). Key reactions of the individual pathways are highlighted in dashed boxes. Genes encoding the individual enzymes of the EMCP and GC are named following the nomenclature established for *Rhodobacter sphaeroides* 2.4.1 and *Escherichia coli* K-12, respectively. The corresponding enzyme names and open reading frames in *P. denitrificans* are listed in Table 1.

Table 1: Genes coding for enzymes of the EMCP and the GC in *Rhodobacter sphaeroides* 2.4.1 and *Escherichia coli* K-12, respectively, and their homologues identified in *P. denitrificans* Pd1222. Key enzymes of the two pathways are highlighted in bold. Missing enzyme homologues are indicated by dashes.

Enzyme		Gene name	Gene ID		
			R. sphaeroides 2.4.1	*E. coli* K-12	*P. denitrificans* Pd1222
EMCP	β-kethothiolase	*phaA*	RSP_ 0745	-	Pden_2026
	Acetoacetyl-CoA reductase	*phaB*	RSP_ 0747	-	Pden_2027
	Crotonyl-CoA carboxylase/reductase	***ccr***	**RSP_ 0960**	**-**	**Pden_3873**
	Ethylmalonyl-CoA/methylmalonyl-CoA epimerase	*epi*	RSP_ 0812	-	Pden_2178
	Ethylmalonyl-CoA mutase	*ecm*	RSP_ 0961	-	Pden_3875
	(*2S*)-methylsuccinyl-CoA dehydrogenase	*mcd*	RSP_ 1679	-	Pden_2840
	Mesaconyl-CoA hydratase	*mch*	RSP_ 0973	-	Pden_0566
	β-methylmalyl-CoA/L-malyl-CoA lyase	*mcl-1*	RSP_ 1771	-	Pden_0799
	(*S*)-malyl-CoA thioesterase	*mcl-2*	RSP_0970	-	Pden_0563
	Propionyl-CoA carboxylase	*pccAB*	RSP_ 2191/2189	-	Pden_3684/3688
	Ethylmalonyl-CoA/methylmalonyl-CoA epimerase	*epi*	RSP_ 0812	-	Pden_2178
	(*2R*)-methylmalonyl-CoA mutase	*mcm*	RSP_ 2912	-	Pden_3681
GC	**Isocitrate lyase**	***aceA***	**-**	**C5Y66_09370**	**Pden_1363**
	Malate synthase	*aceB*	-	C5Y66_09365	Pden_1364

To test whether both the EMCP and the GC are functional and thus operate in *P. denitrificans*, we grew bacterial cells in batch culture on minimal medium supplemented with different carbon sources and quantified the activity of Ccr, the key enzyme of the EMCP, as well as Icl, the key enzyme of the GC, in cell-free extracts obtained from the cultures at mid-log phase (Figure 2).

Activity of Ccr was almost undetectable in cells grown on succinate, and at a very low basal level (<100 mU/mg) in extracts of cells grown on glucose and glycolate. In contrast, the activity of Ccr was significantly higher in extracts of cells grown on

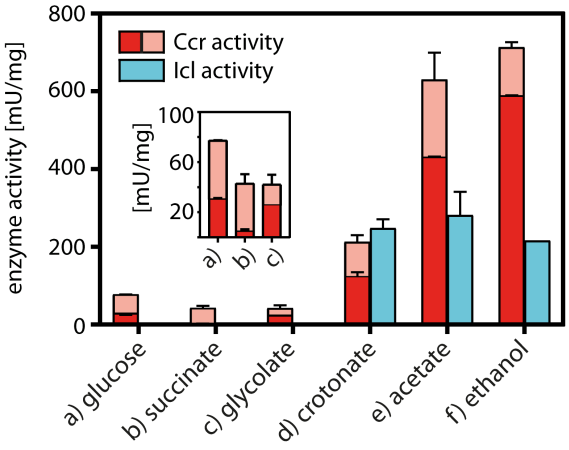

Figure 2: Ccr and Icl enzyme activities in cell-free extracts of *P. denitrificans* grown on different carbon sources. Ccr activity is given as combined activity of reduction and reductive carboxylation of crotonyl-CoA, quantified in the absence (light red) and presence of $NaHCO_3$ (dark red), respectively. Error bars indicate standard deviation.

crotonate, acetate and ethanol. In these extracts, Icl activity was also present, while no Icl activity was detected in extracts of cells grown on glucose, succinate, and glycolate. Together, our data suggest that both the EMCP and the GC are active in *P. denitrificans*. However, while the EMCP is always active at low levels and upregulated in response to growth on substrates requiring acetyl-CoA assimilation, the GC is specifically activated only during growth of *P. denitrificans* on these substrates.

2.4.2 The EMCP is sufficient to sustain growth of *P. denitrificans* on acetate

Next, we tested whether both pathways are essential for acetyl-CoA assimilation in *P. denitrificans*. To that end we aimed to selectively block the GC or EMCP using external inhibitors. Several inhibitors of Icl are known (8). We screened three of them to identify 3-nitropropionate (3-NPA; (9)) as potential candidate for a selective GC inhibitor of *P. denitrificans in vivo*.

3-NPA inhibited purified *P. denitrificans* Icl *in vitro* with an apparent IC50 of 34 µM at concentrations of 100 µM D,L-isocitrate (Figure 3A). Moreover, 3-NPA did not affect growth of *P. denitrificans* on carbon substrates that do not require Icl activity, such as succinate (Figure 3B; Figure S 1E). Notably, 3-NPA did also not affect

growth of *Methylobacterium extorquens* AM1, an EMCP-positive organisms that is closely related to *P. denitrificans*, on acetate (Figure S 1B and E). This suggested

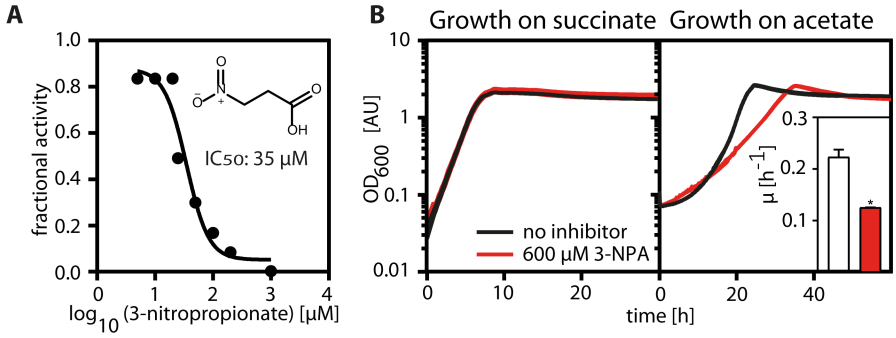

Figure 3: Inhibition of *P. denitrificans* Icl by 3-NPA in vitro (A) and in vivo (B). (A) Recombinant His_6-tagged Icl was pre-incubated at 30°C for 10 min with increasing concentrations of 3-NPA before activity measurements. The fractional activity of Icl is plotted against the log_{10} of the 3-NPA concentration. The apparent IC50 was determined using the log(inhibitor) vs. response function of GraphPad Prism7. (B) Growth of *P. denitrificans* on succinate and acetate in the absence (black line) and presence (red line) of 600 µM 3-NPA. The growth rates on acetate are shown in the inset. Growth on acetate is significantly inhibited by 3-NPA ($p < 0.5$ as determined by an unpaired t-test using GraphPad Prism7). Error bars indicate standard deviation.

to us that 3-NPA acts as GC inhibitor which shows negligible off-target effects in the cell, although additional effects of 3-NPA could not be completely excluded.

When we added increasing concentrations of 3-NPA to *P. denitrificans* growing on acetate, the growth rate was successively decreased from 0.26 ± 0.043 h^{-1} (0 µM 3-NPA) to 0.13 ± 0.005 h^{-1} (600 µM 3-NPA), but not completely abolished (Figure 3B; Figure S 1D). This indicated that the GC is not essential in *P. denitrificans* and that the EMCP is sufficient for acetyl-CoA assimilation.

2.4.3 The use of GC increases the growth rate of *P. denitrificans* on acetate

To estimate the contribution of each pathway to acetyl-CoA assimilation, we individually deleted the genes coding for Ccr and Icl from the genome of *P. denitrificans*, yielding strains Δ*ccr* and Δ*icl*, respectively (Figure 4, Figure S2). During growth on succinate, both deletion strains grew similar to the wild type. However, a shift from succinate to acetate caused pronounced and different strain-specific growth defects.

Δ*ccr* grew with wild type-like growth rates but displayed an extended lag phase (Figure 4). Notably, this lag phase ranged from 15 to 50 h between different experiments (Figure S3). However, when the Δ*ccr* strain was sub-cultured on acetate, the variation in the lag phase disappeared (Figure 4B, blue solid line), and the growth rate corresponded to that of the wild type (Figure 4B and C), indicating that the mutant adapted to acetate.

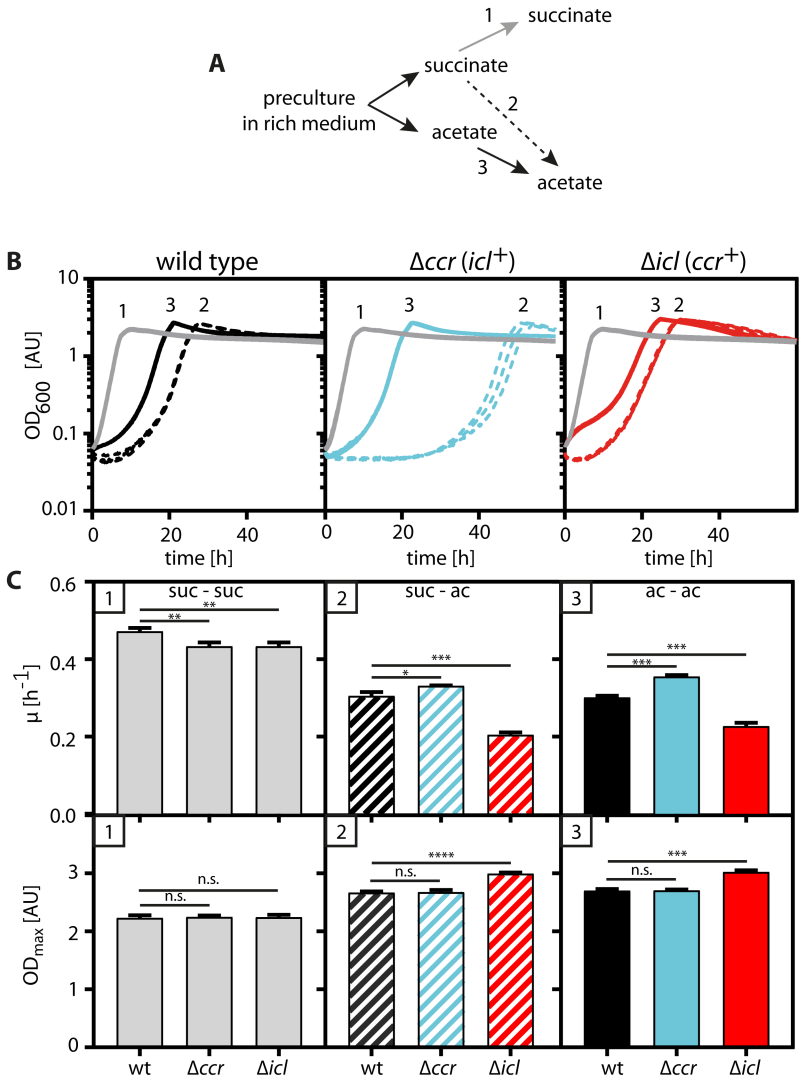

Figure 4: Phenotypic characterization of Δ*ccr* and Δ*icl*. (A) Inoculation scheme. (B) Growth behavior of wild type, Δ*ccr* and Δ*icl P. denitrificans* on succinate (grey lines; 1), after a switch from succinate to acetate (dashed lines; 2), or from acetate to acetate (solid lines; 3). The curves show independently grown triplicates, in some cases the lines overlap. (C) Growth rates and maximum optical densities calculated from the curves shown in (B). Error bars indicate the standard deviation. Asterisks mark the level of significance of growth rate or maximal optical density between wild type and the individual mutants as determined by t-test with the number of asterisks indicating the decimal place of p (*e.g.*, *** $p < 5 \times 10^{-3}$; n.s.: not significant). suc: succinate, ac: acetate.

Δ*icl*, in contrast, did not exhibit a prolonged lag phase, but showed a decreased growth rate on acetate, which is consistent with the results of the 3-NPA inhibition experiments. Together, these results suggest that the GC enables fast growth of *P. denitrificans* on acetate, but unlike the EMCP, requires some time to be induced after a switch onto acetate.

2.4.4 EMCP and GC show a complex expression pattern during switches from succinate to acetate

To follow the expression of the EMCP and the GC *in vivo*, the native *ccr* and *icl* genes of *P. denitrificans* were replaced with constructs encoding translational fusions of Ccr to the red fluorescent protein mCherry and Icl to the cyan fluorescent protein Cerulean, respectively. The resulting strain (*P. denitrificans ccr::ccr-mCherry icl::icl-cerulean*) was continuously monitored by following the total fluorescence of the population during cultivation in 96-well plates (Figure 5).

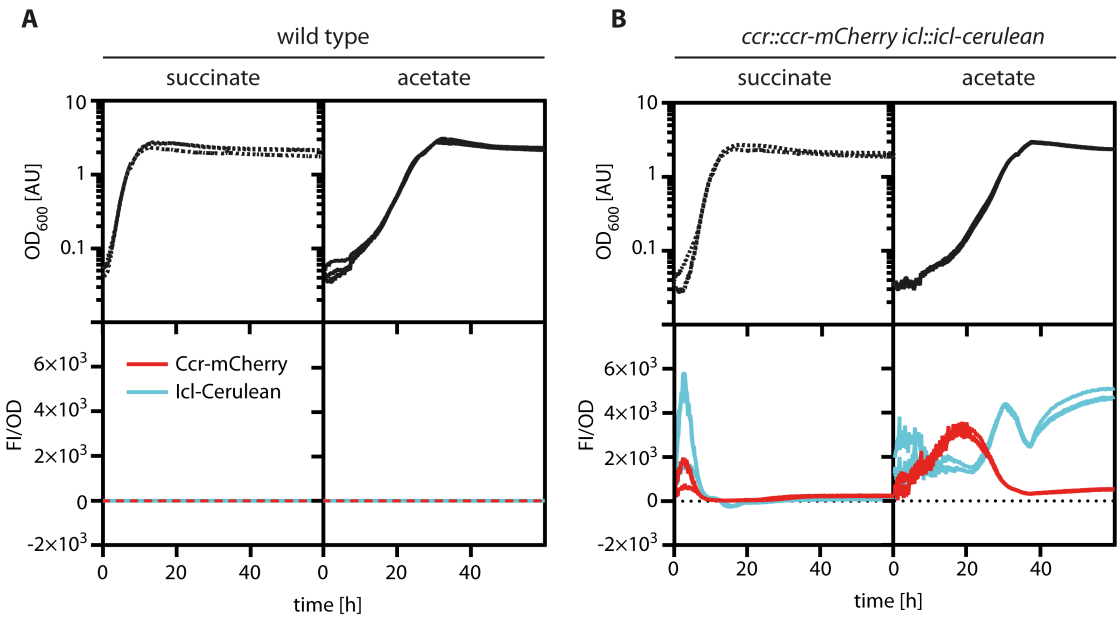

Figure 5: Expression of *ccr* and *icl* in *P. denitrificans* during growth on succinate and acetate. The optical density (OD_{600}) and fluorescence intensity (FI) of the P. denitrificans wild type (A) and *ccr:ccr-mCherry icl::icl-cerulean* strain (B) were monitored during growth on succinate and acetate using a 96-well plate reader. Fluorescence was normalized to OD and corrected by the background signal of the wild type. The Ccr-mCherry level is shown in red and the Icl-Cerulean level is shown in cyan. Growth curves and fluorescent measurements are shown in triplicates, in some cases the lines overlap.

During growth on succinate, cells showed very low levels of mCherry fluorescence and even lower levels of Cerulean fluorescence, which is consistent with our earlier finding that basal Ccr, but no Icl activity could be detected in cell-free extracts of *P. denitrificans* grown on succinate (Figure 2). When shifted from succinate to acetate, the reporter strain showed biphasic *ccr-mCherry* and *icl-cerulean* expression patterns. Ccr-mCherry fluorescence increased within the first 20 h and then decreased gradually at the onset of exponential phase until it again reached a low basal level. By contrast, the production of Icl-Cerulean started only after 20 h, but continued to increase until shortly before the cells entered stationary phase. Subsequently, Icl-Cerulean fluorescence dropped transiently before continuing to rise again in the late stationary phase. Very similar growth-linked expression patterns were observed in reporter strains of *P. denitrificans* carrying only a single Ccr-mCherry or Icl-mCherry fusion (Figure S 5). In summary, our results suggest that acetyl-CoA assimilation in *P. denitrificans* follows a complex regulatory pattern, in which the GC is used for fast and efficient acetyl-CoA assimilation during exponential phase, while the EMCP is used to bypass the time needed for activation of the GC.

2.4.5 Population-wide switch responses monitored by single cell microscopy

To understand whether the transition from EMCP- to GC-driven acetyl-CoA assimilation during the switch to acetate occurred in the whole population or only in a subset of cells, we followed the production of Ccr-mCherry and Icl-Cerulean in *P. denitrificans ccr::ccr-mCherry icl::icl-cerulean* at the single cell level using time-lapse fluorescence microscopy. Here, we imaged cells growing on succinate (Figure 6A and B) and acetate (Figure 6C and D) at two-hour intervals and subjected the images to automated analysis (10) to determine the average fluorescence per cell (Figure 6A and C).

While repeated handling of the cultures for sample collection led to slightly decreased growth rates, the overall expression patterns of *ccr-mCherry* and *icl-cerulean* matched those measured during continuous cultivation in the 96-well plates (Figure 5).

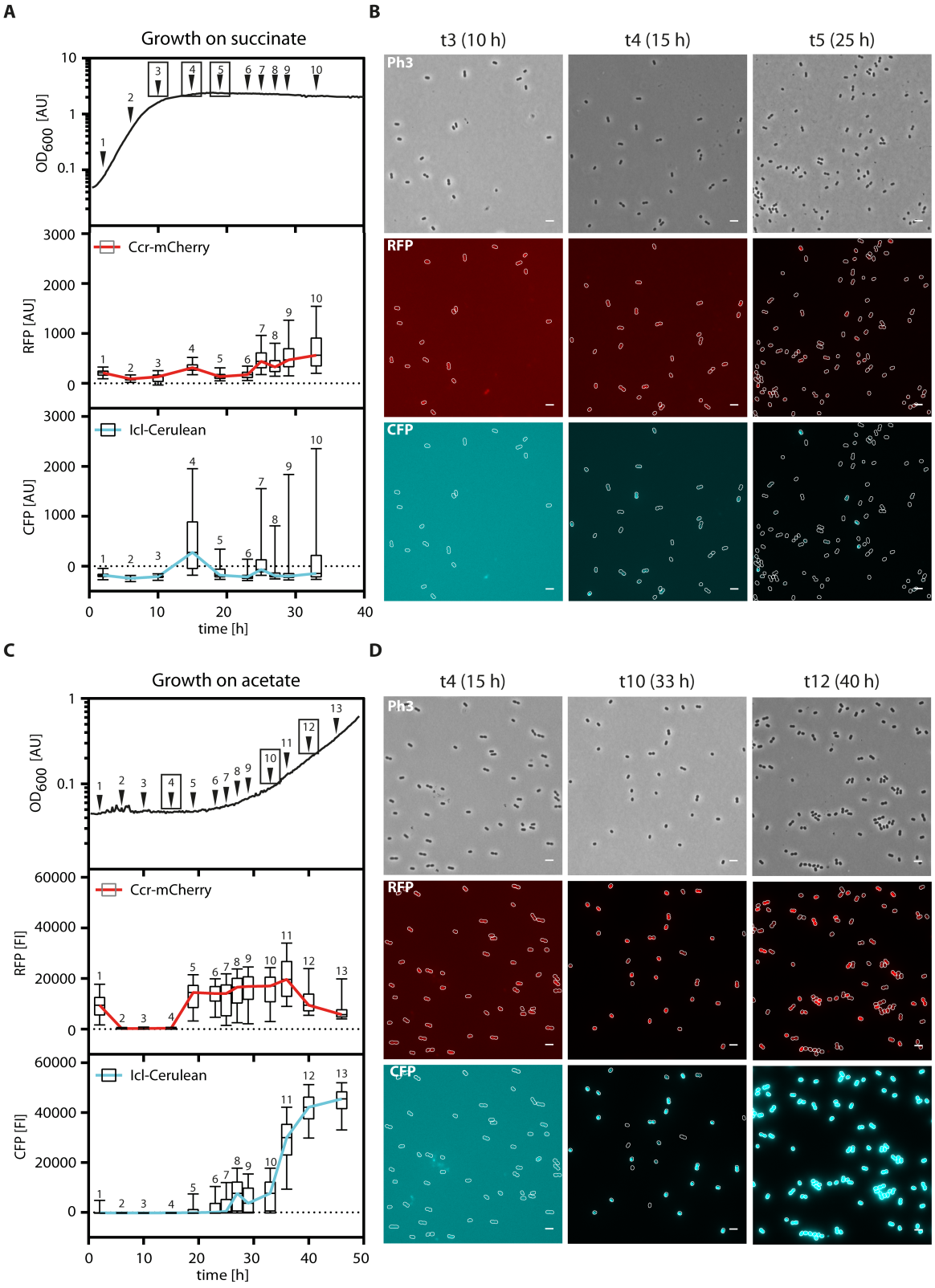

Figure 6: Fluorescence of *P. denitrificans ccr::ccr-mCherry icl::icl-cerulean* during growth on succinate (A, B) and acetate (C, D). At the indicated time points, the cultures were sampled and analyzed microscopically. Images were subjected to automated analysis using BacStalk (10).

(A and C) Distribution of cellular fluorescence intensities (n=450 cells per time point) shown as box plots. The values were corrected for the background fluorescence of the wild type. The margins of the boxes encompass the 25th to 75th percentiles, the lines indicate the median, and the whiskers extend to the 5th and 95th percentile, respectively. The colored lines connect the medians. (B and D) Representative microscopy images. Ph3, phase contrast; RFP, mCherry channel (overlaid with Ph3), CFP, Cerulean channel (overlaid with Ph3).

While no fluorescence was detected for the wild type (negative control; Figure S 4), the reporter strain showed different production patterns for Ccr-mCherry and Icl-Cerulean. On succinate, Ccr was produced at low levels during exponential phase, with increased expression in the stationary phase. By contrast, Icl was detected only at the end of the exponential phase and only in a small fraction of cells, which appeared strongly fluorescent. This implies *icl* expression is heterogeneous in the late exponential phase on succinate, and thus may suggest a bet-hedging-like behavior under these conditions (Figure 6A and B, Figure S 6).

Upon the switch to acetate, Ccr was produced first, whereas Icl was only induced at the onset of the early exponential phase. While some cells switched earlier to Icl production than others, all cells produced Icl in the exponential phase, indicating that the whole population and not only a subset of cells shifted from using the EMCP to using the GC (Figure 6C and D, Figure S 6).

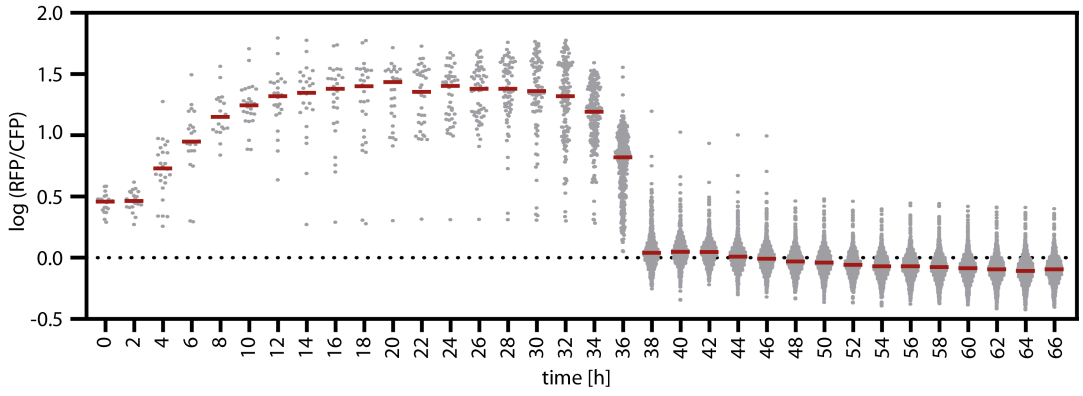

Figure 7: Comparison of Ccr-mCherry (RFP) to Icl-Cerulean (CFP) fluorescence in single cells over time. Succinate-grown cells of the strain *P. denitrificans ccr::ccr-mCherry icl::icl-cerulean* were immobilized in a microfluidic system with a continuous flow of acetate minimal medium. Cell growth and fluorescence intensities were tracked by time-lapse fluorescence microscopy, observing the same field of view for 46 hours. The fluorescence intensities of individual cells, determined via automated image analysis (11), are plotted as the logarithmic ratio of the RFP

and CFP intensities. Grey points represent the values of individual cells. The red lines mark the medians of the sampled populations.

To follow the expression dynamics of *ccr* and *icl* continuously in individual cells, we trapped succinate-grown *P. denitrificans ccr::ccr-mCherry icl::icl-cerulean* in a microfluidic device. We then provided acetate as the sole source of carbon and tracked cell growth and division as well as reporter production by microscopy over the course of time (Supplementary Video 1). This analysis confirmed that essentially all cells switched from the EMCP to the GC, demonstrating that faster acetyl-CoA assimilation is switched on in the whole population and not by individual cells that outgrow the population (Figure 7).

2.5 Discussion

Here we describe an unprecedented (and unexpected) metabolic redundancy in bacterial central carbon metabolism. The chromosome of *P. denitrificans* carries genes for two fundamentally different acetyl-CoA assimilation pathways, the EMCP and the GC. Both pathways are functional and regulated dynamically depending on the growth stage of the cells. The EMCP serves a default function and is expressed at basal levels at all times and on all carbon and free energy sources tested. Upon a switch to acetate, the EMCP is strongly induced at the early stage of growth but then decreases in activity again. The GC, by contrast, is exclusively induced on acetate and reaches peak activity at the late stage of growth, indicating a surprising rewiring of central carbon metabolism in *P. denitrificans* at the onset of the exponential phase.

What might be the reasons for the rewiring of central carbon metabolism in *P. denitrificans*? Individual knock out strains of the EMCP and GC show that the two pathways confer distinct advantages. The EMCP increases the growth yield, while the GC allows faster growth on acetate. How can these differences be explained and what are their consequences?

Importantly, the EMCP is able to fix inorganic carbon to increase biomass yield according to the following equation: 3 acetate + 2 CO_2 + 2 NADPH + 2 quinones → 2 malate + 2 $NADP^+$ + 2 quinols. This stoichiometry allows organisms using the EMCP to gain extra carbon from the environment if additional reducing equivalents

are available to the cell, *e.g.*, through internal storage compounds, such as poly-hydroxybutyrate (PHB), or growth substrates that are comparatively more reduced than average cellular carbon. This is supported by recent calculations that predict an approximately 3% higher yield for *M. extorquens* on methanol when using the EMCP compared to the GC (12). Another important feature of the EMCP is that it does not only enable acetyl-CoA assimilation but is directly linked to PHB metabolism and can also function in the assimilation of propionate, in addition to several dicarboxylic acids. This versatility makes the EMCP an all-purpose pathway that might allow *P. denitrificans* to assimilate several different carbon and free energy sources in parallel, which could explain the constant expression of the EMCP on diverse growth substrates.

The GC on the other hand is a very specialized route that requires only two additional enzymes. The GC requires less protein resources and the thermodynamics of the cycle (*i.e.*, the free energy of the overall process) might become more favorable with the upper limit of free Gibbs energy dissipation rate in *P. denitrificans* (13). Rerouting acetyl-CoA assimilation to the GC thus might allow a higher metabolic flux and consequently faster growth, providing a potential explanation as to why *P. denitrificans* switches to the GC when high concentrations of acetate are available.

Overall, a picture emerges in which metabolic rewiring is a highly coordinated strategy in *P. denitrificans* that allows optimal growth of this species in a changing environment. When the growth substrate changes from succinate to acetate, it is conceivable that the constant expression of the EMCP would facilitate the immediate assimilation of acetate. This could help *P. denitrificans* during the lag phase until the GC is fully induced and thus provide an advantage over other microorganisms that rely on the GC only. Once induced, the GC then could enable increased acetate assimilation rates, which might enable *P. denitrificans* to outcompete microorganisms that solely possess the EMCP.

Out of 48 *Paracoccus* genomes analyzed, 34 possess only a *ccr* homolog, while 9 additionally contain a homolog of *icl* (Figure 8, Figure S 7 and S 8). Only five strains seem to exclusively possess an *icl* homolog. Notably, *ccr* phylogeny largely corresponds to overall strain phylogeny, suggesting that the EMCP is the ancient

acetyl-CoA assimilation strategy in the genus *Paracoccus*. This hypothesis is in line with our experimental observation that the EMCP serves a default function in *P. denitrificans* and is further supported by the fact that other, closely related Alphaproteobacteria possess only the EMCP (4).

Notably, the phenomenon of metabolic rewiring is presumably not restricted to the *Paracoccus* clade alone. Several Alphaproteobacteria show the genetic potential to express multiple acetyl-CoA assimilation pathways (4), suggesting that dynamic rewiring of the central carbon metabolism is a more widespread strategy in nature. This discovery extends recent findings that metabolic degeneracy plays an important role in Alphaproteobacterial metabolism (14). Future experiments will focus on understanding the molecular mechanisms that underlie the coordination of the two acetyl-CoA pathways and their regulation through transcriptional, posttranslational or allosteric regulatory mechanisms (15-18), and on clarifying the evolutionary and ecological significance of dynamic metabolic rewiring as new principle in microbial central carbon metabolism.

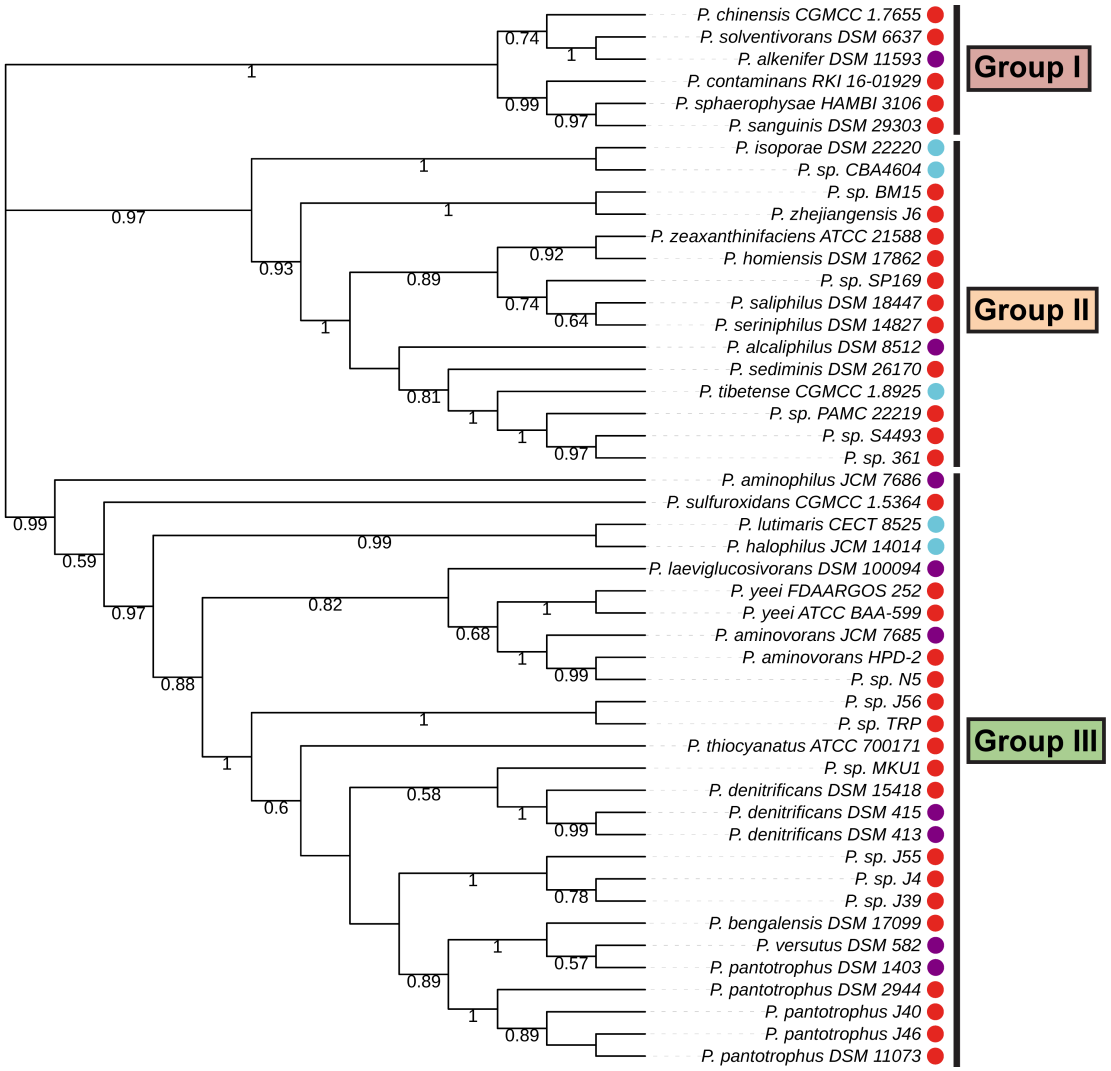

Figure 8: Maximum likelihood phylogenetic tree of *Paracoccus* strains. The phylogenetic tree is based on the concatenated alignments of twelve protein sequences from 48 Paracoccus strains. Bootstrap values ≥ 0.5 are given on the respective nodes; calculated branch lengths of the tree are ignored for the sake of easier visualization. Presence of Ccr is marked with a red dot, presence of Icl is marked with a blue dot, and presence of both enzymes is marked with a purple dot. The 48 strains are clustered in three distinct groups

Acknowledgements

This work was supported by funds from the Germany Research Foundation (Project 192445154 – SFB 987; to T.E. and M.T.). M.C.F.v.T. acknowledges support from the European Molecular Biology Organization (EMBO Long-Term Fellowship ALTF 1396-2015).

Declaration of interests

The authors declare no competing interests.

2.6 Material and Methods

2.6.1 Strains, media and growth conditions

All experiments were performed with *Paracoccus denitrificans* strains DSM413 or Pd1222. The strain preferentially used for all experiments was DSM413, which is the original wild-type strain isolated by Beijerinck in 1908 (19). In cases where genetic manipulation of this strain was not successful, its genetically more tractable derivative Pd1222 (20), was used alternatively. *P. denitrificans* was grown at 30 °C in mineral salt medium (trace elements: TE3-Zn) (21) supplemented with defined carbon sources and adjusted to a total carbon concentration of 120 mM. The density of cultures was determined photometrically at a wavelength of 600 nm. Bacterial growth was monitored over time using TECAN Infinite® 200 PRO plate reader systems (Tecan Trading AG, Switzerland) with Nunclon™ Delta Surface 96-well plates (Thermo Scientific, USA). *In silico* analysis of growth data was performed using the software Prism 7 (GraphPad Software, USA). *Escherichia coli* was grown at 37 °C in Luria Bertani Broth or M9 minimal medium (337 mM NaH_2PO_4, 220 mM KH_2PO_4, 85.5 mM NaCl, 18.7 mM NH_4Cl, 1 mM $MgSO_4$, 0.3 mM $CaCl_2$, 0.13 mM Na_2EDTA, 0.03 mM $FeSO_4$, 1 µg/mL biotine, 1 µg/mL thiamine) supplemented with 60 mM acetate. *Methylobacterium extorquens* AM1 was grown at 30 °C in mineral medium as described previously (22) supplemented with 10 mM acetate. Antibiotic concentrations were used as follows: kanamycin at 25 or 50 µg mL^{-1}, spectinomycin at 50 µg mL^{-1}, tetracycline at 10 µg mL^{-1}.

2.6.2 Chemicals

All chemicals were obtained from Sigma-Aldrich (Steinheim, Germany) and Carl Roth (Karlsruhe, Germany), respectively, and were of highest purity available.

2.6.3 Construction of plasmids

Oligonucleotides and synthetic genes were purchased from Eurofins Deutschland (Hamburg, Germany). All standard cloning techniques were carried out according to (25).

Table 2: Oligonucleotides used for plasmid construction and mutant verification in this study

Oligonucleotide	Sequence	Purpose
NdeI_pKK21-f	TATATCATATGCCCCGGCCCCGGCGCATG	Generation of pTE1624
pKK21-r	TATATCCTAGGGCGGCGCCCCGCCTCCAGCGCGTC	
mCherry-f	TATATCCTAGGGCAGGGAGTGCGGCCGGCAG	
NdeI_mCherry-r	TATATCATATGTCACTTGTACAGCTCGTCCATG	
NdeI_pSYNiclXiclds-f	TATACATATGTCTAGAGGGCCGACAGGATTCGGCC	Generation of pTE1625
HindIII_pSYNccrxccrds-r	TATATAAGCTTGCCGCTGCCGGCCGCACTCCCTGC	
HindIII_cerulean-f	TATATAAGCTTATGGTGAGCAAGGGCGAGGAGC	
NdeI_cerulean-r	TATATCATATGTTACTTGTACAGCTCGTCCATGCCGAG	
NdeI_icl-f	TATACATATGAGCAGAAAGACTTTTTCGGAAATC	Generation of pTE1614
HindIII_icl-r	TATAAAGCTTCTATTCGGCGGCGAACTGGTTCATGGTG	
Pden_3873_ds-f	GGTCAGGCGCTTGTATTGGCCGAACATGTAG	Verification of TJE-KK5
Pden_3873_ups-r	GCGAAAGCGGCATCGCCGTGGTGCGGATGAATTAC	
Pden_1363_ds-f2	CATCCATTCATAGGCGGTGACCACCAGGCCC	Verification of TJE-KK6
Pden_1363_ups-r	GCTGGGACTATATCTTCAGCTATATCAAGAC	
Pden_1363_ds-f2	CATCCATTCATAGGCGGTGACCACCAGGCCC	Verification of TJE-KK10
iclmCherryicIds_seq-f	CAGCATTGCCGAGGCCGACTACCCGGAC	
Pden_1363_ds-f	GACGAGCGCCGTGGTGAGTCTCAGCATGATGG	
Pden_1363_ups-r	GCTGGGACTATATCTTCAGCTATATCAAGAC	
NdeI mCherry-r	TATATCATATGTCACTTGTACAGCTCGTCCATG	Verification of TJE-KK13
Pden_3873_ups-r	GCGAAAGCGGCATCGCCGTGGTGCGGATGAATTAC	
3'-ccr-f	CGCAGGCGCATCTGAAGATGC	
Pden_3873_ds-f	GGTCAGGCGCTTGTATTGGCCGAACATGTAG	
Pden_1363_ds-f2	CATCCATTCATAGGCGGTGACCACCAGGCCC	Verification of TJE-KK14
Pden_1363_ups-r	GCTGGGACTATATCTTCAGCTATATCAAGAC	
HindIII_cerulean-f	TATATAAGCTTATGGTGAGCAAGGGCGAGGAGC	

Markerless genomic deletions and integrations of reporter genes were generated using the pK18*mobsacB* sucrose suicide plasmid system (26).

For the deletion of *ccr* (*Pden_3873*) and *icl* (*Pden_1363*), respectively, fusions of the respective downstream and upstream flanking regions of the genes, each approximately 700 bp in length, were purchased as synthetic genes cloned into the pEX-K4 backbone (pSYNccrflanks (pTE1602) pSYNiclflanks (pTE1604)).

Restriction of the plasmids with PstI and EcoRI, gel-purification of the flanking regions and subsequent ligation into PstI/EcoRI-digested pK18*mobsacB* resulted in plasmids pK18*mobsacB*_ccrflanks (pTE1606) and pK18*mobsacB*_iclflanks (pTE1615).

For the introduction of fluorescent reporter fusions, *ccr* and *icl* were ordered as synthetic genes fused to *evoglowPp1* (27) and *mCherry* (28), respectively, each preceded by a 30-bp linker and followed by the downstream region of the respective genes, yielding plasmids pEX4_ccrevoglowPp1ccrds (pTE1601) and pEX4_iclmCherryicIds (pTE1603).

pTE1603 was digested with SalI and BamHI. Subsequent ligation into SalI/BamHI-cut pK18mobsacB yielded pK18*mobsacB*_iclmCherryicIds (pTE1616).

pTE1601 was amplified with targeted omission of *evoglowPp1* via inverted PCR using primers NdeI_pKK21-f and pKK21-r. *mCherry* was amplified from pTE1603 using primers mCherry-f and NdeI_mCherry-r. Restriction of both fragments with AvrII and NdeI and subsequent ligation of the individual fragments to each other resulted in the plasmid pEX4_ccrmCherryccrds. pEX4-ccrmCherryccrds was digested with SalI and BamHI. Subsequent ligation into SalI/BamHI-cut pK18mobsacB yielded pK18*mobsacB*_ccrmCherryccrds (pTE1624).

pTE1603 was amplified with targeted omission of *mCherry* via inverted PCR using primers NdeI_pSYNiclXicIds-f and HindIII_pSYNccrXccrds-r. *cerulean* (29) was amplified from plasmid pVCERC-6 (30) using primers HindIII_cerulean-f and NdeI_cerulean-r. Restriction of both fragments with HindIII and NdeI and subsequent ligation of the individual fragments to each other resulted in the plasmid pEX4_iclceruleanicIds. Restriction of pEX4_iclceruleanicIds with SalI and BamHI and ligation into SalI/BamHI-cut pK18*mobsacB* yielded pK18*mobsacB*_iclceruleanicIds (pTE1625).

For the heterologous expression of *icl, icl* was amplified from pTE1603 using primers NdeI_icl-for and HindIII_icl. The resulting product was digested with NdeI and HindIII and ligated into NdeI/HindIII-digested pET16b, yielding pET16b_icl (pTE1614).

2.6.4 Genetic manipulation of *P. denitrificans*

The transfer of plasmids into *P. denitrificans* was achieved by biparental mating with the donor strain *E. coli* ST18 (23). Selection of the first integration was performed on LB or methanol mineral medium plates supplemented with 25 µg/mL kanamycin. Colonies were picked and restreaked on LB with kanamycin and LB with 3% sucrose in parallel. Colonies that were kanamycin-resistant and sucrose-sensitive were grown in plain LB for 2 days. Subsequently, cells were plated on methanol mineral medium plates supplemented with 6 % sucrose in serial dilution. Colonies were restreaked on LB with kanamycin and LB with 3 % sucrose in parallel. Kanamycin-sensitive, sucrose-resistant clones were screened for the successful deletion or integration of genes by colony PCR.

Table 3: Strains used in this study

Strain	Genotype or relevant features	Reference
E. coli TOP 10	cloning strain	Invitrogen, USA
E. coli DH5α	cloning strain	Thermo Fisher Scientific, USA
E. coli BL21	protein expression	Thermo Fisher Scientific, USA
E. coli ST18	mating strain	(23)
M. extorquens AM1	wild type	(24)
P. denitrificans DSM413	wild type	(19)
P. denitrificans Pd1222	increased conjugation frequency	(20)
P. denitrificans DSM413 Δ*ccr* (TJE-KK5)	Δ*ccr*	This work
P. denitrificans DSM413 Δ*icl* (TJE-KK6)	Δ*icl*	This work
P. denitrificans Pd1222 *ccr::ccr-mCherry icl::icl-cerulean* (TJE-KK14)	*ccr::ccr-mCherry icl::icl-cerulean*	This work
P. denitrificans Pd1222 *ccr::ccr-mCherry* (TJE-KK13)	*ccr::ccr-mCherry*	This work
P. denitrificans Pd1222 *icl::icl-mCherry* (TJE-KK10)	*icl::icl-mCherry*	This work

2.6.5 Preparation of cell-free extracts

P. denitrificans cultures were grown at 30 °C in mineral medium supplemented with various carbon sources. Cells were harvested at mid-exponential phase, resuspended in ice-cold MOPS/KOH buffer (100 mM, pH 7.2) and lyzed by

sonication (MS-72, 40 %, 3 x 15 pulses). Cell debris was removed by centrifugation at 35 000 x g and 4 °C for 1 h. The total protein concentration of the cell-free extracts was determined with the Bradford assay (31) using bovine serum albumin (BSA) as standard. The catalytic activities of crotonyl-CoA carboxylase/reductase and isocitrate lyase were measured spectrophotometrically as described previously (3, 32).

2.6.6 Synthesis of crotonyl-CoA

Crotonyl-Coenzyme A was synthesized from its anhydride as described before (33).

2.6.7 Live-cell imaging

To monitor gene expression *in vivo*, cells were immobilized on 1% agarose pads and analyzed microscopically using an Axio Observer.Z1 (Zeiss) microscope equipped with a Plan Apochromat 100x/1.4 Oil Ph3 phase contrast objective, an ET-mCherry filter set (Chroma, USA) and a pco-edge sCMOS camera (PCO). Images were recorded with VisiView 3.3.0.6 (Visitron Systems, Germany) and processed with Fiji (34) and Adobe IllustratorCS5 (Adobe Systems, USA). For timelapse imaging, cells were transferred to a B04 CellASIC® ONIX2 microfluidic plate (Merck, Germany) coupled to a ONIX EV262 microfluidic platform (CellASIC, USA), cultivated at 30 °C under continuous medium flow (1 psi) and imaged at regular intervals using the microscope set-up described above. For automated data analysis, images were processed with Fiji (34) and BacStalk (10).

2.6.8 Heterologous production and purification of 6xHis-Icl

Competent *E. coli* BL21 cells were transformed with the expression plasmid pET16b_icl, and grown at 37 °C in Terrific Broth (23.6 g/L yeast extract, 11.8 g/L tryptone, 9.4 g/L K_2HPO_4, 2.2 g/L KH_2PO_4 and 4% (v/v) glycerol) supplemented with ampicillin. Gene expression was induced at OD_{600} = 0.8 by addition of 0.5 mM isopropylthio-galactopyranoside (IPTG). After additional growth at 18 °C for 12 h, cells were harvested, resuspended in 3 volumes of buffer A (500 mM NaCl, 50 mM Tris-HCl, pH 7.9) containing 0.1 mg of DNase I and Protease Inhibitor Cocktail (Sigma-Aldrich, St. Louis, USA), and lyzed by sonication. Lysates were cleared by

centrifugation at 42 000 x g and 4 °C for 45 min. The supernatant was applied onto a pre-equilibrated 1 mL Ni-Sepharose Fast Flow Column (HiTrap™, FF, GE Life Science, UK) and washed with buffer A. Proteins were eluted from the column by the addition of increasing concentrations of buffer B (500 mM NaCl, 50 mM Tris-HCl, 500 mM imidazole, pH7.9) followed by application onto a 5 mL HiTrap® Desalting Column (GE Life Science, UK) for desalting and buffer exchange to storage buffer (buffer A, 10 % glycerol). Protein concentration was determined using a NanoDrop® 2000 spectrometer (Thermo Scientific, USA) and purity was analyzed by SDS-PAGE according to (35).

2.6.9 Measurement of enzyme activities in cell-free extracts and purified protein

Ccr. Enzyme activity of crotonyl-CoA carboxylase/reductase was measured by following the consumption of NADPH spectrophotometrically as described earlier (3).

Icl. Enzyme activity of isocitrate lyase was measured by following the production of a phenylhydrazine-glyoxylate complex as described earlier (32). For the Icl inhibition assay with 3-nitropropionate (3-NPA), the compound was pre-equilibrated in 100 mM MOPS/KOH pH 7.2 oN. Purified isocitrate lyase was incubated in the reaction mixture containing 3-NPA at various concentrations at 30 °C for 10 min before the assay was started by addition of 2 mM D,L-isocitric acid.

2.6.10 Phylogenetic analysis

Sequences of twelve proteins (GapA; GyrA; RecA; RpoA; RpoB; TrpB; 30S ribosomal protein S2; 30S ribosomal protein S3; 30S ribosomal protein S12; 50S ribosomal protein L2; 50S ribosomal protein L3; 50S ribosomal protein L11) from the core proteome of 48 strains of *Paracoccus* were downloaded from the IMG database (36) and aligned using MUSCLE 3.8.31 (37). The alignments were concatenated and used to calculate a phylogenetic tree with MEGA 7.0.14 (38) using the maximum likelihood method with the Le-Gascuel substitution model and 100 bootstrap replicates. The resulting tree was visualized using iTOL (39).

Sequences of Ccr and Icl from 43 and 14 strains of *Paracoccus*, respectively, were downloaded from the IMG database and used to calculate maximum likelihood phylogenetic trees as described above.

2.7 References

1. Kornberg HL, Madsen NB. 1957. Synthesis of C4-dicarboxylic acids from acetate by a glyoxylate bypass of the tricarboxylic acid cycle. Biochim Biophys Acta 24:651-3.

2. Kornberg HL, Krebs HA. 1957. Synthesis of cell constituents from C2-units by a modified tricarboxylic acid cycle. Nature 179:988-91.

3. Erb TJ, Berg IA, Brecht V, Muller M, Fuchs G, Alber BE. 2007. Synthesis of C5-dicarboxylic acids from C2-units involving crotonyl-CoA carboxylase/reductase: the ethylmalonyl-CoA pathway. Proc Natl Acad Sci U S A 104:10631-6.

4. Erb TJ, Fuchs G, Alber BE. 2009. (2S)-Methylsuccinyl-CoA dehydrogenase closes the ethylmalonyl-CoA pathway for acetyl-CoA assimilation. Mol Microbiol 73:992-1008.

5. Erb TJ, Brecht V, Fuchs G, Muller M, Alber BE. 2009. Carboxylation mechanism and stereochemistry of crotonyl-CoA carboxylase/reductase, a carboxylating enoyl-thioester reductase. Proc Natl Acad Sci U S A 106:8871-6.

6. Claassen PAM, Vandenheuvel MHMJ, Zehnder AJB. 1987. Enzyme profiles of *Thiobacillus-versutus* after aerobic and denitrifying growth - regulation of isocitrate lyase. Archives of Microbiology 147:30-36.

7. Claassen PAM, Zehnder AJB. 1986. Isocitrate lyase activity in *Thiobacillus versutus* grown anaerobically on acetate and nitrate. Journal of General Microbiology 132:3179-3185.

8. Lee YV, Wahab HA, Choong YS. 2015. Potential inhibitors for isocitrate lyase of *Mycobacterium tuberculosis* and non-*M. tuberculosis*: a summary. Biomed Res Int 2015:895453.

9. Schloss JV, Cleland WW. 1982. Inhibition of isocitrate lyase by 3-nitropropionate, a reaction-intermediate analogue. Biochemistry 21:4420-7.

10. Hartmann R, van Teeseling MCF, Thanbichler M, Drescher K. 2018. BacStalk: a comprehensive and interactive image analysis software tool for bacterial cell biology. bioRxiv doi:10.1101/360230:360230.

11. Remus-Emsermann MN, Gisler P, Drissner D. 2016. MiniTn7-transposon delivery vectors for inducible or constitutive fluorescent protein expression in *Enterobacteriaceae*. FEMS Microbiol Lett 363.

12. Peyraud R, Schneider K, Kiefer P, Massou S, Vorholt JA, Portais JC. 2011. Genome-scale reconstruction and system level investigation of the metabolic network of *Methylobacterium extorquens* AM1. BMC Syst Biol 5:189.

13. Niebel B, Leupold S, Heinemann M. 2019. An upper limit on Gibbs energy dissipation governs cellular metabolism.

14. Nayak DD, Agashe D, Lee MC, Marx CJ. 2016. Selection maintains apparently degenerate metabolic pathways due to tradeoffs in using methylamine for carbon versus nitrogen. Curr Biol 26:1416-26.

15. Cruz AH, Brock M, Zambuzzi-Carvalho PF, Santos-Silva LK, Troian RF, Goes AM, Soares CM, Pereira M. 2011. Phosphorylation is the major mechanism regulating isocitrate lyase activity in *Paracoccidioides brasiliensis* yeast cells. FEBS J 278:2318-32.

16. Hoyt JC, Reeves HC. 1988. *In vivo* phosphorylation of isocitrate lyase from *Escherichia coli* D5H3G7. Biochem Biophys Res Commun 153:875-80.

17. Robertson EF, Reeves HC. 1989. Phosphorylation of isocitrate lyase in *Escherichia coli*. Biochimie 71:1065-70.

18. Murima P, Zimmermann M, Chopra T, Pojer F, Fonti G, Dal Peraro M, Alonso S, Sauer U, Pethe K, McKinney JD. 2016. A rheostat mechanism governs the bifurcation of carbon flux in *mycobacteria*. Nat Commun 7:12527.

19. Beijerinck M, Minkman D. 1910. Bildung und Verbrauch von Stickoxydul durch Bakterien. Zentbl Bakteriol Parasitenkd Infektionskr Hyg Abt II 25:30-63.

20. de Vries GE, Harms N, Hoogendijk J, Stouthamer AH. 1989. Isolation and characterization of *Paracoccus denitrificans* mutants with increased conjugation frequencies and pleiotropic loss of a (nGATCn) DNA-modifying property. Archives of Microbiology 152:52-57.

21. Hahnke SM, Moosmann P, Erb TJ, Strous M. 2014. An improved medium for the anaerobic growth of *Paracoccus denitrificans* Pd1222. Front Microbiol 5:18.

22. Peyraud R, Kiefer P, Christen P, Massou S, Portais JC, Vorholt JA. 2009. Demonstration of the ethylmalonyl-CoA pathway by using 13C metabolomics. Proc Natl Acad Sci U S A 106:4846-51.

23. Thoma S, Schobert M. 2009. An improved *Escherichia coli* donor strain for diparental mating. FEMS Microbiol Lett 294:127-32.

24. Peel D, Quayle JR. 1961. Microbial growth on C1 compounds. I. Isolation and characterization of *Pseudomonas* AM 1. Biochem J 81:465-9.

25. Sambrook J, Russel, D. W. 2001. Molecular cloning: A laboratory manual. Cold Spring Harbour Laboratory Press.

26. Schafer A, Tauch A, Jager W, Kalinowski J, Thierbach G, Puhler A. 1994. Small mobilizable multi-purpose cloning vectors derived from the *Escherichia coli* plasmids pK18 and pK19: selection of defined deletions in the chromosome of *Corynebacterium glutamicum*. Gene 145:69-73.

27. Drepper T, Eggert T, Circolone F, Heck A, Krauss U, Guterl JK, Wendorff M, Losi A, Gartner W, Jaeger KE. 2007. Reporter proteins for in vivo fluorescence without oxygen. Nat Biotechnol 25:443-5.

28. Shaner NC, Campbell RE, Steinbach PA, Giepmans BNG, Palmer AE, Tsien RY. 2004. Improved monomeric red, orange and yellow fluorescent proteins derived from *Discosoma* sp red fluorescent protein. Nature Biotechnology 22:1567-1572.

29. Rizzo MA, Springer GH, Granada B, Piston DW. 2004. An improved cyan fluorescent protein variant useful for FRET. Nat Biotechnol 22:445-9.

30. Thanbichler M, Iniesta AA, Shapiro L. 2007. A comprehensive set of plasmids for vanillate- and xylose-inducible gene expression in *Caulobacter crescentus*. Nucleic Acids Res 35:e137.

31. Bradford MM. 1976. A rapid and sensitive method for the quantitation of microgram quantities of protein utilizing the principle of protein-dye binding. Anal Biochem 72:248-54.

32. Brock M, Darley D, Textor S, Buckel W. 2001. 2-Methylisocitrate lyases from the bacterium *Escherichia coli* and the filamentous fungus *Aspergillus nidulans*: characterization and comparison of both enzymes. Eur J Biochem 268:3577-86.

33. Peter DM, Vogeli B, Cortina NS, Erb TJ. 2016. A chemo-enzymatic road map to the synthesis of coa esters. Molecules 21:517.

34. Schindelin J, Arganda-Carreras I, Frise E, Kaynig V, Longair M, Pietzsch T, Preibisch S, Rueden C, Saalfeld S, Schmid B, Tinevez JY, White DJ, Hartenstein V, Eliceiri K, Tomancak P, Cardona A. 2012. Fiji: an open-source platform for biological-image analysis. Nat Methods 9:676-82.

35. Laemmli UK. 1970. Cleavage of structural proteins during the assembly of the head of bacteriophage T4. Nature 227:680-5.

36. Markowitz VM, Chen IMA, Palaniappan K, Chu K, Szeto E, Grechkin Y, Ratner A, Jacob B, Huang JH, Williams P, Huntemann M, Anderson I, Mavromatis K, Ivanova NN, Kyrpides NC. 2012. IMG: the integrated microbial genomes database and comparative analysis system. Nucleic Acids Research 40:D115-D122.

37. Edgar RC. 2004. MUSCLE: multiple sequence alignment with high accuracy and high throughput. Nucleic Acids Res 32:1792-7.

38. Kumar S, Stecher G, Tamura K. 2016. MEGA7: Molecular evolutionary genetics analysis version 7.0 for bigger datasets. Molecular Biology and Evolution 33:1870-1874.

39. Letunic I, Bork P. 2016. Interactive tree of life (iTOL) v3: an online tool for the display and annotation of phylogenetic and other trees. Nucleic Acids Research 44:W242-W245.

2.8 Supplementary Information

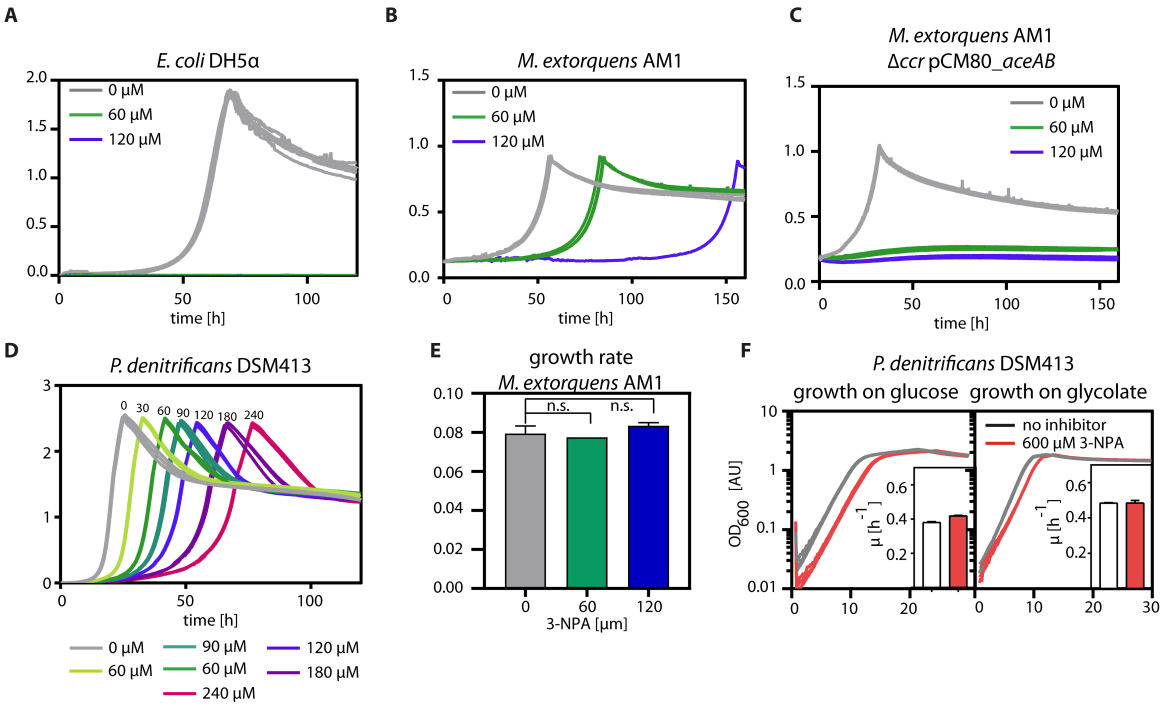

Figure S 1: Testing 3-NPA as suitable compound for the inhibition of Icl in *P. denitrificans in vivo*. 3-NPA was added to acetate minimal medium inoculated with *E. coli* DH5α (A), *M. extorquens* AM1 (B), *M. extorquens* AM1 lacking *ccr* but heterologously expressing the glyoxylate shunt of *E. coli*, and *P. denitrificans* DSM413 (D). (E) Growth rates corresponding to the growth curves in (B). Despite an extension of the lag phase, the growth rate of *M. extorquens* AM1 was not affected by the presence of 3-NPA. n.s.= not significant (F) Growth curves of *P. denitrificans* DSM413 on substrates, which do not require acetyl-CoA assimilation, in the absence and presence of 3-NPA with the corresponding growth rates. Error bars indicate standard deviation.

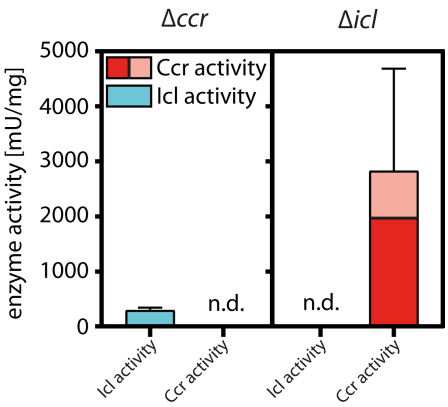

Figure S 2: Enzyme activites in *ccr* and *icl* deletion strains. To confirm the absence of Ccr and Icl in the respective single-deletion backgrounds, enzyme activities were determined in cell-free extracts of the deletion strains grown to mid-exponential phase in acetate minimal medium. n.d.:

not detectable. Dark red: Ccr activity with concomitant carboxylation. Light red: Ccr activity independent of carboxylation. Error bars indicate standard deviation.

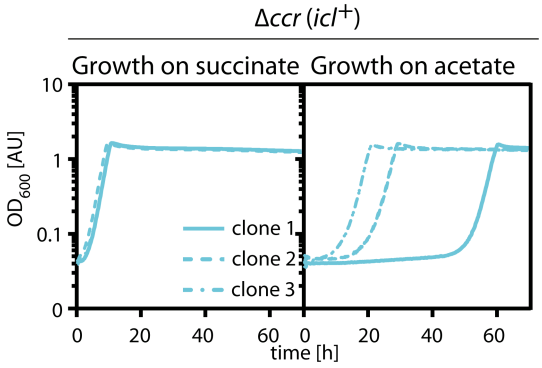

Figure S 3: Growth of individual clones of strain *P. denitrificans* Δ*ccr* on acetate and succinate. Cells were grown in rich medium, washed and shifted to either acetate or succinate minimal medium. While all clones exhibited the same growth behavior on succinate, they displayed different lag phases during growth on acetate. The genotypes of all clones were confirmed by colony PCR after completion of the experiment.

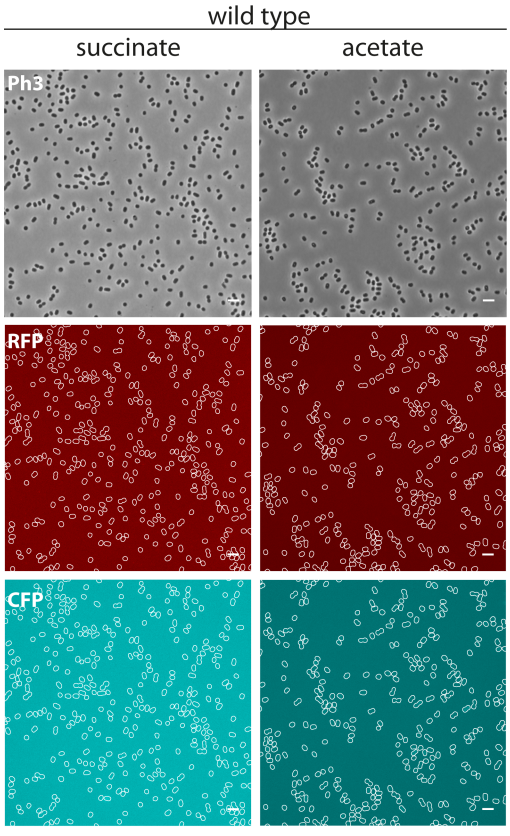

Figure S 4: Fluorescence of the *P. denitrificans* wild type. Cells were grown on succinate and on acetate and analyzed microscopically to exclude the possibility that fluorescence detected in the analysis of *P. denitrificans ccr::ccr-mCherry icl::icl-cerulean* stemmed from autofluorescence of *P. denitrificans*. Scale bar: 3 µm.

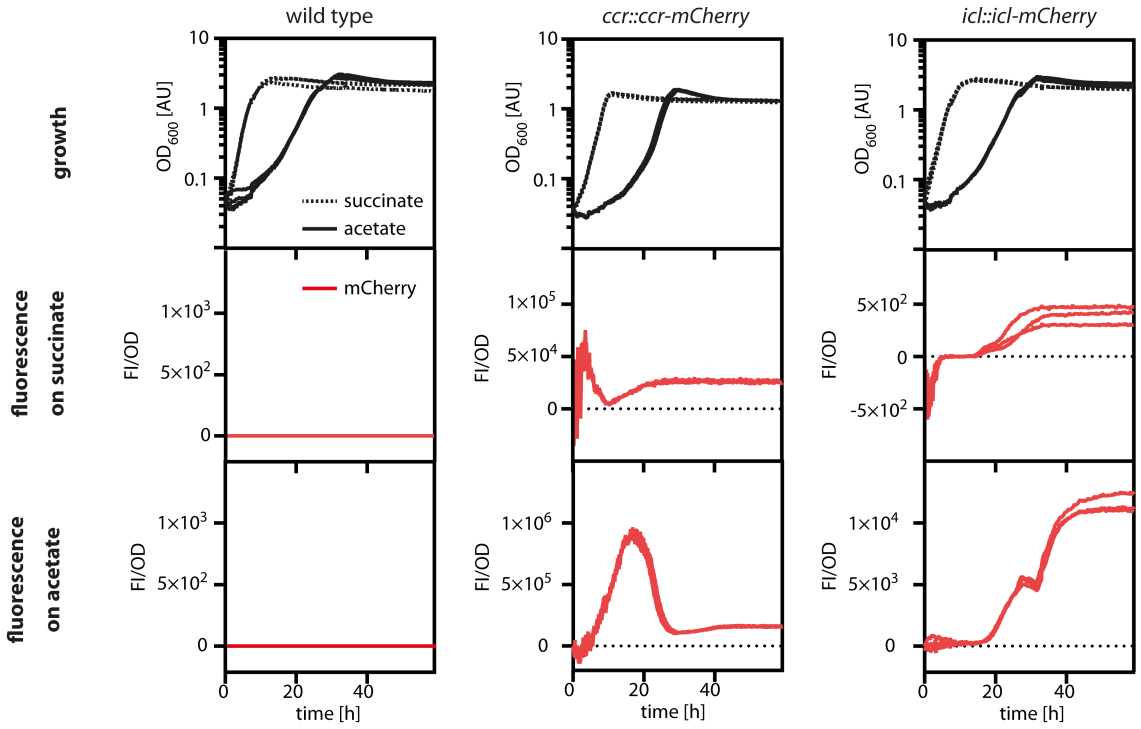

Figure S 5: Production of Ccr-mCherry and Icl-mCherry in *P. denitrificans* single-reporter strains during growth on succinate and acetate. Succinate and acetate cultures were started from washed succinate-grown pre-cultures. Growth curves and fluorescent measurements are shown in triplicates, in some cases the lines overlap. Fluorescence measurements of the individual strains were performed with different gain adjustments. Therefore, the absolute fluorescence intensity values cannot be compared between the different strains.

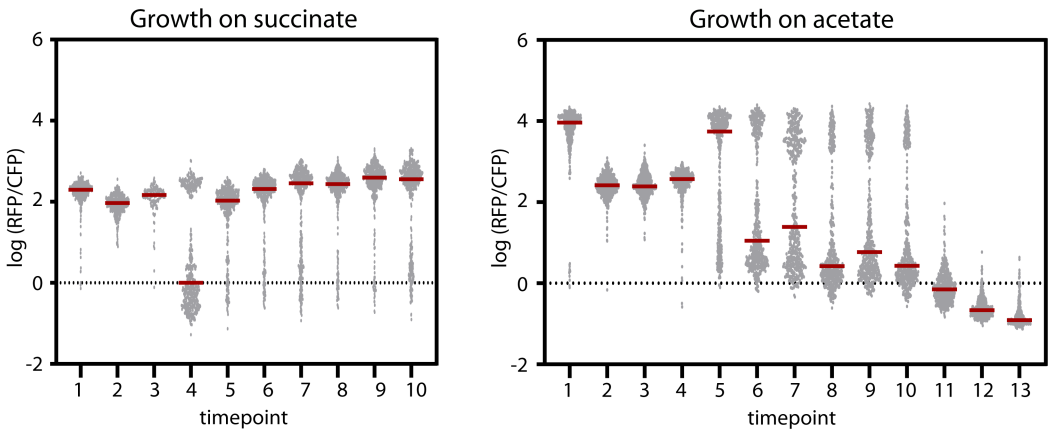

Figure S 6: Comparison of Ccr-mCherry (RFP) to Icl-Cerulean (CFP) fluorescence. RFP and CFP intensities of the strain *P. denitrificans ccr::ccr-mCherry icl::icl-cerulean* grown on succinate and acetate (growth and individual fluorescence intensities shown in Figure 6) are plotted as logarithmic ratios. Grey points represent the values of individual cells. The red lines mark the medians of the sampled populations.

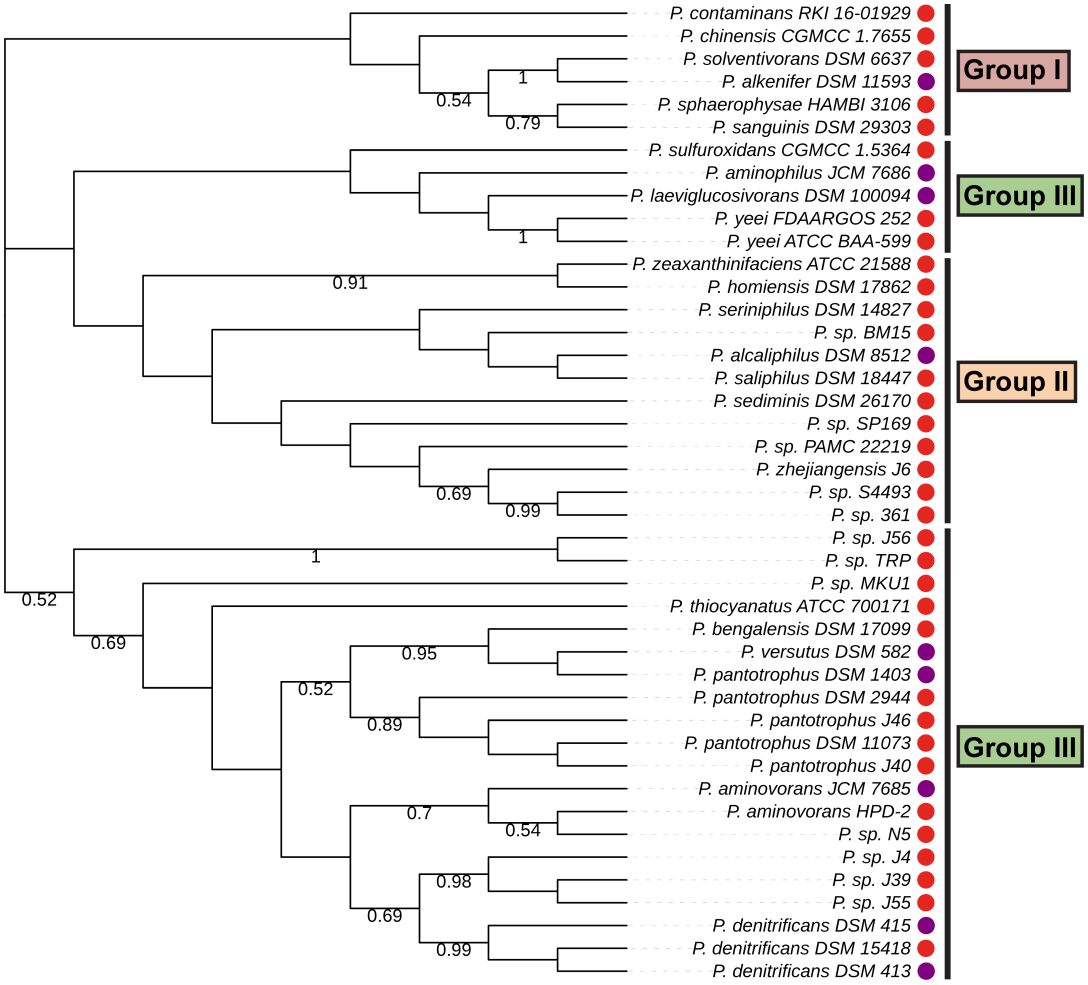

Figure S 7: Maximum likelihood phylogenetic tree of Ccr sequences. The phylogenetic tree is based on Ccr sequences from 43 *Paracoccus* strains. Bootstrap values ≥ 0.5 are given on the respective nodes; calculated branch lengths of the tree are ignored for the sake of easier visualization. Presence of Ccr is marked with a red dot, and presence of both Ccr and Icl is marked with a purple dot. The clustering of the 43 strains is largely similar to the phylogeny shown in Figure 8.

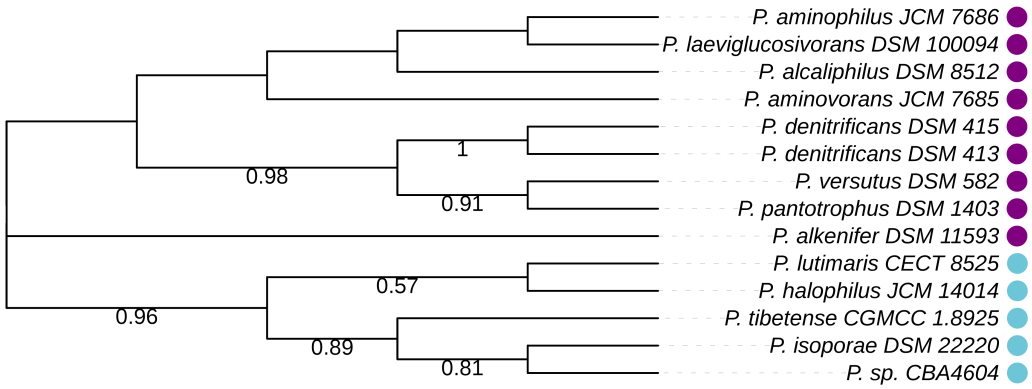

Figure S 8: Maximum likelihood phylogenetic tree of Icl sequences. The phylogenetic tree is based on Icl sequences from 14 *Paracoccus* strains. Bootstrap values ≥ 0.5 are given on the respective

nodes; calculated branch lengths of the tree are ignored for the sake of easier visualization. Presence of Icl is marked with a blue dot, and presence of both Ccr and Icl is marked with a purple dot. Note that the Icl-positive strains of *Paracoccus* can be found in all three phylogenetic groups of the genus (compare Figure 8).

Video S 1: Fluorescence of P. *denitrificans ccr::ccr-mCherry icl::icl-cerulean* during growth on acetate after switch from succinate. Cells were grown in succinate, trapped in a microfluidic device, and continuously flushed with acetate minimal medium. Images were taken every 2 h; time points are indicated on the individual frames of the video. Scale bar: 3 µm.

3 Coordination of functional degeneracy in *P. denitrificans*

Functional degeneracy in *Paracoccus denitrificans* Pd1222 is coordinated via RamB, linking expression of the Glyoxylate Cycle to activity of the Ethylmalonyl-CoA Pathway

Authors: Katharina Kremer[1], Doreen Meier[5], Lisa Theis[1], Stephanie Miller[3], Aerin Rost-Nasshan[3], Yadanar T. Naing[3], Jan Zarzycki[1], Nicole Paczia[4], Javier Serrania[5], Patrick Blumenkamp[6], Alexander Goesmann[6], Anke Becker[2,5], Martin Thanbichler[2,5,7], Georg K. A. Hochberg[5,8,9], Michael S. Carter[3,†] & Tobias J. Erb [1,5]

Affiliations: [1] Department of Biochemistry and Synthetic Metabolism, Max Planck Institute for Terrestrial Microbiology, Marburg, Germany; [2] Department of Biology, University of Marburg, Germany; [3] Department of Biological Sciences, Salisbury University, Maryland, United States; [4] Core Facility for Metabolomics and Small Molecule Mass Spectrometry, Max Planck Institute for terrestrial Microbiology, Marburg, Germany; [5] Center for Synthetic Microbiology (SYNMIKRO), Marburg, Germany; [6] Bioinformatics and Systems Biology, Justus Liebig University Giessen, 35392, Giessen, Germany ; [7] Max Planck Fellow Group Bacterial Cell Biology, Max Planck Institute for Terrestrial Microbiology, Marburg, Germany; [8] Department of Chemistry, University of Marburg, Germany; [8] Evolutionary Biochemistry Group, Max Planck Institute for Terrestrial Microbiology, Marburg, Germany; † current affiliation: Air Force Research Laboratory, Dayton, Ohio, United States

Submitted 12/2022.

Author contributions:

K.K., T.J.E., and M.S.C. designed the study. K.K. planned and performed all genetic and biochemical experiments except for the studies with *R. capsulatus* SB1003. M.S.C. created and analyzed the ScfR sequence similarity network (SSN). K.K., S.M., Y.T.N., and M.S.C. conducted *in silico* identification of the RamB binding sites. D.M., A.B., J.S., P.B., and A.G. generated and analyzed RNAseq data from Pd1222 samples taken by K.K.. M.T. supervised the biolayer interferometry (BLI) experiments. G.K.A.H. supervised the mass photometry (MP) experiments. L.T. contributed to Pd1222 RamB *in vitro* analyses. J.Z. synthesized and purified CoA esters and performed *in silico* structural analysis of Pd1222 RamB. N.P. conduced the LC-MS analysis of the Pd1222 exometabolome from samples taken by K.K.. S.M. and A.R.N. performed genetic studies with *R. capsulatus* SB1003. K.K. and T.J.E. wrote the manuscript.

3.1 Abstract

Metabolic degeneracy describes the phenomenon that cells can use one substrate through different metabolic routes. Metabolic plasticity, on the other hand, refers to the ability of an organism to dynamically rewire its metabolism in response to changing physiological needs. A prime example for this is the dynamic switch between two alternative and seemingly degenerate acetyl-CoA assimilation routes in the Alphaproteobacterium *P. denitrificans* Pd1222: the ethylmalonyl-CoA pathway (EMCP) and the glyoxylate cycle (GC). The EMCP and the GC each tightly control the balance between catabolism and anabolism by shifting flux away from the oxidation of acetyl-CoA in the tricarboxylic acid (TCA) cycle towards biomass formation. However, the simultaneous presence of both the EMCP and GC in *P. denitrificans* Pd1222 raises the question of how this apparent functional degeneracy is globally coordinated during growth. Here, we show that RamB, a transcription factor of the ScfR family, controls expression of the GC in *P. denitrificans* Pd1222. Combining genetic, molecular biological and biochemical approaches, we identify the binding motif of RamB and demonstrate that CoA-thioester intermediates of the EMCP directly bind to the protein. Overall, our study shows that the EMCP and the GC are metabolically and genetically linked with each other, demonstrating a so-far undescribed bacterial strategy to achieve metabolic plasticity, in which one seemingly degenerate metabolic pathway directly drives expression of the other.

3.2 Importance

Carbon metabolism provides organisms with energy and building blocks for cellular functions and growth. The tight regulation between degradation and assimilation of carbon substrates is central for optimal growth. Understanding the underlying mechanisms of metabolic control in bacteria is of importance for applications in health (*e.g.*, targeting of metabolic pathways with new antibiotics, development of resistances) and biotechnology, (*e.g.*, metabolic engineering, introduction of new-to-nature pathways). In this study, we use the Alphaproteobacterium *P. denitrificans* as model organism to study functional degeneracy, a well-known phenomenon of bacteria to use the same carbon source through two different (competing) metabolic routes. We demonstrate that two seemingly degenerate

central carbon metabolic pathways are metabolically and genetically linked with each other, which allows the organism to control the switch between them in a coordinated manner during growth. Our study elucidates the molecular basis of metabolic plasticity in central carbon metabolism, which improves our understanding of how bacterial metabolism is able to partition fluxes between catabolism and anabolism.

3.3 Introduction

Acetyl-CoA is an essential intermediate in central carbon metabolism, where it serves as energy and/or carbon source. While acetyl-CoA is oxidized through the citric acid (TCA) cycle for NADH and ATP generation, bacteria have evolved different strategies for the assimilation of acetyl-CoA into biomass. Several acetyl-CoA assimilation routes have been described to date (1–12) among them the glyoxylate cycle (2, 3) and the ethylmalonyl-CoA pathway (4–7, 12). The glyoxylate cycle (GC) consists of only two enzymes, isocitrate lyase (Icl) and malate synthase (Ms), which branch off the tricarboxylic acid (TCA) cycle and are often organized in one operon under joint transcriptional regulation (13). The ethylmalonyl-CoA pathway (EMCP), instead, is a rather complex pathway that involves at least twelve enzymes (4), among them crotonyl-CoA carboxylase/reductase (Ccr). Ccr catalyzes a unique reaction, the reductive carboxylation of crotonyl-CoA into ethylmalonyl-CoA and is considered the key enzyme of the EMCP (4, 6). In contrast to the GC, genes encoding the EMCP are typically distributed across the host genome (14).

Despite their biochemical and genetic differences, the EMCP and the GC seem to serve a functionally degenerate purpose; both pathways use three or two molecules of acetyl-CoA, respectively, and bypass the decarboxylation steps of the TCA cycle to allow the cell to form the TCA cycle intermediates succinate and malate from acetyl-CoA ((2–5, 7, 12), Figure 3B). This shifts the function of the TCA cycle from acetyl-CoA oxidation (*i.e.*, energy generation) towards acetyl-CoA assimilation (*i.e.*, biomass formation). For optimal growth, bacteria require a tight and fine-tuned regulation of flux between acetyl-CoA oxidation and assimilation (15).

Among various bacteria, different regulatory mechanisms have been described that regulate flux distribution between acetyl-CoA oxidation and assimilation by controlling the enzymes of the TCA cycle as well as the key enzymes of the GC or EMCP, respectively, at the gene and/or protein level (16–20). However, these studies primarily focused on organisms that possess only one of the two alternative acetyl-CoA assimilation pathways, mostly the GC (summarized in (13)). Notably, several organisms exist that harbor both the GC and the EMCP (14, 21–23). These organisms are not only faced with the challenge to distribute metabolic flux between acetyl-CoA oxidation and assimilation, but also with the question of how to coordinate two seemingly functionally degenerate metabolic pathways without compromising fitness.

While 'functional degeneracy' describes the phenomenon that cells can use and metabolize the same substrate through different pathways (1), 'metabolic plasticity' refers to the ability of a cell to dynamically rewire metabolic routes in response to changing physiological needs (24). The latter is well known from cancer cells. There, metabolic plasticity mediates survival and metastatic outgrowth by facilitating the rapid adaptation to changing conditions, which enables cancer cells to outcompete their neighbors by ensuring optimal nutrient supply (25–29). Several examples of functional degeneracy and metabolic plasticity have been observed in microbial communities (30–33) as well as individual bacterial populations. One example is the presence of two functionally degenerate routes for the oxidation of methylamine in *Methylobacterium extorquens* AM1 (34, 35) or the simultaneous existence of the EMCP and GC in several Alphaproteobacteria such as *P. denitrificans* Pd1222 (22) or *Rhodobacter capsulatus* (23). Yet, the molecular mechanisms coordinating functional degeneracy and metabolic plasticity in bacteria remain largely unknown.

Here, we study the regulation of functional degeneracy during acetyl-CoA metabolism in *P. denitrificans* Pd1222. We show that acetyl-CoA metabolism follows a dedicated pattern in which the EMCP and GC are sequentially upregulated during a switch to acetate as the sole carbon source for growth. Using a combination of genetic, molecular biological, and biochemical approaches, we identified the transcriptional regulator controlling the GC in *P. denitrificans* Pd1222,

characterized its DNA-binding site and identify CoA esters as small-molecule ligands that induce a change in the oligomerization state of the protein. Notably, these CoA esters are direct intermediates of the EMCP, implying that the expression of the GC is directly linked to an active EMCP. Altogether, our study demonstrates an as of yet unknown regulatory mechanism in central carbon metabolism in which one seemingly degenerate pathway drives the expression of another.

3.4 Results

3.4.1 The ScfR family of transcription factors are potential regulators of acetate metabolism in *P. denitrificans* Pd1222

To study the regulation of the GC and the EMCP during a switch from succinate to acetate as the sole carbon source for growth, we used the reporter strain *P. denitrificans* Pd1222 *ccr::ccr-mCherry icl::icl-cerulean*, in which the key enzymes of the EMCP (Ccr) and the GC (Icl) were fused to distinct fluorescent proteins. During growth on succinate, neither Ccr-mCherry nor Icl-Cerulean fluorescence was detected (Figure 1A). Upon a switch to acetate, the Ccr-mCherry signal increased first followed by the Icl-Cerulean signal. This sequential activation of key enzymes of the EMPC (Ccr) and the GC (Icl) is in line with earlier reports (22) that additionally showed very basal levels of Ccr (and no Icl) activity in cell extracts of succinate-grown cells and subsequent induction of both enzymes on acetate (Figure 1A and B).

We next aimed to identify potential regulators of acetate metabolism in *P. denitrificans* Pd1222, henceforth termed Pd1222. Notably, several well-known homologs of transcriptional (*e.g.*, IclR (18)) and posttranslational (*e.g.*, AceK (16, 17)) regulators of the GC are absent in Pd1222, indicating that the regulation of this pathway relies on other mechanisms. The family of short-chain fatty acid regulators (ScfR) drew our attention, as several of these proteins are involved in the regulation of central carbon metabolic pathways, in particular acetate and/or propionate assimilation (36). Three known ScfR family members are encoded in the genome of Pd1222 (36), namely Pden_4472, Pden_1365, and Pden_1350. Based on sequence similarity and gene neighborhood analysis, Pden_1350 is

suggested as regulator of the methylcitrate cycle (MccR) and Pden_1365 as regulator of acetate metabolism (RamB), while no specific function could be predicted for Pden_4472 due to its genomic isolation (Figure 1C, (36)).

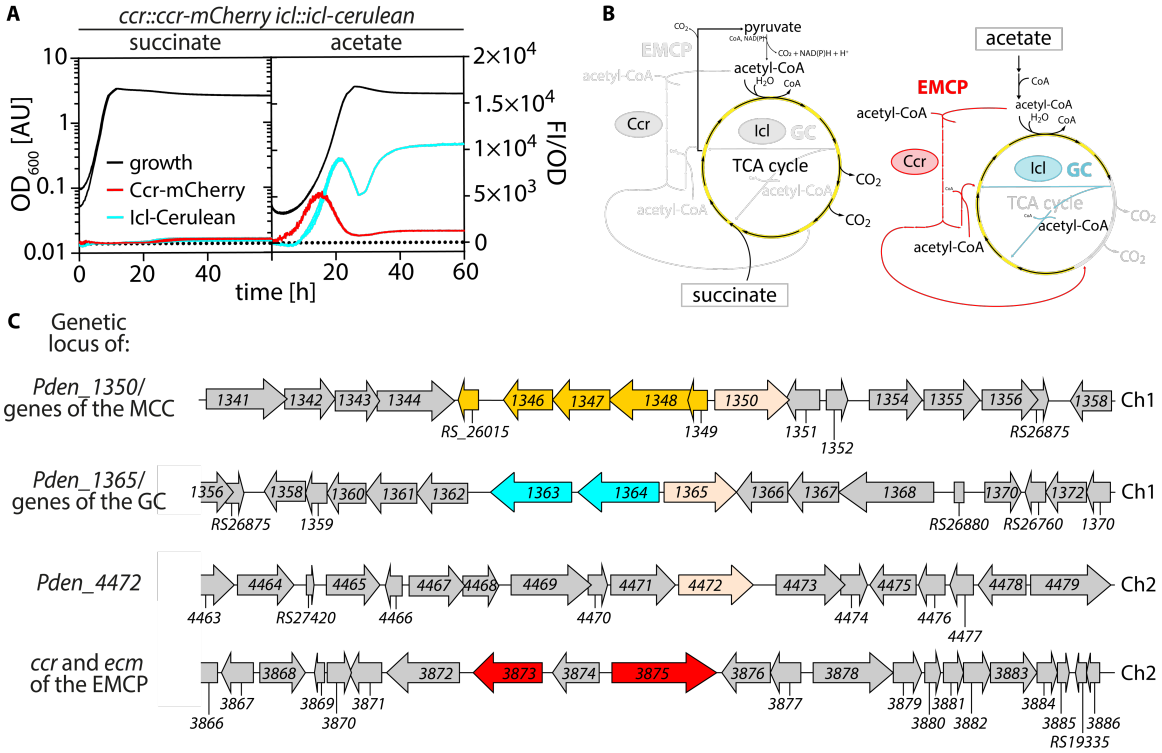

Figure 1: *P. denitrificans* Pd1222 sequentially employs the EMCP and GC for the efficient assimilation of acetyl-CoA. (A) Growth and fluorescence of Pd1222 *ccr::ccr-mCherry icl::icl-cerulean* (TJE-KK12) on succinate and acetate. Growth is given as OD_{600} on the left y-axis of each graph. Fluorescence normalized to OD_{600} is given on the right y-axis of each graph. Replicates are shown as individual curves. (B) Assumed assimilation routes for succinate (left) and acetate (right) in Pd1222. Succinate is assimilated via the TCA cycle. The regeneration of acetyl-CoA from succinate could occur by decarboxylation of malate to pyruvate and subsequent oxidative decarboxylation by pyruvate dehydrogenase (Pdh). The assimilation of acetate requires the activity of the EMCP and GC. (C) Genetic neighborhood of *scfR* homologs as well as the genes encoding the key enzymes of the GC and EMCP. Ch1: chromosome 1; Ch2: chromosome 2. Genes of ScfR homologs (light orange), the MCC (dark orange), the GC (cyan), and the EMCP (red) are highlighted in color. Gene names are given as Pd1222 gene tags (Pden_). For a detailed description of the individual genes of interest and their products, see Table 1.

Table 1: Genes relevant to this study and their corresponding locus tags as well as protein IDs.

	Gene	Product description	Old locus tag	New locus tag	protein ID
EMCP	*phaA*	β-ketothiolase	Pden_2026	PDEN_RS10080	WP_011748315.1
	phaB	Acetoacetyl-CoA reductase	Pden_2027	PDEN_RS10085	WP_011748316.1
	ccr	Crotonyl-CoA carboxylase/reductase	Pden_3873	PDEN_RS19270	WP_011750106.1
	epi	Epimerase	Pden_2178	PDEN_RS10820	WP_011748465.1
	ecm	Ethylmalonyl-CoA mutase	Pden_3875	PDEN_RS19280	WP_041530425.1
	mcd	Methylsuccinyl-CoA dehydrogenase	Pden_2840	PDEN_RS14140	WP_011749115.1
	mch	Mesaconyl-CoA hydratase	Pden_0566	PDEN_RS02820	WP_011746911.1
	mcl-1	β-methylmalyl-CoA/L-malyl-CoA lyase	Pden_0799	PDEN_RS03970	WP_041529775.1
	mcl-2	Malyl-CoA thioesterase	Pden_0563	PDEN_RS02805	WP_011746908.1
	pccA	Propionyl-CoA Carboxylase	Pden_3684	PDEN_RS18285	WP_011749920.1
	pccB		Pden_3688	PDEN_RS18310	WP_011749924.1
	mcm	Methylmalonyl-CoA	Pden_3681	PDEN_RS18265	WP_011749917.1
MCC	*prpD*	2-methylcitrate dehydratase	Pden_1348	PDEN_RS06660	WP_011747670.1
	prpC	2-methylcitrate synthase	Pden_1347	PDEN_RS06655	WP_011747669.1
	prpB	2-methylisocitrate lyase	Pden_1346	PDEN_RS06650	WP_041530157.1
	acyl-CoA thioesterase	Acyl-CoA thioesterase	Pden_1349	PDEN_RS06665	WP_011747671.1
	transcriptional repressor	Transcriptional repressor	n/a	PDEN_RS26015	n/a
GC	*icl (aceA)*	Isocitrate lyase	Pden_1363	PDEN_RS06725	WP_086000156.1
	ms (aceB)	Malate synthase	Pden_1364	PDEN_RS06730	WP_011747683.1
	ramB	Regulator of acetate metabolism	Pden_1365	PDEN_RS06735	WP_011747684.1
	Putative *mccR*	Regulator of methylcitrate cycle	Pden_1350	PDEN_RS06670	WP_011747672.1
	Putative *pccR*	Regulator of methylmalonyl-CoA pathway	Pden_4472	PDEN_RS22285	WP_011750697.1

We used the enzyme similarity tools EFI-EST (37) and Cytoscape (38) to construct a sequence similarity network for ScfR family members in Pd1222 (Supplementary Figure 1). In line with previous predictions (36), Pden_1350 clustered together with PrpR, a recently characterized MccR homolog from *Mycobacterium tuberculosis* (39, 40), while Pden_1365 clustered in a node of RamB-like proteins that belong to subclass 2 and are distinct from the archetypical *Corynebacterium glutamicum* RamB that defines subclass 1 (36, 41). Pden_4472 was located in a node together with the regulator of propionyl-CoA carboxylase (PccR) that has recently been characterized as transcriptional activator of the methylmalonyl-CoA pathway (MMCP) in *Rhodobacter sphaeroides* (Supplementary Figure 1, (36)). Notably, the MMCP is part of the canonical EMCP where it converts propionyl-CoA into succinyl-CoA (see below, Figure 3B). Two additional proteins of Pd1222 appeared in our ScfR network, namely Pden_1785 and Pden_2985. The corresponding genes clustered together with genes for a two-component system and an isocitrate lyase/phosphoenolpyruvate mutase family protein, respectively. Based on the sequence similarity network analysis, we focused on Pden_1350, Pden_1365 and Pden_4472 as potential regulators of acetate metabolism in the following.

3.4.2 Pden_1365 is a RamB homolog that regulates acetate metabolism in Pd1222

To test whether one or several of the ScfRs identified were involved in the regulation of the EMCP or GC, we studied the function of Pden_1350, Pden_1365, and Pden_4472 in Pd1222 *in vivo*. To this end, we deleted each of these genes individually in Pd1222 reporter strains with *ccr-mCherry* or *icl-mCherry* fusions. Neither the deletion of *Pden_4472* nor that of *Pden_1350* affected growth or pathway expression patterns in any of the reporter strains under any condition tested (Supplementary Figure 2A and B), which excludes these genes as regulators of the GC or EMCP in Pd1222. In contrast, and in line with its proposed function, the deletion of *Pden_1365* abolished the production of Icl-mCherry in the *icl::icl-mCherry* reporter background and reduced the growth rate on acetate by 50% compared to the wild-type (WT) strain ($\mu_{icl::icl\text{-}mCherry}$=0.4 h^{-1} vs. $\mu_{icl::icl\text{-}mCherry\Delta Pden\_1365}$=0.2 h^{-1}, Figure 2A, column 2). This phenotype could be complemented by expression of *flag-Pden_1365* from an inducible promoter on plasmid pIND4 ((42), Figure 2A, column 3), while the empty pIND4 had no effect on growth or fluorescence of the *Pden_1365* knockout reporter strain (Figure 2A, column 4). Note that plasmid pIND4 is known to show leaky expression in *P. denitrificans* Pd1222 (42). Accordingly, the Δ*Pden_1365* growth and expression phenotypes could also be complemented by pIND4_*flag-Pden_1365* in the absence of inducer (Figure 2A, column 3, row 3).

Deletion of *Pden_1365* in the WT background confirmed these results. Similar to the *icl::icl-mCherry* Δ*Pden_1365* strain, the *Pden_1365* deletion in the WT reduced the growth rate on acetate two-fold (μ_{WT}=0.4 h^{-1} vs. $\mu_{\Delta Pden\_1365}$=0.2 h^{-1}; Figure 2B). Notably, the growth phenotype of the Δ*Pden_1365* mutant resembled that of a Δ*icl* mutant ((22), $\mu_{\Delta icl}$=0.2 h^{-1}, Figure 2B), suggesting that the growth defect caused by deletion of *Pden_1365* could be caused by a lack of Icl in the cell. Together, these results verified the function of Pden_1365 as regulator of acetate metabolism in Pd1222 and suggested that the protein serves as transcriptional activator for the GC. Therefore, we will refer to Pden_1365 as $RamB_{Pd}$ in the following.

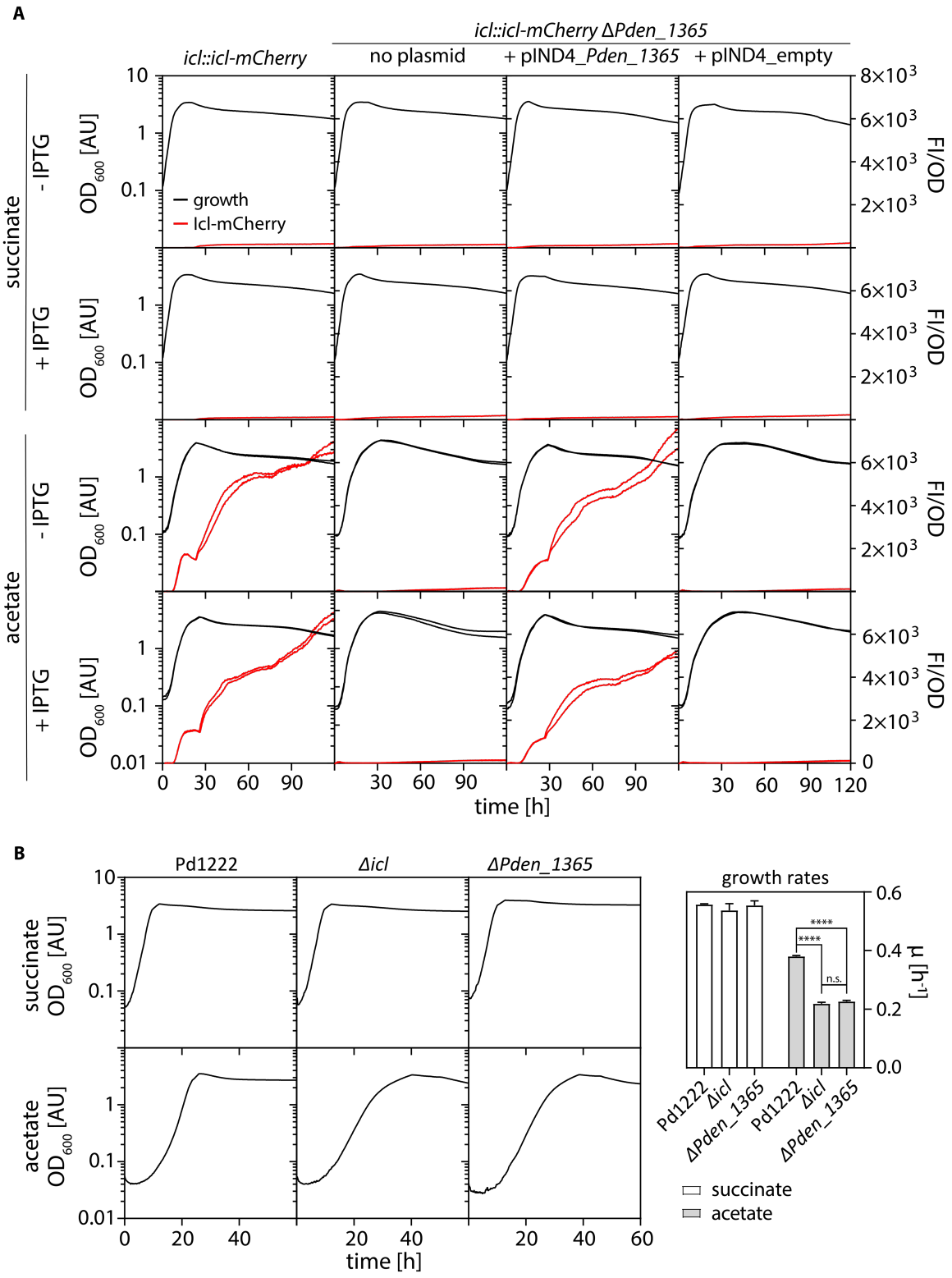

Figure 2: RamB (Pden_1365) is required for efficient production of Icl in *P. denitrificans* Pd1222. (A) Growth and fluorescence of Pd1222 *icl::icl-mCherry* (TJE-KK3), Pd1222 *icl::icl-mCherry* Δ*Pden_1365* (TJE-KK16), Pd1222 *icl::icl-mCherry* Δ*Pden_1365* pIND4_*flag-Pden_1365* (TJE-KK43), and Pd1222 *icl::icl-mCherry* Δ*Pden_1365* pIND4_empty (TJE-KK48) on succinate and acetate in the absence (-) and presence (+) of 0.5 mM IPTG. Growth is given as OD_{600} on the left y-axis. Fluorescence normalized to OD_{600} is given on the right y-axis. Replicates are shown as

individual curves. (B) Growth of Pd1222, Pd1222 Δ*icl* (TJE-KK8) and Pd1222 Δ*Pden_1365* (TJE-KK19) on succinate (upper panels) and acetate (lower panels). Replicates are shown as individual curves. The corresponding growth rates are given on the right. Asterisks indicate the level of significance as determined by t-test (****: p<0.0005), n.s.: not significant.

3.4.3 $RamB_{Pd}$ binds to a conserved motif upstream of the GC operon

Next, we aimed at identifying the promotor region of GC genes that is targeted by the transcription factor $RamB_{Pd}$. The gene encoding $RamB_{Pd}$ (*Pden_1365*) is located in reverse orientation on chromosome 1, directly upstream of the genes for malate synthase (*Pden_1364; aceB*, in the following referred to as *ms*) and *icl* (*Pden_1363*; Figure 1C, row 2). We assessed the upstream region of *ms* as well as the 120 bp intergenic region between *ms* and *icl* in more detail. To that end, we transformed Pd1222 with fluorescence reporter plasmids carrying either the upstream region of *ms* or the *ms-icl* intergenic region fused to a downstream *mCherry* reporter gene (Supplementary Figure 3A). In these experiments during growth with acetate, we detected fluorescent expression for the construct containing the *ms* upstream region, whereas no signal was observed for the *ms-icl* intergenic region or a promoterless *mCherry* gene. The fluorescence pattern obtained with the *ms* upstream region (Supplementary Figure 3D) was comparable to the signal observed for the Pd1222 *icl::icl-mCherry* strain (see above). However, when we analyzed the reporter construct containing the *ms* upstream region in the Δ*ramB* background (Supplementary Figure 3D), we did not observe any fluorescence, supporting the hypothesis that $RamB_{Pd}$ functions as a transcriptional activator. In summary, these results confirmed the role of $RamB_{Pd}$ as the central activator that acts by binding upstream of the *ms* gene.

$RamB_{Pd}$ is a class 2 RamB homolog ((36), Supplementary Figure 1). While specific binding motifs are known (or predicted) for class 1 RamB homologs and other classes of ScfR-type transcription factors, no consensus motif has been described for class 2 RamB homologs to date (36). To identify such a binding motif, we searched for genomes that contain class 2 RamB homologs clustering with a putative GC operon. We identified 67 bacterial genomes that fulfilled this requirement and analyzed the sequences upstream of the GC operon with MEME (Multiple Em for Motive election, (43)) to determine a putative class 2 RamB

binding motif. As is common for ScfR binding sites (36), this binding motif consists of two individual binding boxes that are nearly identical and separated from each other by an 18 bp spacer (Figure 3A). In the Pd1222 genome, this motif is located 82 bp upstream of the *ms* gene. We mutated either one or both binding boxes in a reporter plasmid containing the *ramB-ms* intergenic region fused to an *mCherry* reporter gene (Figure 3A). When introduced into the WT strain, only the reporter construct in which both binding boxes were intact yielded an mCherry signal during growth on acetate, while *mCherry* expression was abolished for constructs where one or both binding boxes were mutated (Figure 3B). In the Pd1222 Δ*ramB* control strain, none of the constructs showed *mCherry* expression, which is consistent with the notion that $RamB_{Pd}$ functions as a transcriptional activator. We further verified these findings *in vitro* by analyzing the interaction of purified $RamB_{Pd}$ (Supplementary Figure 4) with target DNA using biolayer interferometry. To this end, an 80 bp fragment of the *gc* promoter region comprising the two binding boxes separated by an 18 bp spacer and additional 17 bp on each side was immobilized on a biosensor and probed with increasing concentrations of protein, yielding an equilibrium dissociation constant K_D of 1.9 µM (Figure 3C and D). Mutation of any of the two binding boxes resulted in a complete loss of $RamB_{Pd}$ binding (Figure 3C). Altogether, these experiments identified and confirmed the putative binding site of $RamB_{Pd}$.

3.4.4 $RamB_{Pd}$ is a transcriptional activator and repressor

Next, we analyzed the changes in the global transcriptome of the *P. denitrificans* Pd1222 WT and the Δ*ramB* mutant induced upon a switch from succinate to acetate as the sole carbon source during mid-exponential growth (OD_{600} at the time of sampling: 0.8). In the WT, 43 genes were significantly upregulated under this condition (Supplementary Figure 5A, Supplementary Table 1 (see Appendix)). These included genes for acetate-CoA ligases (*Pden_4231*, *Pden_4550*, *Pden_4966*), several transporters as well as several enzymes of core metabolism, such as α-ketoglutarate dehydrogenase (*Pden_4984* and *Pden_4985*) or glucose-1-phosphate dehydrogenase (*Pden_4982*; Supplementary Table 1 (see Appendix)). Notably, genes of the *prp*-operon also showed a strong (300-fold) upregulation on acetate (Figure 4A, Supplementary Figure 5A, Supplementary

Table 1 (see Appendix)). The *prp*-operon encodes the enzymes of the methylcitrate cycle (MCC), which converts propionyl-CoA via methylcitrate and methylisocitrate to succinate and pyruvate (8–11). As propionyl-CoA is an intermediate in the EMCP, upregulation of the MCC indicated that this pathway

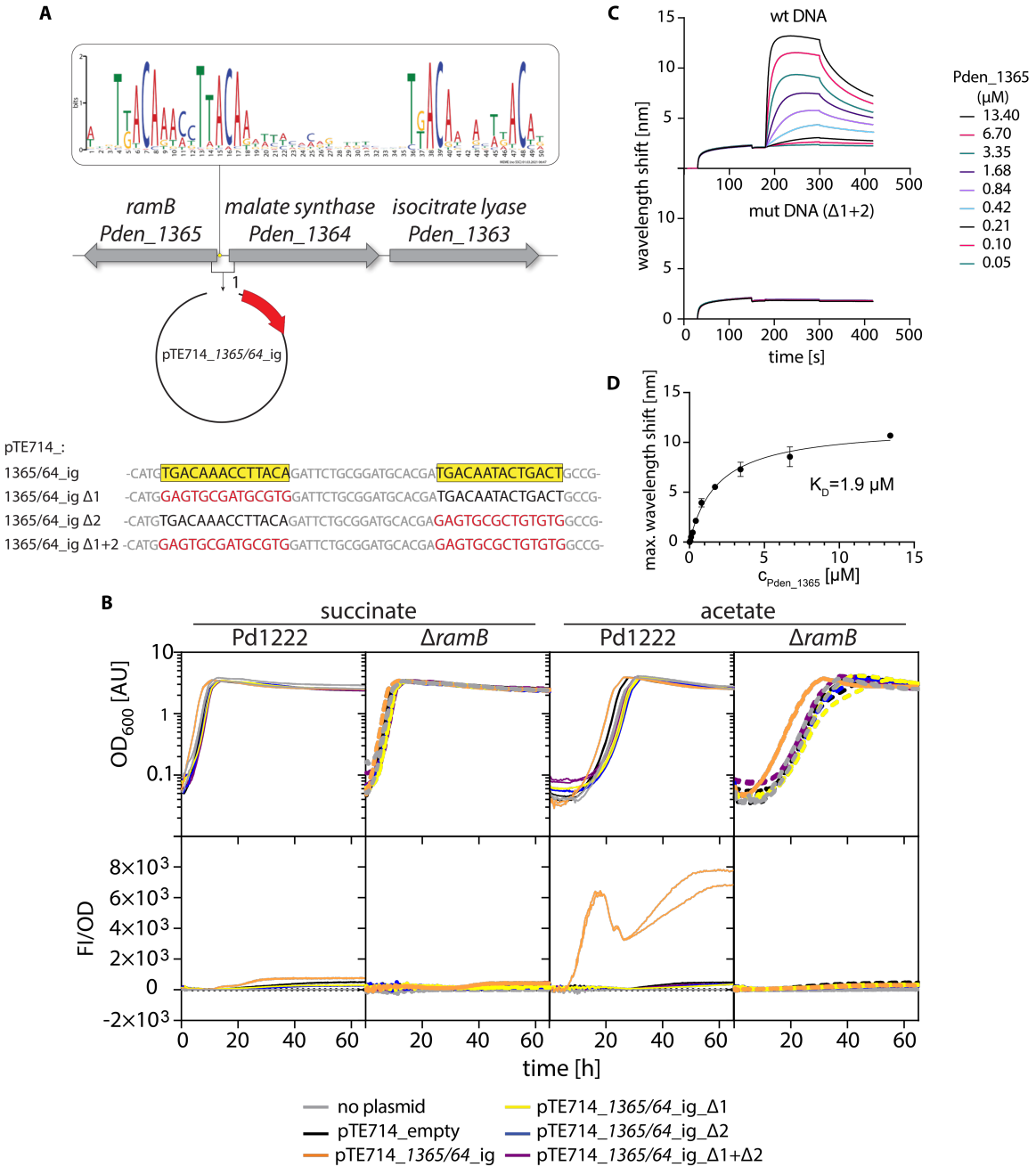

Figure 3: Two binding sites mediate the interaction of RamB$_{Pd}$ with the promoter region of the GC operon. (A) Simplified schematic of the GC operon in *P. denitrificans* Pd1222 in reverse complement, including the consensus binding motif as determined by a sequence alignment using the MEME server (43). To generate a reporter construct for *in vivo* assays, the upstream region of the operon including 50 bp of each flanking open reading frame was integrated upstream of a

promoterless *mCherry* gene in the plasmid pTE714, resulting in the plasmid pTE714_1365/64_ig (pTE1634). Shown at the bottom is the sequence of the binding boxes present in the construct as well as the mutated sequences as present in the derivatives pTE714_1365/64_ig_d1 (pTE1637), pTE714_1365/64_ig_d2 (pTE1638) and pTE714_1365/64_ig_d1+2 (pTE1639). (B) Growth and fluorescence of Pd1222 and Pd1222 Δ*ramB* containing either no plasmid or different derivatives of pTE714 (as indicated) during growth on succinate and acetate. Growth is given as OD_{600} (upper panels), fluorescence is shown normalized to OD_{600} (lower panels). (C) Biolayer interferometry analysis showing the interaction of $RamB_{Pd}$ with its target DNA *in vitro.* A biotinylated 80 bp dsDNA fragment of the promoter region of the GC operon containing intact binding boxes (upper panel) or mutated binding boxes (lower panel; mutations correspond to those present in pTE714_1365/64_ig Δ1+2) was immobilized on Sartorius Octet® SAX2 biosensors. The biosensor tips with immobilized DNA were probed with increasing concentrations of $RamB_{Pd}$ in binding buffer. Wavelength shifts resulting from an increase in the biolayer due to protein association were monitored over the course of time using a BLItz (Forté Bio, USA). (D) Shown are the wavelength shifts reached at equilibrium at the end of the association phase plotted versus the concentration of protein present in the reaction. The K_D was determined as the concentration at which the half-maximal wavelength shift was reached.

might be active in parallel to or instead of the MMCP-branch of the EMCP on acetate (Figure 4B, see discussion). Interestingly, transcripts of *ramB* showed an average of 10 reads, which is below the limit of statistical significance, indicating a very low, basal expression of *ramB* under all conditions in the WT in line with its proposed function as a transcriptional regulator.

In addition and as expected in the WT, expression of EMCP and GC genes was also increased upon growth switch to acetate. GC genes were upregulated more than 600-fold on acetate in mid-exponential phase, while EMCP genes were only slightly upregulated, which is consistent with the observed decrease of EMCP activity in this growth phase (Figure 4A, row 1; Supplementary Table 1 (see Appendix); Supplementary Figure 5A). Unlike in the WT, the expression of GC genes did not change significantly in the Δ*ramB* mutant upon a switch to acetate (Figure 4A, row 2, Supplementary Figure 5B, Supplementary Table 2 (see Appendix)), indicating that $RamB_{Pd}$ acts as an activator of the GC operon. However, while expression of the GC operon was not induced in the Δ*ramB* mutant on acetate, it increased more than 20-fold on succinate compared to the WT (Figure 4A, row 4, Supplementary Figure 5C, Supplementary Table 4 (see

Appendix)), indicating that $RamB_{Pd}$ might serve a dual function as a transcriptional activator on acetate and as a repressor on succinate.

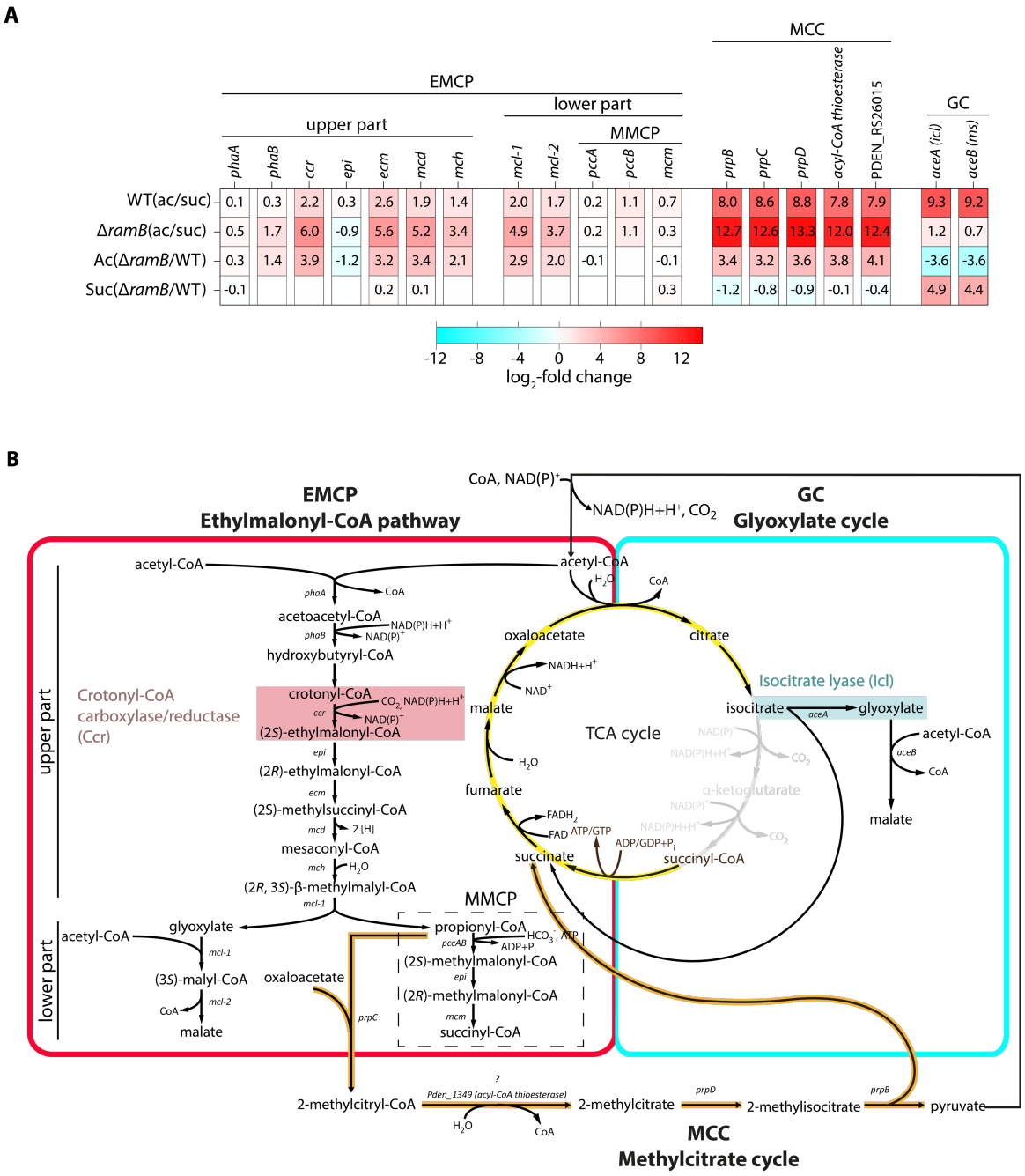

Figure 4: The genes of three pathways are upregulated during growth of *P. denitrificans* Pd1222 on acetate. (A) Regulation of the genes of the EMCP, GC and MCC in Pd1222 and Pd1222 Δ*ramB* during mid-exponential growth phase on acetate and succinate. Data shown are derived from RNAseq-based transcriptome analysis. mRNA profiles were determined from triplicate growth cultures. Differential gene expression (DEseq2-based, Supplementary Table 1-4) is given as log2-fold change in RNA levels between the two conditions indicated in front of each row. (B) Schematic representation of the pathways relevant for acetyl-CoA assimilation in *P. denitrificans* Pd1222 and

their proposed reaction sequences. Genes coding for the enzymes responsible for catalyzing the individual reactions are given in italics. Color code: TCA cycle (yellow), EMCP (red), GC (cyan), MCC (orange). The key reactions of the EMCP and GC, as catalyzed by crotonyl-CoA carboxylase/reductase (Ccr) and isocitrate lyase (Icl), are highlighted with a red and cyan background, respectively. The MMCP (Methylmalonyl-CoA pathway) in the lower EMCP is marked by a dashed box.

This hypothesis is in agreement with the observations that (i) $RamB_{Pd}$ was able to bind its target DNA even in the absence of a potential ligand (Figure 3C and D), (ii) addition of succinate to an acetate-grown culture in mid-log phase resulted in the downregulation of the GC (Supplementary Figure 7A), and (iii) deletion of *ramB* in the *icl::icl-mCherry* background resulted in higher basal mCherry fluorescence on succinate (Supplementary Figure 6). Interestingly, EMCP genes were also strongly upregulated in the Δ*ramB* mutant compared to the WT strain, with 8- to 15-fold higher transcript levels of *ccr*, *ecm*, *mcd*, and *mcl-1* compared to the WT on acetate (Figure 4A, row 3, Supplementary Table 3 (see Appendix), Supplementary Figure 2C). Collectively, these results confirmed the central role of $RamB_{Pd}$ as regulator of acetate metabolism in Pd1222 and suggested that the protein can act both as a transcriptional activator and repressor.

3.4.5 Intermediates of the EMCP bind to $RamB_{Pd}$

Previous studies showed that PrpR (from the MccR group of the ScfR family) from *M. tuberculosis* binds CoA-esters via a dedicated ligand binding pocket (39). Homology modeling using SWISS-MODEL (44) with PrpR as template (39) predicted a similar binding pocket in $RamB_{Pd}$ (Supplementary Figure 9), suggesting that this protein also binds CoA-esters. Notably, the EMCP produces several CoA-ester intermediates and is always induced before the GC in the pre-exponential phase of Pd1222 cultures on acetate (OD600 < 0.1) regardless of the presence of additional carbon sources in the medium (Figure 5D, Supplementary Figure 8B) or the growth state of the pre-culture (Supplementary Figure 7C), suggesting that an active EMCP and/or its CoA-ester intermediates are required for GC expression. This hypothesis was further supported by the fact that a Δ*ccr* mutant showed a prolonged lag phase (between 30 h to 90 h) upon a switch to acetate ((22), Figure 5A and B), while the lag phase was unchanged in a Δ*icl* strain under the same

conditions ((22), Figure 2B), suggesting that $RamB_{Pd}$ might indeed sense an EMCP intermediate.

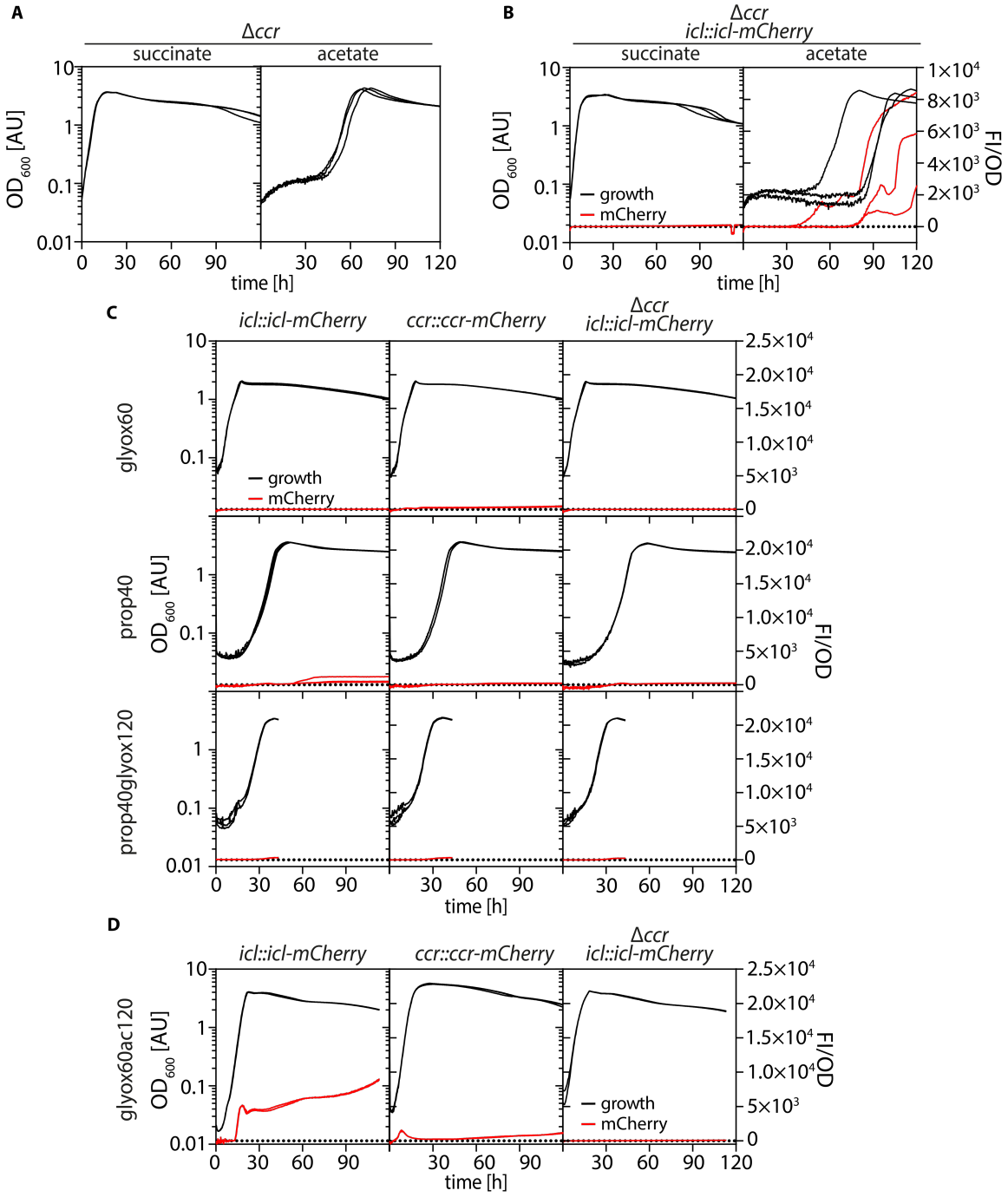

Figure 5: Expression of the GC depends on preceeding activity of the EMCP. Growth of different reporter strains of Pd1222 as indicated. Growth (black) is given as OD_{600} on the left y-axes. Fluorescence normalized to OD_{600} is given as on the right y-axes. Replicates are shown as individual curves. (A) Growth of Pd1222 Δccr (TJE-KK7) on succinate and acetate. (B) Growth of Pd1222 *Δccr icl::icl-mCherry* (TJE-KK40) on succinate and acetate. (C) Growth of Pd1222 *icl::icl-mCherry* (TJE-KK3), Pd1222 *ccr::ccr-mCherry* (TJE-KK11), Pd1222 *Δccr icl::icl-mCherry* (TJE-

KK40) on 60 mM glyoxylate (glyox60), 40 mM propionate (prop40) and 40 mM propionate mixed with 120 mM glyoxylate (prop40glyox120). (D) Growth of the strains described in (C) on 60 mM glyoxylate mixed with 120 mM acetate (glyox60ac120).

To narrow down the list of potential ligands of $RamB_{Pd}$, we tested whether the signal was an intermediate of the upper part (reactions upstream of Mcl-1) or the lower part (reactions downstream of Mcl-1) of the EMCP (Figure 4B). Growth on downstream metabolites, such as glyoxylate, propionate, or a mixture of both carbon sources, had no inducing effect on the expression of *ccr* or *icl*, and thus the EMCP or the GC (Figure 5C). By contrast, growth on upstream substrates such as acetate (Figure 1A), acetate plus glyoxylate (Figure 5D), ethanol, or crotonate induced *icl* expression (22), independently of the presence of additional (*i.e.*, 5% v/v) CO_2, which is an important co-substrate of the EMCP and Ccr as well as propionyl-CoA carboxylase (PccAB) in particular (Supplementary Figure 7B). Altogether, these results indicated that the signal inducing expression of the GC was produced in the upper part of the EMCP. This notion was further supported by the fact that functional Ccr (and presumably an active EMCP) was required to induce *icl*. While *icl* expression was induced during growth on acetate plus glyoxylate (Figure 5D, first panel), it was lost under the same conditions in a Δ*ccr* strain (Figure 5D, last panel). We next aimed to identify the potential ligand of $RamB_{Pd}$. The upper part of the EMCP, including the reactions between the reactions of Ccr and Mcl-1 produces four intermediates, namely (2*S* & 2*R*)-ethylmalonyl-CoA, (2*S*)-methylsuccinyl-CoA, mesaconyl-C1-CoA, and (2*R*/3*S*)-β-methylmalyl-CoA ((4, 12), Figure 4B). To study the effect of the different-CoA esters on $RamB_{Pd}$, we assessed the oligomeric state of $RamB_{Pd}$ *in vitro* in the absence and presence of the different CoA-esters using mass photometry (45, 46). Besides two background peaks at 80 kDa, $RamB_{Pd}$ was detected at a mass corresponding to a molecular weight of approximately 210 kDa (Figure 6A), indicating that $RamB_{Pd}$ forms a tetramer in solution.

Incubation of the protein in the presence of free CoA resulted in a second peak that increased in size with higher concentrations of CoA, until reaching saturation at 62.5 µM CoA with a peak ratio of 1:1 dimer to tetramer. The protein species in this second peak has a molecular weight of ~105 kDa, corresponding to a dimer. These results suggest that the tetrameric $RamB_{Pd}$ complex dissociates into a dimer

upon the addition of CoA. We next tested the influence of the different CoA ester intermediates of the EMCP on dimer formation (Figure 6C-E). Ethylmalonyl-CoA did not induce dimer formation, while methylsuccinyl-CoA (which contained 54 %

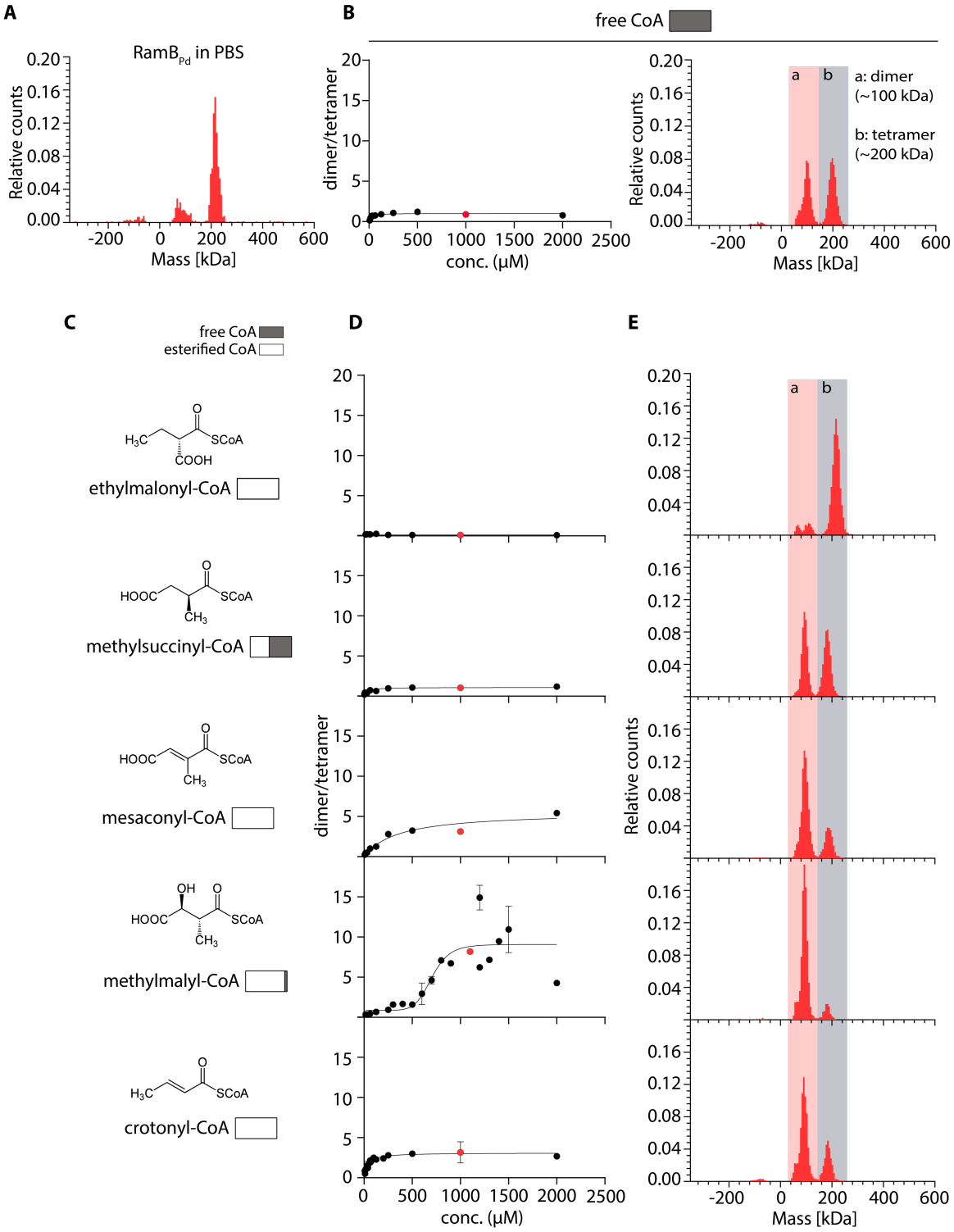

Figure 6: Methylmalyl-CoA induces a change in the oligomeric state of RamB$_{Pd}$. The oligomeric state of RamB$_{Pd}$ was assessed by mass photometry in reactions containing 250 nM protein in PBS buffer with or without supplements as indicated. Relative counts were normalized to

the total count number of each measurement. Red dots indicate the assay concentrations, for which results of the MP measurement are exemplified on the right. Dimer peaks are shown on a red background and indicated with a. Tetramer peaks are shown on a gray background and indicated with b. (A) $RamB_{Pd}$ in PBS buffer. (B) Titration of $RamB_{Pd}$ with rising concentrations of free CoA. $RamB_{Pd}$ was pre-incubated with rising concentrations of free CoA in PBS buffer for 35 min before the measurement. The ratio of dimer/tetramer formed is plotted versus the corresponding concentration of CoA in the assay in triplicate (left panel). Dots represent the mean of three measurements, error bars indicate the standard deviation. An exemplary result of a mass photometry measurement is depicted on the right. (C) Structures and names of the respective CoA-esters used in the assays on the right. The amount of free CoA present in the stock of each CoA-ester is shown as a bar chart with the white area representing the percentage of esterified CoA and the gray area representing the percentage of free CoA. (D) Titration measurements of the interaction of the esters shown in (C) to $RamB_{Pd}$, performed as described in (B). Dots represent the mean of three measurements, error bars indicate the standard deviation. (E) Result of an exemplary mass photometry measurement.

free CoA) showed similar effects as free CoA. Incubation of $RamB_{Pd}$ with mesaconyl-CoA or crotonyl-CoA resulted in a 3:1 ratio of dimers to tetramers. By contrast, incubation with β-methylmalyl-CoA increased the ratio of dimers to tetramers to 9:1, with an apparent K_D of the interaction of 700 µM. The strong shift towards dimer formation at physiologically relevant concentrations suggested that β-methylmalyl-CoA is the preferred ligand of $RamB_{Pd}$.

3.4.6 Acetate assimilation is different in *Rhodobacter capsulatus* SB1003

We finally turned our attention to *Rhodobacter capsulatus* SB1003, an Alphaproteobacterium that is closely related to *P. denitrificans* Pd1222 and possesses the genes of the EMPC, the GC and the MCC as well (47). Like Pd1222, this organism harbors several ScfR family members. Based on their locations in the sequence similarity network (Figure S1) and the neighborhoods of their respective genes, we identified the proteins as putative RamB (regulator of the GC genes), putative PccR (regulator of propionyl-CoA carboxylase), and putative MccR (regulator of the MCC genes; (36)), indicating a similar strategy of *R. capsulatus* SB1003 to assimilate acetate as Pd1222. To test this hypothesis, we deleted the genes of the key enzymes and (putative) regulators of acetate metabolism in *R. capsulatus* SB1003 (*ccr*, *icl*, *pccR*, and *mccR* genes were independently deleted) and analyzed the growth of the mutant strains on different

carbon sources. Deletion of these genes did not affect the growth of *R. capsulatus* SB1003 on malate, the negative control (Figure 7, line 1). As observed for Pd1222, deletion of *ccr* impaired the growth of *R. capsulatus* SB1003 on acetate (Figure 7, column 3, line 2), emphasizing the importance of the EMCP for its ability to assimilate acetyl-CoA. However, unlike in Pd1222, deletion of *icl* did not affect the growth of *R. capsulatus* SB1003 on acetate (Figure 7, column 2, line 2), indicating that Icl (and likely the GC) plays a minor role in acetyl-CoA assimilation in this species. Deletion of the regulatory *pccR* or *mccR* genes did not affect growth on acetate, but the deletion of *pccR* uniquely impaired growth on propionate. Deletion of *mccR* left growth of *R. capsulatus* SB1003 on propionate and CO_2 unaffected, indicating that the MCC was not able to substitute for the loss of the expression of MMCP genes, which requires PccR (Figure 7, column 4, line 3; (36)). In summary, these findings suggested that despite the presence of a common set of pathways and regulators, acetate metabolism strongly differs between these two organisms.

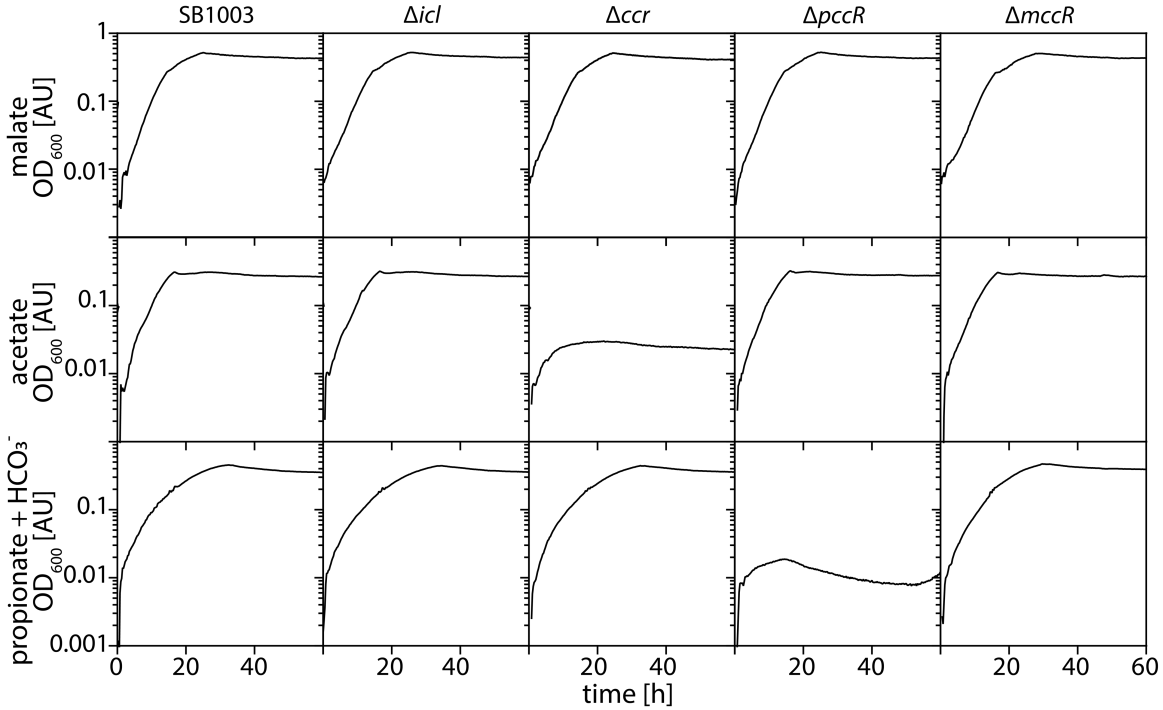

Figure 7: *R. capsulatus* SB1003 shows different employment patterns of the EMCP and GC. The growth of SB1003 (wt), SB1003 Δ*icl,* SB1003 Δ*ccr*, SB1003 Δ*pccR*, SB1003 Δ*mccR* on malate, acetate and propionate supplemented with HCO_3^- is shown as OD_{600}. All carbon sources are provided at a concentration of 10 mM each.

3.5 Discussion

Organisms must balance metabolic flux between catabolic and anabolic routes during growth. One of the key intermediates in central carbon metabolism is acetyl-CoA, which can be either oxidized in the citric acid cycle (catabolism) or assimilated into biomass (anabolism). Notably, the Alphaproteobacterium *P. denitrificans* Pd1222 employs two functionally degenerate acetyl-CoA assimilation pathways, the EMCP and the GC. It has been suggested that the EMCP represents the ancestral pathway in *P. denitrificans* Pd1222, while the GC was likely acquired through lateral gene transfer (22). The existence of two apparently redundant central metabolic traits in one organism is surprising and raises the question why *P. denitrificans* Pd1222 uses two parallel acetyl-CoA assimilation strategies and how the expression and activity of the two pathways are coordinated during growth of *P. denitrificans* Pd1222.

Here, we propose a novel mechanism of transcriptional control of GC genes that involves metabolic cross-talk via RamB, a regulator of the ScfR family that binds upstream of the GC operon (Figure 8). Induction of the GC is driven by flux through the EMCP, an alternative pathway for assimilating the same initial substrate.

The hypothesis that RamB links the expression of the GC to the activity of the EMCP is supported by several findings. First, the EMCP is (always) active at very basal levels in *P. denitrificans* Pd1222 and becomes upregulated in the pre-exponential growth phase after a switch to acetate and prior to induction of the GC. Second, deletion of the EMCP-essential *ccr* gene results in a significantly prolonged lag in GC expression. Third, *in vitro* experiments with purified $RamB_{Pd}$ show that several intermediates of the EMCP, and in particular β-methylmalyl-CoA, cause a shift from the tetrameric to the dimeric state of $RamB_{Pd}$ at physiologically relevant ligand concentrations.

Our findings show that *P. denitrificans* Pd1222 achieves metabolic plasticity through a complex entanglement and coordination of functionally degenerate central carbon metabolic pathways. Functional degeneracy is not uncommon in prokaryotes, and Alphaproteobacteria in particular. *Methylobacterium extorquens* AM1, a related methylotroph, for instance, features two different methylamine

assimilation routes that serve different purposes and confer distinct advantages under different growth conditions (34, 35). In the case of acetyl-CoA assimilation in *P. denitrificans* Pd1222, the EMCP might serve as a basic assimilation route, which is replaced by the more specialized and more efficient GC, when high fluxes require a strong commitment to acetyl-CoA assimilation (22).

This work clarifies the molecular basis of GC regulation in *P. denitrificans* Pd1222, but several questions remain unanswered. While upregulation of the GC requires an active EMCP, as shown in this work, the mechanism upregulating the EMCP itself remains enigmatic. In addition, the regulation of acetate metabolism in *P. denitrificans* Pd1222 is more complex and seems to involve catabolite repression, because succinate suppresses acetate metabolism (Supplementary Figure 8) but apparently not EMCP expression. Moreover, externally added succinate directly represses the expression of GC genes. This indicates a (post-)transcriptional/translational feedback loop and points to a more integrated regulation of acetate metabolism in the context of central carbon metabolism in *P. denitrificans* Pd1222. This hypothesis is further supported by the observation that the deletion of *ramB* or *icl* increases EMCP expression, possibly to compensate for the loss of GC activity.

An interesting finding of our study is that the MCC is upregulated in addition to the EMCP and GC during growth on acetate (and even further increased in absence of a functional GC in the Δ*ramB* mutant). This indicates that propionyl-CoA might be additionally assimilated through the MCC under these conditions, possibly as a strategy to prevent accumulation of potentially toxic concentrations of propionyl-CoA in the cell (48). In any way, the additional upregulation of the MCC represents an interesting variation of the EMCP that might add to the functional degeneracy of *P. dentrificans* Pd1222 and, potentially, other organisms expressing the EMCP and the MCC.

We would like to note that the functional degeneracy of acetyl-CoA assimilation routes is accompanied by regulatory degeneracy: although *R. capsulatus* SB1003 possesses in principle the same metabolic capabilities (*i.e.*, codes for the EMCP, GC and MCC) and homologous regulatory proteins (*i.e.*, RamB, PccR, MccR), the regulation of acetate metabolism (*i.e.*, the induction of the different pathways), and

the relevance of functional degeneracy of acetyl-CoA assimilation differs from *P. denitrificans* Pd1222. Future studies focusing on acetyl-CoA assimilation in *P. dentrificans* Pd1222 and/or *R. capsulatus* SB1003 will shed more light on and thus eventually complete our picture of functional degeneracy and metabolic plasticity in Alphaproteobacteria.

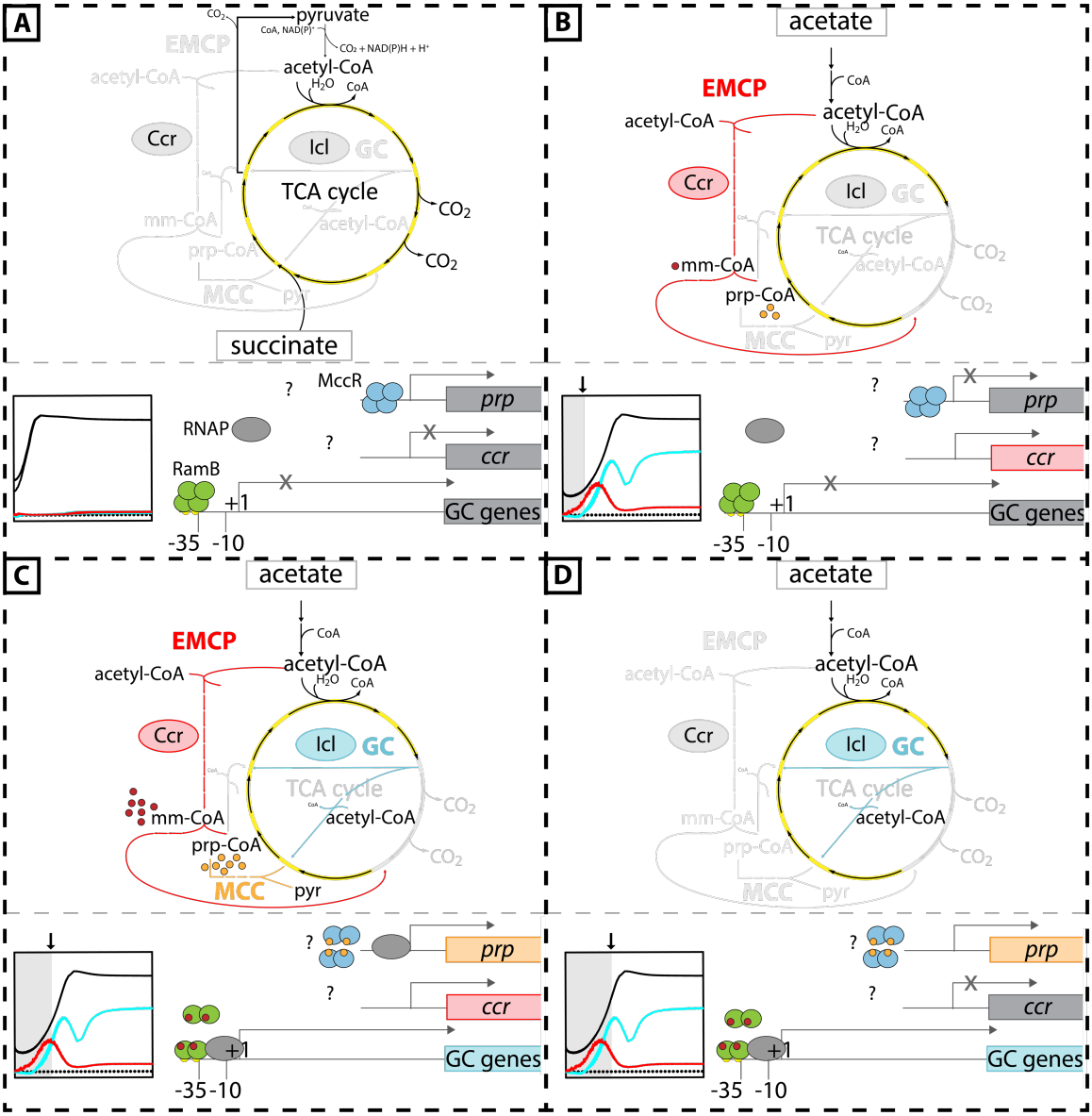

Figure 8: Hypothetical regulation of acetyl-CoA metabolism in *P. denitrificans* Pd1222. Shown is the interplay of the MCC, the EMCP, and the GC during growth on succinate (A) and growth on acetate (B-D). The different stages of growth on acetate depicted are indicated in the growth curve by arrows and gray background. Regulator binding sites, the -35 and -10 boxes as well as the transcription start site (+1) are shown for the GC operon. (A) Assimilation of succinate occurs via the TCA cycle. Neither the genes of the MCC (*prp*-operon), the EMCP (here shown on the example of *ccr*), nor the GC are expressed at relevant levels under this condition. Expression

of the *prp* operon might be negatively or positively regulated by MccR (Pden_1350; here shown is an example for negative regulation). Expression of the GC genes is repressed by a blockage of transcription through binding of tetrameric RamB to the *gc* promoter. (B) When the cells are shifted to growth on acetate, genes of the EMCP are initially upregulated. The resulting flux through the EMCP produces the metabolites methylmalyl-CoA (mm-CoA) and propionyl-CoA (prp-CoA). Due to low activity or the lack of propionyl-CoA carboxylase (PccAB) and other propionyl-CoA converting enzymes, propionyl-CoA accumulates, which leads to a backup in the EMCP and consequently an accumulation of methylmalyl-CoA. (C) propionyl-CoA might stimulate MccR to trigger expression of the *prp*-genes, resulting in the metabolization of propionyl-CoA by the now produced MCC enzymes. Binding of methylmalyl-CoA to RamB promotes a decay of the tetrameric inhibitory RamB complex into dimers. In the dimeric form, RamB stays bound to the *gc* promoter, but now promotes expression of the GC genes through positive interaction with RNA polymerase (RNAP). (D) A yet unknown signal leads to downregulation of the EMCP, while the GC remains upregulated.

3.6 Material and Methods

3.6.1 Chemicals

All chemicals used in this study were obtained from Sigma-Aldrich (Steinheim, Germany) and Carl Roth (Karlsruhe, Germany) unless specified otherwise and were of the highest purity available.

3.6.2 Strains, medium and cultivation conditions

All plasmids and strains used in this study are listed in Table 2. *Escherichia coli* was grown in Luria Bertani (LB) medium in the presence of appropriate antibiotics (Ampicillin [100 µg/mL]; Gentamycin [30 µg/mL]; Kanamycin [50 µg/mL]; Streptomycin [20 µg/mL]; Tetracycline [10 µg/mL]) at 37 °C. For the cultivation of *E. coli* ST18, media were supplemented with 5-aminolevulinic acid [50 µg/mL]. *Paracoccus denitrificans* was grown in the presence of appropriate antibiotics (Kanamycin [50 µg/mL]; Spectinomycin [50 µg/mL]; Rifampicin [30 µg/mL], Tetracycline [10 µg/mL]) in LB medium or mineral salt medium supplemented with trace elements TE3-Zn (49) and defined carbon compounds at a total carbon concentration of 120 mM at 30 °C. For strains carrying derivatives of the suicide plasmid pK18mobsacB, LB medium was replaced with SOB medium to lower the risk of point mutations in the *sacB* gene. *R. capsulatus* was grown at 30°C with peptone yeast extract (PYE) medium, as well as a modified version of minimal media (7) that, undiluted, contained 20X salt solution (20 g/L NH_4Cl, 6 g/L

$MgSO_4 \cdot 7H_2O$, 3 g/L KCl, 0.1 g/L $CaCl_2 \cdot 2H_2O$, 0.05 g/L $FeSO_4 \cdot 7H_2O$), 20X phosphate buffer, pH 7.0 (500 mM KH_2PO_4, 500 mM Na_2HPO_4), 1000X trace elements solution (0.5 g/L NaEDTA, 0.3 g/L $FeSO_4 \cdot 7H_2O$, 0.003 g/L $MnCl_2 \cdot 4H_2O$, 0.005 g/L $CoCl_2 \cdot 6H_2O$, 0.001 g/L $CuCl_2 \cdot 2H_2O$, 0.002 g/L $NiCl_2 \cdot 6H_2O$, 0.003 g/L $Na_2MoO_4 \cdot 2H_2O$, 0.005 $ZnSO_4 \cdot 7H_2O$, 0.002 g/L H_3BO_3), and 1000X vitamin solution (0.1 g/L cyanocobalamin, 0.3 g/L pyridoxamine-2 HCl, 0.1 g/L calcium-D(+)-pantothenate, 0.2 g/L thiamine dichloride, 0.2 g/L nicotinic acid, 0.08 g/L 4-aminobenzoic acid, 0.02 g/L, D(+)-biotin) with defined carbon sources as indicated for individual experiments at a concentration of 10 mM each. The optical density at 600 nm (OD_{600}) of cultures was determined using a Spectroquant® Prove 300 spectrophotometer (Merck, Germany). Growth and fluorescence measurements on *P. denitrificans* Pd1222 and its derivatives were performed in black VisiView 96-well plates with an optical bottom (Perkin Elmer, USA) in a Tecan M200 Pro plate reader system (Tecan, Switzerland). Growth was followed by measuring the OD_{600} at regular intervals. The fluorescence of mCherry was measured at an emission wavelength of 610 nm after excitation at 575 nm with a constant gain of 120. The fluorescence of Cerulean was measured at an emission wavelength of 475 nm after excitation at 433 nm with a constant gain of 90. The growth of *R. capsulatus* SB1003 and its derivatives was followed in a SpectraMax i3 plate reader (Molecular Devices, USA) by monitoring the OD_{600}.

Table 2: Strains and plasmids used in this study.

Strain/Plasmid name	Organism/ backbone	Genotype/description	Resistance	Source/ Reference
TOP10	*Escherichia coli*	F⁻*mcr*A Δ(*mrr-hsd*RMS-*mcr*BC) φ80*lac*ZΔM15 Δ*lac*X74 *rec*A1 *ara*D139 Δ(*ara-leu*)7697 *gal*U *gal*K λ⁻*rps*L(Str^R) *end*A1 *nup*G		Invitrogen, USA
DH5α	*Escherichia coli*	F⁻ φ80*lac*ZΔM15 Δ(*lac*ZYA-*arg*F)U169 *rec*A1 *end*A1 *hsd*R17(r_K^-, m_K^+) *pho*A *sup*E44 λ⁻*thi*-1 *gyr*A96 *rel*A1		New England Biolabs
S17-1	*Escherichia coli*	*pro, res⁻ hsdR17 (rK⁻ mK⁺) recA⁻* with an integrated *RP4-2-Tc::Mu-Km::Tn7*, Tp^r		(63)
ST18	*Escherichia coli*	S17 λ*pir*Δ*hemA*		(50)
BL21 AI	*Escherichia coli*	F⁻*ompT hsdS*$_B$ (r_B^-, m_B^-) *gal dcm ara*B::T7RNAP-*tet*A		Novagen, Germany
Rosetta™ (DE3)pLysS	*Escherichia coli*	F⁻ *ompT hsdS*$_B$(r_B^- m_B^-) *gal dcm* (DE3) pLysSRARE	Cam	Novagen, Germany
Pd1222	*Paracoccus denitrificans*	wildtype with increased conjugation efficiency	Spec, Rif	(64)

TJE-KK3	*Paracoccus denitrificans*	Pd1222 *icl::icl-mCherry*	Spec, Rif	(22)
TJE-KK7	*Paracoccus denitrificans*	Pd1222 Δ*ccr*	Spec, Rif	(22)
TJE-KK8	*Paracoccus denitrificans*	Pd1222 Δ*icl*	Spec, Rif	(22)
TJE-KK11	*Paracoccus denitrificans*	Pd1222 *ccr::ccr-mCherry*	Spec, Rif	(22)
TJE-KK12	*Paracoccus denitrificans*	Pd1222 *ccr::ccr-mCherry icl::icl-cerulean*	Spec, Rif	(22)
TJE-KK15	*Paracoccus denitrificans*	Pd1222 *ccr::ccr-mCherry icl::icl-cerulean* Δ*Pden_4472*	Spec, Rif	this work
TJE-KK16	*Paracoccus denitrificans*	Pd1222 *icl::icl-mCherry* Δ*ramB*	Spec, Rif	this work
TJE-KK17	*Paracoccus denitrificans*	Pd1222 *ccr::ccr-mCherry* Δ*Pden_1350*	Spec, Rif	this work
TJE-KK18	*Paracoccus denitrificans*	Pd1222 *icl::icl-mCherry* Δ*Pden_4472*	Spec, Rif	this work
TJE-KK20	*Paracoccus denitrificans*	Pd1222 *ccr::ccr-mCherry icl::icl-cerulean* Δ*ramB*	Spec, Rif	this work
TJE-KK23	*Paracoccus denitrificans*	Pd1222 pTE714	Spec, Rif	this work
TJE-KK24	*Paracoccus denitrificans*	Pd1222 Δ*ramB* pTE714	Spec, Rif	this work
TJE-KK32	*Paracoccus denitrificans*	Pd1222 Δ*ramB* pTE714_*1365/1364*_ig	Spec, Rif	this work
TJE-KK33	*Paracoccus denitrificans*	Pd1222 pTE714_*1365/1364*_ig	Spec, Rif	this work
TJE-KK40	*Paracoccus denitrificans*	Pd1222 Δ*ccr icl::icl-mCherry*	Spec, Rif	this work
TJE-KK42	*Paracoccus denitrificans*	Pd1222 *icl::icl-mCherry* pIND4_FLAG-r*amB*	Spec, Rif	this work
TJE-KK43	*Paracoccus denitrificans*	Pd1222 *icl::icl-mCherry* Δ*ramB* pIND4_FLAG-*ramB*	Spec, Rif	this work
TJE-KK47	*Paracoccus denitrificans*	Pd1222 *icl::icl-mCherry* Δ*ramB* pIND4	Spec, Rif	this work
TJE-KK51	*Paracoccus denitrificans*	Pd1222 pTE714_*1365/64*_ig_d1	Spec, Rif, Tet	this work
TJE-KK52	*Paracoccus denitrificans*	Pd1222 pTE714_*1365/64*_ig_d2	Spec, Rif, Tet	this work
TJE-KK53	*Paracoccus denitrificans*	Pd1222 pTE714_*1365/64*_ig_d1+2	Spec, Rif, Tet	this work
TJE-KK54	*Paracoccus denitrificans*	Pd1222 Δ*ramB* pTE714_*1365/64*_ig_d1	Spec, Rif, Tet	this work
TJE-KK55	*Paracoccus denitrificans*	Pd1222 Δ*ramB* pTE714_*1365/64*_ig_d2	Spec, Rif, Tet	this work
TJE-KK56	*Paracoccus denitrificans*	Pd1222 Δ*ramB* pTE714_*1365/64*_ig_d1+2	Spec, Rif, Tet	this work
TJE-KK57	*Paracoccus denitrificans*	Pd1222 pTE770	Spec, Rif, Tet	this work
TJE-KK58	*Paracoccus denitrificans*	Pd1222 Δ*ramB* pTE770	Spec, Rif, Tet	this work
TJE-KK60	*Paracoccus denitrificans*	Pd1222 icl::icl-mCherry ΔramB ΔPden_4472	Spec, Rif, Tet	this work
SB1003	*Rhodobacter capsulatus*	wildtype		this work

Δ*ccr*	*Rhodobacter capsulatus*	SB1003 Δ16020		this work
Δ*icl*	*Rhodobacter capsulatus*	SB1003 Δ16495		this work
Δ*pccR*	*Rhodobacter capsulatus*	SB1003 Δ04520-		this work
Δ*mccR*	*Rhodobacter capsulatus*	SB1003 Δ16525-		this work
pTB146		backbone for oe of *his-sumo*-tagged genes	Amp	(62)
pTB145		*his-ulp1*	Amp	(62)
pK18mobsacB		backbone for double homologous recombination	Kan	(65)
pTE714		pTE100	Tet	(66)
pIND4		backbone for oe of *his*-tagged genes in Alphaproteobacteria	Kan	(42)
Plasmids for *Paracoccus denitrificans* Pd1222				
pTE770		pTE714_*mCherry*	Tet	(66)
pTE1615	pK18mobsacB	pK18mobsacB_*icl*-flanks	Kan	(22)
pTE1616	pK18mobsacB	pK18mobsacB_*icl-mCherry-iclds*	Kan	(22)
pTE1630	pK18mobsacB	pK18mobsacB_*Pden1350*-flanks	Kan	this work
pTE1631	pK18mobsacB	pK18mobsacB_P*den1365*-flanks	Kan	this work
pTE1632	pK18mobsacB	pK18mobsacB_*Pden4472*-flanks	Kan	this work
pTE1633	pTE714	pTE714_*1364/1363*_ig	Tet	this work
pTE1634	pTE714	pTE714_*1365/1364*_ig	Tet	this work
pTE1637	pTE714	pTE714_*1365/1364*_ig_d1	Tet	this work
pTE1638	pTE714	pTE714_*1365/1364*_ig_d2_new	Tet	this work
pTE1639	pTE714	pTE714_*1365/1364*_ig_d1+2_new	Tet	this work
pTE5000	pIND4	pIND4_*FLAG-ramB* (original *his*-tag of pIND4 was removed in this construct)	Kan	this work
Plasmids for *Escherichia coli*				
pTE5007	pTB146	pTB146_r*amB*	Amp	this work
Plasmids for *Rhodobacter capsulatus* SB1003				
pJM009	pK18mobsacB	pK18mobsacB_*ccr*-flanks	Kan	this work
pYN011	pK18mobsacB	pK18mobsacB_*icl*-flanks	Kan	this work
pYN019	pK18mobsacB	pK18mobsacB_*pccR*-flanks	Kan	this work
pRK005	pK18mobsacB	pK18mobsacB_*mccR*-flanks	Kan	this work

Spec: spectinomycin; Rif: rifampicin; Tet: tetracyclin, Kan: kanamycin; Amp: ampicillin; Cam: chloramphenicol

Table 3: Oligonucleotides used in this study. Recognition sites for restriction enzymes are underlined in the given sequences.

#	Name	Sequence	Cloning method/ purpose	Construction of plasmid	Restriction site/ modification
1	1350-1-f	TCGAGCTCGGTACCCGGGGATCCTCTAGAGGGATCGGCGGGATGTTGT	Gibson assembly	pTE1630	
2	1350-1-r	CTGCGGGCAGGCGGGGCTGGGCGAGATCCCCAGG	Gibson assembly	pTE1630	
3	1350-2-f	GGGATCTCGCCCAGCCCCGCCTGCCCGCAGCGC	Gibson assembly	pTE1630	
4	1350-2-r	CGGCCAGTGCCAAGCTTGCATGCCTGCAGGATCGCGTTCAGCCGCAGCAGGACCG	Gibson assembly	pTE1630	
5	1365-1-f	GAATTCGAGCTCGGTACCCGGGGATCCTCTAGAGCGGCGGGCAGGGTCTCGATCA	Gibson assembly	pTE1631	
6	1365-1-r	GCGGGCCGAGCAATCCGGGACGCCCAGCTCGGCCGCCA	Gibson assembly	pTE1631	
7	1365-2-f	GGCGGCCGAGCTGGGCGTCCCGGATTGCTCGGCCCGCG	Gibson assembly	pTE1631	
8	1365-2-r	GACGGCCAGTGCCAAGCTTGCATGCCTGCAGGCGCGGGCGACCCGGCCCC	Gibson assembly	pTE1631	
9	4472-1-f	TCGAGCTCGGTACCCGGGGATCCTCTAGAGTGCGCGACATCGTGCCGG	Gibson assembly	pTE1632	

10	4472-1-r	GCAGTTCGGCCGGGGTGAAACGCCCA GCCGGTC	Gibson assembly	pTE1632	
11	4472-2-f	CGGCTGGGCGTTTCACCCCGGCCGAA CTGCCATCAGCGTT	Gibson assembly	pTE1632	
12	4472-2-r	ACGGCCAGTGCCAAGCTTGCATGCCT GCAGGCCATCGGCGGCGGCCAGGG	Gibson assembly	pTE1632	
13	EcoRI_Pden1364-f	GATATGAATTCCTGCCCGATTTCATCA CCG	restriction/ ligation	pTE1633	EcoRI
14	XbaI_STOP_Pden136 3-r	cgTTCTAGATCAGTAGCGGGACGACAC CTC	restriction/ ligation	pTE1633	XbaI
15	EcoRI_STOP_Pden13 65-r	GATATGAATTCTCAGCGCAGCACGCGC AGG	restriction/ ligation	pTE1634	EcoRI
16	XbaI_STOP_Pden136 4-r	CGTCTAGATCAGGCGCGCAGGACGAC GGG	restriction/ ligation	pTE1634	XbaI
17	1365_5UTR_binding1 _mut-f	ATGCGTGGATTCTGCGGATGCACGATG ACAATACT	KLD	pTE1637	
18	1365_5UTR_binding1 _mut-r	CGCACTCCATGGCCCGAGGCGAGAAA CTGATCATC	KLD	pTE1637	
19	1365_5UTR_binding2 _mut-r	GCACTCTCGTGCATCCGCAGAATCTGT AAGGTTTG	KLD	pTE1638	
20	binding2_mut2-f	GCTGTGTGGCCGCACCCATTGCTTTCA AAGCAATA	KLD	pTE1638/39	
21	binding12_mut2-r	GCACTCTCGTGCATCCGCAGAATCCAC GCATCGCA	KLD	pTE1639	
22	pIND4-f	GCTTAATTAGCTGAGCTTGGAC	Gibson assembly	pTE5000	
23	FLAG_pIND4-r	ATCGTCATCATCTTTGTAATCAATATCA TGGTCTTTGTAGTCACCGTCGTGATCC TTATAGTCCATGGTTAATTTCTCCTCTT TAATTCTAG	Gibson assembly	pTE5000	
24	FLAG_linker_1365-f	GATTACAAAGATGATGACGATAAACTT CATCCTAGGGCAGGGAGTGCGGCCGG CAGCG	Gibson assembly	pTE5000	
25	pIND4_1365-r	AAGCTCAGCTAATTAAGCCTAACCCTC CTCGAAGCTGAAGATC	Gibson assembly	pTE5000	
26	Pden1365-f_NOSTRT	CACAGAGAACAGATTGGTGCCCGAGG CGAGAAACTGATCATC	Gibson assembly	pTE5007	
27	pTB146_1365-r(2)	ACGGAGCTCTGCTCTTCTCTAACCCTC CTCGAAGCTGAAGATCG	Gibson assembly	pTE5007	
28	pLT1-f	GGTGCCCGAGGCGAGAAACTG	KLD	pTE5007	
29	pLT1-r	ACCAATCTGTTCTCTGTGAGCC	KLD	pTE5007	
30	D16020UpF1	CTTGCATGCCTGCAGGTCGACTCTAGA GCCACGGCGATGTAAAGCGACAAAAG	Gibson assembly	pMJ009	
31	D16020UpR1	GGTGCGCAGCCCCATCTCGCCGATTT CGTAAAGGTCTTTCTC	Gibson assembly	pMJ009	
32	D16020DnF1	ATCGGCGAGATGGGGCTGCGCACCTT TGAAGATG	Gibson assembly	pMJ009	
33	D16020DnR1	GAATTCGAGCTCGGTACCCGGGGATC CGGGCGGATTCCCACAGGAACG	Gibson assembly	pMJ009	
34	D16495UpF1	CTTGCATGCCTGCAGGTCGACTCTAGA CGGCACGGCTGGTCAAGGTCTG	Gibson assembly	pYN011	
35	D16495UpR1	CGTGTCGCCCAGGACCGCCTTGATCAT CTGCTG	Gibson assembly	pYN011	
36	D16495DnF1	ATCAAGGCGGTCCTGGGCGACACGTT CAAGGAGATG	Gibson assembly	pYN011	
37	D16495DnR1	GAATTCGAGCTCGGTACCCGGGGATC CACGGTTGGCTGCACTGGATCGAAG	Gibson assembly	pYN011	
38	D04520UpF1	CTTGCATGCCTGCAGGTCGACTCTAGA GCATGGACCGGATGGTGCTTTCG	Gibson assembly	pYN019	
39	D04520UpR3	TTCCATGTCGTCGCGCAGTTTCACACC GGCATAAAG	Gibson assembly	pYN019	
40	D04520DnF2	GTGAAACTGCGCGACGACATGGAACT GGGCAATCCG	Gibson assembly	pYN019	
41	D04520DnR2	GAATTCGAGCTCGGTACCCGGGGATC CCTGTCGGATCAAGGGCAACATCTC	Gibson assembly	pYN019	
42	D16525UpF1	CTTGCATGCCTGCAGGTCGACTCTAGA CGCACCAGTTCGACCTGAATTTCATAG C	Gibson assembly	pPK005	
43	D16525UpR1	CCACAGATAGCTCCGCACCCCCATGAA TGCCTTTG	Gibson assembly	pPK005	
44	D16525DnF1	ATGGGGGTGCGGAGCTATCTGTGGAT CGCCCGACAG	Gibson assembly	pPK005	

45	D16525DnR1	GAATTCGAGCTCGGTACCCGGGGATC CAGCGCGATGACCCTTGACGATG	Gibson assembly	pPK005	
46	bs_wt-f	TCTCGCCTCGGGCCATGTGACAAACCT TACAGATTCTGCGGATGCACGATGACA ATACTGACTGCCGCACCCATTGCTTT	BLITz		5'-biotinylation
47	bs_wt-r	AAAGCAATGGGTGCGGCAGTCAGTATT GTCATCGTGCATCCGCAGAATCTGTAA GGTTTGTCACATGGCCCGAGGCGAGA	BLITz		
48	bs_mut12-f	TCTCGCCTCGGGCCATGGAGTGCGAT GCGTGGATTCTGCGGATGCACGAGAG TGCGCTGTGTGGCCGCACCCATTGCTT T	BLITz		5'-biotinylation
49	bs_mut12-r	AAAGCAATGGGTGCGGCCACACAGCG CACTCTCGTGCATCCGCAGAATCCACG CATCGCACTCCATGGCCCGAGGCGAG A	BLITz		

3.6.3 Genetic manipulation of *P. denitrificans*

The transfer of plasmids to *P. denitrificans* was achieved by biparental mating using *E. coli* ST18 as a donor strain (50). The deletion of genes from the *P. denitrificans* genome was carried out as described (22) with LB medium being replaced with SOB medium. The transfer of replicative plasmids to *P. denitrificans* was done according to (51). The selection of transformants occurred on mineral salt medium supplemented with 120 mM methanol and appropriate antibiotics. The successful transfer of plasmids and the deletion of genes were verified by colony PCR. All strains and plasmids used in this study are listed in Table 2.

3.6.4 Genetic manipulation of *R. capsulatus*

R. capsulatus and *E. coli* cultures were grown overnight for at least 24 hours. *R. capsulatus* and *E. coli* S17-1 were allowed to conjugate for at least 24 hours to transfer the desired plasmids into *R. capsulatus*. *R. capsulatus* strains containing the plasmids were selected using PYE with 20 µg/mL kanamycin, followed by colony PCR. Plasmid-containing cells were grown in liquid PYE with no antibiotics for at least 24 hours. Cultures were then centrifuged, diluted, and plated on PYE agar + 10% sucrose or nutrient agar (NA) + 10% sucrose. Colonies were patch-plated in parallel onto PYE agar and PYE agar with antibiotics. Colonies that grew on PYE agar but not on PYE agar with antibiotics were identified as potential deletion or fusion strains. PCR was was performed to confirm the deletion of the desired gene.

3.6.5 Generation of plasmids

Plasmids pTE1630-pTE1632 were generated by amplification of the up- and downstream genomic regions of targeted genes from Pd1222 genomic DNA with oligonucleotides 1-12 and subsequent Gibson assembly (52) of matching PCR products as indicated in Table 3 with EcoRI-linearized, dephosphorylated pK18mobsacB. Plasmids pTE1633 and pTE1634 were generated by amplification of inserts from Pd1222 gDNA with oligonucleotides 13-16 and subsequent ligation of adequately restricted PCR products into equally restricted and dephosphorylated pTE714. Plasmids pTE1637-1639 were generated by inverse amplification of pTE1634 with oligonucleotides 17-21, followed by removal of the template strand with DpnI, phosphorylation and ligation (KLD reaction). Plasmid pTE5000 was generated by inverse amplification of pIND4 with oligonucleotides 22-23, amplification of Pden_1365 with oligonucleotides 24-25 from Pd1222 genomic DNA and subsequent Gibson assembly of the resulting fragments. Plasmid pTE5007 was generated in two stepts. First, the insert fragment was amplified from Pd1222 gDNA with oligonucleotides 26-27 and inserted into SapI-restricted pTB146 by Gibson assembly. A missing codon for a glycine-residue in the future Ulp1 recognition site was then inserted into the resulting construct by inverse amplification with oligonucleotides 28-29 and followed by a KLD reaction. Plasmids pMJ009, pYN011, pYN019, pPK005 were generated by amplification of upstream and downstream genomic regions of targeted genes from SB1003 genomic DNA and subsequent Gibson assembly of matching products according to Table 3 with BamHI- and XbaI-linearized, dephosphorylated pK18mobsacB. All oligonucleotides used in this study and their purpose are listed in Table 3.

3.6.6 Global transcriptome analysis

Samples for transcriptome analysis were taken in triplicates from succinate- and acetate-growing cultures of *P. denitrificans* Pd1222 and the Pd1222 Δ*ramB* deletion at OD_{600} 0.8. For sample collection, 2 mL of culture were transferred into sterile 2 mL Eppendorf tubes and pelleted by centrifugation at 10 000 x g and 4 °C for 10 min. Supernatant was discarded and samples were snap-frozen at – 80 °C. Storage of samples occurred at -80 °C until further usage. The Qiagen miRNeasy Kit was used for total RNA isolation starting from a pellet of 4 mL cultured cells.

The pellet was resuspended in 1 mL QiAzol lysis reagent and homogenized in a FastPrep sample preparation system using Lysing Matrix B containing 0.1 mm silica beads (MP biomedicals) and the following settings: 4x 6,500 rpm for 20 sec, 15 sec break. The supernatant was transferred into a new tube and RNA isolation was performed according to the manufacturer's instruction including the optional on column DNaseI digestion. Depletion of rRNA was performed and cDNA libraries were prepared with the Illumina® Stranded Total RNA Prep Kit (Ligation with Ribo-Zero Plus; Illumina, USA). Library quality was assessed with the fragment analyzer employing the Agilent HS NGS Fragment kit (Agilent, USA). Quantification of libraries was done by qPCR and the KAPA library quantification Kit (Roche, Switzerland) in a qTOWER3 G Thermal Cycler (Analytic Jena, Germany). Libraries were paired-end sequenced on an Illumina MiSeq using the MiSeq reagent kit V3 featuring 150 bp read length. Sequencing data are available from ArrayExpress (reference number: E-MTAB-12482). The differential gene expression analysis was done as described elsewhere (53) using the RNA-seq pipeline Curare 0.3.1 (https://github.com/pblumenkamp/Curare). Briefly, reads were preprocessed with Trim Galore 0.6.7 (54) and Cutadapt 3.5 (55) with a quality and length threshold setting of 20 (phred score and base pairs, respectively). Preprocessed reads were aligned to the Pden1222 genome (chromosome 1: NC_008686.1, chromosome 2: NC_008687.1, plasmid: NC_008688.1) using Bowtie2 2.4.4 in "very-sensitive" mode and with "–mm" option (56).The resulting SAM/BAM files were processed with SAMtools 1.13 (57). Read-to-feature assignment was done using featureCounts (58) of the subread 2.0.1 package (59). Normalized read counts were then calculated and differential gene expression determined with DESeq2 1.32.0 (Supplementary Tables 1-4 (see Appendix)) (60). For verification and analysis of the results, GenExVis 0.4.1 (https://github.com/pblumenkamp/GenExVis) was used.

3.6.7 Synthesis of CoA esters

Synthesis of CoA esters was performed as described (61) unless specified otherwise. β-Methylmalyl-CoA was synthesized from propionyl-CoA and a 12-fold molar excess of glyoxylate (in buffer: 100 mM MOPS/KOH pH 7.5, 5 mM $MgCl_2$) using heterologously expressed and purified *Rhodobacter sphaeroides* Mcl-1

(accession number ACI22682) as catalyst. The resulting esters were purified via preparative HPLC-MS with a 1260 Infinity II LC System (Agilent, USA) in combination with a 6130 Single Quadrupole LC/MS (Agilent, USA). Lyophilized CoA esters were stored at -80 °C and dissolved in ddH_2O before use. The concentrations of the respective CoA esters were determined photometrically using a Carry 60 UV-Vis spectrophotometer (Agilent, USA) and calculated from the absorbance at 260 nm using defined extinction coefficients (22,300 M^{-1} cm^{-1} for α-β-unsaturated fatty acid CoA thioesters and 16,400 M^{-1} cm^{-1} for saturated ones). The amount of free sulfhydryl groups (indicating free CoA) present in the samples was quantified by treatment with Ellman's reagent (DNTB) in EDTA-HEPES/KOH buffer (15 mM EDTA, 200 mM HEPES-KOH pH 7.8) and subsequent measurement of the absorbance at 412 nm (extinction coefficient: 14,000 M^{-1} cm^{-1}).

3.6.8 Heterologous production and purification of proteins

6xhis-sumo-ramB was heterologously expressed from plasmid pTE5007, respectively, in *E. coli* BL21 AI (Novagen, Germany) grown in terrific broth (TB; 24 g/L yeast extract, 20 g/L tryptone, 0.017 M KH_2PO_4, 0.072 M K_2HPO_4, 10 % (w/v) glycerol) in the presence of ampicillin. Gene expression was induced by addition of 0.25 % arabinose and 0.5 mM IPTG when the cultures had reached an OD_{600} of 1.0-2.0. *6xhis-ulp1* was expressed from plasmid pTB145 (62) in *E. coli* Rosetta™ (DE3)pLysS (Novagen, Germany) grown in TB supplemented with ampicillin and gentamycin. Gene expression was induced by addition of 0.5 mM IPTG when cultures had reached an OD_{600} of 1.0-2.0. Overproduction of all proteins occurred at 25°C overnight and was verified by SDS-PAGE analysis of culture samples taken before and after induction. The cultures were harvested by centrifugation at 8,000 x g and 10°C for 15 min. For lysis, the cells were resuspended in buffer A (50 mM Tris, 500 mM NaCl, pH 7.8) supplemented with 0.5 mM DTT, DNase I, and 5 mM $MgCl_2$ and treated by 4 cycles of sonication (50 %, 1s pulse, 60 s) using a Sonopuls GM200 sonicator (BANDELIN, Germany). Cell lysates were cleared by ultracentrifugation at 100 000 x g and 4 °C for 45 min followed by filtration through a Filtropur S 0.45 µm filter (Sarstedt, Germany). His-tagged proteins in cell lysate were loaded on pre-equilibrated Ni-NTA agarose beads in Protino drop down columns (Macherey-Nagel, Germany), washed with buffer A and eluted with

increasing concentrations of buffer B (50 mM Tris, 500 mM NaCl, 500 mM imidazole, pH 7.8). Buffer exchange was performed with Cytiva PD-10 Desalting columns (Cytiva, USA) and elution in desalting buffer (50 mM Tris, 350 mM NaCl, 10% glycerol, pH 7.8). His-SUMO tag was cleaved off by treatment of the fusion proteins with His-Ulp1 protease (1 U per 2 µg of target protein) in desalting buffer, followed by removal of His-SUMO protein with pre-equilibrated Ni-NTA agarose beads. Successful purification of proteins, as well as proteolytic cleavage of tags was verified by SDS-PAGE. Protein concentrations were determined using a NanoDrop™ 2000 (Thermo Scientific, USA).

3.6.9 Mass photometry

The molecular weights of protein-protein/protein-DNA complexes were determined in phosphate buffered saline (PBS; pH 7.4) on 1.5 H, 24 x 60 mm microscope coverslips (Carl Roth, Germany) and Culture Well™ Reusable Gaskets (GRACE BIO-LABS, USA) using a Refeyn One^{MP} mass photometer (Refeyn Ltd, UK) with the AcquireMP software (Refeyn Ltd, UK). A previously measured standard was used at a concentration of 20 nM as a reference. The processing and analysis of mass photometry images was performed using DiscoverMP (Refeyn Ltd, UK).

3.6.10 Biolayer interferometry (BLI)

The analysis of protein-DNA interactions by BLI was performed using Sartorius Octet® SAX2 biosensors in binding buffer (desalting buffer supplemented with 0.01 % Tween 20 and 10 µM bovine serum albumin (BSA)) on a BLItz® platform (FortéBio, USA). Biotinylated dsDNA at 40 µM concentration was generated by annealing oligos 46 and 47 for wt DNA with intact binding sites and oligos 48 and 49 (Table 3) for DNA with mutated binding sites in Phusion high GC buffer (Thermo Scientific, USA) dsDNA stocks were diluted 20-fold in binding buffer to reach a working concentration of 2 µM. To immobilize biotinylated dsDNA fragments on the biosensor tips, 4 µL of the 2 µM stock were applied to the sample drop holder and the biosensor tip was placed in it. DNA loading was followed for 120 s until equilibrium was reached. Afterwards, the biosensor tip was transferred back into binding buffer to wash off excess DNA fragments for 30 s. The association of protein with the DNA-loaded biosensor tip was followed as described for DNA

loading. After each sample loading step, the sample drop holder was cleaned with 0.5 M NaOH, followed by two washes with ddH_2O. After the association step, the biosensor tip was transferred into binding buffer again and protein dissociation was followed for 120 s. A new biosensor tip was used for each measurement.

Data availability

Sequencing data are available from ArrayExpress (reference number: E-MTAB-12482).

Author contributions

K.K., T.J.E., and M.S.C. designed the study. K.K. planned and performed all genetic and biochemical experiments except for the studies with *R. capsulatus* SB1003. M.S.C. created and analyzed the ScfR sequence similarity network (SSN). K.K., Y.T.N., S.M., and M.S.C. conducted *in silico* identification of the RamB binding sites. D.M., A.B., J.S., P.B., and A.G. generated and analyzed RNAseq data from Pd1222 samples taken by K.K.. M.T. supervised the biolayer interferometry (BLI) experiments. G.K.A.H. supervised the mass photometry (MP) experiments. L.T. contributed to Pd1222 RamB *in vitro* analyses. J.Z. synthesized and purified CoA esters and performed *in silico* structural analysis of Pd1222 RamB. N.P. conduced the LC-MS analysis of the Pd1222 exometabolome from samples taken by K.K.. S.M. and A.R.N. performed genetic studies with *R. capsulatus* SB1003. K.K. and T.J.E. wrote the manuscript.

Acknowledgements

We acknowledge technical assistance by the Bioinformatics Core Facility at the professorship of Systems Biology at JLU Giessen and provision of compute resources and general support by the BiGi service center (BMBF grant 031A533) within the de.NBI network." The RNA-Seq bioinformatics analysis was supported by the German Research Foundation (DFG FOR5116 - project number 43319410).

3.7 References

1. Schada Von Borzyskowski L, Bernhardsgrütter I, Erb TJ. 2020. Biochemical unity revisited: microbial central carbon metabolism holds new discoveries, multi-tasking pathways, and redundancies with a reason. Biol Chem 401:1429–1441.

2. Kornberg HL, Madsen NB. 1957. Synthesis of C4-dicarboxylic acids from acetate by a "glyoxylate bypass" of the tricarboxylic acid cycle. Biochim Biophys Acta 24:651–653.

3. Kornberg HL, Krebs HA. 1957. Synthesis of cell constituents from C2-Units by a modified tricarboxylic acid cycle. Nature 179:988–991.

4. Erb TJ, Berg IA, Brecht V, Müller M, Fuchs G, Alber BE. 2007. Synthesis of C5-dicarboxylic acids from C2-units involving crotonyl-CoA carboxylase/reductase: The ethylmalonyl-CoA pathway. Proc Natl Acad Sci U S A 104:10631–10636.

5. Peyraud R, Kiefer P, Christen P, Massou S, Portais JC, Vorholt JA. 2009. Demonstration of the ethylmalonyl-CoA pathway by using ^{13}C metabolomics. Proc Natl Acad Sci U S A 106:4846–4851.

6. Han L, Reynolds KA. 1997. A novel alternate anaplerotic pathway to the glyoxylate cycle in Streptomycetes. J Bacteriol 179:5157–5164.

7. Alber BE, Spanheimer R, Ebenau-Jehle C, Fuchs G. 2006. Study of an alternate glyoxylate cycle for acetate assimilation by *Rhodobacter sphaeroides*. Mol Microbiol 61:297–309.

8. Horswill AR, Escalante-Semerena JC. 1999. *Salmonella typhimurium* LT2 catabolizes propionate via the 2-methylcitric acid cycle. J Bacteriol 181:5615–5623.

9. Horswill AR, Escalante-Semerena JC. 1997. Propionate catabolism in *Salmonella typhimurium* LT2: two divergently transcribed units comprise the *prp* locus at 8.5 centisomes, *prpR* encodes a member of the sigma-54 family of activators, and the *prpBCDE* genes constitute an operon. J Bacteriol 179:928–940.

10. Upton AM, McKinney JD. 2007. Role of the methylcitrate cycle in propionate metabolism and detoxification in *Mycobacterium smegmatis*. Microbiology (Reading) 153:3973–3982.

11. Tabuchi T, Hara S. 1974. Production of 2-methylisocitric acid from n-paraffins by mutants of *Candida lipolytica.* Agric Biol Chem 38:1105–1106.

12. Erb TJ, Fuchs G, Alber BE. 2009. (2S)-Methylsuccinyl-CoA dehydrogenase closes the ethylmalonyl-CoA pathway for acetyl-CoA assimilation. Mol Microbiol 73:992–1008.

13. Dolan SK, Welch M. 2018. The glyoxylate shunt, 60 years on. Annual review of microbiology *72*, 309-330.

14. Erb TJ, Brecht V, Fuchs G, Müller M, Alber BE. 2009. Carboxylation mechanism and stereochemistry of crotonyl-CoA carboxylase/reductase, a carboxylating enoyl-thioester reductase. Proc Natl Acad Sci U S A 106:8871–8876.

15. Russell JB, Cook GM. 1995. Energetics of bacterial growth: balance of anabolic and catabolic reactions. Microbiol Rev 59:48–62.

16. Laporte DC, Koshland DE. 1982. A protein with kinase and phosphatase activities involved in regulation of tricarboxylic acid cycle. Nature 300:458–460.

17. Garnak M, Reeves HC. 1979. Phosphorylation of isocitrate dehydrogenase of *Escherichia coli*. Science 203:1111–1112.

18. Cortay JC, Negre D, Galinier A, Duclos B, Perriere G, Cozzone AJ. 1991. Regulation of the acetate operon in *Escherichia coli*: purification and functional characterization of the IclR repressor. EMBO J 10:675–679.

19. Gui L, Sunnarborg A, Laporte DC. 1996. Regulated expression of a repressor protein: FadR activates *iclR*. J Bacteriol 178:4704.

20. Hu B, Lidstrom M. 2012. CcrR, a TetR family transcriptional regulator, activates the transcription of a gene of the ethylmalonyl coenzyme A pathway in *Methylobacterium extorquens* AM1. J Bacteriol 194:2802–2808.

21. Alber BE. 2010. Biotechnological potential of the ethylmalonyl-CoA pathway. Applied Microbiology and Biotechnology 2010 89:1 89:17–25.

22. Kremer K, van Teeseling MCF, von Borzyskowski LS, Bernhardsgrütter I, van Spanning RJM, Gates AJ, Remus-Emsermann MNP, Thanbichler M, Erb TJ. 2019. Dynamic metabolic rewiring enables efficient acetyl coenzyme A assimilation in *Paracoccus denitrificans*. mBio 10.

23. Petushkova E, Mayorova E, Tsygankov A. 2021. TCA cycle replenishing pathways in photosynthetic purple non-sulfur bacteria growing with acetate. Life 11.

24. Fendt SM, Frezza C, Erez A. 2020. Targeting metabolic plasticity and flexibility dynamics for cancer therapy. Cancer Discov 10:1797–1807.

25. Andrzejewski S, Klimcakova E, Johnson RM, Tabariès S, Annis MG, McGuirk S, Northey JJ, Chénard V, Sriram U, Papadopoli DJ, Siegel PM, St-Pierre J. 2017. PGC-1α Promotes

Breast Cancer Metastasis and Confers Bioenergetic Flexibility against Metabolic Drugs. Cell Metab 26:778-787.e5.

26. Dupuy F, Tabariès S, Andrzejewski S, Dong Z, Blagih J, Annis MG, Omeroglu A, Gao D, Leung S, Amir E, Clemons M, Aguilar-Mahecha A, Basik M, Vincent EE, St.-Pierre J, Jones RG, Siegel PM. 2015. PDK1-dependent metabolic reprogramming dictates metastatic potential in breast cancer. Cell Metab 22:577–589.

27. Loo JM, Scherl A, Nguyen A, Man FY, Weinberg E, Zeng Z, Saltz L, Paty PB, Tavazoie SF. 2015. extracellular metabolic energetics can promote cancer progression. Cell 160:393.

28. Jiang L, Shestov AA, Swain P, Yang C, Parker SJ, Wang QA, Terada LS, Adams ND, McCabe MT, Pietrak B, Schmidt S, Metallo CM, Dranka BP, Schwartz B, Deberardinis RJ. 2016. Reductive carboxylation supports redox homeostasis during anchorage-independent growth. Nature 532:255–258.

29. Labuschagne CF, Cheung EC, Blagih J, Domart MC, Vousden KH. 2019. Cell clustering promotes a metabolic switch that supports metastatic colonization. Cell Metab 30:720-734.e5.

30. Moradali MF, Davey ME. 2021. Metabolic plasticity enables lifestyle transitions of *Porphyromonas gingivalis*. npj Biofilms and Microbiomes 7:1–13.

31. Allison SD, Martiny JBH. 2008. Resistance, resilience, and redundancy in microbial communities. Proc Natl Acad Sci U S A 105:11512.

32. Comte J, Fauteux L, del Giorgio PA. 2013. Links between metabolic plasticity and functional redundancy in freshwater bacterioplankton communities. Front Microbiol 4.

33. Trivedi CB, Stamps BW, Lau GE, Grasby SE, Templeton AS, Spear JR. 2020. Microbial metabolic redundancy is a key mechanism in a sulfur-rich glacial ecosystem. mSystems 5.

34. Nayak DD, Marx CJ. 2014. Methylamine utilization via the N-methylglutamate pathway in *Methylobacterium extorquens* PA1 involves a novel flow of carbon through C1 assimilation and dissimilation pathways. J Bacteriol 196:4130–4139.

35. Nayak DD, Marx CJ. 2015. Experimental horizontal gene transfer of methylamine dehydrogenase mimics prevalent exchange in nature and overcomes the methylamine growth constraints posed by the sub-optimal N-Methylglutamate pathway. Microorganisms 3:60–79.

36. Carter MS, Alber BE. 2015. Transcriptional regulation by the short-chain fatty acyl coenzyme A regulator (ScfR) PccR controls propionyl coenzyme A assimilation by *Rhodobacter sphaeroides*. J Bacteriol 197:3048–3056.

37. Zallot R, Oberg N, Gerlt JA. 2019. The EFI web resource for genomic enzymology tools: leveraging protein, genome, and metagenome databases to discover novel enzymes and metabolic pathways. Biochemistry 58:4169–4182.

38. Shannon P, Markiel A, Ozier O, Baliga NS, Wang JT, Ramage D, Amin N, Schwikowski B, Ideker T. 2003. Cytoscape: a software environment for integrated models of biomolecular interaction networks. Genome Res 13:2498–2504.

39. Tang S, Hicks ND, Cheng YS, Silva A, Fortune SM, Sacchettini JC. 2019. Structural and functional insight into the *Mycobacterium tuberculosis* protein PrpR reveals a novel type of transcription factor. Nucleic Acids Res 47:9934–9949.

40. Masiewicz P, Brzostek A, Wolański M, Dziadek J, Zakrzewska-Czerwińska J. 2012. A novel role of the PrpR as a transcription factor involved in the regulation of methylcitrate pathway in *Mycobacterium tuberculosis.* PLoS One 7.

41. Gerstmeir R, Cramer A, Dangel P, Schaffer S, Eikmanns BJ. 2004. RamB, a novel transcriptional regulator of genes involved in acetate metabolism of *Corynebacterium glutamicum*. J Bacteriol 186:2798–2809.

42. Ind AC, Porter SL, Brown MT, Byles ED, de Beyer JA, Godfrey SA, Armitage JP. 2009. Inducible-expression plasmid for *Rhodobacter sphaeroides* and *Paracoccus denitrificans*. Appl Environ Microbiol 75:6613.

43. Bailey TL, Elkan C. 1994. Fitting a mixture model by expectation maximization to discover motifs in biopolymers.

44. Waterhouse A, Bertoni M, Bienert S, Studer G, Tauriello G, Gumienny R, Heer FT, de Beer TAP, Rempfer C, Bordoli L, Lepore R, Schwede T. 2018. SWISS-MODEL: homology modelling of protein structures and complexes. Nucleic Acids Res 46:W296–W303.

45. Young G, Hundt N, Cole D, Fineberg A, Andrecka J, Tyler A, Olerinyova A, Ansari A, Marklund EG, Collier MP, Chandler SA, Tkachenko O, Allen J, Crispin M, Billington N, Takagi Y, Sellers JR, Eichmann C, Selenko P, Frey L, Riek R, Galpin MR, Struwe WB, Benesch JLP, Kukura P. 2018. Quantitative mass imaging of single biological macromolecules. Science 360:423–427.

46. Cole D, Young G, Weigel A, Sebesta A, Kukura P. 2017. Label-free single-molecule imaging with numerical-aperture-shaped interferometric scattering microscopy. ACS Photonics 4:211–216.

47. Petushkova EP, Tsygankov AA. 2017. Acetate metabolism in the purple non-sulfur bacterium *Rhodobacter capsulatus*. Biochemistry (Mosc) 82:587–605.

48. Maruyama K, Kitamura H. 1985. mechanisms of growth inhibition by propionate and restoration of the growth by sodium bicarbonate or acetate in *Rhodopseudomonas sphaeroides S*. The Journal of Biochemistry 98:819–824.

49. Hahnke SM, Moosmann P, Erb TJ, Strous M. 2014. An improved medium for the anaerobic growth of *Paracoccus denitrificans* Pd1222. Front Microbiol 5.

50. Thoma S, Schobert M. 2009. An improved *Escherichia coli* donor strain for diparental mating. FEMS Microbiol Lett 294:127–132.

51. Schada von Borzyskowski L, Severi F, Krüger K, Hermann L, Gilardet A, Sippel F, Pommerenke B, Claus P, Cortina NS, Glatter T, Zauner S, Zarzycki J, Fuchs BM, Bremer E, Maier UG, Amann RI, Erb TJ. 2019. Marine Proteobacteria metabolize glycolate via the β-hydroxyaspartate cycle. Nature 575:500–504.

52. Gibson DG, Young L, Chuang RY, Venter JC, Hutchison CA, Smith HO. 2009. Enzymatic assembly of DNA molecules up to several hundred kilobases. Nature Methods 6:343–345.

53. Kuzmich S, Blumenkamp P, Meier D, Szadkowski D, Goesmann A, Becker A, Søgaard-Andersen L. 2022. CRP-Like Transcriptional regulator MrpC curbs c-di-GMP and 3',3'-cGAMP nucleotide levels during development in *Myxococcus xanthus*. mBio 13.

54. Krueger F, James F, Ewels P, Afyounian E, Schuster-Boeckler B. FelixKrueger/TrimGalore: v0.6.7 - DOI via Zenodo (0.6.7).

55. Martin M. 2011. Cutadapt removes adapter sequences from high-throughput sequencing reads. EMBnet J 17:10–12.

56. Langmead B, Salzberg SL. 2012. Fast gapped-read alignment with Bowtie 2. Nat Methods 9:357–359.

57. Li H, Handsaker B, Wysoker A, Fennell T, Ruan J, Homer N, Marth G, Abecasis G, Durbin R. 2009. The sequence alignment/map format and SAMtools. Bioinformatics 25:2078–2079.

58. Liao Y, Smyth GK, Shi W. 2014. featureCounts: an efficient general purpose program for assigning sequence reads to genomic features. Bioinformatics 30:923–930.

59. Liao Y, Smyth GK, Shi W. 2019. The R package Rsubread is easier, faster, cheaper and better for alignment and quantification of RNA sequencing reads. Nucleic Acids Res 47.

60. Love MI, Huber W, Anders S. 2014. Moderated estimation of fold change and dispersion for RNA-seq data with DESeq2. Genome Biol 15.

61. Peter DM, Vögeli B, Cortina NS, Erb TJ. 2016. A chemo-enzymatic road map to the synthesis of CoA esters. Molecules 21.

62. Bendezú FO, Hale CA, Bernhardt TG, de Boer PAJ. 2009. RodZ (YfgA) is required for proper assembly of the MreB actin cytoskeleton and cell shape in *Escherichia coli*. EMBO J 28:193.

63. Simon R, Priefer U, Pühler A. 1983. A broad host range mobilization system for in vivo genetic engineering: transposon mutagenesis in Gram negative bacteria. Bio/Technology 1:784–791.

64. de Vries GE, Harms N, Hoogendijk J, Stouthamer AH. 1989. Isolation and characterization *of Paracoccus denitrificans* mutants with increased conjugation frequencies and pleiotropic loss of a (nGATCn) DNA-modifying property. Archives of Microbiology 152:52–57.

65. Wang P, Yu Z, Li B, Cai X, Zeng Z, Chen X, Wang X. 2015. Development of an efficient conjugation-based genetic manipulation system for *Pseudoalteromonas*. Microb Cell Fact 14:1–11.

66. Schada Von Borzyskowski L, Remus-Emsermann M, Weishaupt R, Vorholt JA, Erb TJ. 2015. A set of versatile brick vectors and promoters for the assembly, expression, and integration of synthetic operons in *Methylobacterium extorquens* AM1 and other Alphaproteobacteria. ACS Synth Biol 4:430–443.

3.8 Supplementary Information

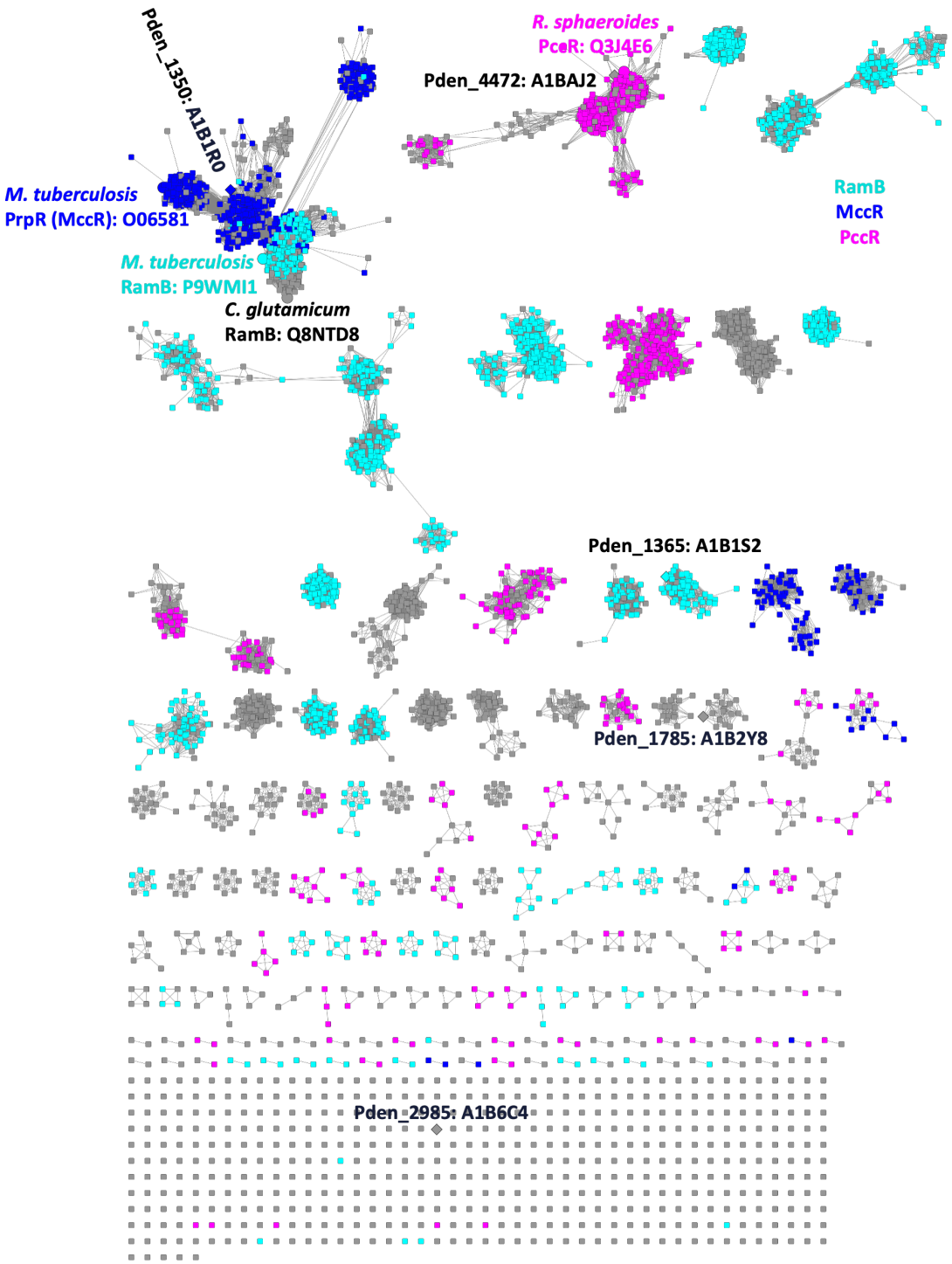

Supplementary Figure 1: Sequence similarity network (SSN) of the ScfR family (PF09856). The network was generated by EFI-EST using UniProt version 2022_03 and InterPro version 90. Nodes represent proteins from the ScfR family. Lines (edges) connect nodes whose proteins are related by alignment scores better than e^{-151}. EFI-GNT was used to identify conserved genome neighborhoods that encoded the proteins from the SSN in the figure. Nodes are colored according

to the neighborhoods in which the respective proteins are encoded. Proteins identified as RamB (teal) are encoded in neighborhoods that included *aceA* and/or *aceB*. Proteins identified as MccR (blue) are encoded in neighborhoods that include at least two of the following: *prpB*, *prpC*, or *prpD*. Proteins identified as PccR (pink) are encoded in neighborhoods that included *pccA, pcc*B, or *mcm*. Proteins represented by gray nodes are not encoded in neighborhoods that included the aforementioned genes. Circular nodes are marked with the Swiss-Prot annotation and UniProt identifiers of the respective proteins. Diamond nodes represent proteins of *Paracoccus denitrificans* Pd1222 and are labeled with the respective Pden_ gene tags and UniProt identifiers in black.

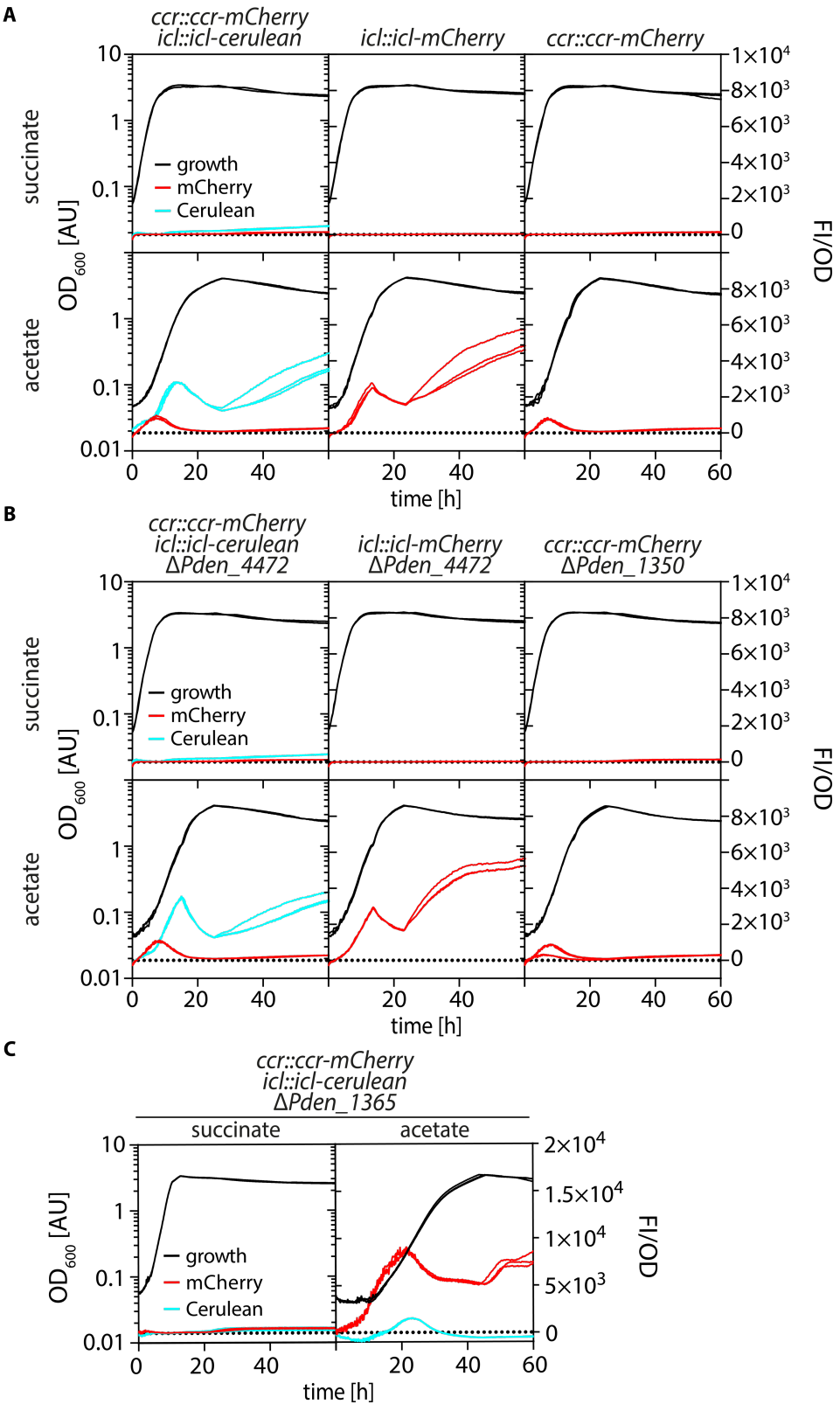

Supplementary Figure 2: Deletion of *scfR* homologues in different Pd1222 reporter backgrounds. Growth is given as OD_{600} on the left y-axis. Fluorescence normalized to OD_{600} is depicted on the right y-axis. Replicates are shown as individual curves. Genotypes indicating the respective fluorescent fusions present in the different strains are given above the panels. Growth

and fluorescence of unaffected *scfR* mutants (B) and their parental strains (A) on succinate (upper rows) and acetate (lower rows). (C) Growth and fluorescence of *ccr::ccr-mCherry icl::icl-cerulean* Δ*Pden_1365* (TJE-KK20) on succinate and acetate.

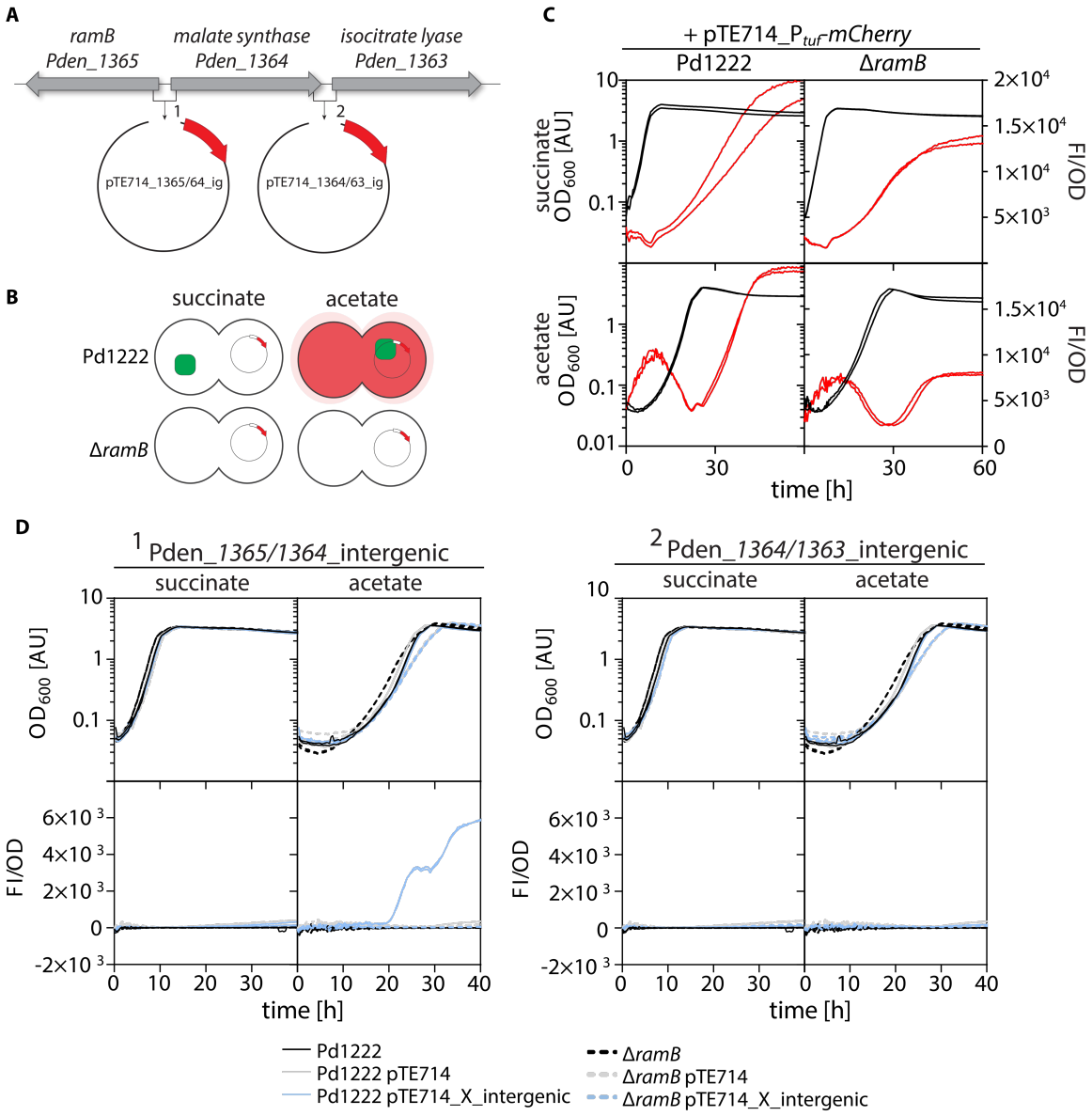

Supplementary Figure 3: The genes of the GC are organized in an operon. (A) Simplified depiction of the GC genes in reverse complement. *icl* (*Pden_1363*) and *ms* (*Pden_1364*) are separated by an intergenic region of 120 bp. *ms* and *ramB* (*Pden_1365*) are separated by 134 bp. The individual intergenic regions including 50 bp of their respective flanking open reading frames (ORFs) were integrated into plasmid pTE714, yielding plasmids pTE714_1365/64_ig (pTE1634) and pTE714_1364/63_ig (pTE1633), respectively. In the resulting plasmids, the intergenic regions are followed by an otherwise promoterless *mCherry* gene. (B) Predicted outcome of the reporter assay. In wild-type Pd1222, RamB is present but inactive during growth on succinate. When shifted to acetate, the regulator is activated and induces gene expression from the promoter region of its target gene. If the reporter plasmid present in the cell carries this region, expression of *mCherry*

will be induced, resulting in fluorescence of the cell. In the Δ*ramB* mutant, gene expression from the reporter plasmids cannot be induced due to the lack of regulator. (C and D) Growth and fluorescence of Pd1222 and Pd1222 Δ*ramB* carrying different variants of pTE714. Growth is depicted as OD_{600} on the left y-axis. Fluorescence corrected by OD_{600} is given on the right y-axis. (C) Positive controls. The Pd1222 strains carry a derivative of pTE714 (pTE770) with *mCherry* under the control of the constitutive P_{tuf} promoter. Here, an mCherry signal was detected in all strains under all conditions, verifying the functionality of the *mCherry* gene as a reliable reporter. (D) Fluorescence reporter assay with Pd1222 strains carrying different versions (1 or 2) of the reporter constructs indicated above the panels.

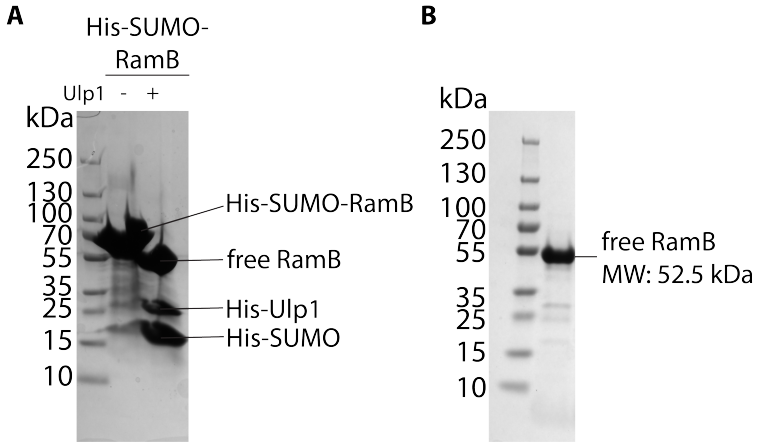

Supplementary Figure 4: Purification of free Pden_1365 ($RamB_{Pd}$). Molecular weights: His-SUMO-Pden_1365 (65.2 kDa), free Pden_1365 (52.5 kDa), His-Ulp1 (27.0 kDa), His-SUMO-tag (12.7 kDa). (A) SDS gel with His-SUMO-Pden_1365 after purification via affinity chromatography from BL21 AI cell extracts before (-) and after proteolytic cleavage with His-Ulp1 (+). (B) SDS-gel with free Pden_1365 after removal of His-Ulp1 and the cleaved His-SUMO-tag.

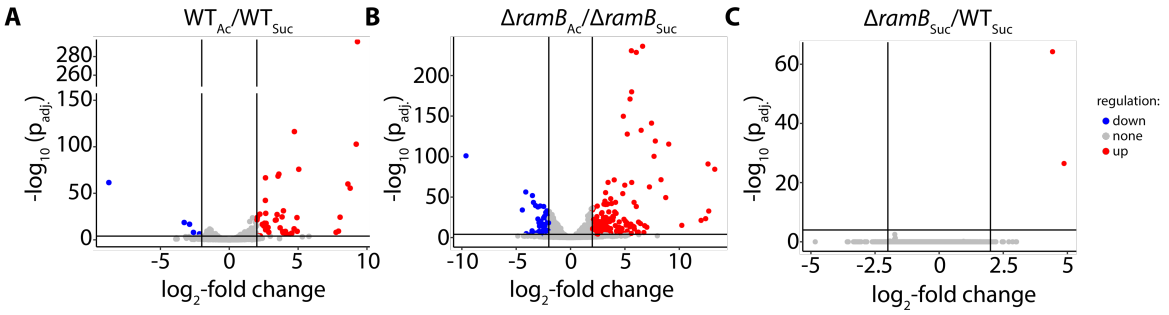

Supplementary Figure 5: Volcano plots showing the regulation of genes in Pd1222 WT and Δ*ramB* under different conditions. Dots represent individual genes. Thresholds above which genes were considered significantly up- or downregulated are indicated by black lines. (A) Regulation of genes in Pd1222 WT during growth on acetate vs. succinate. (B) Regulation of genes in Pd1222 Δ*ramB* during growth on acetate vs. succinate. (C) Regulation of genes on succinate in Pd1222 Δ*ramB* vs. WT.

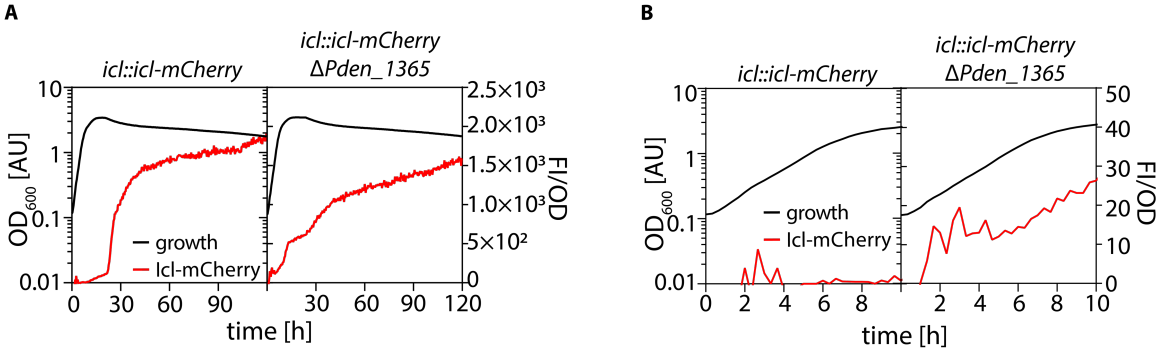

Supplementary Figure 6: Growth and fluorescence of Pd1222 *icl::icl-mCherry* (TJE-KK3) and Pd1222 *icl::icl-mCherry* Δ*Pden_1365* (TJE-KK16) on succinate. Growth is depicted as OD_{600} on the left y-axes, fluorescence normalized to OD_{600} is given as on the right y-axes. Shown are data from the same experiment as in Figure 2 with an adjusted right y-axis (A) and adjusted right y- and x-axes (B) for a better representation of the basal mCherry fluorescence observed during exponential growth of the strains on succinate.

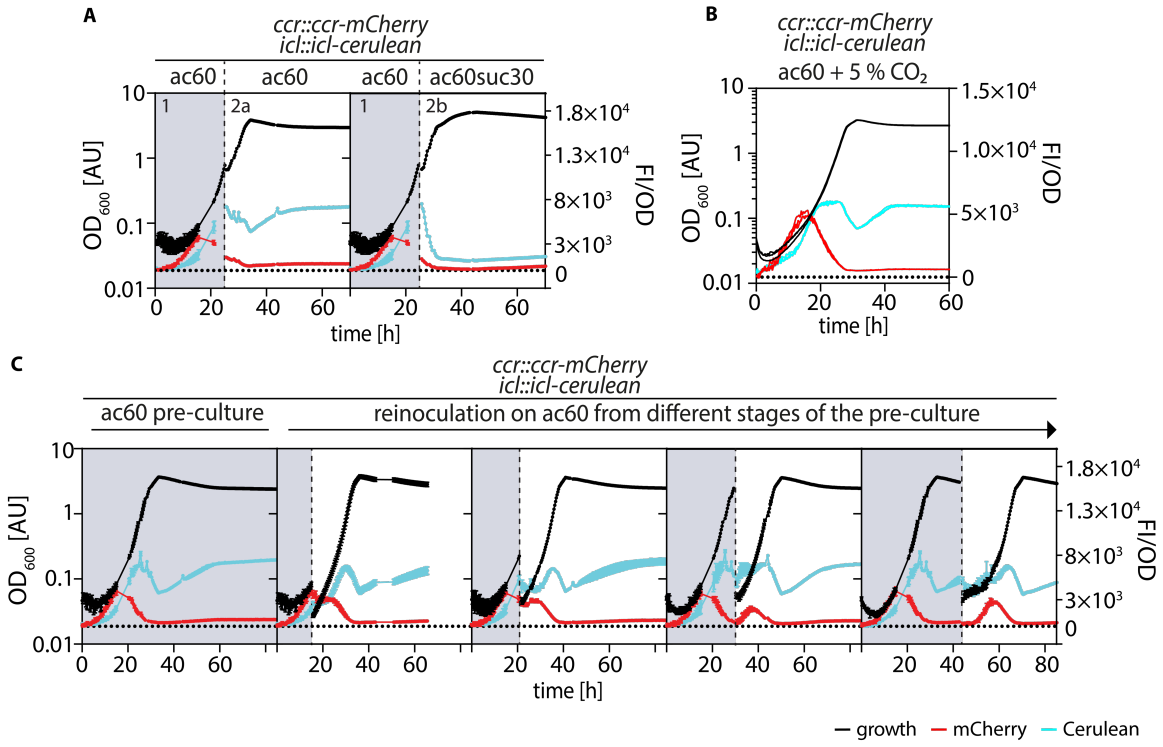

Supplementary Figure 7: Influence of additional carbon sources and pre-culture growth state on *ccr* and *icl* expression. Growth and fluorescence of Pd1222 *ccr::ccr-mCherry icl::icl-cerulean* (TJE-KK12) on different carbon sources. Growth is given as OD_{600} on the left y-axes, fluorescence normalized to OD_{600} is depicted as on the right y-axes. (A) Cells were grown to mid-exponential phase on 60 mM acetate (1; gray background), then washed and resuspended in fresh 60 mM acetate medium (2a; white background) or 60 mM acetate medium supplemented with 30 mM succinate (2b; white background). (B) Cells were grown on 60 mM acetate with a constant supply with 5 % CO_2 in the atmosphere. (C) Cells were grown to different growth stages in 60 mM

acetate medium (gray background) and used to re-inoculate fresh cultures to a starting OD_{600} of 0.05 (white background).

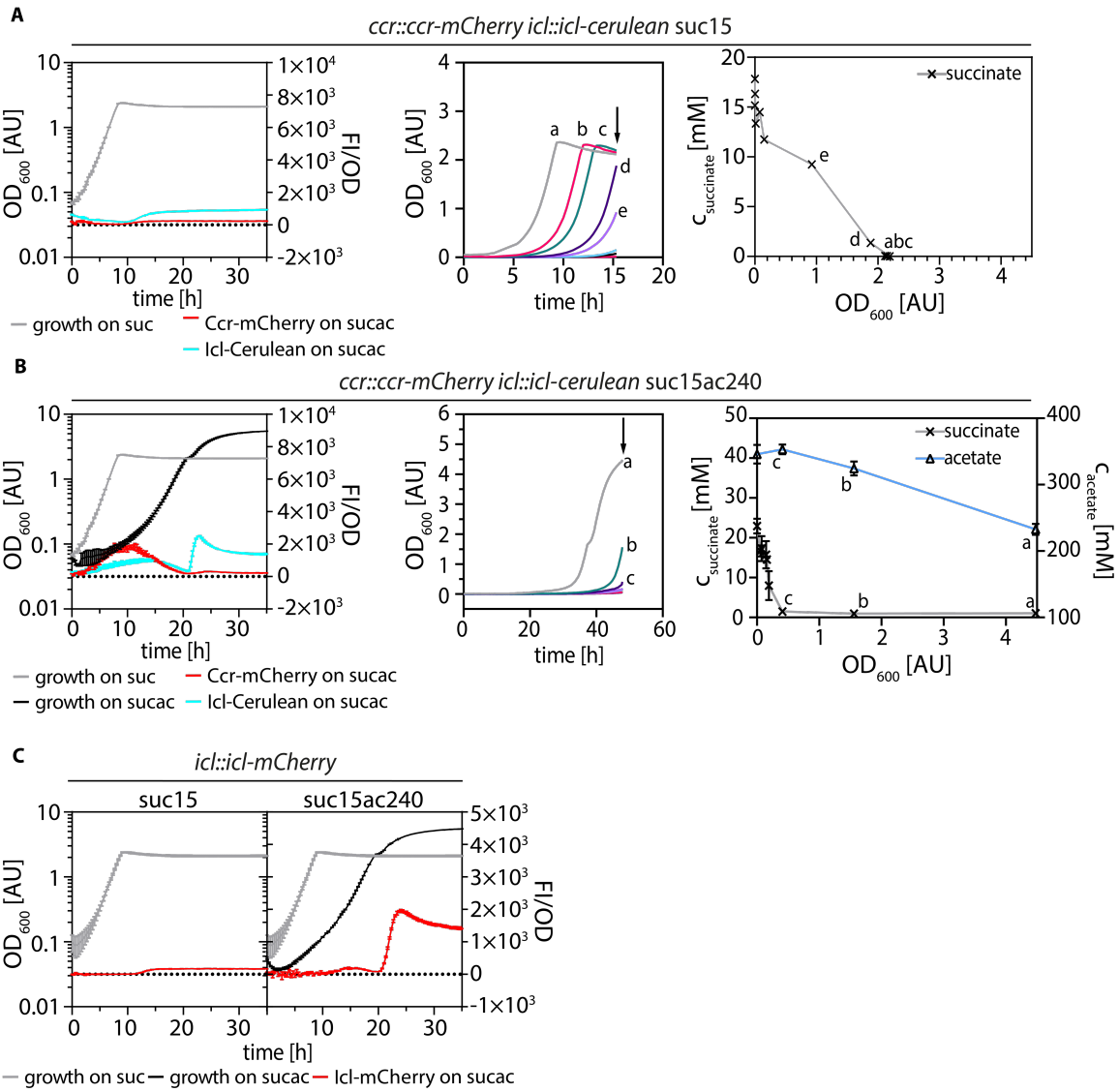

Supplementary Figure 8: Expression of the GC occurs only upon metabolization of acetate. Growth is depicted as OD_{600} on the left y-axes, fluorescence normalized to OD_{600} is depicted as on the right y-axes. (A) Left panel: Growth and fluorescence of Pd1222 *ccr::ccr-mCherry icl::icl-cerulean* (TJE-KK12) on 15 mM succinate. Middle panel: Growth of TJE-KK12 on 15 mM succinate to different optical densities. At the timepoints indicated by arrows, growth was stopped and the cultures were passed through a MultiScreen$_{HTS}$-GV 0.22 µM filter plate (Millipore, Germany) to remove cells from the spent medium. Spent medium was then analyzed for the concentrations of succinate and acetate by LC-MS as shown in the right panel. Right panel: Concentrations of succinate and acetate in spent medium of the cultures shown in the middle panel after removal of cells. The measured carbon source concentrations are plotted versus the corresponding OD_{600} of the cultures prior to filtration. (B) Left panel: Growth and fluorescence of TJE-KK12 on 15 mM succinate plus 240 mM acetate (black). To demonstrate the maximal reachable OD_{600} on 15 mM

succinate only, the growth of TJE-KK12 on 15 mM succinate is shown in addition (gray). Middle and right panels: as described in (A). (C) Growth and fluorescence of Pd1222 *icl::icl-mCherry* (TJE-KK3) on 15 mM succinate (left panel, gray curve) and 15 mM succinate plus 240 mM acetate (right panel, black curve). To demonstrate the maximal reachable OD_{600} on 15 mM succinate only, the growth of TJE-KK12 on 15 mM succinate is additionally shown in the right panel (gray).

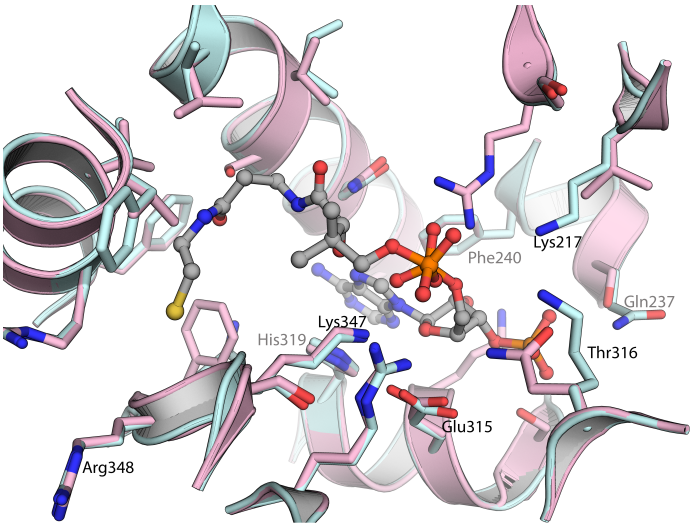

Supplementary Figure 9: Pd1222 $RamB_{Pd}$ contains a CoA binding cavity. Superposition of a Pd1222 $RamB_{Pd}$ homology model (pink) and *M. tuberculosis* PrpR (teal, PDB 6CYY). Depicted is the CoA binding site with bound CoA (grey) as observed in PrpR (39). Amino acid residues described to be engaged in the coordination of CoA in *M. tuberculosis* PrpR (39) are labeled. These binding site residues are well-conserved in $RamB_{Pd}$ with only few exceptions. Lys217 is replaced by Leu211, Gln237 is replaced by Ser231, and Thr316 is replaced by Gln310 in $RamB_{Pd}$.

4 Discussion and Outlook

4.1 About the existence of functional degeneracy

4.1.1 Two distinct acetyl-CoA assimilation routes in *P. denitrificans*

This work focused on the examination of two distinct replenishment pathways in *P. denitrificans*: the glyoxylate cycle (GC) and the ethylmalonyl-CoA pathway (EMCP). With both facilitating the assimilation of acetyl-CoA into malate and succinate, the GC and the EMCP show a seemingly redundant function. This represents an example of functional degeneracy, a phenomenon which is recognized in central metabolism of bacteria today (1). It contrasts with the canonical picture of metabolism, which assumed a biochemical unity between all organisms of all domains of life, from "*E. coli* to an elephant" (2, 3). While functional degeneracy between different organisms is quite a prevalent situation (4–6), the simultaneous presence of two functionally degenerate pathways in one organism is less common.

In accordance with the above, most bacterial species possess either the GC (roughly 33 % of all bacteria) or the EMCP (roughly 7 % of all bacteria), while only few hold the genetic potential for both (roughly 1 %; (7)). The given numbers for the abundance of the GC and the EMCP stem from 2009 (7). Since then, the number of sequenced genomes available has increased drastically. The distribution of the GC and the EMCP in the domain of bacteria was therefore reevaluated with the use of AnnoTree (8), a platform that identifies the presence of a specific gene of interest based on KEGG or PFAM annotations in sequenced genomes (Figure 1). Genomes encoding homologs of Icl (key enzyme of the GC) were considered positive for the GC, genomes encoding homologs of Ccr (key enzyme of the EMCP) and Mcd (2(*S*)-methylsuccinyl-CoA dehydrogenase) were considered positive for the EMCP.

From over 29 000 sequenced bacterial genomes present in the database at this point, the GC was found in roughly one third of all genomes (9623 in absolute numbers), whereby roughly 2 % of these (233 of the 9623) additionally encoded the EMCP (which equals below 1 % of all 29 000 genomes in the data base). Roughly 5 % of all genomes (1444 in absolute numbers) held the EMCP as standalone route. In the remaining 60 % of genomes, no evidence for the presence

of either the GC or the EMCP was found, which suggests that the affiliated organisms either possess alternative routes to the GC and the EMCP or are incapable of acetate assimilation.

In conclusion, despite the drastic increase in available bacterial genome sequences, the relative distribution of the GC and the EMCP in the domain of bacteria still show the same trend as that determined in 2009 (7). This suggests that the given numbers might, in fact, reflect the environmental distribution of the pathways. Followingly, the coexistence of the EMCP and the GC in the same organism, as is the case in *P. denitrificans*, remains to be considered a peculiarity.

However, the existence of functional degeneracy in single organisms is not exclusive for the co-occurrence of the GC and the EMCP but also exists for other metabolic pathways. An example for this is the presence of two distinct metabolic pathways for the oxidation of methylamine in the Alphaproteobacterium *M. extorquens* AM1 (9) that will be referred to again in section 1.2 of this Chapter.

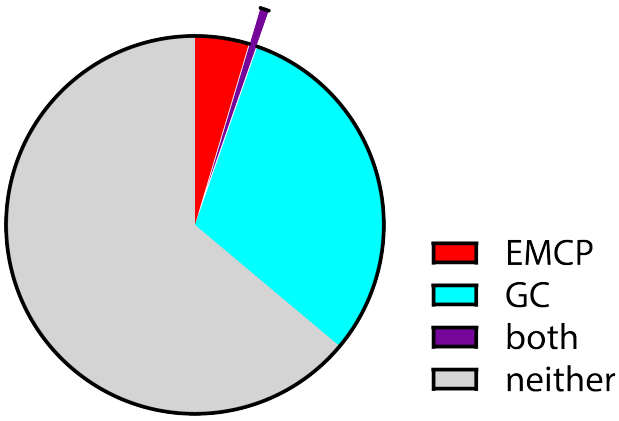

Figure 1: Abundance of the GC and EMCP in the domain of bacteria. The analysis was conducted with the use of AnnoTree (8). Homologs of Icl (KEGG: K01637) marked the presence of the GC, while homologs of Ccr (KEGG: K14446) and Mcd (KEGG: K14448) marked the presence of the EMCP. Shown are the fractions of genomes that contain the individual pathways in relation to approximately 29 000 reference genomes. The fraction of genomes encoding both, the GC and EMCP is accentuated. Note that the precise number of total reference genomes in the database was not supplied by (8). Therefore, percentages given might deviate slightly.

4.1.2 Importance of functional degeneracy in acetyl-CoA assimilation

The presence of two distinct, but functionally degenerate acetyl-CoA assimilation routes in *P. denitrificans* raised the question what the importance and biological purpose of this unusual metabolic setup in the bacterium is.

In Chapter 2 of this work, it was shown that the GC and the EMCP are, in fact, not completely degenerate in their function but confer different advantages and disadvantages on their host.

The GC is a short pathway that processes its initial substrate acetyl-CoA in only two steps. This facilitates little energy demand for enzyme production combined with fast substrate conversion and in sum leads to accelerated bacterial growth. However, the GC is a route strongly specialized for the assimilation of acetyl-CoA and is therefore of no use for the cell when it does not need to assimilate the latter. Tight repression of the GC genes in the absence of acetyl-CoA or the presence of alternative carbon sources, such as succinate, might, thus, be an efficient strategy of the cell to avoid dispensable gene expression and enzyme production.

The EMCP, on the other hand, is a much longer pathway that (i) offers the potential to assimilate a greater variety of substrates that can enter the pathway at different levels and (ii) mediates the assimilation of additional biomass from CO_2. For these reasons, higher growth yields can be achieved with the use of the EMCP than with that of the GC (10). Moreover, the pathway contains two reductive steps that consume reducing equivalents (PhaB reaction and Ccr reaction), which might especially offer the cell the potential to dispose excess electrons during growth on reduced carbon substrates, such as butyrate. A similar effect has been reported in the related *P. pantotrophus*, which uses the periplasmic ubiquinol-Nap reductase as electron sink for the resolution of electron overflow on butyrate (11).

At all advantages of the EMCP, it comes at the disadvantage of significantly higher maintenance costs due to the requirement for more *de novo* synthesis and turnover of metabolic enzymes as well as provision of more and partially costly cofactors. Additionally, the long sequence of this pathway also slows down the conversion rate of acetyl-CoA in comparison to the GC and ultimately leads to slower growth rates.

For the reasons given above, the GC and the EMCP seem to hold a trade-off between growth speed and growth yield that is for example also found between fermentative and respirative routes in catabolism (12). A selective switch between the two pathways in *P. denitrificans* might be an elegant strategy of the bacterium to get the best out of both routes and thereby maximize its efficiency for acetyl-CoA assimilation under changing environmental conditions.

Similar observations have been made in *M. extorquens* PA1, a closely related strain to *M. exorquens* AM1. Unlike its relative AM1, PA1 lacks functional degeneracy for methylamine oxidation and instead only contains one route for this, namely the N-methylglutamate pathway (9). Introduction of the second functionally degenerate route from *M. extorquens* AM1 that involves methylamine dehydrogenase was shown to significantly increase the growth speed and fitness of the PA1 strain (13), demonstrating the benefit of functional degeneracy in this organism as well.

4.1.3 Two distinct propionyl-CoA assimilation routes in *P. denitrificans*

Another factor that adds to the functional degeneracy in *P. denitrificans* is the presence of genes for the methylcitrate cycle (MCC encoded by the *prp*-operon (14)) in addition to the methylmalonyl-CoA pathway (MMCP) (15). Both pathways assimilate propionyl-CoA. While the MMCP converts propionyl-CoA and CO_2 into succinyl-CoA (16), the MCC converts propionyl-CoA and oxaloacetate into succinate and pyruvate (17–19). The MMCP is known to act on the metabolization of propionyl-CoA in the lower part of the EMCP ((20, 21); see Chapter 1, Figure 2A for illustration). The MCC has never been reported to be involved in acetyl-CoA assimilation via the EMCP, but instead is reported as pathway for the assimilation of propionate or propionyl-CoA derived from the degradation of odd chain fatty acids (17, 22).

To test whether the potential for two distinct propionyl-CoA assimilation routes is common, AnnoTree (8) was used to examine the abundance of the MCC and MMCP in bacteria. Thereby, the quantitative representation of the MMCP and the MCC appeared approximately equal. Roughly 24 % of all genomes (6910 in absolute numbers) encoded the MMCP but not the MCC and roughly 18 % (5236

in absolute numbers) encoded the MCC but not the MMCP. Only roughly 3 % (827 in total numbers) of all genomes showed the presence of the MCC and the MMCP at the same time (Figure 2). Like the coexistence of the GC and the EMCP, the simultaneous presence of the MCC and the MMCP in the genome of *P. denitrificans,* thus, appears to be unusual as well.

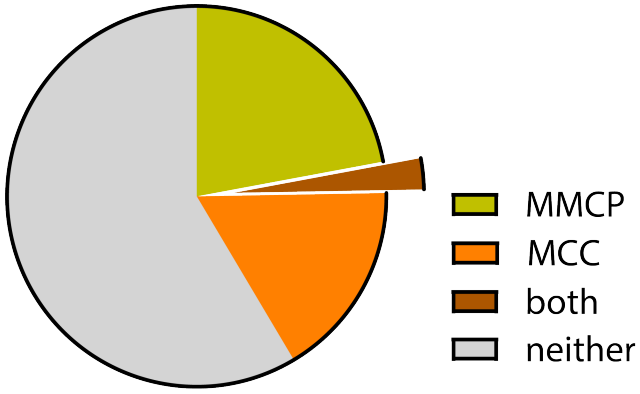

Figure 2: Abundance of the MMCP and MCC in the domain of bacteria. The analysis was conducted with the use of AnnoTree (8). Homologs of propionyl-CoA carboxylase (PccAB; KEGG: K01965 and KEGG: K01966) marked the presence of the MMCP, while homologs of methylisocitrate synthase (PrpC; KEGG: K01659) marked the presence of the MCC. Shown are the fractions of genomes that contain the individual pathways in relation to approximately 29 000 reference genomes. The fraction of genomes encoding both, the MMCP and MCC is accentuated. Note that the precise number of total reference genomes in the database was not supplied by (8). Therefore, percentages given might deviate slightly from the actual situation.

Moreover, while the MMCP seems to be the predominant propionyl-CoA assimilation route in Alphaproteobacteria (Figure 3A), the MCC is mainly represented in Gammaproteobacteria (Figure 3B). This corresponds to the distribution of the EMCP and the GC (7), whereby the EMCP is mainly contained in Alphaproteobacteria (Figure 3C) like *M. extorquens* or *R. sphaeroides,* while the GC is typically found in Gammaproteobacteria (Figure 3D) like *Escherichia coli* and *Salmonella enterica*.

The predominant co-occurrence of the EMCP with the MMCP, and the GC with the MCC, respectively, highlights a strong pair-wise association of acetyl-CoA and propionyl-CoA assimilation routes in bacteria. This is also reflected in species of other bacterial phyla, as for example in *Mycobacterium tuberculosis* (23–26). Here, the MCC and the GC are strongly entangled and do not only share regulatory

players (26, 27). In fact, the GC's key enzyme Icl even substitutes the function of methylisocitrate lyase (PrpB), an important enzyme of the MCC, which is missing in *M. tuberculosis* (24, 28).

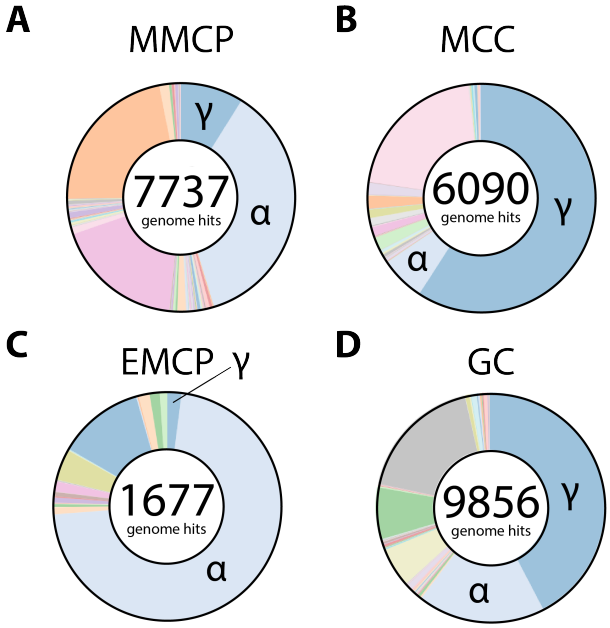

Figure 3: Representation of the MMCP (A), MCC (B), EMCP (C), and GC (D) in different bacterial classes. The analysis was conducted with the use of AnnoTree (8). Homologs for methylisocitrate synthase (PrpC; KEGG: K01659) marked the presence of the MCC, homologs for propionyl-CoA carboxylase (PccAB; KEGG: K01965 and KEGG: K01966) marked the presence of the MMCP, homologs for Ccr (KEGG: K14446) and Mcd (KEGG: K14448) marked the presence of the EMCP, homologs for Icl (KEGG: K01637) marked the presence of the GC. Shown in the center are the absolute numbers of genomes that encode the individual pathways. Their relative representation in the different classes of bacteria is indicated in colors. Alpha- and Gammaproteobacteria are marked by Greek letters. Note that in this analysis, a small percentage of genomes that encode the MMCP additionally encode the MCC and vice versa. Also, a small percentage of genomes that encode the EMCP additionally encode the GC and vice versa.

As a short digress, it is tempting to speculate that this entanglement of the GC and MCC in *M. tuberculosis* could be the expression of a long-standing evolutionary adaptation which resulted from conserved co-occurrence of these pathways and wherein due to a redundancy of methylisocitrate lyase and isocitrate lyase one enzyme was eventually lost. Of course, the apparent bifunctionality of Icl in *M. tuberculosis* could have also emerged the other way around, whereby first the *prpB* gene would have been lost from the genome and Icl would have then consequently adapted promiscuity to accept 2-methylisocitrate in addition to

isocitrate. In any way, the situation in *M. tuberculosis* is peculiar as this organism does not only encode one, but instead two isoforms of isocitrate lyase (29), that are both known to act in the GC and the MCC (24, 28, 30).

4.1.4 Importance of functional degeneracy in propionyl-CoA assimilation

In Chapter 2 of this work, it was shown that the interplay and dynamic metabolic rewiring of two acetyl-CoA assimilation routes in *P. denitrificans* confers an advantage on the bacterium that allows it to maximize its efficiency for acetyl-CoA assimilation ((10), here discussed in section 1.2). However, what the purpose of two propionyl-CoA assimilation strategies is remains unclear.

We have detected a strong upregulation of the genes of the MCC in addition to the genes of the GC and the EMCP during assimilation of acetyl-CoA in *P. denitrificans* (15). This upregulation of the MCC during acetyl-CoA assimilation could serve the sufficient metabolization of propionyl-CoA, which arises as intermediate in the EMCP (see Chapter 1, Figure 2A for schematic overview of the EMCP). A potential accumulation of propionyl-CoA could be caused by slow reactivity of propionyl-CoA carboxylase (PccAB) and/or a shortage in CO_2 or required cofactors (ATP, biotin, vitamin B_{12}). Notably, propionyl-CoA is known to have toxic effects at high intracellular concentrations (22). While the reasons for the toxicity of the metabolite are not entirely resolved until today, one important factor contributing to this seems to be its characteristic to inhibit pyruvate dehydrogenase (PDH; (31)). This could especially pose a problem to the cell upon a growth switch from acetate (or other compounds that are exclusively assimilated via acetyl-CoA) to other carbon substrates that depend on the PDH reaction for the generation of acetyl-CoA from pyruvate (32). Additionally, propionyl-CoA toxicity could also be a consequence of drainage of the CoA pool caused through sequestration of CoA.

The MCC has been reported to work towards the detoxification of propionyl-CoA in other organisms, such as *Mycobacterium smegmatis* (23). Followingly, it could be the case that *P. denitrificans* employs the MCC in addition to the MMCP to ensure fast metabolization of propionyl-CoA that arises during metabolic flux through the EMCP. In accordance with this, the data presented in Chapter 3 of this

work show a higher upregulation of the MCC genes in a Δ*icl* mutant that lacked the GC and instead relied stronger on the EMCP for assimilation of acetyl-CoA (15).

Besides this, our finding could potentially suggest that a variation of the EMCP might be present in *P. denitrificans*, in which the MMCP is inactive and the MCC is used in its place for further metabolization of the arising propionyl-CoA. This hypothesis is especially supported by the fact that an upregulation of the genes of the upper EMCP, but no significant upregulation of the MMCP genes (of the lower EMCP) was found during acetyl-CoA assimilation. This observation, however, could also be reflective of a constitutive expression and use of the MMCP in the metabolism of *P. denitrificans.*

To objectively understand the purpose of the simultaneous presence of the MMCP and the MCC in *P. denitrificans,* the data presented in this work must be extended by several experiments. These include (i) thorough measurements of activities of the MMCP (*e.g.*, PccAB) and the MCC enzymes in crude extracts of acetate-grown and/or propionate grown *P. denitrificans* cells in comparison to succinate or malate grown cells (negative control), (ii) dynamic metabolome analyses, which indicate metabolic flux through the individual pathways, and (iii) knock out and reporter studies that shed light on the essentiality and functional roles of the individual pathways in the cell under different conditions. Importantly, testing of the presence and absence of additionally provided cofactors, such as CO_2, biotin, and vitamin B_{12} must be combined with this. Note that *P. denitrificans* is capable of de-novo biosynthesis of biotin as well as vitamin B12, which is why the vitamins were not externally provided in the growth medium for *P. denitrificans* to this point.

4.1.5 Potential existence of a modified EMCP

To test whether variations of the EMCP, in which the MMCP would be replaced or extended by the MCC, are generally likely to exist, the abundance of the individual pathways in the domain of bacteria was analyzed via AnnoTree (8). With a simultaneous representation in only 0.4 % (123 in absolute numbers) of all genomes in the database, the analysis shows that the EMCP and the MCC hardly ever co-occur in a single organism. Notably, 46 % of the organisms that did show the genetic potential for both, the EMCP and the MCC, belong to the class of

Alphaproteobacteria (Figure 4A). From all 123 genomes that encoded the upper part of the EMCP and the MCC, 100 additionally possessed the potential for the MMCP (Figure 4B). The remaining 23 genomes coded for the upper part of the EMCP and the MCC, but not the MMCP. The organisms corresponding to these identified genomes are listed in Table 1 at the end of this Chapter. Note that Ccr is not exclusively used in the context of the EMCP in primary metabolism, but also occurs in secondary metabolism of some microorganisms as part of polyketide synthase complexes (33). Therefore, it is not clear whether the 23 identified organisms that contain the *ccr* and *mcd* genes without the MMCP possess the genes as part of the EMCP or rather for other purposes.

The rare association of the MCC with the EMCP makes the existence of a modified EMCP that uses the MCC instead of the MMCP for metabolization of propionyl-CoA generally unlikely. Additional knowledge about the metabolism, the occurrence and the evolution of the 23 organisms that encode the upper EMCP and the MCC but not the MMCP is required for further speculations whether a modified EMCP might yet exist here.

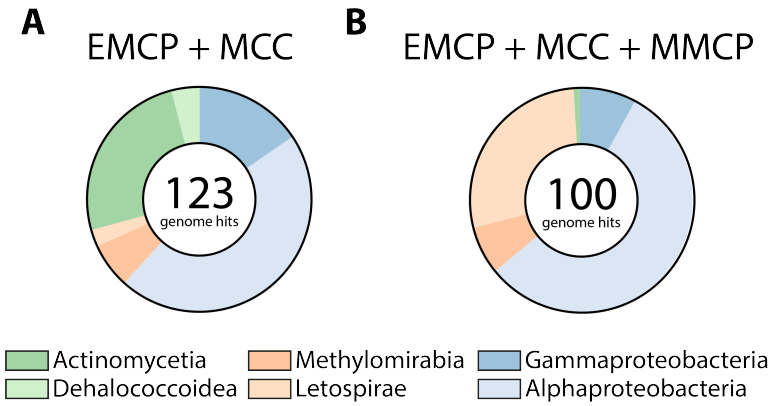

Figure 4: Representation of the EMCP, MCC and MMCP in different bacterial classes. The analysis was conducted with the use of AnnoTree (8). Homologs for Ccr (KEGG: K14446) and Mcd (KEGG: K14448) marked the presence of the EMCP, Homologs for methylisocitrate synthase (PrpC; KEGG: K01659) marked the presence of the MCC, homologs for propionyl-CoA carboxylase (PccAB; KEGG: K01965 and KEGG: K01966) marked the presence of the MMCP. Shown in the center are the absolute numbers of genomes that encoded the EMCP and MCC (A) and the EMCP, MCC, and MMCP (B), respectively. Their relative representation in the different classes of bacteria is indicated in colors.

4.1.6 Emergence and conservation of functional degeneracy in *P. denitrificans* and related Alphaproteobacteria

Finally, the simultaneous presence of the GC, the EMCP including the MMCP, and the MCC is extremely rare. According to analysis with AnnoTree (8), this set of pathways can only be found in 0.2 % (62 in total numbers) of genomes in the database. These 0.2 % mainly belong to the phylum Proteobacteria, but also to the distantly related phyla Actinobacteriota and Methylomirabilota (Figure 5). This raises the question how these organisms obtained this unique metabolic equipment.

In Chapter 2, the hypothesis has been presented that ancestors of *P. denitrificans* originally possessed the EMCP and additionally obtained the GC by horizontal gene transfer (10). This hypothesis is supported by the following observations. (i) The EMCP seems to be a housekeeping-like pathway in *P. denitrificans* with very basal constitutive activity and upregulation on acetate, while the GC is usually tightly repressed and only specifically activated for assimilation of acetyl-CoA (10). (ii) Deletion of the EMCP from the genome of *P. denitrificans* results in a growth defect that renders cells incapable to initiate growth for approximately 60 hours after switch to acetate, which is significantly more severe than the effect caused by deletion of the GC (10, 15). (iii) The predominant acetyl-CoA assimilation route found in Alphaproteobacteria is the EMCP, while the GC is predominantly found in Gammaproteobacteria (see discussion above). (iv) Accordingly, the predominant acetyl-CoA assimilation route found in the genus *Paracoccus* is the EMCP, while only few species contain the EMCP in combination with the GC, and even less contain the GC (but not the EMCP) as standalone route (10, 34). (v) The phylogeny of *ccr* corresponds largely to the overall strain phylogeny of the genus *Paracoccus*, which suggests that it has been held by members of this genus for a long time (10). (vi) Finally, *P. denitrificans* has a multipartite genome that consists of two chromosomes and one mega plasmid, whereby the genes of the EMCP lie dispersed over the genome, while the genes of the GC are clustered in an operon on chromosome 1. There, the GC operon lies near the genes of the MCC (15), which is the propionyl-CoA assimilation route usually associated with the GC in Gammaproteobacteria (see above; of 4172 Gammaproteobacteria that contain the

GC, 3167 additionally possess the MCC). However, the genes of the GC and the MCC in the genus *Paracoccus* show only little sequence similarity to those of representative Gammaproteobacteria like *Escherichia coli* and *Salmonella enterica* (35), which suggests that the pathways might have been obtained by an ancestor of *P. denitrificans* and related species at an earlier timepoint in evolution. The phylogeny of *icl* and the gene for methylisocitrate lyase in these strains should be studied in more detail to follow up on this hypothesis.

Additional evidence for the potential acquirement of metabolic genes via horizontal gene transfer in the genus *Paracoccus* is known from *P. aminophilus* (34, 35). Here, the presence of a methylotrophy island has been shown that was likely obtained by an earlier ancestor via horizontal gene transfer and from there vertically passed on to the bacterium. The methylotrophy island lies on an extrachromosomal element (pAMV1) in *P. aminophilus*, which also contains genes for the GC and the MCC (35). In line with our observations from *P. denitrificans* (10, 15), the authors of the mentioned publications have reported a reduction in growth rate of *P. aminophilus* on acetate upon the deletion of the GC genes from the extrachromosomal island (35). Notably, *P. aminophilus* is like *P. denitrificans* one of the only 62 species that possess the genetic potential for the EMCP (including the MMCP), the GC, and the MCC (see Table 2 at the end of this Chapter). This suggests that the functional degeneracy present in these bacteria might serve a common function and is coordinated similarly. Contrasting to that, however, is the finding presented in Chapter 3 of this study that *Rhodobacter capsulatus*, another closely related bacterium of *P. denitrificans* and *P. aminophilus* that also possesses genes for the above-mentioned set of pathways was unaffected by the deletion of the GC during growth on acetate (15). This suggests a minor and, most importantly, different role of the GC in *R. capsulatus* than in *P. denitrificans* and *P. aminophilus.* Additional studies with *R. capsulatus* and other species with the same metabolic equipment are needed to expand the findings of this work to better understand the conservation of the functional degeneracy present in these bacteria.

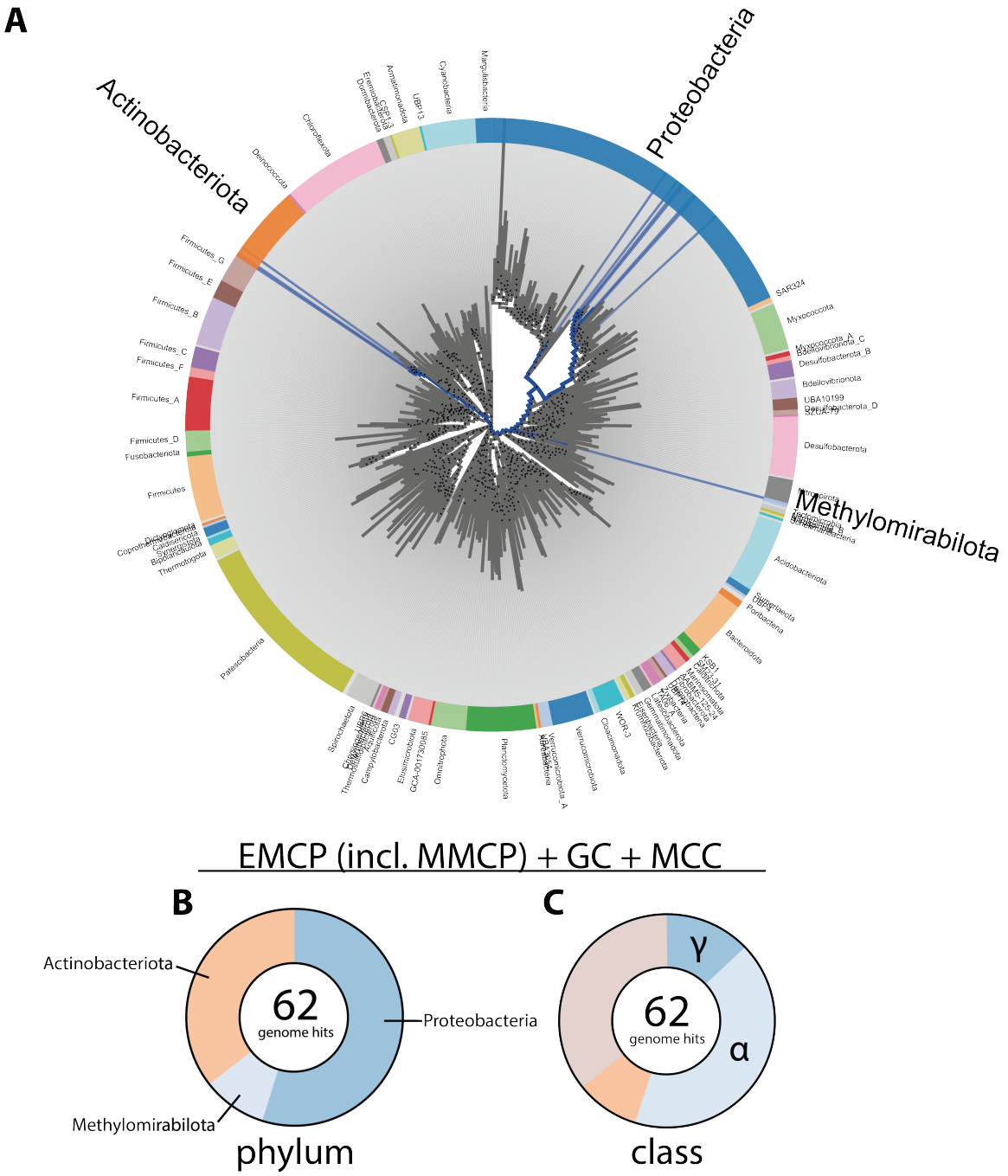

Figure 5: Phylogeny showing the distribution of the pathway set consisting of the EMCP (including MMCP), GC and MCC in bacteria. (A) Phylogenetic tree representing the domain of bacteria, in which blue paths lead to genomes of organisms that simultaneously encode the pathways of interest. Phyla that contain these genomes (Actinobacteriota, Proteobacteria, Methylomirabilota) are highlighted in large font size. (B) Representation of the pathways of interest in the individual phyla in the domain of bacteria. (C) Representation of the pathways of interest in individual classes of the phylum Proteobacteria. The analysis was conducted with AnnoTree (8). Homologs for Icl (KEGG: K01637), Ccr (KEGG: K14446), Mcd (KEGG: K14448), propionyl-CoA carboxylase (PccAB; KEGG: K01965 and KEGG: K01966), and methylisocitrate synthase (PrpC; KEGG: K01659) marked the presence of the desired set of pathways.

4.2 About the mediation of metabolic plasticity

The ability of cells to selectively switch in between different metabolic routes based on their physiological needs is referred to as metabolic plasticity. The phenomenon is specifically studied in cancer cells, which depend on a rapid adaptation of their metabolic program in response to changing environmental conditions for metastatic outgrowth (36–39).

Based on the thorough analysis of reporter strains, we have also reported metabolic plasticity during acetyl-CoA assimilation in *P. denitrificans* (10, 15). For this, we have demonstrated that during growth on succinate, *P. denitrificans* expresses neither the genes of the EMCP nor the GC at significant levels. (Note that a low activity of Ccr is still detectable in extracts of succinate-grown *P. denitrificans* cells, showing that the EMCP is not completely turned off on succinate, but expressed at a very basal level). However, a growth shift to acetate stimulates the bacterium to induce both pathways in a sequential fashion. Thereby, an initial upregulation of the EMCP during the lag phase is superseded by the GC upon the transition to the exponential phase of growth (10, 15). Notably, this effect has also been observed on single cell level, which is why it did not have to be interpreted as an artificial pattern that could have resulted from an inhomogenic gene expression in the cultures (10).

4.2.1 Regulation of the GC in *P. denitrificans* through the dual-mode transcription factor RamB

The discovery of dynamic rewiring between the EMCP and the GC in *P. denitrificans* during growth on acetate raised the question how the bacterium regulates this metabolic plasticity. While regulation of the EMCP remains enigmatic, this work has proposed the existence of a mechanism for linking expression of the GC to flux through the EMCP via the dual-mode transcription factor $RamB_{Pd}$ (15). RamB (regulator of acetate metabolism; (40)) is a member of the ScfR family (short chain fatty acid metabolism regulators), which holds several transcription factors involved in controlling a variety of metabolic pathways, amongst them routes for acetate and propionate assimilation (41).

RamB as a transcriptional repressor

Studies of RamB in other model organisms, such as *C. glutamicum* or *M. tuberculosis* have suggested a role of the protein as transcriptional repressor of the GC genes ((26, 42–45); see Chapter 1, Figure 4 for overview). In line with this, we have detected a repressive function of RamB in *P. denitrificans* during growth on succinate as well (15). This is reflected by the following findings: (i) Icl activity is not at all detectable in crude extracts of succinate grown *P. denitrificans* cells (10), (ii) *icl*-reporter strains of *P. denitrificans* do not indicate *icl* expression on succinate (10, 15), (iii) transcripts of the GC genes cannot be found in the RNA profiles of succinate grown *P. denitrificans* cells (15), (iv) *ramB*-deletion strains, in contrast, show a basal expression of the GC genes on succinate (15), and (v) $RamB_{Pd}$ shows specific interaction with its operator motif in the *gc* promoter region *in vitro* in the absence of inducing ligands (15). Notably, the common operator motif for *P. denitrificans* RamB (hereafter referred to as $RamB_{Pd}$) was unknown before and newly discovered in this work as well (15, 41).

RamB as transcriptional activator

Even more important than the repressive function of $RamB_{Pd}$ and as first example in literature to our knowledge, this work has also demonstrated a function of $RamB_{Pd}$ as transcriptional activator that mediates expression of the GC genes in *P. denitrificans* upon growth switch to acetate (15). This characteristic of $RamB_{Pd}$ is reflected by the following findings: (i) while *icl*-reporter strains of otherwise wildtype background indicate a strong upregulation of *icl* during growth on acetate, this upregulation is missing in Δ*ramB* mutants, (ii) RNAseq analyses show a missing upregulation of the GC genes on acetate in Δ*ramB* cells, (iii) Δ*ramB* mutants display the same growth defect as Δ*icl* strains with reduced growth rate on acetate in comparison to wildtype, and (iv) the defect displayed by Δ*ramB* mutants can be complemented by the ectopic expression of *ramB* in these cells.

Together, this makes $RamB_{Pd}$ a dual-mode transcription factor with repressive as well as activating functions on the GC genes. As shown in Chapter 3, its mode of action is likely defined by the oligomerization state of the protein. Thereby, $RamB_{Pd}$ presumably functions as transcriptional repressor when present in the tetrameric

state and becomes a transcriptional activator when transposed to the dimeric state. The decay of the tetrameric into dimeric complexes, in turn, is likely triggered by binding of β-methylmalyl-CoA, an intermediate that arises upon metabolic flux through the EMCP (15). Note that β-methylmalyl-CoA is presumably a unique intermediate of the EMCP in *P. denitrificans,* as other routes like the 3-hydroxypropionate bi-cycle (46) that could potentially also produce β-methylmalyl-CoA are missing from the organism. In accordance with this, this work has demonstrated that the preceding activity of the EMCP is needed to induce expression of the GC genes in *P. denitrificans* (10, 15). Moreover, binding of CoA and esterified derivatives thereof were shown to induce the decay of tetrameric $RamB_{Pd}$ *in vitro*, whereby β-methylmalyl-CoA evoked this effect the strongest (15).

Note that $RamB_{Pd}$ is a homolog of RamB subclass 2 proteins, whereby the RamB homologs investigated in the other studies mentioned above (26, 42–45) belong to RamB subclass 1 (41). For this reason, functional differences between the proteins are not unlikely.

RamB as putative iron-sensor

Other examples for homologs of the ScfR family are the regulator of propionyl-CoA carboxylase PccR (involved in regulation of the MMCP (41)) and the regulator of the *prp*-operon PrpR (involved in regulation of the MCC (14, 27, 47)). These have been studied in different bacteria, respectively. In line with the findings presented in this work, CoA binding to ScfR homologs has been demonstrated in a structural study on the transcriptional activator PrpR from *M. tuberculosis* as well (47). Here, like $RamB_{Pd}$, PrpR has also been reported as tetrameric complex. Additionally, CoA binding and ordered function of PrpR have been suggested to depend on the presence of a [4Fe-4S]-cluster, which is coordinated by a C-X_2-C-X_4-C motif in the C-terminal region of the individual PrpB subunits. While the authors also proposed CoA-esters as inducing ligands of the protein, they additionally speculated on a role of PrpR as iron-sensor based on the detected importance of the [4Fe-4S]-cluster for the function of the protein.

The [4Fe-4S]-cluster is reported as highly stable in PrpR (47). It is also present in $RamB_{Pd}$, where we did not investigate its specific function so far. However, an

association of iron limitation with an upregulation of the GC has been reported for marine heterotrophic bacteria (48). Here, it has been proposed that the upregulation of the GC could be a strategy to redirect metabolism away from usage of the respiratory chain, which requires iron for the transport of electrons and is, thus, significantly hindered upon iron limitation. Also other studies have reported on a transcriptional upregulation of the GC genes under iron-limiting conditions (49), which also appears to be a consequence of the encounter of oxidative stress in bacterial cells (49, 50). It might, followingly, be the case that an involvement in these processes applies for RamB in *P. denitrificans* in addition to its CoA-sensing capacity.

On the mechanism of work of RamB-mediated regulation of transcription in *P. denitrificans*

As discussed above, $RamB_{Pd}$ has been characterized as dual-mode transcription factor in this work with repressing as well as activating function on the GC genes. The function of the protein is presumably defined by its oligomeric state, whereby tetrameric $RamB_{Pd}$ might function as transcriptional repressor, while dimeric $RamB_{Pd}$ might function as transcriptional activator. The switch in the oligomeric state of the protein is controlled by the absence or presence of the effector molecule β-methylmalyl-CoA, an intermediate of the EMCP, which accumulates upon metabolic flux through the pathway (15).

Moreover, the consensus sequence of the operator motif that mediates binding of RamB subclass 2 homologs to their target promoter region has been presented in Chapter 3 of this study (15). In *P. denitrificans*, this operator motif consists of two individual binding boxes that are separated by an 18 bp spacer, whereby the second box of the motif seems to overlap with the -35 element in the promoter of the GC operon (Figure 6). In Chapter 3 of this work it has been shown that both binding boxes are required for $RamB_{Pd}$-activated expression of the GC genes. The overlapping operator site arrangement with the -35 box of the promoter found in the GC operon is typical for transcriptional activation from class II promoters (51, 52). It differs from that from class I promoters therein as the operator sites in the latter lie further upstream of the -35 and -10 elements (53).

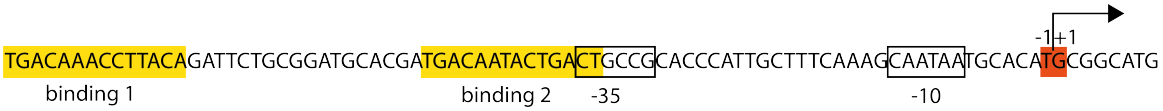

Figure 6: Architecture of promoter elements in the GC operon. Shown is the promoter region of the GC operon in reverse complement. The operator motif for RamB consists of two 14 bp-binding boxes (yellow background) that are separated by an 18 bp-spacer. Binding box 2 overlaps with the predicted –35 element of the promoter as typical for promoters subjected to class II transcriptional activation. The predicted –10 element as well as the predicted transcription start site (+1; red background) are also shown. Analysis of the promoter elements in the GC operon was conducted by Doreen Meier based on known consensus sequences for σ^{70}-targeted promoters from *Sinorhizobium meliloti* (54).

Note that prerequisite for transcription initiation in bacteria is the assembly of the RNA polymerase (RNAP) that consists of the four apo enzymatic subunits αββ‘ and ω, which are complemented by the σ factor to form the functional RNAP holoenzyme. The σ factor mediates selective promoter recognition and binding of the bacterial RNAP, which is required for the formation of transcription initiation complexes on the DNA, from which transcription ultimately proceeds (55–59). According to their structure and evolution, sigma factors are divided into two distinct classes: the major σ^{70} class and the enhancer-dependent σ^{54} class (60). The major σ^{70} class comprises the vast majority of cytoplasmic and extra cytoplasmic sigma factors involved in housekeeping, general stress responses, flagella assembly, chemotaxis, developmental processes, and physiological adaptation of cells to environmental signals (56).

Class II transcriptional activation usually involves σ^{70}-driven formation of transcription complexes (61). Thereby, different contributions of the involved transcriptional activators are discussed that include hypotheses on the stabilization of transcription complexes at different stages of the transcription initiation process (*i.e.*, recruitment of RNAP; stabilization of the closed complex; stabilization of the open complex; transition between the closed and the open complex (62)), as well as the induction of conformational changes in the RNAP (63). Notably, the most-widely used model to study transcriptional activation from class I and class II promoters is the catabolite activator protein (CAP) from *Escherichia coli* (53) or homologs thereof (51), respectively. In support of our hypothesis that $RamB_{Pd}$ is

present in the dimeric state when functional as activator, transcriptional activators of the CAP-type are usually described as homodimers as well (51, 63–66).

While the mechanism of transcriptional activation through dimeric $RamB_{Pd}$ is potentially shared with other transcriptional activators (see above), the mechanism of transcriptional repression by tetrameric $RamB_{Pd}$ is less conclusive. Examples of tetrameric transcriptional repressors, such as the LacI repressor of the *lac*-operon from *E. coli*, are well-known in literature (67). Typically, the tight repressive mechanism of these proteins results from steric occlusion of the RNAP from the promoter or the inhibition of its promoter escape (68). This is often additionally enhanced by DNA-loop formation through binding of the oligomeric transcription factor to multiple operator motifs present in different regions on the host DNA (69–71).

The mechanism of DNA-looping is not exclusive to tetrameric transcription factors but also conserved for others, like the dimeric AraC protein that controls expression of the *araBAD* genes in dependence on the absence and presence of arabinose in *E. coli*. Interestingly, AraC is like $RamB_{Pd}$ a dual mode transcription factor, activity of which switches between activation and inhibition of transcription in response to effector binding (72–75). Unlike observed for $RamB_{Pd}$, the conformational change caused by effector binding to the dimeric AraC protein does not affect its oligomeric state. Alternatively, it repositions its N-terminal DNA binding arms to enable binding to alternative operator sites in the DNA (I_1 and I_2 instead of I_1 and O_2 as in repressive mode). Binding of AraC to these alternative operator sites (I_1 and I_2) eliminates DNA-looping and instead mediates the activation of transcription through direct positive interactions of the AraC dimer with the RNAP (76).

No additional operator sites for $RamB_{Pd}$ could be detected by *in-silico* analysis of the *P. denitrificans* genome that would indicate a potential DNA-looping mechanism for repression of gene expression mediated by binding of the tetrameric $RamB_{Pd}$ complex. As mentioned above, in Chapter 3 of this work it was shown that the presence of both binding boxes of the operator motif is required for $RamB_{Pd}$-mediated activation of gene expression *in vivo*. Moreover, it was shown that *in vitro* binding of tetrameric $RamB_{Pd}$ to DNA depends on the presence of the identified operator motif consisting of the two binding boxes and the 18 bp spacer

as well. Together, this suggests that in repressive as well as activating mode, RamB might bind to the same operator sites in the promoter. The bound tetrameric $RamB_{Pd}$ complex might thereby be sufficient for steric occlusion of the RNAP from the *gc* promoter without additional DNA looping in repressive mode, while the bound dimeric $RamB_{Pd}$ complex might instead positively interact with the RNAP to promote transcription in activating mode.

After all, it could also be the case that additional operator sites for $RamB_{Pd}$ are present in the DNA that were missed by *in silico* analyses. A chromatin immunoprecipitation DNA sequencing (ChIP-seq) experiment could provide more insights into this. Additionally, this experiment would allow to identify other putative target genes of $RamB_{Pd}$ if any are present.

Finally, the model proposed in Chapter 3 of this study, according to which flux through the EMCP results in the accumulation of β-methylmalyl-CoA, which, in turn, is the effector molecule inducing RamB-activated expression of the GC genes could be verified via LC-MS. Here, an endometabolome analysis of acetate grown *P. denitrificans* cells could give information about the intracellular concentrations of different CoA-esters of the EMCP at different timepoints during *P. denitrificans* growth on acetate. Dynamic labelling experiments with ^{13}C-acetate could additionally demonstrate the metabolic fluxes through the individual pathways.

4.2.2 The picture of GC regulation is not complete

In other organisms like *E. coli, M. tuberculosis*, or *C. glutamicum* abundance and activity of the GC enzymes is controlled by several layers of regulation. These involve the action of multiple regulators that control gene expression on transcriptional level (26, 27, 40, 42, 43, 47, 77–79), regulators that introduce posttranslational modifications into the GC enzymes (80–86), as well as allosteric regulation of the GC enzymes through effector binding (28) (see Chapter 1, Section 1.5). While this work has characterized one aspect of the transcriptional regulation of the GC operon through $RamB_{Pd}$ (15), additional regulatory layers might be present in *P. denitrificans.* These remain to be investigated in future studies to complete the picture of GC regulation in the model organism.

4.2.3 Regulation of the EMCP

While this work has presented insights into the molecular basis of transcriptional regulation of the GC, the regulators and mechanisms controlling the EMCP remain largely enigmatic and should be subject to future studies (15). In preparation for this, the knowledge gathered on the regulation of the EMCP so far will be discussed in detail below.

Please note, that unlike the GC genes, the EMCP genes are not organized in an operon but instead lie dispersed over the genome of *P. denitrificans*. For reasons of simplification, the genetic regulation of the EMCP described below mainly refers to the regulation of the gene encoding Ccr, the key enzyme of this pathway. It might, however, be different for genes encoding the remaining EMCP enzymes.

The EMCP and the GC are regulated individually

Several experiments presented in this work have shown that the EMCP (indicated by the abundance and activity of its key enzyme Ccr) is always transiently upregulated in the lag phase of *P. denitrificans* cultures on acetate after growth switch from alternative carbon sources. It is then downregulated upon transition of the cultures to the exponential phase. Notably, the downregulation of the EMCP upon transition of acetate-growing *P. denitrificans* cultures to exponential growth phase coincides with an upregulation of the GC (indicated by the abundance and activity of its key enzyme Icl) (10, 15).

Because of this apparently synchronized regulation of the GC and the EMCP, one could even speculate that both pathways are controlled by the same transcriptional regulator (*i.e.*, RamB) that acts as activator on the GC genes and as repressor on the EMCP genes (or *ccr*, respectively). This hypothesis is especially supported by the fact that mutants of *P. denitrificans* that lack RamB are incapable of upregulating the GC and at the same time show an enhanced and prolonged upregulation of the EMCP (10, 15).

However, several other findings indicate that the GC and the EMCP are regulated individually, which suggests that the absent downregulation of the EMCP in Δ*ramB* mutants is rather an indirect effect to compensate for the lack of a functional GC

mediated by a regulator other than RamB. This hypothesis is supported by the following findings: (i) putative operator sites for RamB are absent in the genomic vicinity of the *ccr* gene and (ii) the regulation of the EMCP and the GC can become desynchronized under certain conditions.

Desynchronized regulation of the EMCP and the GC is for example displayed by acetate-growing cultures of *P. denitrificans* reporter strains when they are started from acetate-grown precultures in which the GC had already been expressed. Here, a constant upregulation of the GC does not affect the regulation of the EMCP. Instead, the EMCP shows the same characteristic transient upregulation at low densities of the cultures as observed in pre-exponential cultures after growth switch to acetate from alternative carbon sources, a condition under which the GC is not initially expressed (see Chapter 3, Supplementary Figure 7 for comparison).

Another example for desynchronized regulation of the EMCP and the GC can be seen in cultures of *P. denitrificans* reporter strains on a mixture of acetate and succinate as carbon sources. While cultures growing on these compounds display an initial transient upregulation of the EMCP (or Ccr, respectively), upregulation of the GC does not coincide with downregulation of the EMCP in this case. Instead, it lags behind until all succinate in the medium has been consumed and acetate is the only carbon source left (see Chapter 3, Supplementary Figure 8 for comparison).

Acetate or acetyl-CoA, respectively, as signal molecule inducing upregulation of the EMCP

The fact that the additional presence of succinate in acetate-growing cultures suppresses induction of the GC genes but not induction of the *ccr* gene, suggests that the genetic regulatory machineries controlling the GC and the EMCP respond to different signal molecules.

While β-methylmalyl-CoA is suggested as effector molecule that triggers expression of the GC genes ((15), see discussion above), the inducing molecule of the EMCP or the *ccr* gene, respectively, might, in fact, be acetate or acetyl-CoA when present at significant levels.

Additional mechanisms prevent flux through the EMCP in the presence of succinate

If induction of the GC genes occurs in response to accumulation of β-methylmalyl-CoA, induction of the GC will always be expected as a consequence of flux through the EMCP. However, while the EMCP or *ccr*, respectively, are induced in *P. denitrificans* cells on mixtures of acetate and succinate, induction of the GC does not proceed before complete consumption of succinate (see discussion above). If the above-mentioned hypothesis is true, this finding indicates that despite the upregulation of the EMCP on mixtures of succinate and acetate, additional mechanisms prevent or significantly lower the metabolization of acetyl-CoA through the EMCP under these conditions.

The exometabolome analysis presented in Chapter 3 of this work (see Chapter 3, Supplementary Figure 8 for comparison) displays the corresponding acetate and succinate concentrations in the medium of *P. denitrificans* grown on this carbon source mixture. It supports the aforementioned hypothesis as it shows that the acetate levels present in the medium of these cultures only start to decrease after succinate is completely consumed.

Flux through the EMCP during growth on a mixture of succinate and acetate might be prevented by different means that could involve (i) posttranslational/allosteric inactivation of Ccr, (ii) transcriptional suppression or posttranslational/allosteric inactivation of an EMCP enzyme upstream or downstream of Ccr, or (iii) a catabolite repression system that prevents cellular uptake of acetate in the presence of succinate.

More insights into this could be provided by the following experiments. Transcriptional suppression of a gene encoding an upstream or downstream EMCP enzyme of Ccr could be excluded by an extension of the RNA-seq analysis presented in Chapter 3 of this work (15) through likewise analysis of samples of *P. denitrificans* grown on a mixture of succinate and acetate. Inactivation of Ccr could be tested by measuring the activity of the protein in crude extracts of acetate+succinate-grown cells. Identification of putative posttranslational modifications of EMCP enzymes under different conditions could occur via LC-MS

analysis with similar methods as previously performed for Icl1 in *M. tuberculosis* (86). Finally, exploration of metabolic fluxes via dynamic labelling experiments with a combination of ^{13}C acetate and ^{12}C succinate and subsequent LC-MS analysis could verify the prevented metabolization of acetate in the presence of succinate.

How to identify transcriptional regulators of the *ccr* gene

While genetic regulation of *ccr* appears to be present in *P. denitrificans* (10, 15), the underlying mechanisms and regulators behind it could not be identified to this point.

In *M. extorquens* AM1, *ccr* is transcriptionally controlled by the TetR-type activator CcrR ((87), see Chapter 1, section 1.5.5). No homologs of this protein can be found in *P. denitrificans* Pd1222 according to BLAST analysis, suggesting that an alternative player controls expression of *ccr* here.

As stated above, the genes of the EMCP lie dispersed over the genome of *P. denitrificans*, which consists of two chromosomes and a megaplasmid. The *ccr* gene (*Pden_3873*) lies on chromosome 2, where it is located on the reverse strand. It is not clustered together with any genes for putative transcriptional regulators. It might either be transcribed into a monocistronic RNA or co-transcribed with a gene coding for a α/β-hydrolase (*Pden_3874*) that lies 191 bp upstream on the reverse strand of chromosome 2 as well. Interestingly, the *ecm* gene (*Pden_3875*), which codes for the EMCP enzyme ethylmalonyl-CoA mutase, lies 244 bp upstream of *Pden_3874* in reverse direction of *Pden_3873* and *Pden_3874* (Figure 7). In most organisms that encode the EMCP, *ccr* and *ecm* are clustered together in the genome (88). The genes are, moreover, known to be co-transcribed in some (89) but not all organisms (87).

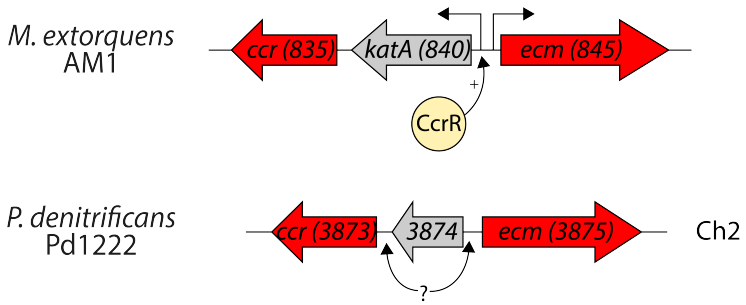

Figure 7: Locus of *ccr* and *ecm* in *M. extorquens* AM1 and *P. denitrificans* Pd1222. Numbers of MEXAM1_RS_ and Pden_ locus tags are given in brackets. In *M. extorquens*, CcrR activates transcription of *ccr* and *katA* into a polycistronic mRNA. The promoter region controlling expression of *ccr* and associated regulatory proteins in *P. denitrificans* are unknown. Ch2: chromosome 2.

The gene architecture of *ccr* and *ecm* in *P. denitrificans* is similar to that in *M. extorquens* AM1 ((87), Figure 7). Here, *ccr* is known to be co-transcribed with *katA*, a gene encoding a catalse, while *ecm* is known to be transcribed into an individual mRNA. It might, thus, be the case that in *P. denitrificans*, the *ccr* gene *(Pden_3873*) is co-transcribed with the neighboring gene for the α/β-hydrolase (*Pden_3874*), while *ecm* (*Pden_3875*) is transcribed individually as well. According to sequence analysis with BPROM (90), putative promoter elements can be found in the intergenic regions upstream of both *Pden_3873* and *Pden_3874/Pden_3875* Similar reporter experiments as those performed to identify the promoter region of the GC operon ((15), see Chapter 3, Supplementary Figure 3 for comparison) could allow to locate the promoter region of the *ccr* gene. *P. denitrificans* strains carrying suitable reporter constructs for this exist and are listed in Table 3 at the end of this chapter.

Once the *ccr* promoter region is located, identification of regulators targeting this region could occur by pull-down assays and following LC-MS analysis of the isolated proteins as described in literature before (91, 92).

4.3 Perspectives for the future

Anaplerotic reaction sequences like the GC and the EMCP are not only relevant for bacterial growth in the natural context. They also possess a great potential for biotechnological applications (93–95). Here, they can serve the production of multicarbon, value-added chemicals from cheap building blocks such as acetate, ethanol, or even the widely available greenhouse gas CO_2 (96, 97).

In fact, several CoA-ester intermediates of the EMCP represent platform chemicals for industry (93, 97). For this reason, bacterial strains that possess the EMCP, as for example *M. extorquens* AM1, are used as hosts for metabolic engineering to develop microbial cell factories capable of making and excreting the desired CoA esters or the functionalized carboxylic acids thereof, respectively, or other value-

added compounds. However, these approaches still hold several constraints due to incomplete understanding of the host metabolism as well as the lack of applicable regulatory modules to achieve control and/or a targeted rewiring of metabolic pathways (94, 97).

Moreover, the use of the EMCP or Ccr, in particular, in biotechnological applications does not only hold the chance to produce value-added compounds from cheap resources. At the same time, it allows to tackle a major environmental threat our society is faced with today: the ever-rising atmospheric concentrations of the greenhouse gas CO_2, which represent one of the main driving forces of global warming (98). Here, the capability of the EMCP's key enzyme Ccr to fix CO_2 much faster and more efficient than Rubisco ((99); the key enzyme of CO_2 fixation in photosynthesis) is highly beneficial. It is exploited in new-to-nature pathways that use atmospheric CO_2 for the production of value-added chemicals as for example the CETCH (crotonyl–coenzyme A (CoA)/ethylmalonyl-CoA/hydroxy-butyryl-CoA) cycle, which simultaneously aims at counteracting the problem of rising atmospheric CO_2 concentrations (100). While the CETCH cycle is at this point only functional as an *in vitro* pathway, its implantation into living cells, such as algae or bacteria, could be a promising solution in the future to develop autotrophic production chassis that function as CO_2 sinks at the same time (95, 101, 102).

Different examples for the beneficial use of replenishment pathways in metabolic engineering and synthetic biology have been presented above. According to Max Planck's famous saying, '*Insight must precede application'*, the successful implantation of alienated metabolic pathways or, even more, the realization of synthetic reaction sequences *in vivo* requires the extension of our current understanding of bacterial metabolism.

Full elucidation of the regulation of the GC and the EMCP in *P. denitrificans* as well as further characterization of the bacterium's metabolic network will contribute to this overall goal. Here, the principles of metabolic regulation found in *P. denitrificans* could be abstracted to develop (i) biosensors from characterized transcription factors that can serve the dynamic readout of metabolites (103, 104) in *in vivo* and *in vitro* systems as well as (ii) regulatory modules to control

(synthetic) pathways in metabolically engineered cells (105, 106). Additionally, a thorough understanding of the metabolism of *P. denitrificans* might make the organism a favorable, highly flexible (10, 15), well-characterized (10, 15, 107–111), genetically tractable (112), and facultatively autotrophic (113) host for the implementation of synthetic metabolic pathways in the future.

4.4 Conclusion

Overall, this work has shed light on the unique and highly flexible metabolism of *P. denitrificans*. It has shown the presence of functional degeneracy in metabolism on multiple examples, attempted to explain its biological purpose and evolution, and presented the molecular basis of metabolic plasticity. The presented findings highlight the modularity of central carbon metabolism and the possibilities to adopt functionally degenerate pathways for different purposes and environmental conditions. Together, this contributes to a new, overhauled picture of metabolism and expands our understanding of its regulation. Together, this might set the basis for new applications in synthetic biology and metabolic engineering in the future.

.

4.5 References

1. Schada Von Borzyskowski L, Bernhardsgrütter I, Erb TJ. 2020. Biochemical unity revisited: Microbial central carbon metabolism holds new discoveries, multi-tasking pathways, and redundancies with a reason. Biol Chem 401:1429–1441.

2. Singleton R, Singleton DR. 2017. Remembering Our Forebears: Albert Jan Kluyver and the unity of life. J Hist Biol 50:169–218.

3. Allen GE. 2005. Mechanism, vitalism and organicism in late nineteenth and twentieth-century biology: the importance of historical context. Stud Hist Philos Biol Biomed Sci 36:261–283.

4. Comte J, Fauteux L, del Giorgio PA. 2013. Links between metabolic plasticity and functional redundancy in freshwater bacterioplankton communities. Front Microbiol 4.

5. Allison SD, Martiny JBH. 2008. Resistance, resilience, and redundancy in microbial communities. Proc Natl Acad Sci U S A 105:11512.

6. Trivedi CB, Stamps BW, Lau GE, Grasby SE, Templeton AS, Spear JR. 2020. Microbial metabolic redundancy is a key mechanism in a sulfur-rich glacial ecosystem. mSystems 5.

7. Erb TJ. 2009. The ethylmalonyl-CoA pathway, a novel acetyl-CoA assimilation strategy. Dissertation.

8. Mendler K, Chen H, Parks DH, Lobb B, Hug LA, Doxey AC. 2019. AnnoTree: visualization and exploration of a functionally annotated microbial tree of life. Nucleic Acids Res 47:4442–4448.

9. Nayak DD, Marx CJ. 2014. Methylamine utilization via the N-methylglutamate pathway in *Methylobacterium extorquens* PA1 involves a novel flow of carbon through C1 assimilation and dissimilation pathways. J Bacteriol 196:4130–4139.

10. Kremer K, van Teeseling MCF, von Borzyskowski LS, Bernhardsgrütter I, van Spanning RJM, Gates AJ, Remus-Emsermann MNP, Thanbichler M, Erb TJ. 2019. Dynamic metabolic rewiring enables efficient acetyl coenzyme a assimilation in *Paracoccus denitrificans*. mBio 10.

11. Ellington MJK, Bhakoo KK, Sawers G, Richardson DJ, Ferguson SJ. 2002. Hierarchy of carbon source selection in *Paracoccus pantotrophus*: Strict correlation between reduction state of the carbon substrate and aerobic expression of the *nap* operon. J Bacteriol 184:4767–4774.

12. Pfeiffer T, Schuster S, Bonhoeffer S. 2001. Cooperation and competition in the evolution of ATP-producing pathways. Science 292:504–507.

13. Nayak DD, Marx CJ. 2015. Experimental horizontal gene transfer of methylamine dehydrogenase mimics prevalent exchange in nature and overcomes the methylamine growth constraints posed by the sub-optimal n-methylglutamate pathway. Microorganisms 3:60–79.

14. Horswill AR, Escalante-Semerena JC. 1997. Propionate catabolism in *Salmonella typhimurium* LT2: two divergently transcribed units comprise the *prp* locus at 8.5 centisomes, *prpR* encodes a member of the sigma-54 family of activators, and the *prpBCDE* genes constitute an operon. J Bacteriol 179:928–940.

15. Kremer K, Meier D, Theis L, Miller S, Rost-Nasshan A, Naing YT, Zarzycki J, Paczia N, Serrania J, Blumenkamp P, Goesmann A, Becker A, Thanbichler M, Hochberg GKA, Carter MS, Erb TJ. 2022. Functional degeneracy in *Paracoccus denitrificans* Pd1222 is coordinated via RamB, linking expression of the glyoxylate cycle to activity of the ethylmalonyl-CoA pathway. Submitted.

16. Mancia F, Evans PR. 1998. Conformational changes on substrate binding to methylmalonyl CoA mutase and new insights into the free radical mechanism. Structure 6:711–720.

17. Textor S, Wendisch VF, de Graaf AA, Müller U, Linder MI, Linder D, Buckel W. 1997. Propionate oxidation in *Escherichia coli*: evidence for operation of a methylcitrate cycle in bacteria. Archives of Microbiology 168:428–436.

18. Tabuchi T, Uchiyama H. 1975. Methylcitrate condensing and methylisocitrate cleaving enzymes; evidence for the pathway of oxidation of propionyl-coa to pyruvate via C7-tricarboxylic acids. Agric Biol Chem 39:2035–2042.

19. Tabuchi T, Hara S. 1974. Production of 2-methylisocitric acid from n-paraffins by mutants of *Candida lipolytica*. Agric Biol Chem 38:1105–1106.

20. Erb TJ, Berg IA, Brecht V, Müller M, Fuchs G, Alber BE. 2007. Synthesis of C5-dicarboxylic acids from C2-units involving crotonyl-CoA carboxylase/reductase: The ethylmalonyl-CoA pathway. Proc Natl Acad Sci U S A 104:10631–10636.

21. Peyraud R, Kiefer P, Christen P, Massou S, Portais JC, Vorholt JA. 2009. Demonstration of the ethylmalonyl-CoA pathway by using ^{13}C metabolomics. Proc Natl Acad Sci U S A 106:4846–4851.

22. Dolan SK, Wijaya A, Geddis SM, Spring DR, Silva-Rocha R, Welch M. 2018. Loving the poison: The methylcitrate cycle and bacterial pathogenesis. Microbiology (Reading) 164:251–259.

23. Upton AM, McKinney JD. 2007. Role of the methylcitrate cycle in propionate metabolism and detoxification in *Mycobacterium smegmatis*. Microbiology (N Y) 153:3973–3982.

24. Gould TA, van de Langemheen H, Muñoz-Elías EJ, McKinney JD, Sacchettini JC. 2006. Dual role of isocitrate lyase 1 in the glyoxylate and methylcitrate cycles in *Mycobacterium tuberculosis*. Mol Microbiol 61:940–947.

25. Eoh H, Rhee KY. 2014. Methylcitrate cycle defines the bactericidal essentiality of isocitrate lyase for survival of *Mycobacterium tuberculosis* on fatty acids. Proc Natl Acad Sci U S A 111:4976–4981.

26. Antelmann H, Bashiri G, Wang J, Serafini A, Qi N, She G-L, Du W, Ye B-C. 2021. *Mycobacterium smegmatis* GlnR regulates the glyoxylate cycle and the methylcitrate cycle on fatty acid metabolism by repressing *icl* transcription. Front Microbiol.

27. Masiewicz P, Brzostek A, Wolański M, Dziadek J, Zakrzewska-Czerwińska J. 2012. A novel role of the PrpR as a transcription factor involved in the regulation of methylcitrate pathway in *Mycobacterium tuberculosis*. PLoS One 7.

28. Bhusal RP, Jiao W, Kwai BXC, Reynisson J, Collins AJ, Sperry J, Bashiri G, Leung IKH. 2019. Acetyl-CoA-mediated activation of *Mycobacterium tuberculosis* isocitrate lyase 2. Nature Communications 2019 10:1 10:1–7.

29. Cole ST, Brosch R, Parkhill J, Garnier T, Churcher C, Harris D, Gordon S v., Eiglmeier K, Gas S, Barry CE, Tekaia F, Badcock K, Basham D, Brown D, Chillingworth T, Connor R, Davies R, Devlin K, Feltwell T, Gentles S, Hamlin N, Holroyd S, Hornsby T, Jagels K, Krogh A, McLean J, Moule S, Murphy L, Oliver K, Osborne J, Quail MA, Rajahdream MA, Rogers J, Rutter S, Seeger K, Skelton J, Squares R, Squares S, Sulsten JE, Taylor K, Whitehead S, Bartell BG. 1998. Deciphering the biology of *Mycobacterium tuberculosis* from the complete genome sequence. Nature 396:190–190.

30. Muñoz-Elías EJ, McKinney JD. 2005. *M. tuberculosis* isocitrate lyases 1 and 2 are jointly required for *in vivo* growth and virulence. Nat Med 11:638.

31. Brock M, Buckel W. 2004. On the mechanism of action of the antifungal agent propionate. Propionyl-CoA inhibits glucose metabolism in *Aspergillus nidulans*. Eur J Biochem 271:3227–3241.

32. Patel MS, Roche TE. 1990. Molecular biology and biochemistry of pyruvate dehydrogenase complexes1. The FASEB Journal 4:3224–3233.

33. Chan YA, Podevels AM, Kevany BM, Thomas MG. 2009. Biosynthesis of polyketide synthase extender units. Nat Prod Rep 26:90.

34. Dziewit L, Czarnecki J, Prochwicz E, Wibberg D, Schüter A, Pühler A, Bartosik D. 2015. Genome-guided insight into the methylotrophy of *Paracoccus aminophilus* JCM 7686. Front Microbiol 6:852.

35. Czarnecki J, Dziewit L, Puzyna M, Prochwicz E, Tudek A, Wibberg D, Schlüter A, Pühler A, Bartosik D. 2017. Lifestyle-determining extrachromosomal replicon pAMV1 and its contribution to the carbon metabolism of the methylotrophic bacterium *Paracoccus aminovorans* JCM 7685. Environ Microbiol 19:4536–4550.

36. Mosier JA, Schwager SC, Boyajian DA, Reinhart-King CA. 2021. Cancer cell metabolic plasticity in migration and metastasis. Clinical & Experimental Metastasis 38:343–359.

37. Loo JM, Scherl A, Nguyen A, Man FY, Weinberg E, Zeng Z, Saltz L, Paty PB, Tavazoie SF. 2015. extracellular metabolic energetics can promote cancer progression. Cell 160:393.

38. Fendt SM, Frezza C, Erez A. 2020. Targeting metabolic plasticity and flexibility dynamics for cancer therapy. Cancer Discov 10:1797–1807.

39. Andrzejewski S, Klimcakova E, Johnson RM, Tabariès S, Annis MG, McGuirk S, Northey JJ, Chénard V, Sriram U, Papadopoli DJ, Siegel PM, St-Pierre J. 2017. PGC-1α promotes breast cancer metastasis and confers bioenergetic flexibility against metabolic drugs. Cell Metab 26:778-787.e5.

40. Gerstmeir R, Cramer A, Dangel P, Schaffer S, Eikmanns BJ. 2004. RamB, a novel transcriptional regulator of genes involved in acetate metabolism of *Corynebacterium glutamicum*. J Bacteriol 186:2798–2809.

41. Carter MS, Alber BE. 2015. Transcriptional regulation by the short-chain fatty acyl coenzyme A regulator (ScfR) PccR controls propionyl coenzyme A assimilation by *Rhodobacter sphaeroides*. J Bacteriol 197:3048–3056.

42. Auchter M, Cramer A, Hüser A, Rückert C, Emer D, Schwarz P, Arndt A, Lange C, Kalinowski J, Wendisch VF, Eikmanns BJ. 2011. RamA and RamB are global transcriptional regulators in *Corynebacterium glutamicum* and control genes for enzymes of the central metabolism. J Biotechnol 154:126–139.

43. Cramer A, Auchter M, Frunzke J, Bott M, Eikmanns BJ. 2007. RamB, the transcriptional regulator of acetate metabolism in *Corynebacterium glutamicum*, is subject to regulation by RamA and RamB. J Bacteriol 189:1145–1149.

44. Datta P, Shi L, Bibi N, Balázsi G, Gennaro ML. 2011. Regulation of central metabolism genes of *Mycobacterium tuberculosis* by parallel feed-forward loops controlled by sigma factor E (σE). J Bacteriol 193:1154.

45. Micklinghoff JC, Breitinger KJ, Schmidt M, Geffers R, Eikmanns BJ, Bange FC. 2009. Role of the transcriptional regulator RamB (Rv0465c) in the control of the glyoxylate cycle in *Mycobacterium tuberculosis*. J Bacteriol 191:7260–7269.

46. Zarzycki J, Fuchs G. 2011. Coassimilation of organic substrates via the autotrophic 3-hydroxypropionate bi-cycle in *Chloroflexus aurantiacus*. Appl Environ Microbiol 77:6181–6188.

47. Tang S, Hicks ND, Cheng YS, Silva A, Fortune SM, Sacchettini JC. 2019. Structural and functional insight into the *Mycobacterium tuberculosis* protein PrpR reveals a novel type of transcription factor. Nucleic Acids Res 47:9934–9949.

48. Koedooder C, Guéneuguès A, van Geersdaële R, Vergé V, Bouget FY, Labreuche Y, Obernosterer I, Blain S. 2018. The role of the glyoxylate shunt in the acclimation to iron limitation in marine heterotrophic bacteria. Front Mar Sci 5:435.

49. Ha S, Shin B, Park W. 2018. Lack of glyoxylate shunt dysregulates iron homeostasis in *Pseudomonas aeruginosa*. Microbiology (Reading) 164:587–599.

50. Ahn S, Jung J, Jang IA, Madsen EL, Park W. 2016. Role of glyoxylate shunt in oxidative stress response. J Biol Chem 291:11928.

51. Feng Y, Zhang Y, Ebright RH. 2016. Structural basis of transcription activation. Science 352:1330–1333.

52. Browning DF, Busby SJW. 2004. The regulation of bacterial transcription initiation. Nat Rev Microbiol 2:57–65.

53. Busby S, Ebright RH. 1999. Transcription activation by catabolite activator protein (CAP). J Mol Biol 293:199–213.

54. Schlüter JP, Reinkensmeier J, Barnett MJ, Lang C, Krol E, Giegerich R, Long SR, Becker A. 2013. Global mapping of transcription start sites and promoter motifs in the symbiotic α-proteobacterium *Sinorhizobium meliloti* 1021. BMC Genomics 14:1–21.

55. Feklistov A, Darst SA. 2011. Structural basis for promoter-10 element recognition by the bacterial RNA polymerase σ subunit. Cell 147:1257–1269.

56. Feklístov A, Sharon BD, Darst SA, Gross CA. 2014. Bacterial sigma factors: a historical, structural, and genomic perspective. Annu Rev Microbiol 68:357–376.

57. Paget MS. 2015. Bacterial sigma factors and anti-sigma factors: structure, function and distribution. Biomolecules 5:1245.

58. Khesin RB, Shemyakin MF, Gorlenko ZM, Mindlin SZ, Ilyina TS. 1969. Studies on the RNA polymerase in *Escherichia coli* K12 using the mutation affecting its activity. J Mol Biol 42:401–411.

59. Travers AA, Burgess RR. 1969. Cyclic re-use of the RNA polymerase sigma factor. Nature 222:537–540.

60. Buck M, Gallegos MT, Studholme DJ, Guo Y, Gralla JD. 2000. The bacterial enhancer-dependent sigma(54) (sigma(N)) transcription factor. J Bacteriol 182:4129–4136.

61. Kumar A, Grimes B, Fujita N, Makino K, Malloch RA, Hayward RS, Ishihama A. 1994. Role of the sigma70 subunit of *Escherichia coli* RNA polymerase in transcription activation. J Mol Biol 235:405–413.

62. Liu B, Hong C, Huang RK, Yu Z, Steitz TA. 2017. Structural basis of bacterial transcription activation. Science 358:947–951.

63. Shi W, Jiang Y, Deng Y, Dong Z, Liu B. 2020. Visualization of two architectures in class-II CAP-dependent transcription activation. PLoS Biol 18:e3000706.

64. Schultz SC, Shields GC, Steitz TA. 1991. Crystal structure of a CAP-DNA complex: the DNA is bent by 90 degrees. Science 253:1001–1007.

65. de Crombrugghe B, Busby S, Buc H. 1984. Cyclic AMP receptor protein: Role in transcription activation. Science 224:831–838.

66. Hao M, Ye F, Jovanovic M, Kotta-Loizou I, Xu Q, Qin X, Buck M, Zhang X, Wang M. 2022. structures of class i and class ii transcription complexes reveal the molecular basis of RamA-dependent transcription activation. Advanced Science 9.

67. Payankaulam S, Li LM, Arnosti DN. 2010. Transcriptional repression: Conserved and evolved features. Current Biology 20:R764–R771.

68. Lee J, Goldfarb A. 1991. Lac repressor acts by modifying the initial transcribing complex so that it cannot leave the promoter. Cell 66:793–798.

69. Schlax PJ, Capp MW, Record MT. 1995. Inhibition of transcription initiation by lac repressor. J Mol Biol 245:331–350.

70. Majors J. 1975. Initiation of i*n vitro* mRNA synthesis from the wild-type lac promoter. Proceedings of the National Academy of Sciences 72:4394–4398.

71. Lewis M. 1996. Response: DNA looping and lac repressor--CAP interaction. Science 274:1931–1932.

72. Greenblatt J, Schleif R. 1971. Arabinose C protein: regulation of the arabinose operon i*n vitro*. Nature New Biology 233:166–170.

73. Englesberg E. 1961. Enzymatic characterization of 17 L-arabinose negative mutants of *Escherichia coli*. J Bacteriol 81:996–1006.

74. Sheppard DE, Englesberg E. 1967. Further evidence for positive control of the L-arabinose system by gene *araC*. J Mol Biol 25:443–454.

75. Ross JJ, Gryczynski U, Schleif R. 2003. Mutational analysis of residue roles in AraC function. J Mol Biol 328:85–93.

76. Zhang X, Reeder T, Schleif R. 1996. Transcription activation parameters at ara p*BAD*. J Mol Biol 258:14–24.

77. Gui L, Sunnarborg A, Laporte DC. 1996. Regulated expression of a repressor protein: FadR activates *iclR*. J Bacteriol 178:4704–4709.

78. Cortay JC, Negre D, Galinier A, Duclos B, Perriere G, Cozzone AJ. 1991. Regulation of the acetate operon in *Escherichia coli*: purification and functional characterization of the IclR repressor. EMBO J 10:675–679.

79. Lorca GL, Ezersky A, Lunin V v., Walker JR, Altamentova S, Evdokimova E, Vedadi M, Bochkarev A, Savchenko A. 2007. Glyoxylate and pyruvate are antagonistic effectors of the *Escherichia coli* IclR transcriptional regulator. J Biol Chem 282:16476–16491.

80. Laportes DC, Thorsness PE, Koshland DE. 1985. Compensatory phosphorylation of isocitrate dehydrogenase. A mechanism for adaptation to the intracellular environment. J Biol Chem 260:10563–10568.

81. Garnak M, Reeves HC. 1979. Phosphorylation of Isocitrate dehydrogenase of *Escherichia coli*. Science 203:1111–1112.

82. Laporte DC, Koshland DE. 1982. A protein with kinase and phosphatase activities involved in regulation of tricarboxylic acid cycle. Nature 300:458–460.

83. Laporte DC, Koshland DE. 1983. Phosphorylation of isocitrate dehydrogenase as a demonstration of enhanced sensitivity in covalent regulation. Nature 305:286–290.

84. Zheng J, Jia Z. 2010. Structure of the bifunctional isocitrate dehydrogenase kinase/phosphatase. Nature 465:961–965.

85. Miller SP, Chen R, Karschnia EJ, Romfo C, Dean A, LaPorte DC. 2000. Locations of the regulatory sites for isocitrate dehydrogenase kinase/phosphatase. J Biol Chem 275:833–839.

86. Bi J, Wang Y, Yu H, Qian X, Wang H, Liu J, Zhang X. 2017. Modulation of central carbon metabolism by acetylation of isocitrate lyase in *Mycobacterium tuberculosis*. Scientific Reports 7:1–11.

87. Hu B, Lidstrom M. 2012. CcrR, a TetR family transcriptional regulator, activates the transcription of a gene of the ethylmalonyl coenzyme a pathway in *Methylobacterium extorquens* AM1. J Bacteriol 194:2802–2808.

88. Erb TJ, Rétey J, Fuchs G, Alber BE. 2008. Ethylmalonyl-CoA mutase from *Rhodobacter sphaeroides* defines a new subclade of coenzyme B12-dependent Acyl-CoA mutases. J Biol Chem 283:32283–32293.

89. Blažič M, Kosec G, Baebler Š, Gruden K, Petković H. 2015. Roles of the crotonyl-CoA carboxylase/reductase homologues in acetate assimilation and biosynthesis of immunosuppressant FK506 in *Streptomyces tsukubaensis*. Microb Cell Fact 14:164.

90. Solovyev V, Salamov A. 2011. Automatic annotation of microbial genomes and metagenomic sequences. Metagenomics and its Applications in Agriculture, Biomedicine and Environmental Studies (Ed RW Li) 61–78.

91. Subhadra B, Ray D, Han JY, Bae KH, Lee JK. 2015. Identification of the regulators binding to the upstream region of *glxR* in *Corynebacterium glutamicum*. J Microbiol Biotechnol 25:1216–1226.

92. Leßmeier L, Alkhateeb RS, Schulte F, Steffens T, Loka TP, Pühler A, Niehaus K, Vorhölter FJ. 2016. Applying DNA affinity chromatography to specifically screen for sucrose-related DNA-binding transcriptional regulators of *Xanthomonas campestris*. J Biotechnol 232:89–98.

93. Alber BE. 2011. Biotechnological potential of the ethylmalonyl-CoA pathway. Appl Microbiol Biotechnol 89:17–25.

94. Severi F. 2022. New central carbon metabolic pathways in Alphaproteobacteria: from natural to synthetic metabolism. Dissertation.

95. Schada von Borzyskowski L. 2017. Exploring alternative solutions in the central carbon metabolism of *Methylobacterium extorquens* AM1 by metabolic engineering. Dissertation.

96. Diehl C, Gerlinger PD, Paczia N, Erb TJ. 2022. Synthetic anaplerotic modules for the direct synthesis of complex molecules from CO2. Nature Chemical Biology 2022 1–8.

97. Schada Von Borzyskowski L, Sonntag F, Pöschel L, Vorholt JA, Schrader J, Erb TJ, Buchhaupt M. 2018. Replacing the ethylmalonyl-coa pathway with the glyoxylate shunt provides metabolic flexibility in the central carbon metabolism of *Methylobacterium extorquens* AM1. ACS Synth Biol 7:86–97.

98. Yoro KO, Daramola MO. 2020. CO2 emission sources, greenhouse gases, and the global warming effect. Advances in Carbon Capture: Methods, Technologies and Applications 3–28.

99. Erb TJ, Brecht V, Fuchs G, Müller M, Alber BE. 2009. Carboxylation mechanism and stereochemistry of crotonyl-CoA carboxylase/reductase, a carboxylating enoyl-thioester reductase. Proc Natl Acad Sci U S A 106:8871–8876.

100. Schwander T, von Borzyskowski LS, Burgener S, Cortina NS, Erb TJ. 2016. A synthetic pathway for the fixation of carbon dioxide *in vitro*. Science 354:900–904.

101. Carrillo Camacho M. 2020. Implementation of CO2 fixation pathways into *Methylorubrum extorquens* AM1. Dissertation.

102. Miller TE. 2020. Building a light driven synthetic carbon dioxide fixation cycle within microdroplets. Dissertation.

103. Mitchler MM, Garcia JM, Montero NE, Williams GJ. 2021. Transcription factor-based biosensors: A molecular-guided approach for natural product engineering. Curr Opin Biotechnol 69:172.

104. Zhang Y, Shi S. 2021. Transcription factor-based biosensor for dynamic control in yeast for natural product synthesis. Front Bioeng Biotechnol 9:1.

105. He F, Murabito E, Westerhoff H v. 2016. Synthetic biology and regulatory networks: where metabolic systems biology meets control engineering. J R Soc Interface 13.

106. Na D, Kim TY, Lee SY. 2010. Construction and optimization of synthetic pathways in metabolic engineering. Curr Opin Microbiol 13:363–370.

107. Jarman OD, Biner O, Wright JJ, Hirst J. 2021. *Paracoccus denitrificans*: a genetically tractable model system for studying respiratory complex I. Scientific Reports 11:1–14.

108. Olaya-Abril A, Hidalgo-Carrillo J, Luque-Almagro VM, Fuentes-Almagro C, Urbano FJ, Moreno-Vivián C, Richardson DJ, Roldán MD. 2018. Exploring the denitrification proteome of *Paracoccus denitrificans* PD1222. Front Microbiol 9:1137.

109. de Gier JL, Lübben M, Reijnders WNM, Tipker CA, Slotboom D -J, van Spanning RJM, Stouthamer AH, van der Oost J. 1994. The terminal oxidases of *Paracoccus denitrificans*. Mol Microbiol 13:183–196.

110. Giannopoulos G, Sullivan MJ, Hartop KR, Rowley G, Gates AJ, Watmough NJ, Richardson DJ. 2017. Tuning the modular *Paracoccus denitrificans* respirome to adapt from aerobic respiration to anaerobic denitrification. Environ Microbiol 19:4953–4964.

111. Bordel S, van Spanning RJM, Santos-Beneit F. 2021. Imaging and modelling of poly(3-hydroxybutyrate) synthesis in *Paracoccus denitrificans*. AMB Express 11:1–8.

112. de Vries GE, Harms N, Hoogendijk J, Stouthamer AH. 1989. Isolation and characterization of *Paracoccus denitrificans* mutants with increased conjugation frequencies and pleiotropic loss of a (nGATCn) DNA-modifying property. Archives of Microbiology 152:52–57.

113. van Verseveld HW, Stouthamer AH. 1978. Growth yields and the efficiency of oxidative phosphorylation during autotrophic growth of *Paracoccus denitrificans* on methanol and formate. Arch Microbiol 118:21–26.

Table 1: List of species/genomes that encode the EMCP and MCC, but not the MMCP

1	*Pseudomonas*_E sp002356535	12	SWB02 sp900696695
2	LZORAL124-50-18 sp002747395	13	AR37 sp003220345
3	*Oleiphilus messinensis*	14	*Leptospira_B selangorensis*
4	*Paraburkholderia* sp004353905	15	*Leptospira_A ilyithenensis*
5	*Paraburkholderia unamae*	16	*Turneriella parva*
6	P*aucimonas* sp003590835	17	*Saccharopolyspora spinosa*
7	*Acidovorax_C* sp001725235	18	A*urantimicrobium* sp003325955
8	*Achromobacter xylosoxidans*_C	19	SURF-43 sp004297315
9	*Achromobacter insolitus*	20	UBA2979 sp002725365
10	*Accumulibacter phosphatis*_A	21	UBA2979 sp002701625
11	2-12-FULL-62-58 sp001771985	22	GCA-002718395 sp003228125

Table 2: List of species/genomes that encode the EMCP (including the MMCP), GC, and MCC

1	*Accumulibacter* sp005524045	32	*Sneathiella* sp002694385
2	*Accumulibacter phosphatis*_B	33	*Sneathiella* sp002428885
3	*Accumulibacter phosphatis*_E	34	*Insolitispirillum peregrinum*
4	*Accumulibacter* sp000584975	35	AR31 sp003220495
5	*Accumulibacter phosphatis*_C	36	AR31 sp003220685
6	*Accumulibacter aalborgensis*	37	AR31 sp003221515
7	*Accumulibacter phosphatis*_F	38	20CM-2-70-11 sp003220315
8	*Accumulibacter* sp000585075	39	20CM-2-70-11 sp003221695
9	*Methylobacterium gossipiicola*	40	AR19 sp003220595
10	*Hyphomicrobium* sp003987725	41	*Nocardia speluncae*
11	*Hyphomicrobium denitrificans*	42	*Nocardia pseudovaccinii*
12	*Rhodomicrobium udaipurense*	43	*Nocardia veterana*
13	*Pseudodonghicola xiamenensis*	44	*Rhodococcus wratislaviensis*
14	*Celeribacter ethanolicus*	45	*Rhodococcus jostii*
15	*Celeribacter persicus*	46	*Rhodococcus opacus_C*
16	*Rhodovulum sulfidophilum*	47	*Rhodococcus rhodnii*
17	*Paracoccus versutus*	48	*Rhodococcus fascians*
18	*Paracoccus* sp002359815	49	*Amycolatopsis antarctica*
19	*Paracoccus denitrificans*	50	*Kutzneria albida*
20	*Paracoccus aminovorans*	51	*Sciscionella marina*
21	*Paracoccus aminophilus*	52	*Streptomyces yokosukanensis*
22	*Paracoccus alkenifer*	53	*Streptomyces griseofuscus*
23	*Rhodobacter capsulatus*	54	*Streptomyces murinus*
24	*Rhodobacter capsulatus_C*	55	*Streptomyces* sp003259585
25	*Rhodobacter capsulatus_B*	56	*Streptomyces antibioticus*_B
26	*Xinfangfangia* sp900105075	57	*Streptomyces* sp900091845
27	*Xinfangfangia humi*	58	*Streptomyces albidoflavus*
28	*Pararhodobacter aggregans*	59	*Streptomyces klenkii*
29	*Amaricoccus* sp003241785	60	*Streptomyces griseocarneus*
30	*Hyphomonas* sp002282565	61	*Kitasatospora purpeofusca*
31	*Zavarzinia compransoris*	62	*Kribbella antibiotica*

Table 3: Strains and plasmids for identification of the promoter region controlling the *ccr* gene

Strain/Plasmid	Description	Creator
TJE-KK49	*P. denitrificans* Pd1222 pTE5005	Katharina Kremer/Fabia Weiser
TJE-KK50	*P. denitrificans* Pd1222 pTE5006	Katharina Kremer/Fabia Weiser
pTE5005	pTE714_3873/3874_ig	Katharina Kremer/Fabia Weiser
pTE5006	pTE714_3874/3875_ig	Katharina Kremer/Fabia Weiser

III ACKNOWLEDGEMENTS

[redacted]

[redacted]

IV CURRICULUM VITAE

[redacted]

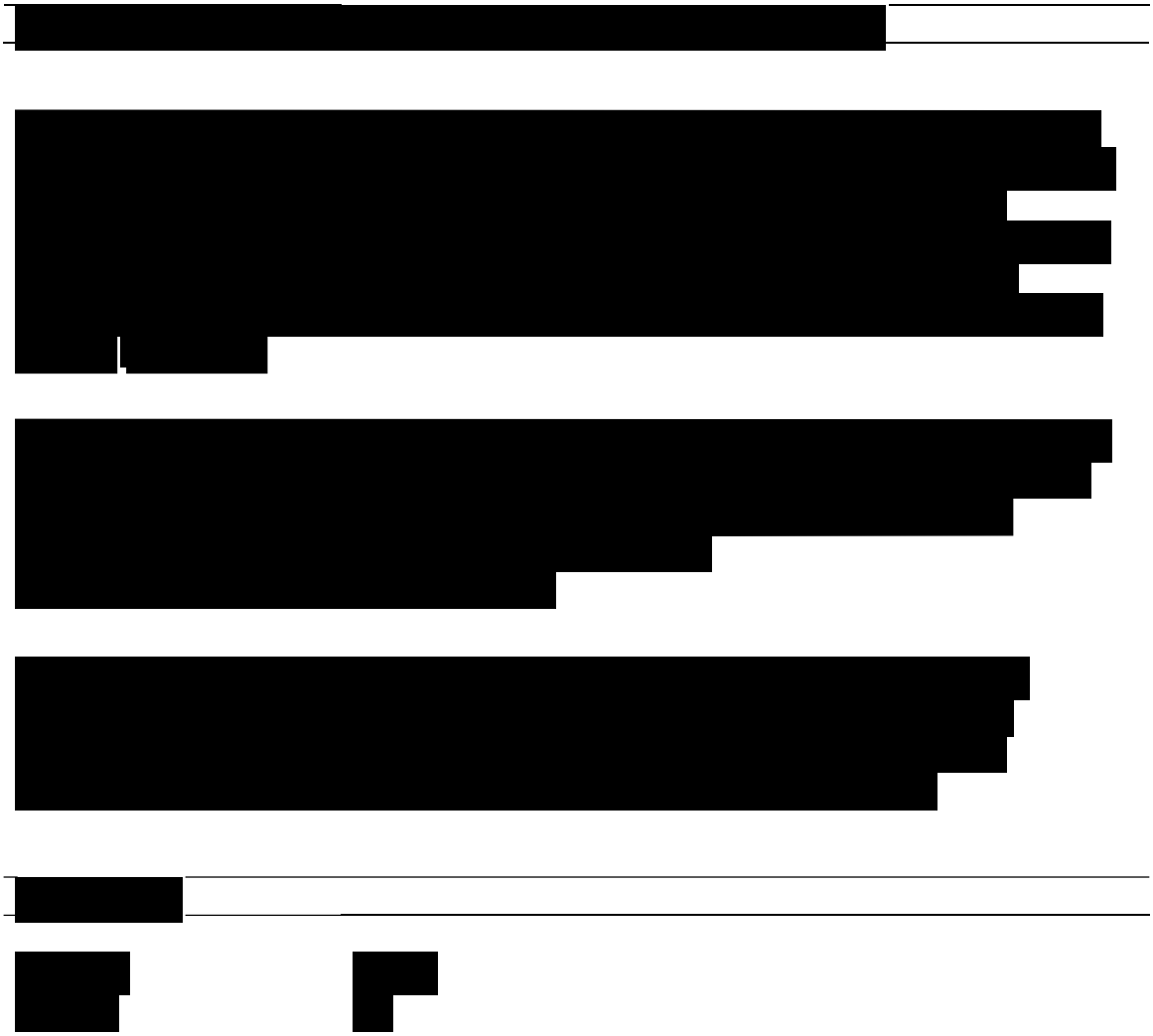

V APPENDIX

Supplementary Table 1: Top regulated genes WT_{Ac}/WT_{Suc}. Listed are all genes regulated above a threshold of log_2-fold 2.0 in the Pd1222 wild type on acetate compared to Pd1222 on succinate.

gene_id	Gene	padj	neg. log10 (padjust)	pvalue	log2-Fold Change	Regu-lation	CDS/product description	old locus tag	new locus tag
cds-WP_086000156.1	*aceA*	9.73E-297	296	2.76E-300	9.3	up	aceA	Pden_1363	PDEN_RS06725
cds-WP_011747683.1	*aceB*	1.61E-103	103	1.37E-106	9.2	up	aceB	Pden_1364	PDEN_RS06730
cds-WP_011747670.1	*prpD*	3.09E-56	56	8.77E-59	8.8	up	prpD	Pden_1348	PDEN_RS06660
cds-WP_011747669.1	*prpC*	9.99E-61	60	2.55E-63	8.6	up	prpC	Pden_1347	PDEN_RS06655
cds-WP_041530157.1	*prpB*	4.97E-25	24	2.40E-27	8.0	up	prpB	Pden_1346	PDEN_RS06650
cds-PDEN_RS26015		5.16E-10	9	6.59E-12	7.9	up	transcriptional repressor	-	PDEN_RS26015
cds-WP_011747671.1		9.57E-09	8	1.47E-10	7.8	up	thioesterase	Pden_1349	PDEN_RS06665
cds-WP_011750441.1		1.50E-76	76	1.71E-79	5.0	up	DUF485 domain-containing protein CDS	Pden_4212	PDEN_RS20985
cds-WP_011751202.1		7.18E-10	9	9.37E-12	4.9	up	alphakteoacid-dh subunit beta	Pden_4984	PDEN_RS24785
cds-WP_011750439.1		1.34E-24	24	7.21E-27	4.9	up	response regulator	Pden_4210	PDEN_RS20975
cds-WP_011750440.1		4.74E-117	116	2.69E-120	4.7	up	cation acetate symporter	Pden_4211	PDEN_RS20980
cds-WP_011746654.1		1.39E-12	12	1.46E-14	4.7	up	tricarboxylate transporter	Pden_0307	PDEN_RS01490
WP_011751203.1		7.25E-08	7	1.30E-09	4.5	up	PDH E1 suA	Pden_4985	PDEN_RS24790
cds-WP_011751200.1		6.28E-07	6	1.30E-08	4.4	up	Glc1-DH	Pden_4982	PDEN_RS24775
cds-WP_011747582.1		2.12E-07	7	4.04E-09	4.1	up	metal ABC transporter substrate-binding protein CDS	Pden_1259	PDEN_RS06215
cds-WP_011747581.1		8.73E-10	9	1.16E-11	4.1	up	manganese/iron ABC transporter ATP-binding protein CDS	Pden_1258	PDEN_RS06210
cds-WP_011746655.1		6.40E-32	31	2.18E-34	3.9	up	tripartite tricarboxylate transporter substrate binding protein CDS	Pden_0308	PDEN_RS01495
cds-WP_011747580.1		1.81E-08	8	2.93E-10	3.9	up	metal ABC transporter permease CDS	Pden_1257	PDEN_RS06205
cds-WP_049792306.1		1.53E-09	9	2.13E-11	3.9	up	hypothetical protein	Pden_1351	PDEN_RS06675
cds-WP_011746653.1		2.40E-25	25	1.09E-27	3.8	up	tripartite tricarboxylate transporter permease CDS	Pden_0306	PDEN_RS01485
cds-WP_011747579.1		1.24E-13	13	1.23E-15	3.7	up	metal ABC transporter permease CDS	Pden_1256	PDEN_RS06200
cds-WP_011750442.1		2.35E-71	71	3.34E-74	3.6	up	acs (acetate CoA ligase)	Pden_4213	PDEN_RS20990
cds-WP_011750774.1		3.47E-69	68	5.90E-72	3.5	up	acs (acetate CoA ligase)	Pden_4550	PDEN_RS22665
cds-WP_041530430.1		6.20E-28	27	2.64E-30	3.5	up	PALP-dep enzyme	Pden_3920	PDEN_RS19505
cds-WP_011750154.1		3.85E-22	21	2.40E-24	3.4	up	aminotransferase class V-fold PLP-dependent enzyme CDS	Pden_3921	PDEN_RS19510
cds-WP_011750438.1		8.16E-22	21	5.32E-24	3.3	up	bifunctional enoyl-CoA hydratase/phosphate acetyltransferase CDS	Pden_4209	PDEN_RS20970
cds-WP_011751214.1		7.01E-09	8	1.06E-10	2.9	up	acs (acetate CoA ligase)	Pden_4996	PDEN_RS24845
cds-WP_011750151.1		5.19E-14	13	5.01E-16	2.8	up	ornithine cyclodeaminase family protein CDS	Pden_3918	PDEN_RS19495
cds-WP_011750150.1		1.87E-18	18	1.48E-20	2.7	up	purine permease CDS	Pden_3917	PDEN_RS19490
cds-WP_011750630.1		3.59E-29	28	1.32E-31	2.6	up	hypothetical protein	Pden_4404	PDEN_RS21930
cds-WP_011750629.1		1.85E-11	11	2.04E-13	2.6	up	tripartite tricarboxylate transporter TctB family protein CDS	Pden_4403	PDEN_RS21925
cds-WP_011750527.1		2.31E-67	67	4.58E-70	2.6	up	acnA (aconitat hydratase)	Pden_4301	PDEN_RS21425
cds-WP_041530425.1		4.35E-43	42	1.36E-45	2.6	up	ecm	Pden_3875	PDEN_RS19280
cds-WP_011750152.1		1.38E-18	18	1.06E-20	2.6	up	DSD1 family PLP-dependent enzyme CDS	Pden_3919	PDEN_RS19500

cds-WP_011750790.1		1.39E-15	15	1.26E-17	2.5	up	EamA family transporter CDS	Pden_4566	PDEN_RS22745
cds-WP_011750791.1		2.52E-17	17	2.15E-19	2.4	up	bifunctional aconitate hydratase 2/2-methylisocitrate dehydratase CDS	Pden_4567	PDEN_RS22750
cds-WP_011750599.1		5.04E-05	4	1.32E-06	2.3	up	TonB-dependent siderophore receptor CDS	Pden_4373	PDEN_RS21785
cds-WP_011750106.1	*ccrA*	2.52E-28	28	1.00E-30	2.2	up	Crotonyl-CoA carboxylase/reductase	Pden_3873	PDEN_RS19270
cds-WP_011750149.1		5.04E-05	4	1.33E-06	2.1	up	8-oxoguanine deaminase CDS	Pden_3916	PDEN_RS19485
cds-WP_011749235.1		6.77E-25	24	3.46E-27	2.0	up	NADP-dependent isocitrate dehydrogenase CDS	Pden_2961	PDEN_RS14750
cds-WP_041529775.1		2.72E-22	22	1.62E-24	2.0	up	L-malyl-CoA/beta-methylmalyl-CoA lyase CDS	Pden_0799	PDEN_RS03970
cds-WP_011747496.1		3.95E-07	6	7.97E-09	-2.2	down	TonB-dependent receptor CDS	Pden_1171	PDEN_RS05800
cds-WP_128492943.1		1.05E-08	8	1.65E-10	-2.6	down	ammonium transporter CDS	Pden_2032	PDEN_RS10105
cds-WP_011750899.1		1.83E-17	17	1.50E-19	-2.9	down	rpmC CDS ribosomal protein	Pden_0767	PDEN_RS03810
cds-WP_164901616.1		2.35E-19	19	1.73E-21	-3.3	down	TonB-dependent siderophore receptor CDS	Pden_3029	PDEN_RS15110
cds-WP_011750985.1		2.88E-62	62	6.54E-65	-8.7	down	dicarboxylate/amino acid:cation symporter CDS	Pden_4765	PDEN_RS23720

Supplementary Table 2: Top regulated genes KO_{Ac}/KO_{Suc}. Listed are all genes regulated above a threshold of log_2-fold 2.0 in Pd1222 Δ*ramB* on acetate compared to Pd1222 Δ*ramB* on succinate.

gene_id	Gene	padj	neg. log10 (padjust)	pvalue	log2-Fold Change	Regu-lation	CDS/product description	Old locus tag	New locus tag
cds-WP_011747670.1	prpD	4.30972E-85	84	1.40169E-87	13.3	up	MmgE/PrpD family protein CDS	Pden_1348	
cds-WP_041530157.1	prpB	1.85554E-33	33	1.97141E-35	12.7	up	prpB CDS	Pden_1346	
cds-WP_011747669.1	prpC	1.37001E-91	91	4.15876E-94	12.6	up	prpC	Pden_1347	
cds-PDEN_RS26015	-	4.46679E-24	23	8.23238E-26	12.4	up	transcriptional repressor prp-operon	-	PDEN_RS26015
cds-WP_011747671.1	-	5.70502E-22	21	1.28648E-23	12.0	up	acyl-CoA thioesterase CDS	Pden_1349	PDEN_RS06665
cds-WP_011750346.1	-	7.43866E-16	15	2.91934E-17	10.2	up	VOC family protein CDS	Pden_4115	PDEN_RS20505
cds-PDEN_RS20500	-	4.0324E-116	115	9.6177E-119	9.0	up	acyl-CoA/acyl-ACP dehydrogenase CDS	Pden_4113	PDEN_RS20500
cds-WP_049792306.1	-	4.03678E-50	49	2.27572E-52	8.8	up	hypothetical protein CDS	Pden_1351	PDEN_RS06675
cds-WP_011750347.1	-	3.70507E-72	71	1.28537E-74	8.3	up	hypothetical protein CDS	Pden_4116	PDEN_RS20510
cds-WP_011750351.1	-	6.5218E-120	119	1.4141E-122	7.8	up	TRAP transporter large permease subunit CDS	Pden_4120	PDEN_RS20530
cds-WP_198140555.1	-	4.8799E-101	100	1.3755E-103	7.7	up	TRAP transporter small permease subunit CDS	Pden_4121	PDEN_RS20535
cds-WP_011750353.1	-	5.4393E-142	141	8.2557E-145	7.4	up	TRAP transporter substrate-binding protein CDS	Pden_4122	PDEN_RS20540
cds-WP_011750439.1	-	2.9281E-63	63	1.33326E-65	7.3	up	response regulator CDS	Pden_4210	PDEN_RS20975
cds-WP_011750635.1	-	1.61018E-13	13	8.55364E-15	7.0	up	hydantoinase B/oxoprolinase family protein CDS	Pden_4409	PDEN_RS21955
cds-WP_011750345.1	-	1.94225E-15	15	8.0436E-17	6.8	up	maoC family dehydratase	Pden_4111	PDEN_RS20490
cds-WP_011751204.1	-	5.17068E-07	6	6.9062E-08	6.7	up	NAD(+)/NADH kinase CDS	Pden_4986	PDEN_RS24795
cds-WP_011750440.1	-	6.8547E-237	236	1.4863E-240	6.6	up	cation acetate symporter CDS	Pden_4211	PDEN_RS20980
cds-WP_011750441.1	-	3.4732E-133	132	6.0246E-136	6.5	up	DUF485 domain-containing protein CDS	Pden_4212	PDEN_RS20985
cds-WP_011746370.1	-	5.13834E-18	17	1.57092E-19	6.4	up	methanol/ethanol family PQQ-dependent dehydrogenase CDS	Pden_0020	PDEN_RS00105
cds-WP_011750437.1	-	6.91563E-20	19	1.84437E-21	6.3	up	acetate/propionate family kinase CDS	Pden_4208	PDEN_RS20965
cds-WP_011748741.1	-	1.67472E-07	7	2.04074E-08	6.2	up	filamentous hemagglutinin N-terminal domain-containing protein CDS	Pden_2461	PDEN_RS12235
cds-WP_011746372.1	-	6.01885E-07	6	8.14346E-08	6.1	up	substrate-binding domain-containing protein CDS	Pden_0022	PDEN_RS00115
cds-WP_011750350.1	-	4.48668E-39	38	3.98859E-41	6.0	up	fumarat hydratase	Pden_4119	PDEN_RS20525
cds-WP_011750106.1	ccrA	2.5411E-229	229	1.6529E-232	6.0	up	ccrA	Pden_3873	PDEN_RS18165

cds-WP_011751203.1	-	2.28313E-11	11	1.63767E-12	5.9	up	thiamine pyrophosphate-dependent dehydrogenase E1 component subunit alpha CDS	Pden_4985	PDEN_RS24790
cds-WP_011750195.1	-	3.23154E-44	43	2.10204E-46	5.8	up	coA transferase	Pden_4112	PDEN_RS20495
cds-WP_011750344.1	-	4.55829E-14	13	2.18426E-15	5.8	up	coA ester lyase	Pden_4110	PDEN_RS20485
cds-WP_011751200.1	-	8.77269E-15	14	3.95646E-16	5.7	up	glucose 1-dehydrogenase CDS	Pden_4982	PDEN_RS24775
cds-WP_011750438.1	-	8.75216E-69	68	3.60562E-71	5.6	up	bifunctional enoyl-CoA hydratase/phosphate acetyltransferase CDS	Pden_4209	PDEN_RS20970
cds-WP_011750442.1	acs	1.1766E-180	180	1.0205E-183	5.6	up	acetyl-CoA ligase	Pden_4213	PDEN_RS20990
cds-WP_041530425.1	-	2.2765E-231	231	9.8719E-235	5.6	up	protein meaA CDS/mcm	Pden_3875	PDEN_RS19280
cds-WP_011748740.1	-	6.56687E-06	5	1.04369E-06	5.6	up	ShlB/FhaC/HecB family hemolysin secretion/activation protein CDS	Pden_2460	PDEN_RS12230
cds-WP_011746374.1	-	2.45305E-17	17	7.92506E-19	5.5	up	SRPBCC family protein CDS	Pden_0024	PDEN_RS00125
cds-WP_011750774.1	acs	9.1521E-172	171	9.9221E-175	5.5	up	acetate coA ligase CDS	Pden_4550	PDEN_RS22665
cds-WP_041530124.1	hydA	4.9607E-14	13	2.39861E-15	5.5	up	dihidropyrimidinase	Pden_1112	PDEN_RS05510
cds-WP_011749115.1	-	1.7495E-128	128	3.4141E-131	5.2	up	acyl-CoA/acyl-ACP dehydrogenase CDS	Pden_2840	PDEN_RS14140
cds-WP_011747441.1	-	9.94657E-09	8	1.00285E-09	5.2	up	Zn dependent hydrolase	Pden_1113	PDEN_RS05515
cds-WP_081465060.1	-	4.66576E-19	18	1.3455E-20	5.2	up	ompA family protein	Pden_2459	PDEN_RS25615
cds-WP_011751202.1	-	4.32877E-16	15	1.58621E-17	5.1	up	coA ester lyase	Pden_4110	PDEN_RS20485
cds-WP_011748724.1	tssC	6.37613E-21	20	1.54841E-22	5.0	up	tssC CDS (part of type VI secretion system)	Pden_2444	PDEN_RS12150
cds-WP_011750349.1	-	1.99488E-65	65	8.65081E-68	5.0	up	acyl-CoA/Acyl-ACP-DH	Pden_4113	PDEN_RS20500
cds-PDEN_RS26020	-	5.51764E-06	5	8.63777E-07	5.0	up	ribonucleoside triphosphate reductase CDS	Pden_1345	PDEN_RS26020
cds-WP_011749103.1	fdxH	2.50497E-23	23	4.9969E-25	4.9	up	fdxH CDS (formate dh)	Pden_2828	PDEN_RS14080
cds-WP_041529775.1	-	1.7325E-150	150	2.2538E-153	4.9	up	L-malyl-CoA/beta-methylmalyl-CoA lyase CDS = mcl-1	Pden_0799	PDEN_RS03970
cds-WP_011750348.1	-	5.14592E-55	54	2.67784E-57	4.8	up	class I SAM-dependent methyltransferase CDS	Pden_4117	PDEN_RS20515
cds-WP_011751201.1	-	6.59275E-12	11	4.3742E-13	4.7	up	acetoin dehydrogenase dihydrolipoyllysine-residue acetyltransferase subunit CDS	Pden_4983	PDEN_RS24780
cds-WP_011748644.1	pqqC	6.64845E-07	6	9.09621E-08	4.7	up	pyrroloquinoline-quinone synthase PqqC	Pden_2361	PDEN_RS11725
cds-WP_011749179.1	-	1.03188E-08	8	1.04261E-09	4.7	up	enoyl-CoA hydratase/isomerase family protein CDS	Pden_2905	PDEN_RS14470
cds-WP_011750428.1	-	1.94702E-12	12	1.20739E-13	4.6	up	hypothetical protein CDS	Pden_4199	PDEN_RS20920
cds-WP_049792275.1	-	4.54269E-13	12	2.59048E-14	4.5	up	ABC transporter substrate-binding protein CDS	Pden_0026	PDEN_RS00135
cds-WP_011748651.1	-	4.6819E-20	19	1.23849E-21	4.5	up	DUF779 protein	Pden_2368	PDEN_RS11765
cds-WP_011746378.1	-	2.3877E-13	13	1.30464E-14	4.4	up	hypothetical protein CDS	Pden_0028	PDEN_RS00145
cds-WP_011748177.1	-	3.11737E-07	7	4.00148E-08	4.4	up	DUF2147 domain-containing protein CDS	Pden_1885	PDEN_RS09315
cds-WP_011748723.1	tssB	1.23541E-08	8	1.26702E-09	4.4	up	type VI secretion system contractile sheath small subunit	Pden_2443	PDEN_RS12145
cds-WP_011748725.1	-	7.58753E-13	12	4.54067E-14	4.4	up	type VI secretion system tube protein Hcp CDS	Pden_2445	PDEN_RS12155
cds-WP_011750780.1	-	1.16669E-05	5	1.94027E-06	4.4	up	3'-5' exonuclease CDS	Pden_4556	PDEN_RS22695
cds-WP_049792433.1	-	9.07072E-12	11	6.13631E-13	4.4	up	hydantoinase/oxoprolinase family protein CDS	Pden_4408	PDEN_RS21950
cds-WP_024843519.1	pqqA	1.79816E-07	7	2.20676E-08	4.3	up	pqqA CDS (pyroloquinone synthesis)	-	PDEN_RS11735
cds-WP_011748645.1	pqqB	7.90747E-09	8	7.86975E-10	4.2	up	pyrroloquinoline quinone biosynthesis protein PqqB	Pden_2362	PDEN_RS11730
cds-WP_011748641.1	-	2.18742E-05	5	3.81803E-06	4.2	up	quinoprotein dehydrogenase-associated SoxYZ-likecarrier CDS	Pden_2358	PDEN_RS11710
cds-WP_041530319.1	-	1.33483E-30	30	1.59184E-32	4.2	up	AMP-binding protein CDS	Pden_2909	PDEN_RS14490
cds-WP_041530599.1	-	3.16588E-44	43	1.99069E-46	4.1	up	MaoC family dehydratase CDS	Pden_3661	PDEN_RS18165
cds-WP_011746377.1	-	1.5629E-15	15	6.40476E-17	4.1	up	YVTN family beta-propeller repeat protein CDS	Pden_0027	PDEN_RS00140
cds-WP_011746655.1	-	1.8323E-32	32	2.06591E-34	4.1	up	tripartite tricarboxylate transporter substrate binding protein CDS	Pden_0308	PDEN_RS01495

cds-WP_198140528.1	fdnG	6.11179E-72	71	2.25283E-74	4.0	up	fdnG CDS (formate dh)	Pden_2829	PDEN_RS14085
cds-WP_011748650.1	adhP	5.07158E-26	25	8.35732E-28	3.9	up	alcohol-DH	Pden_2367	PDEN_RS11760
cds-WP_011748649.1	-	6.78671E-27	26	1.00064E-28	3.9	up	aldehyde dehydrogenase family protein CDS	Pden_2366	PDEN_RS11755
cds-WP_011749181.1	-	2.93138E-22	22	6.48311E-24	3.9	up	acetyl-CoA C-acyltransferase CDS	Pden_2907	PDEN_RS14480
cds-WP_011749960.1	-	9.56337E-43	42	6.63547E-45	3.8	up	LuxR family transcriptional regulator CDS	Pden_3724	PDEN_RS18480
cds-WP_011746908.1	mcl-2	1.01917E-48	48	5.9665E-51	3.7	up	CoA ester lyase CDS	Pden_0563	PDEN_RS02805
cds-WP_011751217.1	-	1.01323E-06	6	1.43021E-07	3.7	up	branched-chain amino acid ABC transporter permease CDS	Pden_4999	PDEN_RS24860
cds-WP_155984334.1	-	7.53288E-12	11	5.0633E-13	3.7	up	hypothetical protein CDS	-	PDEN_RS26985
cds-WP_011750691.1	-	1.80466E-20	20	4.61729E-22	3.6	up	hypothetical protein CDS	Pden_4466	PDEN_RS22255
cds-WP_011750942.1	-	8.5441E-24	23	1.61174E-25	3.6	up	nitrate reductase cytochrome c-type subunit CDS	Pden_4722	PDEN_RS23505
cds-WP_011747066.1	-	1.75818E-32	32	1.94422E-34	3.5	up	patatin-like phospholipase family protein CDS	Pden_0721	PDEN_RS03585
cds-WP_011746869.1	-	1.01414E-10	10	7.78413E-12	3.5	up	purine-nucleoside phosphorylase CDS	Pden_0524	PDEN_RS02610
cds-WP_011750427.1	-	7.30621E-06	5	1.16912E-06	3.5	up	RiPP maturation radical SAM C-methyltransferase CDS	Pden_4198	PDEN_RS20915
cds-WP_011746654.1	-	9.80012E-09	8	9.85962E-10	3.5	up	tripartite tricarboxylate transporter TctB family protein CDS	Pden_0307	PDEN_RS01490
cds-WP_011748720.1	tssH	1.43033E-10	10	1.11958E-11	3.5	up	tssH CDS (type IV secretion system ATPase)	Pden_2440	PDEN_RS12130
cds-WP_011746911.1	-	7.95539E-69	68	3.10488E-71	3.4	up	MaoC family dehydratase CDS	Pden_0566	PDEN_RS02820
cds-WP_011749579.1	-	4.64028E-11	10	3.43091E-12	3.4	up	hypothetical protein CDS	Pden_3318	PDEN_RS16475
cds-WP_011748365.1	-	3.04568E-42	42	2.17926E-44	3.4	up	hypothetical protein CDS	Pden_2078	PDEN_RS10325
cds-WP_011749102.1	-	2.5488E-13	13	1.40924E-14	3.4	up	formate dehydrogenase subunit gamma CDS	Pden_2827	PDEN_RS14075
cds-WP_011746653.1	-	1.13916E-21	21	2.64288E-23	3.4	up	tripartite tricarboxylate transporter permease CDS	Pden_0306	PDEN_RS01485
cds-WP_011749182.1	-	6.91107E-11	10	5.15483E-12	3.4	up	SDR family NAD(P)-dependent oxidoreductase CDS	Pden_2908	PDEN_RS14485
cds-WP_011750943.1	-	1.13687E-41	41	8.6276E-44	3.4	up	cytochrome c3 family protein CDS	Pden_4723	PDEN_RS23510
cds-WP_011750777.1	-	1.54807E-11	11	1.09761E-12	3.3	up	hypothetical protein CDS	Pden_4553	PDEN_RS22680
cds-WP_011749876.1	-	1.72693E-06	6	2.52001E-07	3.3	up	glutathione S-transferase CDS	Pden_3640	PDEN_RS18050
cds-WP_011749180.1	-	4.30404E-16	15	1.56782E-17	3.3	up	acyl-CoA dehydrogenase family protein CDS	Pden_2906	PDEN_RS14475
cds-WP_011751197.1	-	1.07524E-09	9	9.62865E-11	3.3	up	sigma-54-dependent Fis family transcriptional regulator CDS	Pden_4979	PDEN_RS24760
cds-WP_011746754.1	-	4.65539E-07	6	6.1574E-08	3.3	up	glutathione S-transferase family protein CDS	Pden_0407	PDEN_RS02020
cds-WP_011748943.1	-	9.8708E-26	25	1.66939E-27	3.2	up	acetyl-CoA C-acyltransferase family protein CDS	Pden_2663	PDEN_RS13255
cds-WP_011748761.1	-	3.21781E-06	5	4.87694E-07	3.2	up	VWA domain-containing protein CDS	Pden_2481	PDEN_RS12330
cds-WP_011750941.1	napA	3.08196E-56	56	1.53697E-58	3.2	up	nitrate reductase	Pden_4721	PDEN_RS23500
cds-WP_011750776.1	-	1.51575E-41	41	1.18315E-43	3.2	up	cation acetate symporter CDS	Pden_4552	PDEN_RS22675
cds-WP_011750775.1	-	7.95356E-16	15	3.13865E-17	3.2	up	DUF4212 domain-containing protein CDS	Pden_4551	PDEN_RS22670
cds-WP_011749819.1	-	1.9589E-05	5	3.38517E-06	3.2	up	helix-turn-helix transcriptional regulator CDS	Pden_3582	PDEN_RS17750
cds-WP_011749580.1	-	9.75971E-11	10	7.46512E-12	3.2	up	hypothetical protein CDS	Pden_3319	PDEN_RS16480
cds-WP_011747141.1	-	1.29467E-05	5	2.16995E-06	3.2	up	ABC transporter permease CDS	Pden_0801	PDEN_RS03985
cds-WP_011750768.1	-	9.64117E-07	6	1.3567E-07	3.2	up	TRAP transporter small permease subunit CDS	Pden_4544	PDEN_RS22635
cds-WP_041530739.1	-	1.80032E-05	5	3.09551E-06	3.2	up	branched-chain amino acid ABC transporter permease CDS	Pden_5000	PDEN_RS24865
cds-WP_011746909.1	-	1.03606E-45	45	6.29002E-48	3.2	up	NnrU family protein CDS	Pden_0564	PDEN_RS02810
cds-WP_011749262.1	-	5.60611E-13	12	3.24551E-14	3.1	up	response regulator transcription factor CDS	Pden_2990	PDEN_RS14925
cds-WP_011749695.1	-	7.58016E-09	8	7.52756E-10	3.1	up	efflux RND transporter periplasmic adaptor subunit CDS	Pden_3447	PDEN_RS17075
cds-WP_011750423.1	-	1.23293E-17	17	3.90302E-19	3.1	up	SARP family transcriptional regulator CDS	Pden_4194	PDEN_RS20895

cds-WP_011749875.1	-	2.94793E-08	8	3.21511E-09	3.1	up	ATP-grasp domain-containing protein CDS	Pden_3639	PDEN_RS18045
cds-WP_011749887.1	aqpZ	1.05782E-11	11	7.40844E-13	3.1	up	aqpZ CDS (aquaporin)	Pden_3651	PDEN_RS18105
cds-WP_011748964.1	-	5.80276E-42	41	4.27784E-44	3.1	up	DUF2853 family protein CDS	Pden_2684	PDEN_RS13360
cds-WP_011749581.1	-	3.95201E-24	23	7.19794E-26	3.1	up	VWA domain-containing protein CDS	Pden_3320	PDEN_RS16485
cds-WP_011746380.1	-	6.05177E-05	4	1.14947E-05	3.0	up	ABC transporter permease CDS	Pden_0030	PDEN_RS00155
cds-WP_011749577.1	-	3.20521E-08	7	3.51656E-09	3.0	up	hypothetical protein CDS	Pden_3316	PDEN_RS16465
cds-WP_074810587.1	-	1.11666E-25	25	1.91275E-27	3.0	up	YdcH family protein CDS (methyltransferase)	Pden_2029	PDEN_RS10090
cds-WP_011749106.1	-	2.39457E-17	17	7.68422E-19	3.0	up	hybrid-cluster NAD(P)-dependent oxidoreductase CDS	Pden_2831	PDEN_RS14095
cds-WP_011746935.1	-	4.84807E-15	14	2.08675E-16	3.0	up	outer membrane protein transport protein CDS	Pden_0590	PDEN_RS02940
cds-WP_011750977.1	-	1.56669E-22	22	3.36301E-24	3.0	up	3-methyl-2-oxobutanoate dehydrogenase (2-methylpropanoyl-transferring) subunit alpha CDS	Pden_4757	PDEN_RS23680
cds-WP_011749391.1	-	1.08733E-14	14	4.97455E-16	3.0	up	recombinase family protein CDS	Pden_3123	PDEN_RS15550
cds-WP_011750769.1	-	5.31956E-16	15	1.98388E-17	3.0	up	TRAP transporter large permease subunit CDS	Pden_4545	PDEN_RS22640
cds-WP_011748715.1	-	4.62323E-05	4	8.55078E-06	3.0	up	hypothetical protein CDS	Pden_2435	PDEN_RS12105
cds-WP_011750436.1	-	6.0014E-08	7	6.88365E-09	3.0	up	polyhydroxyalkanoic acid synthase CDS	Pden_4207	PDEN_RS20960
cds-WP_011749263.1	-	1.51237E-07	7	1.83308E-08	2.9	up	HAMP domain-containing protein CDS	Pden_2991	PDEN_RS14930
cds-WP_011749578.1	-	3.98472E-09	8	3.87067E-10	2.9	up	hypothetical protein CDS	Pden_3317	PDEN_RS16470
cds-WP_011749835.1	-	5.12081E-10	9	4.38578E-11	2.9	up	hypothetical protein CDS	Pden_3599	PDEN_RS27125
cds-WP_011749582.1	-	5.81499E-08	7	6.6194E-09	2.9	up	hypothetical protein CDS	Pden_3321	PDEN_RS16490
cds-WP_011748551.1	mscL	1.59977E-31	31	1.8731E-33	2.9	up	mscL CDS (mechanosensitive channel protein)	Pden_2265	PDEN_RS11260
cds-WP_011751071.1	-	3.42961E-13	12	1.93343E-14	2.9	up	caspase family protein	Pden_4852	PDEN_RS24150
cds-WP_011746365.1	gfa	4.61173E-07	6	6.08965E-08	2.9	up	gfa CDS (glutathion synthase)	Pden_0015	PDEN_RS00080
cds-WP_011749647.1	-	5.68427E-05	4	1.07843E-05	2.9	up	twin-arginine translocation pathway signal CDS	Pden_3398	PDEN_RS16825
cds-WP_011747579.1	-	3.74546E-09	8	3.63014E-10	2.9	up	metal ABC transporter permease CDS	Pden_1256	PDEN_RS06200
cds-WP_011746795.1	-	5.42676E-13	12	3.12992E-14	2.9	up	hypothetical protein CDS	Pden_0448	PDEN_RS02230
cds-WP_011749944.1	-	1.00326E-09	9	8.89709E-11	2.9	up	DUF1330 domain-containing protein CDS	Pden_3708	PDEN_RS18410
cds-WP_011749576.1	-	9.90065E-13	12	5.98933E-14	2.8	up	hypothetical protein CDS	Pden_3315	PDEN_RS27080
cds-WP_011746910.1	-	1.93264E-30	30	2.38856E-32	2.8	up	DUF1737 domain-containing protein CDS	Pden_0565	PDEN_RS02815
cds-WP_011748722.1	-	4.96211E-05	4	9.26361E-06	2.8	up	type VI secretion system ImpA family N-terminal domain-containing protein CDS	Pden_2442	PDEN_RS12140
cds-WP_011751215.1	-	5.21718E-05	4	9.83029E-06	2.8	up	ABC transporter ATP-binding protein CDS	Pden_4997	PDEN_RS24850
cds-WP_011749873.1	-	6.00185E-13	12	3.50064E-14	2.8	up	methylcrotonoyl-CoA carboxylase CDS	Pden_3637	PDEN_RS18035
cds-WP_049792328.1	-	3.82534E-06	5	5.88896E-07	2.8	up	sigma-54-dependent Fis family transcriptional regulator CDS	Pden_2365	PDEN_RS11750
cds-WP_011748735.1	tssI	3.57935E-09	8	3.4381E-10	2.8	up	type VI secretion system tip protein VgrG	Pden_2455	PDEN_RS12205
cds-WP_011748395.1	-	3.31588E-07	6	4.27786E-08	2.8	up	Crp/Fnr family transcriptional regulator CDS	Pden_2108	PDEN_RS10470
cds-WP_011750754.1	-	5.86663E-08	7	6.70363E-09	2.8	up	sodium:solute symporter family protein CDS	Pden_4529	PDEN_RS22575
cds-WP_011746794.1	-	3.60495E-20	19	9.37976E-22	2.8	up	hypothetical protein CDS	Pden_0447	PDEN_RS02225
cds-WP_011750770.1	dctP	1.08124E-18	18	3.16493E-20	2.8	up	dctP CDS	Pden_4546	PDEN_RS22645
cds-WP_164901615.1	-	6.64984E-08	7	7.65626E-09	2.8	up	hypothetical protein CDS	-	PDEN_RS27345
cds-WP_011750560.1	-	6.2623E-13	12	3.66614E-14	2.7	up	APC family permease CDS	Pden_4334	PDEN_RS21580
cds-WP_011750863.1	-	1.06349E-12	12	6.47964E-14	2.7	up	tyrosinase family protein CDS	Pden_4643	PDEN_RS23115
cds-WP_011749264.1	-	3.38897E-08	7	3.74756E-09	2.7	up	protein MoxZ CDS	Pden_2992	PDEN_RS14935
cds-WP_049792297.1	-	8.8447E-06	5	1.43832E-06	2.7	up	DNA/RNA non-specific endonuclease CDS	Pden_0949	PDEN_RS04715

cds-WP_011750773.1	-	1.26297E-13	13	6.54488E-15	2.6	up	iron-containing alcohol dehydrogenase CDS	Pden_4549	PDEN_RS22660
cds-WP_011749107.1	-	1.78847E-20	20	4.49832E-22	2.6	up	aromatic ring-hydroxylating dioxygenase subunit alpha CDS	Pden_2832	PDEN_RS14100
cds-WP_011746953.1	-	2.64213E-19	19	7.3329E-21	2.6	up	peptide ABC transporter substrate-binding protein CDS	Pden_0608	PDEN_RS03025
cds-WP_011750740.1	-	4.10865E-17	16	1.37193E-18	2.6	up	VOC family protein CDS	Pden_4515	PDEN_RS22505
cds-WP_011750633.1	-	2.99821E-05	5	5.35674E-06	2.6	up	allantoin permease CDS	Pden_4407	PDEN_RS21945
cds-WP_011746952.1	-	6.55491E-16	15	2.51565E-17	2.6	up	ABC transporter permease CDS	Pden_0607	PDEN_RS03020
cds-WP_011750487.1	xdhB	1.1606E-13	13	5.98923E-15	2.6	up	xanthine dehydrogenase molybdopterin binding subunit	Pden_4258	PDEN_RS21210
cds-WP_011750418.1	ugpA	4.02813E-19	18	1.13542E-20	2.6	up	sn-glycerol-3-phosphate ABC transporter permeaseUgpA	Pden_4189	PDEN_RS20870
cds-WP_011750978.1	-	2.46167E-09	9	2.30582E-10	2.6	up	alpha-ketoacid dehydrogenase subunit beta CDS	Pden_4758	PDEN_RS23685
cds-WP_011746738.1	-	4.50678E-05	4	8.2963E-06	2.6	up	hypothetical protein CDS	Pden_0391	PDEN_RS01930
cds-WP_011746796.1	-	1.38646E-13	13	7.27501E-15	2.6	up	DNA polymerase III subunit epsilon CDS	Pden_0449	PDEN_RS25930
cds-WP_011750417.1	ugpE	1.59096E-18	18	4.69147E-20	2.6	up	sn-glycerol-3-phosphate ABC transporter permeaseUgpE	Pden_4188	PDEN_RS20865
cds-WP_011746954.1	-	8.56217E-15	14	3.84295E-16	2.6	up	ABC transporter ATP-binding protein CDS	Pden_0609	PDEN_RS03030
cds-WP_128492982.1	-	5.46752E-08	7	6.20016E-09	2.6	up	hypothetical protein CDS	-	PDEN_RS04720
cds-WP_011747391.1	-	4.88201E-09	8	4.79521E-10	2.6	up	flavin reductase family protein CDS	Pden_1062	PDEN_RS05275
cds-WP_011750940.1	-	4.0844E-11	10	2.99334E-12	2.6	up	chaperone NapD CDS	Pden_4720	PDEN_RS23495
cds-WP_011750059.1	-	1.01888E-11	11	7.11358E-13	2.6	up	CoA-binding protein CDS	Pden_3824	PDEN_RS19025
cds-WP_011746951.1	-	7.02985E-07	6	9.63327E-08	2.6	up	ABC transporter permease CDS	Pden_0606	PDEN_RS03015
cds-WP_011746870.1	-	5.34176E-17	16	1.80684E-18	2.5	up	ABC transporter permease CDS	Pden_0525	PDEN_RS02615
cds-WP_041529929.1	-	7.64945E-10	9	6.71732E-11	2.5	up	hypothetical protein CDS	-	PDEN_RS10215
cds-WP_011749574.1	-	9.43538E-11	10	7.18087E-12	2.5	up	molybdopterin-dependent oxidoreductase CDS	Pden_3313	PDEN_RS16450
cds-WP_011747752.1	bioB	2.76344E-15	15	1.15643E-16	2.5	up	bioB CDS (part of biotin synthesis/import cluster)	Pden_1433	PDEN_RS07085
cds-WP_198140556.1	-	5.14456E-05	4	9.67116E-06	2.5	up	hydantoinase/oxoprolinase family protein CDS	Pden_4263	PDEN_RS21235
cds-WP_011751198.1	-	2.51754E-08	8	2.71296E-09	2.5	up	2,3-butanediol dehydrogenase CDS	Pden_4980	PDEN_RS24765
cds-WP_011746553.1	-	1.33024E-05	5	2.23821E-06	2.5	up	SDR family oxidoreductase CDS	Pden_0206	PDEN_RS00990
cds-WP_011748717.1	-	2.12119E-05	5	3.69783E-06	2.5	up	DUF4150 domain-containing protein CDS	Pden_2437	PDEN_RS25610
cds-WP_011748261.1	-	5.64885E-05	4	1.07008E-05	2.5	up	recombinase family protein CDS	Pden_1972	PDEN_RS26105
cds-WP_011750702.1	-	7.23386E-10	9	6.28963E-11	2.5	up	CBS domain-containing protein CDS	Pden_4477	PDEN_RS22310
cds-WP_011747298.1	-	1.31044E-39	39	1.10813E-41	2.5	up	hypothetical protein CDS	Pden_0959	PDEN_RS04770
cds-WP_041530327.1	-	1.54435E-05	5	2.63002E-06	2.5	up	hypothetical protein CDS	-	PDEN_RS15600
cds-WP_011747675.1	-	1.78372E-07	7	2.18517E-08	2.4	up	methionine synthase CDS	Pden_1355	PDEN_RS06690
cds-WP_011748716.1	-	6.6643E-12	11	4.43612E-13	2.4	up	hypothetical protein CDS	Pden_2436	PDEN_RS12110
cds-WP_011748294.1	-	1.52114E-08	8	1.56996E-09	2.4	up	acyl-CoA synthetase CDS	Pden_2005	PDEN_RS09970
cds-WP_011748341.1	-	2.10131E-07	7	2.60614E-08	2.4	up	hypothetical protein CDS	Pden_2053	PDEN_RS10205
cds-WP_041530076.1	-	8.93522E-22	21	2.03425E-23	2.4	up	ABC transporter permease CDS	Pden_0526	PDEN_RS02620
cds-WP_011748015.1	-	3.9757E-08	7	4.46534E-09	2.4	up	malonyl-CoA decarboxylase CDS	Pden_1720	PDEN_RS08455
cds-WP_011750419.1	ugpB	1.17588E-26	26	1.81022E-28	2.4	up	ugpB CDS (glycerol-3-p permease)	Pden_4190	PDEN_RS20875
cds-WP_011747674.1	-	3.06796E-07	7	3.93141E-08	2.4	up	DUF1852 domain-containing protein CDS	Pden_1354	PDEN_RS06685
cds-WP_128492935.1	-	2.92407E-12	12	1.864E-13	2.4	up	hypothetical protein CDS	Pden_1356	PDEN_RS26870
cds-WP_011747140.1	-	4.98541E-07	6	6.6155E-08	2.4	up	ABC transporter ATP-binding protein CDS	Pden_0800	PDEN_RS03980
cds-WP_011750862.1	-	3.99193E-18	17	1.21177E-19	2.4	up	hypothetical protein CDS	Pden_4642	PDEN_RS23110

cds-WP_011751042.1	-	8.26721E-07	6	1.14992E-07	2.4	up	SDR family oxidoreductase CDS	Pden_4822	PDEN_RS24005
cds-WP_011750489.1	guaD	5.69731E-12	11	3.74303E-13	2.4	up	guaD CDS	Pden_4260	PDEN_RS21220
cds-WP_011747600.1	-	5.66681E-23	22	1.16727E-24	2.4	up	purine permease CDS	Pden_1277	PDEN_RS06305
cds-WP_011750082.1	-	2.45053E-12	12	1.54619E-13	2.4	up	site-specific integrase CDS	Pden_3849	PDEN_RS19160
cds-WP_011750861.1	-	1.49889E-10	10	1.17649E-11	2.4	up	hypothetical protein CDS	Pden_4641	PDEN_RS23105
cds-WP_011751214.1	-	2.19471E-08	8	2.32224E-09	2.4	up	acetate--CoA ligase family protein CDS	Pden_4996	PDEN_RS24845
cds-WP_011749717.1	-	8.16135E-16	15	3.25605E-17	2.3	up	hypothetical protein CDS	Pden_3470	PDEN_RS17190
cds-WP_011750980.1	lpdA	3.72321E-06	5	5.7156E-07	2.3	up	lpdA CDS	Pden_4760	PDEN_RS23695
cds-WP_011748944.1	-	3.69179E-10	9	3.09784E-11	2.3	up	LysR family transcriptional regulator CDS	Pden_2664	PDEN_RS13260
cds-WP_011750771.1	-	9.48495E-12	11	6.49879E-13	2.3	up	glutamine synthetase CDS	Pden_4547	PDEN_RS22650
cds-WP_011749534.1	-	1.38238E-09	9	1.2439E-10	2.3	up	LysR family transcriptional regulator CDS	Pden_3271	PDEN_RS16245
cds-WP_011750772.1	-	6.89098E-08	7	7.97871E-09	2.3	up	aldehyde dehydrogenase family protein CDS	Pden_4548	PDEN_RS22655
cds-WP_011746947.1	-	4.88398E-14	13	2.35092E-15	2.3	up	hypothetical protein CDS	Pden_0602	PDEN_RS02995
cds-WP_041530454.1	-	3.6689E-08	7	4.10484E-09	2.3	up	glycosyltransferase family 2 protein CDS	Pden_4162	PDEN_RS20735
cds-WP_011747779.1	-	8.09818E-05	4	1.56275E-05	2.3	up	GNAT family N-acetyltransferase CDS	Pden_1461	PDEN_RS07200
cds-WP_011748633.1	-	5.56367E-05	4	1.05193E-05	2.3	up	hypothetical protein CDS	Pden_2350	PDEN_RS11670
cds-WP_011751039.1	-	9.28236E-10	9	8.21162E-11	2.3	up	acetyl-CoA acetyltransferase CDS	Pden_4819	PDEN_RS23990
cds-WP_011748185.1	msrB	1.28044E-05	5	2.14332E-06	2.3	up	msrB CDS	Pden_1893	PDEN_RS09355
cds-WP_128493090.1	-	2.5118E-06	6	3.74156E-07	2.3	up	hypothetical protein CDS	Pden_3848	PDEN_RS19155
cds-WP_011748543.1	-	9.43538E-11	10	7.16121E-12	2.2	up	NAD-dependent succinate-semialdehyde dehydrogenase CDS	Pden_2257	PDEN_RS11220
cds-WP_011750493.1	-	7.28019E-23	22	1.51539E-24	2.2	up	sigma-54-dependent Fis family transcriptional regulator CDS	Pden_4264	PDEN_RS21240
cds-WP_011749132.1	-	2.86647E-10	10	2.35558E-11	2.2	up	formate dehydrogenase beta subunit CDS	Pden_2857	PDEN_RS14225
cds-WP_041529877.1	-	2.15456E-10	10	1.73318E-11	2.2	up	LacI family DNA-binding transcriptional regulator CDS	Pden_1685	PDEN_RS08280
cds-WP_011749587.1	-	1.56436E-05	5	2.66945E-06	2.2	up	recombinase family protein CDS	Pden_0106	PDEN_RS00535
cds-WP_011749390.1	-	1.1514E-08	8	1.17337E-09	2.2	up	tyrosine-type recombinase/integrase CDS	Pden_3122	PDEN_RS15545
cds-WP_011750707.1	mmsB	1.76933E-11	11	1.26216E-12	2.2	up	3-hydroxyisobutyrate dehydrogenase	Pden_4482	PDEN_RS22335
cds-WP_011748636.1	-	3.39695E-08	7	3.76375E-09	2.2	up	FIST C-terminal domain-containing protein CDS	Pden_2353	PDEN_RS11685
cds-WP_074810797.1	-	5.71194E-13	12	3.31917E-14	2.2	up	hypothetical protein CDS	Pden_0973	PDEN_RS04850
cds-WP_128493044.1	-	2.07601E-05	5	3.60555E-06	2.2	up	hypothetical protein CDS	Pden_3322	PDEN_RS16495
cds-WP_011747100.1	-	4.53575E-10	9	3.84536E-11	2.2	up	hypothetical protein CDS	Pden_0757	PDEN_RS03760
cds-WP_157137424.1	-	1.35322E-20	20	3.37425E-22	2.2	up	hypothetical protein CDS		PDEN_RS26815
cds-WP_011747881.1	-	1.44805E-15	15	5.90274E-17	2.2	up	TRAP transporter substrate-binding protein CDS	Pden_1563	PDEN_RS07680
cds-WP_011747751.1	-	8.98662E-05	4	1.75757E-05	2.2	up	biotin transporter BioY CDS	Pden_1432	PDEN_RS07080
cds-WP_157137429.1	-	8.70516E-06	5	1.41374E-06	2.2	up	hypothetical protein CDS		PDEN_RS26875
cds-WP_011750416.1	-	1.88572E-09	9	1.73771E-10	2.2	up	sn-glycerol-3-phosphate import ATP-binding protein UgpC CDS	Pden_4187	PDEN_RS20860
cds-WP_011748634.1	-	4.83278E-06	5	7.54467E-07	2.2	up	hypothetical protein CDS	Pden_2351	PDEN_RS11675
cds-WP_011750486.1	xdhA	3.23361E-08	7	3.55473E-09	2.2	up	xanthine dehydrogenase small subunit	Pden_4257	PDEN_RS21205
cds-WP_011749823.1	-	8.16135E-16	15	3.25456E-17	2.2	up	transglutaminase domain-containing protein CDS	Pden_3586	PDEN_RS17770
cds-WP_011751037.1	-	9.94574E-12	11	6.92234E-13	2.2	up	TRAP transporter substrate-binding protein CDS	Pden_4817	PDEN_RS23980
cds-WP_011746571.1	-	1.80288E-21	21	4.22184E-23	2.2	up	sigma-54-dependent Fis family transcriptional regulator CDS	Pden_0224	PDEN_RS01080
cds-WP_011749101.1	fdhE	4.08026E-09	8	3.97233E-10	2.2	up	fdhE CDS	Pden_2826	PDEN_RS14070
cds-WP_198140519.1	-	3.56041E-12	11	2.29281E-13	2.1	up	Na/Pi symporter CDS	Pden_0816	PDEN_RS04055
cds-WP_011749131.1	fdhF	2.5938E-15	15	1.07981E-16	2.1	up	formate dehydrogenase subunit alpha	Pden_2856	PDEN_RS14220

cds-WP_011749201.1	-	3.42724E-17	16	1.13696E-18	2.1	up	L-lactate permease CDS	Pden_2927	PDEN_RS14580
cds-WP_011749696.1	-	3.18621E-23	22	6.494E-25	2.1	up	multidrug efflux RND transporter permease subunit CDS	Pden_3448	PDEN_RS17080
cds-WP_011746900.1	-	2.84316E-37	37	2.65082E-39	2.1	up	2-oxoglutarate dehydrogenase E1 component CDS	Pden_0555	PDEN_RS02770
cds-WP_011746873.1	-	2.76775E-14	14	1.30826E-15	2.1	up	BMP family ABC transporter substrate-binding protein CDS	Pden_0528	PDEN_RS02630
cds-WP_011748622.1	-	1.33414E-07	7	1.60548E-08	2.1	up	4-aminobutyrate--2-oxoglutarate transaminase CDS	Pden_2338	PDEN_RS11610
cds-WP_011749743.1	-	1.36678E-10	10	1.06687E-11	2.1	up	TRAP transporter substrate-binding protein CDS	Pden_3497	PDEN_RS17330
cds-WP_011751040.1	-	4.57072E-13	12	2.61637E-14	2.1	up	acyl-CoA synthetase CDS	Pden_4820	PDEN_RS23995
cds-WP_011749869.1	-	1.64513E-15	15	6.77741E-17	2.1	up	isovaleryl-CoA dehydrogenase CDS	Pden_3633	PDEN_RS18015
cds-WP_011750239.1	-	9.57349E-08	7	1.12715E-08	2.1	up	DUF2945 domain-containing protein CDS	Pden_4005	PDEN_RS19945
cds-WP_011747578.1	-	8.65655E-09	8	8.65279E-10	2.1	up	SDR family oxidoreductase CDS	Pden_1255	PDEN_RS06195
cds-WP_011746872.1	-	9.5675E-09	8	9.60484E-10	2.1	up	ABC transporter ATP-binding protein CDS	Pden_0527	PDEN_RS02625
cds-WP_041529795.1	-	9.51651E-07	6	1.33503E-07	2.1	up	hypothetical protein CDS	Pden_0978	PDEN_RS04875
cds-WP_011747142.1	-	6.56117E-05	4	1.25334E-05	2.1	up	ABC transporter permease CDS	Pden_0802	PDEN_RS03990
cds-WP_011750101.1	-	4.08146E-10	9	3.43366E-11	2.1	up	zinc metallopeptidase CDS	Pden_3868	PDEN_RS19245
cds-WP_041529728.1	-	4.24381E-08	7	4.78487E-09	2.0	up	hypothetical protein CDS	Pden_0347	PDEN_RS01705
cds-WP_011750741.1	-	3.14314E-10	10	2.58975E-11	2.0	up	VOC family protein CDS	Pden_4516	PDEN_RS22510
cds-WP_128492954.1	-	5.9106E-10	9	5.10065E-11	2.0	up	tyrosine-type recombinase/integrase CDS	Pden_2419	PDEN_RS12025
cds-WP_011746899.1	odhB	6.06734E-35	34	6.05156E-37	2.0	up	2-oxoglutarate dehydrogenase complex dihydrolipoyllysine-residue succinyltransferase	Pden_0554	PDEN_RS02765
cds-WP_104493368.1	-	9.22046E-12	11	6.26583E-13	2.0	up	hypothetical protein CDS	Pden_0393	PDEN_RS01940
cds-WP_011749712.1	-	2.10941E-05	5	3.66814E-06	2.0	up	Rieske 2Fe-2S domain-containing protein CDS	Pden_3465	PDEN_RS17165
cds-WP_011749575.1	-	3.78018E-07	6	4.94243E-08	2.0	up	hypothetical protein CDS	Pden_3314	PDEN_RS16455
cds-WP_081465042.1	-	3.96294E-06	5	6.11799E-07	2.0	up	rhomboid family intramembrane serine protease CDS	Pden_2337	PDEN_RS11605
cds-WP_041529953.1	-	1.12582E-09	9	1.0106E-10	2.0	up	Arc family DNA-binding protein CDS	Pden_2281	PDEN_RS26955
cds-WP_164901601.1	-	5.09035E-05	4	9.54717E-06	2.0	up	hypothetical protein CDS		PDEN_RS27300
cds-WP_011747299.1	phaR	2.14211E-21	21	5.1091E-23	2.0	up	polyhydroxyalkanoate synthesis repressor PhaR	Pden_0960	PDEN_RS04775
cds-WP_011748334.1	-	6.65088E-08	7	7.67188E-09	-2.0	down	TonB-dependent receptor CDS	Pden_2046	PDEN_RS10170
cds-WP_011747230.1	rpsF	1.62712E-26	26	2.54017E-28	-2.0	down	rpsF CDS	Pden_0891	PDEN_RS04425
cds-WP_011748873.1	-	1.56791E-13	13	8.2951E-15	-2.0	down	RNA-binding protein CDS	Pden_2593	PDEN_RS12885
cds-WP_011749934.1	-	3.25276E-07	6	4.18232E-08	-2.0	down	RNA methyltransferase CDS	Pden_3698	PDEN_RS18360
cds-WP_011748055.1	ilvC	2.75472E-10	10	2.25777E-11	-2.0	down	ketol-acid reductoisomerase	Pden_1760	PDEN_RS08665
cds-WP_011747229.1	-	7.58753E-13	12	4.53118E-14	-2.0	down	30S ribosomal protein S18 CDS	Pden_0890	PDEN_RS04420
cds-WP_041530668.1	-	2.35576E-06	6	3.48869E-07	-2.0	down	hypothetical protein CDS	Pden_4302	PDEN_RS21430
cds-WP_041530731.1	-	6.49124E-19	18	1.88601E-20	-2.0	down	altronate dehydratase CDS	Pden_4928	PDEN_RS24515
cds-WP_010400236.1	rpsS	2.86461E-07	7	3.64597E-08	-2.0	down	30S ribosomal protein S19	Pden_0763	PDEN_RS03790
cds-WP_011748577.1	-	8.03332E-05	4	1.54849E-05	-2.0	down	glycosyl transferase CDS	Pden_2293	PDEN_RS11390
cds-WP_011747088.1	rplK	5.48385E-17	16	1.86679E-18	-2.0	down	50S ribosomal protein L11	Pden_0743	PDEN_RS03695
cds-WP_011747028.1	tolQ	9.96023E-13	12	6.04698E-14	-2.0	down	tolQ CDS	Pden_0683	PDEN_RS03395
cds-WP_011747109.1	rpsQ	1.96741E-07	7	2.423E-08	-2.0	down	30S ribosomal protein S17	Pden_0768	PDEN_RS03815
cds-WP_011750311.1	-	6.36432E-18	17	1.97333E-19	-2.0	down	50S ribosomal protein L25/general stress proteinCtc CDS	Pden_4077	PDEN_RS20310
cds-WP_041530730.1	-	1.00529E-07	7	1.19099E-08	-2.0	down	amino acid ABC transporter permease CDS	Pden_4924	PDEN_RS24495
cds-WP_011750529.1	rpsD	7.40185E-13	12	4.39745E-14	-2.1	down	30S ribosomal protein S4	Pden_4303	PDEN_RS21435
cds-WP_011748890.1	-	2.60821E-06	6	3.89083E-07	-2.1	down	TonB-dependent receptor CDS	Pden_2610	PDEN_RS12975

cds-WP_104491135.1	-	5.30849E-09	8	5.23713E-10	-2.1	down	H-type lectin domain-containing protein CDS	Pden_3820	PDEN_RS19005
cds-WP_041529773.1	rpmC	7.36309E-13	12	4.35846E-14	-2.1	down	50S ribosomal protein L29	Pden_0767	PDEN_RS03810
cds-WP_011749035.1	rpsO	1.66471E-10	10	1.31387E-11	-2.1	down	30S ribosomal protein S15	Pden_2760	PDEN_RS13740
cds-WP_011750809.1	-	1.94114E-09	9	1.79299E-10	-2.1	down	co-chaperone GroES CDS	Pden_4586	PDEN_RS22840
cds-WP_011747105.1	rplV	3.39651E-10	9	2.82061E-11	-2.1	down	50S ribosomal protein L22	Pden_0764	PDEN_RS03795
cds-WP_011751150.1	-	1.12779E-05	5	1.86824E-06	-2.1	down	SDR family oxidoreductase CDS	Pden_4932	PDEN_RS24535
cds-WP_011747103.1	-	1.04265E-13	13	5.35793E-15	-2.1	down	50S ribosomal protein L23 CDS	Pden_0761	PDEN_RS03780
cds-WP_010400243.1	rplN	1.79749E-20	20	4.55998E-22	-2.1	down	rplN CDS	Pden_0769	PDEN_RS03820
cds-WP_011747115.1	rplR	1.77872E-14	14	8.3305E-16	-2.1	down	rplR CDS	Pden_0775	PDEN_RS03850
cds-WP_041529977.1	-	4.64011E-11	10	3.42072E-12	-2.1	down	non-ribosomal peptide synthetase CDS	Pden_2564	PDEN_RS12745
cds-WP_011748559.1	rplT	1.39224E-17	17	4.43754E-19	-2.1	down	50S ribosomal protein L20	Pden_2273	PDEN_RS11300
cds-WP_011748041.1	ndk	9.24805E-22	21	2.12553E-23	-2.1	down	nucleoside-diphosphate kinase	Pden_1746	PDEN_RS08590
cds-WP_041530417.1	-	3.39964E-06	5	5.17465E-07	-2.1	down	hypothetical protein CDS		PDEN_RS19080
cds-WP_041530427.1	-	1.52466E-09	9	1.37854E-10	-2.1	down	chorismate mutase CDS	Pden_3880	PDEN_RS19305
cds-WP_011747113.1	rpsH	1.50647E-19	19	4.08301E-21	-2.1	down	30S ribosomal protein S8	Pden_0773	PDEN_RS03840
cds-WP_011746353.1	mnmE	5.01848E-15	14	2.17627E-16	-2.1	down	tRNA uridine-5-carboxymethylaminomethyl(34) synthesis GTPase MnmE	Pden_0003	PDEN_RS00020
cds-WP_011747114.1	rplF	8.58302E-24	23	1.6377E-25	-2.1	down	50S ribosomal protein L6	Pden_0774	PDEN_RS03845
cds-WP_011750114.1	rpsP	1.87962E-27	27	2.64908E-29	-2.1	down	30S ribosomal protein S16	Pden_3881	PDEN_RS19310
cds-WP_011749243.1	rplM	7.8E-29	28	1.03166E-30	-2.1	down	50S ribosomal protein L13	Pden_2969	PDEN_RS14790
cds-WP_011750112.1	-	9.79608E-07	6	1.38063E-07	-2.1	down	GNAT family N-acetyltransferase CDS	Pden_3879	PDEN_RS19300
cds-WP_011749491.1	-	4.78384E-15	14	2.0434E-16	-2.1	down	enoyl-CoA hydratase/isomerase family protein CDS	Pden_3225	PDEN_RS16020
cds-WP_011747231.1	-	3.199E-10	9	2.64272E-11	-2.2	down	polyisoprenoid-binding protein CDS	Pden_0892	PDEN_RS04430
cds-WP_011749482.1	-	5.07436E-14	13	2.46998E-15	-2.2	down	NAD(P)-dependent oxidoreductase CDS	Pden_3256	PDEN_RS16165
cds-WP_011749481.1	-	4.4001E-16	15	1.62189E-17	-2.2	down	carboxymuconolactone decarboxylase family protein CDS	Pden_3257	PDEN_RS16170
cds-WP_011747030.1	tolA	1.28906E-12	12	7.88194E-14	-2.2	down	cell envelope integrity protein TolA	Pden_0685	PDEN_RS03405
cds-WP_011747029.1	-	9.12503E-11	10	6.90511E-12	-2.2	down	ExbD/TolR family protein CDS	Pden_0684	PDEN_RS03400
cds-WP_011750115.1	rimM	1.00562E-33	33	1.04661E-35	-2.2	down	16S rRNA processing protein RimM	Pden_3882	PDEN_RS19315
cds-WP_011751144.1	-	1.27925E-06	6	1.8279E-07	-2.2	down	amino acid ABC transporter ATP-binding protein CDS	Pden_4926	PDEN_RS24505
cds-WP_011748418.1	-	4.72334E-10	9	4.02488E-11	-2.2	down	GNAT family N-acetyltransferase CDS	Pden_2131	PDEN_RS10585
cds-WP_011749734.1	-	4.17521E-06	5	6.48189E-07	-2.2	down	FAD-dependent monooxygenase CDS	Pden_3488	PDEN_RS17285
cds-WP_011747112.1	rpsN	6.33318E-15	14	2.80132E-16	-2.2	down	30S ribosomal protein S14	Pden_0772	PDEN_RS03835
cds-WP_011749475.1	dctP	2.00951E-08	8	2.11756E-09	-2.2	down	TRAP transporter substrate-binding protein DctP	Pden_3209	PDEN_RS15945
cds-WP_011746516.1	-	7.18256E-13	12	4.23603E-14	-2.2	down	cupin domain-containing protein CDS	Pden_0167	PDEN_RS00805
cds-WP_011750335.1	-	4.7603E-27	26	6.91545E-29	-2.2	down	GNAT family N-acetyltransferase CDS	Pden_4101	PDEN_RS20440
cds-WP_011746938.1	-	1.06554E-09	9	9.51867E-11	-2.2	down	hypothetical protein CDS	Pden_0593	PDEN_RS02955
cds-WP_011747080.1	-	4.42051E-16	15	1.639E-17	-2.3	down	dienelactone hydrolase family protein CDS	Pden_0735	PDEN_RS03650
cds-WP_011747110.1	-	3.64938E-15	14	1.54299E-16	-2.3	down	50S ribosomal protein L24 CDS	Pden_0770	PDEN_RS03825
cds-WP_011750599.1	-	1.11461E-05	5	1.84275E-06	-2.3	down	TonB-dependent siderophore receptor CDS	Pden_4373	PDEN_RS21785
cds-WP_011747395.1	-	2.50982E-06	6	3.73317E-07	-2.3	down	hypothetical protein CDS	Pden_1066	PDEN_RS05295
cds-WP_011748329.1	-	1.05151E-31	31	1.20837E-33	-2.3	down	aspartate aminotransferase family protein CDS	Pden_2041	PDEN_RS10145
cds-WP_011749962.1	rpsB	2.85785E-26	26	4.58545E-28	-2.3	down	30S ribosomal protein S2	Pden_3726	PDEN_RS18490
cds-WP_011750900.1	-	3.40184E-07	6	4.4091E-08	-2.3	down	MaoC family dehydratase CDS	Pden_4680	PDEN_RS23300
cds-WP_011747117.1	rpmD	3.34279E-16	15	1.21042E-17	-2.3	down	50S ribosomal protein L30	Pden_0777	PDEN_RS03860

cds-WP_011750640.1	gabT	3.41155E-08	7	3.78733E-09	-2.3	down	4-aminobutyrate--2-oxoglutarate transaminase	Pden_4414	PDEN_RS21980
cds-WP_019353022.1	groES	3.56599E-10	9	2.97681E-11	-2.3	down	co-chaperone GroES		PDEN_RS18130
cds-WP_011749493.1	-	6.23656E-14	13	3.05608E-15	-2.4	down	CoA transferase CDS	Pden_3227	PDEN_RS16030
cds-WP_041530483.1	-	3.94797E-15	14	1.6778E-16	-2.4	down	DUF1775 domain-containing protein CDS	Pden_4444	PDEN_RS22135
cds-WP_011749303.1	-	6.3387E-06	5	1.00468E-06	-2.4	down	ABC transporter substrate-binding protein CDS	Pden_3033	PDEN_RS15130
cds-WP_011749492.1	-	2.61895E-16	16	9.31284E-18	-2.4	down	thiolase family protein CDS	Pden_3226	PDEN_RS16025
cds-WP_011747619.1	-	3.76874E-07	6	4.91931E-08	-2.4	down	DegT/DnrJ/EryC1/StrS family aminotransferase CDS	Pden_1296	PDEN_RS06400
cds-WP_011750312.1	trmFO	6.17576E-17	16	2.11572E-18	-2.4	down	methylenetetrahydrofolate--tRNA-(uracil(54)- C(5))-methyltransferase (FADH(2)-oxidizing) TrmFO	Pden_4078	PDEN_RS20315
cds-WP_011747084.1	-	6.95284E-27	26	1.04021E-28	-2.4	down	ABC transporter ATP-binding protein CDS	Pden_0739	PDEN_RS03670
cds-WP_011750569.1	cysT	2.98425E-06	6	4.48414E-07	-2.4	down	sulfate ABC transporter permease subunit CysT	Pden_4343	PDEN_RS21630
cds-WP_198140538.1	-	6.71859E-16	15	2.59304E-17	-2.4	down	AMP-binding protein CDS	Pden_3230	PDEN_RS16045
cds-WP_011751149.1	-	1.80674E-09	9	1.66101E-10	-2.4	down	zinc-binding alcohol dehydrogenase family protein CDS	Pden_4931	PDEN_RS24530
cds-WP_011749495.1	-	2.28546E-16	16	8.02786E-18	-2.4	down	MaoC family dehydratase N-terminal domain-containing protein CDS	Pden_3229	PDEN_RS16040
cds-WP_011747111.1	rplE	1.40972E-11	11	9.96462E-13	-2.5	down	rplE CDS	Pden_0771	PDEN_RS03830
cds-WP_011750669.1	-	3.24357E-15	14	1.36438E-16	-2.5	down	SCO family protein CDS	Pden_4443	PDEN_RS22130
cds-WP_011750945.1	-	5.97674E-07	6	8.06057E-08	-2.5	down	hypothetical protein CDS	Pden_4725	PDEN_RS23520
cds-WP_011749961.1	-	3.7282E-39	38	3.23348E-41	-2.5	down	elongation factor Ts CDS	Pden_3725	PDEN_RS18485
cds-WP_011746417.1	tnpB	2.53926E-08	8	2.74188E-09	-2.5	down	IS66 family insertion sequence element accessoryprotein TnpB	Pden_0067	PDEN_RS00375
cds-WP_011747189.1	-	4.2325E-25	24	7.43348E-27	-2.5	down	porin family protein CDS	Pden_0849	PDEN_RS04220
cds-WP_011746845.1	-	1.7296E-09	9	1.57884E-10	-2.5	down	VOC family protein CDS	Pden_0500	PDEN_RS02485
cds-PDEN_RS14835	-	9.02857E-06	5	1.47018E-06	-2.5	down	?	Pden_2973	PDEN_RS14835
cds-WP_011751143.1	-	2.50718E-07	7	3.14757E-08	-2.6	down	amino acid ABC transporter permease CDS	Pden_4925	PDEN_RS24500
cds-WP_011750484.1	-	1.07338E-05	5	1.76646E-06	-2.6	down	Hsp70 family protein CDS	Pden_4255	PDEN_RS21195
cds-WP_011747262.1	-	5.76323E-16	15	2.16184E-17	-2.6	down	hypothetical protein CDS	Pden_0923	PDEN_RS04585
cds-WP_011747154.1	-	2.90382E-19	19	8.12215E-21	-2.7	down	phosphoglycerate dehydrogenase CDS	Pden_0814	PDEN_RS04045
cds-WP_104494388.1	-	1.52458E-06	6	2.2115E-07	-2.7	down	TetR family transcriptional regulator CDS	Pden_2940	PDEN_RS14645
cds-WP_011749494.1	-	8.69252E-21	20	2.12978E-22	-2.7	down	aldehyde dehydrogenase CDS	Pden_3228	PDEN_RS16035
cds-WP_011749216.1	-	1.0367E-39	39	8.5418E-42	-2.8	down	multidrug efflux RND transporter permease subunit CDS	Pden_2942	PDEN_RS14655
cds-WP_011747531.1	ureC	3.40184E-07	6	4.41089E-08	-2.8	down	urease subunit alpha	Pden_1208	PDEN_RS05985
cds-WP_041529781.1	-	2.97041E-07	7	3.78992E-08	-2.8	down	hypothetical protein CDS		PDEN_RS04285
cds-WP_011748469.1	-	7.60771E-15	14	3.38157E-16	-2.9	down	DUF1800 domain-containing protein CDS	Pden_2182	PDEN_RS10840
cds-WP_011747118.1	-	1.8687E-08	8	1.95703E-09	-2.9	down	hypothetical protein CDS	Pden_0778	PDEN_RS03865
cds-WP_128492943.1	-	4.32341E-19	18	1.22803E-20	-2.9	down	ammonium transporter CDS	Pden_2032	PDEN_RS10105
cds-WP_011749215.1	-	1.18288E-07	7	1.41507E-08	-3.0	down	efflux RND transporter periplasmic adaptor subunit CDS	Pden_2941	PDEN_RS14650
cds-WP_011750899.1	-	1.09018E-23	23	2.10377E-25	-3.0	down	6,7-dimethyl-8-ribityllumazine synthase CDS	Pden_4679	PDEN_RS23295
cds-WP_011750642.1	-	1.61074E-38	38	1.46685E-40	-3.0	down	NAD-dependent succinate-semialdehyde dehydrogenase CDS	Pden_4416	PDEN_RS21990
cds-WP_011750125.1	pdhA	2.83234E-40	40	2.27226E-42	-3.2	down	pyruvate dehydrogenase (acetyl-transferring) E1 component subunit alpha	Pden_3892	PDEN_RS19370
cds-WP_011749301.1	-	2.84838E-06	6	4.26145E-07	-3.3	down	iron ABC transporter permease CDS	Pden_3031	PDEN_RS15120
cds-WP_011750124.1	-	3.9234E-44	43	2.63715E-46	-3.4	down	pyruvate dehydrogenase complex E1 component subunit beta CDS	Pden_3891	PDEN_RS19365

cds-WP_011750123.1	-	1.41783E-52	52	7.68553E-55	-3.5	down	pyruvate dehydrogenase complex dihydrolipoamide acetyltransferase CDS	Pden_3890	PDEN_RS19360
cds-WP_011749300.1	-	4.60306E-09	8	4.50125E-10	-3.5	down	class I SAM-dependent methyltransferase CDS	Pden_3030	PDEN_RS15115
cds-WP_011748558.1	-	3.00914E-05	5	5.38278E-06	-3.6	down	cytochrome P450 CDS	Pden_2272	PDEN_RS11295
cds-WP_011747493.1	-	1.13413E-05	5	1.88119E-06	-4.1	down	ABC transporter substrate-binding protein CDS	Pden_1168	PDEN_RS05785
cds-WP_011748511.1	-	5.21305E-57	56	2.48671E-59	-4.1	down	NADP-dependent malic enzyme CDS	Pden_2224	PDEN_RS11050
cds-WP_164901616.1	-	8.65261E-35	34	8.81771E-37	-4.4	down	TonB-dependent siderophore receptor CDS	Pden_3029	PDEN_RS15110
cds-_011750985.1	-	1.2001E-101	101	3.1225E-104	-9.6	down	dicarboxylate/amino acid:cation symporter CDS	Pden_4765	PDEN_RS23720

Supplementary Table 3: Top regulated genes KO_{Ac}/WT_{Ac}. Listed are all genes regulated above a threshold of log_2-fold 2.0 in Pd1222 Δ*ramB* on acetate in relation to Pd1222 wildtype on acetate

gene_id	Gene	padj	neg. log10 (padjust)	pvalue	log2-Fold Change	Regulation	CDS/product description	Old locus tag	New locus tag
cds-WP_011747670.1	prpD	4.30972E-85	84	1.40169E-87	13.3	up	MmgE/PrpD family protein CDS	Pden_1348	
cds-WP_041530157.1	prpB	1.85554E-33	33	1.97141E-35	12.7	up	prpB CDS	Pden_1346	
cds-WP_011747669.1	prpC	1.37001E-91	91	4.15876E-94	12.6	up	prpC	Pden_1347	
cds-PDEN_RS26015	-	4.46679E-24	23	8.23238E-26	12.4	up	transcriptional repressor prp-operon	-	PDEN_RS26015
cds-WP_011747671.1	-	5.70502E-22	21	1.28648E-23	12.0	up	acyl-CoA thioesterase CDS	Pden_1349	PDEN_RS06665
cds-WP_011750346.1	-	7.43866E-16	15	2.91934E-17	10.2	up	VOC family protein CDS	Pden_4115	PDEN_RS20505
cds-PDEN_RS20500	-	4.0324E-116	115	9.6177E-119	9.0	up	acyl-CoA/acyl-ACP dehydrogenase CDS	Pden_4113	PDEN_RS20500
cds-WP_049792306.1	-	4.03678E-50	49	2.27572E-52	8.8	up	hypothetical protein CDS	Pden_1351	PDEN_RS06675
cds-WP_011750347.1	-	3.70507E-72	71	1.28537E-74	8.3	up	hypothetical protein CDS	Pden_4116	PDEN_RS20510
cds-WP_011750351.1	-	6.5218E-120	119	1.4141E-122	7.8	up	TRAP transporter large permease subunit CDS	Pden_4120	PDEN_RS20530
cds-WP_198140555.1	-	4.8799E-101	100	1.3755E-103	7.7	up	TRAP transporter small permease subunit CDS	Pden_4121	PDEN_RS20535
cds-WP_011750353.1	-	5.4393E-142	141	8.2557E-145	7.4	up	TRAP transporter substrate-binding protein CDS	Pden_4122	PDEN_RS20540
cds-WP_011750439.1	-	2.9281E-63	63	1.33326E-65	7.3	up	response regulator CDS	Pden_4210	PDEN_RS20975
cds-WP_011750635.1	-	1.61018E-13	13	8.55364E-15	7.0	up	hydantoinase B/oxoprolinase family protein CDS	Pden_4409	PDEN_RS21955
cds-WP_011750345.1	-	1.94225E-15	15	8.0436E-17	6.8	up	maoC family dehydratase	Pden_4111	PDEN_RS20490
cds-WP_011751204.1	-	5.17068E-07	6	6.9062E-08	6.7	up	NAD(+)/NADH kinase CDS	Pden_4986	PDEN_RS24795
cds-WP_011750440.1	-	6.8547E-237	236	1.4863E-240	6.6	up	cation acetate symporter CDS	Pden_4211	PDEN_RS20980
cds-WP_011750441.1	-	3.4732E-133	132	6.0246E-136	6.5	up	DUF485 domain-containing protein CDS	Pden_4212	PDEN_RS20985
cds-WP_011746370.1	-	5.13834E-18	17	1.57092E-19	6.4	up	methanol/ethanol family PQQ-dependent dehydrogenase CDS	Pden_0020	PDEN_RS00105
cds-WP_011750437.1	-	6.91563E-20	19	1.84437E-21	6.3	up	acetate/propionate family kinase CDS	Pden_4208	PDEN_RS20965
cds-WP_011748741.1	-	1.67472E-07	7	2.04074E-08	6.2	up	filamentous hemagglutinin N-terminal domain-containing protein CDS	Pden_2461	PDEN_RS12235
cds-WP_011746372.1	-	6.01885E-07	6	8.14346E-08	6.1	up	substrate-binding domain-containing protein CDS	Pden_0022	PDEN_RS00115
cds-WP_011750350.1	-	4.48668E-39	38	3.98859E-41	6.0	up	fumarat hydratase	Pden_4119	PDEN_RS20525
cds-WP_011750106.1	ccrA	2.5411E-229	229	1.6529E-232	6.0	up	ccrA	Pden_3873	PDEN_RS18165

cds-WP_011751203.1	-	2.28313E-11	11	1.63767E-12	5.9	up	thiamine pyrophosphate-dependent dehydrogenase E1 component subunit alpha CDS	Pden_4985	PDEN_RS24790
cds-WP_011750195.1	-	3.23154E-44	43	2.10204E-46	5.8	up	coA transferase	Pden_4112	PDEN_RS20495
cds-WP_011750344.1	-	4.55829E-14	13	2.18426E-15	5.8	up	coA ester lyase	Pden_4110	PDEN_RS20485
cds-WP_011751200.1	-	8.77269E-15	14	3.95646E-16	5.7	up	glucose 1-dehydrogenase CDS	Pden_4982	PDEN_RS24775
cds-WP_011750438.1	-	8.75216E-69	68	3.60562E-71	5.6	up	bifunctional enoyl-CoA hydratase/phosphate acetyltransferase CDS	Pden_4209	PDEN_RS20970
cds-WP_011750442.1	acs	1.1766E-180	180	1.0205E-183	5.6	up	acetyl-CoA ligase	Pden_4213	PDEN_RS20990
cds-WP_041530425.1	-	2.2765E-231	231	9.8719E-235	5.6	up	protein meaA CDS/mcm	Pden_3875	PDEN_RS19280
cds-WP_011748740.1	-	6.56687E-06	5	1.04369E-06	5.6	up	ShlB/FhaC/HecB family hemolysin secretion/activation protein CDS	Pden_2460	PDEN_RS12230
cds-WP_011746374.1	-	2.45305E-17	17	7.92506E-19	5.5	up	SRPBCC family protein CDS	Pden_0024	PDEN_RS00125
cds-WP_011750774.1	acs	9.1521E-172	171	9.9221E-175	5.5	up	acetate coA ligase CDS	Pden_4550	PDEN_RS22665
cds-WP_041530124.1	hydA	4.9607E-14	13	2.39861E-15	5.5	up	dihidropyrimidinase	Pden_1112	PDEN_RS05510
cds-WP_011749115.1	-	1.7495E-128	128	3.4141E-131	5.2	up	acyl-CoA/acyl-ACP dehydrogenase CDS	Pden_2840	PDEN_RS14140
cds-WP_011747441.1	-	9.94657E-09	8	1.00285E-09	5.2	up	Zn dependent hydrolase	Pden_1113	PDEN_RS05515
cds-WP_081465060.1	-	4.66576E-19	18	1.3455E-20	5.2	up	ompA family protein	Pden_2459	PDEN_RS25615
cds-WP_011751202.1	-	4.32877E-16	15	1.58621E-17	5.1	up	coA ester lyase	Pden_4110	PDEN_RS20485
cds-WP_011748724.1	tssC	6.37613E-21	20	1.54841E-22	5.0	up	tssC CDS (part of type VI secretion system)	Pden_2444	PDEN_RS12150
cds-WP_011750349.1	-	1.99488E-65	65	8.65081E-68	5.0	up	acyl-CoA/Acyl-ACP-DH	Pden_4113	PDEN_RS20500
cds-PDEN_RS26020	-	5.51764E-06	5	8.63777E-07	5.0	up	ribonucleoside triphosphate reductase CDS	Pden_1345	PDEN_RS26020
cds-WP_011749103.1	fdxH	2.50497E-23	23	4.9969E-25	4.9	up	fdxH CDS (formate dh)	Pden_2828	PDEN_RS14080
cds-WP_041529775.1	-	1.7325E-150	150	2.2538E-153	4.9	up	L-malyl-CoA/beta-methylmalyl-CoA lyase CDS = mcl-1	Pden_0799	PDEN_RS03970
cds-WP_011750348.1	-	5.14592E-55	54	2.67784E-57	4.8	up	class I SAM-dependent methyltransferase CDS	Pden_4117	PDEN_RS20515
cds-WP_011751201.1	-	6.59275E-12	11	4.3742E-13	4.7	up	acetoin dehydrogenase dihydrolipoyllysine-residue acetyltransferase subunit CDS	Pden_4983	PDEN_RS24780
cds-WP_011748644.1	pqqC	6.64845E-07	6	9.09621E-08	4.7	up	pyrroloquinoline-quinone synthase PqqC	Pden_2361	PDEN_RS11725
cds-WP_011749179.1	-	1.03188E-08	8	1.04261E-09	4.7	up	enoyl-CoA hydratase/isomerase family protein CDS	Pden_2905	PDEN_RS14470
cds-WP_011750428.1	-	1.94702E-12	12	1.20739E-13	4.6	up	hypothetical protein CDS	Pden_4199	PDEN_RS20920
cds-WP_049792275.1	-	4.54269E-13	12	2.59048E-14	4.5	up	ABC transporter substrate-binding protein CDS	Pden_0026	PDEN_RS00135
cds-WP_011748651.1	-	4.6819E-20	19	1.23849E-21	4.5	up	DUF779 protein	Pden_2368	PDEN_RS11765
cds-WP_011746378.1	-	2.3877E-13	13	1.30464E-14	4.4	up	hypothetical protein CDS	Pden_0028	PDEN_RS00145
cds-WP_011748177.1	-	3.11737E-07	7	4.00148E-08	4.4	up	DUF2147 domain-containing protein CDS	Pden_1885	PDEN_RS09315
cds-WP_011748723.1	tssB	1.23541E-08	8	1.26702E-09	4.4	up	type VI secretion system contractile sheath small subunit	Pden_2443	PDEN_RS12145
cds-WP_011748725.1	-	7.58753E-13	12	4.54067E-14	4.4	up	type VI secretion system tube protein Hcp CDS	Pden_2445	PDEN_RS12155

cds-WP_011750780.1	-	1.16669E-05	5	1.94027E-06	4.4	up	3'-5' exonuclease CDS	Pden_4556	PDEN_RS22695
cds-WP_049792433.1	-	9.07072E-12	11	6.13631E-13	4.4	up	hydantoinase/oxoprolinase family protein CDS	Pden_4408	PDEN_RS21950
cds-WP_024843519.1	pqqA	1.79816E-07	7	2.20676E-08	4.3	up	pqqA CDS (pyroloquinone synthesis)	-	PDEN_RS11735
cds-WP_011748645.1	pqqB	7.90747E-09	8	7.86975E-10	4.2	up	pyrroloquinoline quinone biosynthesis protein PqqB	Pden_2362	PDEN_RS11730
cds-WP_011748641.1	-	2.18742E-05	5	3.81803E-06	4.2	up	quinoprotein dehydrogenase-associated SoxYZ-likecarrier CDS	Pden_2358	PDEN_RS11710
cds-WP_041530319.1	-	1.33483E-30	30	1.59184E-32	4.2	up	AMP-binding protein CDS	Pden_2909	PDEN_RS14490
cds-WP_041530599.1	-	3.16588E-44	43	1.99069E-46	4.1	up	MaoC family dehydratase CDS	Pden_3661	PDEN_RS18165
cds-WP_011746377.1	-	1.5629E-15	15	6.40476E-17	4.1	up	YVTN family beta-propeller repeat protein CDS	Pden_0027	PDEN_RS00140
cds-WP_011746655.1	-	1.8323E-32	32	2.06591E-34	4.1	up	tripartite tricarboxylate transporter substrate binding protein CDS	Pden_0308	PDEN_RS01495
cds-WP_198140528.1	fdnG	6.11179E-72	71	2.25283E-74	4.0	up	fdnG CDS (formate dh)	Pden_2829	PDEN_RS14085
cds-WP_011748650.1	adhP	5.07158E-26	25	8.35732E-28	3.9	up	alcohol-DH	Pden_2367	PDEN_RS11760
cds-WP_011748649.1	-	6.78671E-27	26	1.00064E-28	3.9	up	aldehyde dehydrogenase family protein CDS	Pden_2366	PDEN_RS11755
cds-WP_011749181.1	-	2.93138E-22	22	6.48311E-24	3.9	up	acetyl-CoA C-acyltransferase CDS	Pden_2907	PDEN_RS14480
cds-WP_011749960.1	-	9.56337E-43	42	6.63547E-45	3.8	up	LuxR family transcriptional regulator CDS	Pden_3724	PDEN_RS18480
cds-WP_011746908.1	mcl-2	1.01917E-48	48	5.9665E-51	3.7	up	CoA ester lyase CDS	Pden_0563	PDEN_RS02805
cds-WP_011751217.1	-	1.01323E-06	6	1.43021E-07	3.7	up	branched-chain amino acid ABC transporter permease CDS	Pden_4999	PDEN_RS24860
cds-WP_155984334.1	-	7.53288E-12	11	5.0633E-13	3.7	up	hypothetical protein CDS	-	PDEN_RS26985
cds-WP_011750691.1	-	1.80466E-20	20	4.61729E-22	3.6	up	hypothetical protein CDS	Pden_4466	PDEN_RS22255
cds-WP_011750942.1	-	8.5441E-24	23	1.61174E-25	3.6	up	nitrate reductase cytochrome c-type subunit CDS	Pden_4722	PDEN_RS23505
cds-WP_011747066.1	-	1.75818E-32	32	1.94422E-34	3.5	up	patatin-like phospholipase family protein CDS	Pden_0721	PDEN_RS03585
cds-WP_011746869.1	-	1.01414E-10	10	7.78413E-12	3.5	up	purine-nucleoside phosphorylase CDS	Pden_0524	PDEN_RS02610
cds-WP_011750427.1	-	7.30621E-06	5	1.16912E-06	3.5	up	RiPP maturation radical SAM C-methyltransferase CDS	Pden_4198	PDEN_RS20915
cds-WP_011746654.1	-	9.80012E-09	8	9.85962E-10	3.5	up	tripartite tricarboxylate transporter TctB family protein CDS	Pden_0307	PDEN_RS01490
cds-WP_011748720.1	tssH	1.43033E-10	10	1.11958E-11	3.5	up	tssH CDS (type IV secretion system ATPase)	Pden_2440	PDEN_RS12130
cds-WP_011746911.1	-	7.95539E-69	68	3.10488E-71	3.4	up	MaoC family dehydratase CDS	Pden_0566	PDEN_RS02820
cds-WP_011749579.1	-	4.64028E-11	10	3.43091E-12	3.4	up	hypothetical protein CDS	Pden_3318	PDEN_RS16475
cds-WP_011748365.1	-	3.04568E-42	42	2.17926E-44	3.4	up	hypothetical protein CDS	Pden_2078	PDEN_RS10325
cds-WP_011749102.1	-	2.5488E-13	13	1.40924E-14	3.4	up	formate dehydrogenase subunit gamma CDS	Pden_2827	PDEN_RS14075
cds-WP_011746653.1	-	1.13916E-21	21	2.64288E-23	3.4	up	tripartite tricarboxylate transporter permease CDS	Pden_0306	PDEN_RS01485
cds-WP_011749182.1	-	6.91107E-11	10	5.15483E-12	3.4	up	SDR family NAD(P)-dependent oxidoreductase CDS	Pden_2908	PDEN_RS14485
cds-WP_011750943.1	-	1.13687E-41	41	8.6276E-44	3.4	up	cytochrome c3 family protein CDS	Pden_4723	PDEN_RS23510
cds-WP_011750777.1	-	1.54807E-11	11	1.09761E-12	3.3	up	hypothetical protein CDS	Pden_4553	PDEN_RS22680

cds-WP_011749876.1	-	1.72693E-06	6	2.52001E-07	3.3	up	glutathione S-transferase CDS	Pden_3640	PDEN_RS18050
cds-WP_011749180.1	-	4.30404E-16	15	1.56782E-17	3.3	up	acyl-CoA dehydrogenase family protein CDS	Pden_2906	PDEN_RS14475
cds-WP_011751197.1	-	1.07524E-09	9	9.62865E-11	3.3	up	sigma-54-dependent Fis family transcriptional regulator CDS	Pden_4979	PDEN_RS24760
cds-WP_011746754.1	-	4.65539E-07	6	6.1574E-08	3.3	up	glutathione S-transferase family protein CDS	Pden_0407	PDEN_RS02020
cds-WP_011748943.1	-	9.8708E-26	25	1.66939E-27	3.2	up	acetyl-CoA C-acyltransferase family protein CDS	Pden_2663	PDEN_RS13255
cds-WP_011748761.1	-	3.21781E-06	5	4.87694E-07	3.2	up	VWA domain-containing protein CDS	Pden_2481	PDEN_RS12330
cds-WP_011750941.1	napA	3.08196E-56	56	1.53697E-58	3.2	up	nitrate reductase	Pden_4721	PDEN_RS23500
cds-WP_011750776.1	-	1.51575E-41	41	1.18315E-43	3.2	up	cation acetate symporter CDS	Pden_4552	PDEN_RS22675
cds-WP_011750775.1	-	7.95356E-16	15	3.13865E-17	3.2	up	DUF4212 domain-containing protein CDS	Pden_4551	PDEN_RS22670
cds-WP_011749819.1	-	1.9589E-05	5	3.38517E-06	3.2	up	helix-turn-helix transcriptional regulator CDS	Pden_3582	PDEN_RS17750
cds-WP_011749580.1	-	9.75971E-11	10	7.46512E-12	3.2	up	hypothetical protein CDS	Pden_3319	PDEN_RS16480
cds-WP_011747141.1	-	1.29467E-05	5	2.16995E-06	3.2	up	ABC transporter permease CDS	Pden_0801	PDEN_RS03985
cds-WP_011750768.1	-	9.64117E-07	6	1.3567E-07	3.2	up	TRAP transporter small permease subunit CDS	Pden_4544	PDEN_RS22635
cds-WP_041530739.1	-	1.80032E-05	5	3.09551E-06	3.2	up	branched-chain amino acid ABC transporter permease CDS	Pden_5000	PDEN_RS24865
cds-WP_011746909.1	-	1.03606E-45	45	6.29002E-48	3.2	up	NnrU family protein CDS	Pden_0564	PDEN_RS02810
cds-WP_011749262.1	-	5.60611E-13	12	3.24551E-14	3.1	up	response regulator transcription factor CDS	Pden_2990	PDEN_RS14925
cds-WP_011749695.1	-	7.58016E-09	8	7.52756E-10	3.1	up	efflux RND transporter periplasmic adaptor subunit CDS	Pden_3447	PDEN_RS17075
cds-WP_011750423.1	-	1.23293E-17	17	3.90302E-19	3.1	up	SARP family transcriptional regulator CDS	Pden_4194	PDEN_RS20895
cds-WP_011749875.1	-	2.94793E-08	8	3.21511E-09	3.1	up	ATP-grasp domain-containing protein CDS	Pden_3639	PDEN_RS18045
cds-WP_011749887.1	aqpZ	1.05782E-11	11	7.40844E-13	3.1	up	aqpZ CDS (aquaporin)	Pden_3651	PDEN_RS18105
cds-WP_011748964.1	-	5.80276E-42	41	4.27784E-44	3.1	up	DUF2853 family protein CDS	Pden_2684	PDEN_RS13360
cds-WP_011749581.1	-	3.95201E-24	23	7.19794E-26	3.1	up	VWA domain-containing protein CDS	Pden_3320	PDEN_RS16485
cds-WP_011746380.1	-	6.05177E-05	4	1.14947E-05	3.0	up	ABC transporter permease CDS	Pden_0030	PDEN_RS00155
cds-WP_011749577.1	-	3.20521E-08	7	3.51656E-09	3.0	up	hypothetical protein CDS	Pden_3316	PDEN_RS16465
cds-WP_074810587.1	-	1.11666E-25	25	1.91275E-27	3.0	up	YdcH family protein CDS (methyltransferase)	Pden_2029	PDEN_RS10090
cds-WP_011749106.1	-	2.39457E-17	17	7.68422E-19	3.0	up	hybrid-cluster NAD(P)-dependent oxidoreductase CDS	Pden_2831	PDEN_RS14095
cds-WP_011746935.1	-	4.84807E-15	14	2.08675E-16	3.0	up	outer membrane protein transport protein CDS	Pden_0590	PDEN_RS02940
cds-WP_011750977.1	-	1.56669E-22	22	3.36301E-24	3.0	up	3-methyl-2-oxobutanoate dehydrogenase (2-methylpropanoyl-transferring) subunit alpha CDS	Pden_4757	PDEN_RS23680
cds-WP_011749391.1	-	1.08733E-14	14	4.97455E-16	3.0	up	recombinase family protein CDS	Pden_3123	PDEN_RS15550
cds-WP_011750769.1	-	5.31956E-16	15	1.98388E-17	3.0	up	TRAP transporter large permease subunit CDS	Pden_4545	PDEN_RS22640
cds-WP_011748715.1	-	4.62323E-05	4	8.55078E-06	3.0	up	hypothetical protein CDS	Pden_2435	PDEN_RS12105
cds-WP_011750436.1	-	6.0014E-08	7	6.88365E-09	3.0	up	polyhydroxyalkanoic acid synthase CDS	Pden_4207	PDEN_RS20960

cds-WP_011749263.1	-	1.51237E-07	7	1.83308E-08	2.9	up	HAMP domain-containing protein CDS	Pden_2991	PDEN_RS14930
cds-WP_011749578.1	-	3.98472E-09	8	3.87067E-10	2.9	up	hypothetical protein CDS	Pden_3317	PDEN_RS16470
cds-WP_011749835.1	-	5.12081E-10	9	4.38578E-11	2.9	up	hypothetical protein CDS	Pden_3599	PDEN_RS27125
cds-WP_011749582.1	-	5.81499E-08	7	6.6194E-09	2.9	up	hypothetical protein CDS	Pden_3321	PDEN_RS16490
cds-WP_011748551.1	mscL	1.59977E-31	31	1.8731E-33	2.9	up	mscL CDS (mechanosensitive channel protein)	Pden_2265	PDEN_RS11260
cds-WP_011751071.1	-	3.42961E-13	12	1.93343E-14	2.9	up	caspase family protein	Pden_4852	PDEN_RS24150
cds-WP_011746365.1	gfa	4.61173E-07	6	6.08965E-08	2.9	up	gfa CDS (glutathion synthase)	Pden_0015	PDEN_RS00080
cds-WP_011749647.1	-	5.68427E-05	4	1.07843E-05	2.9	up	twin-arginine translocation pathway signal CDS	Pden_3398	PDEN_RS16825
cds-WP_011747579.1	-	3.74546E-09	8	3.63014E-10	2.9	up	metal ABC transporter permease CDS	Pden_1256	PDEN_RS06200
cds-WP_011746795.1	-	5.42676E-13	12	3.12992E-14	2.9	up	hypothetical protein CDS	Pden_0448	PDEN_RS02230
cds-WP_011749944.1	-	1.00326E-09	9	8.89709E-11	2.9	up	DUF1330 domain-containing protein CDS	Pden_3708	PDEN_RS18410
cds-WP_011749576.1	-	9.90065E-13	12	5.98933E-14	2.8	up	hypothetical protein CDS	Pden_3315	PDEN_RS27080
cds-WP_011746910.1	-	1.93264E-30	30	2.38856E-32	2.8	up	DUF1737 domain-containing protein CDS	Pden_0565	PDEN_RS02815
cds-WP_011748722.1	-	4.96211E-05	4	9.26361E-06	2.8	up	type VI secretion system ImpA family N-terminal domain-containing protein CDS	Pden_2442	PDEN_RS12140
cds-WP_011751215.1	-	5.21718E-05	4	9.83029E-06	2.8	up	ABC transporter ATP-binding protein CDS	Pden_4997	PDEN_RS24850
cds-WP_011749873.1	-	6.00185E-13	12	3.50064E-14	2.8	up	methylcrotonoyl-CoA carboxylase CDS	Pden_3637	PDEN_RS18035
cds-WP_049792328.1	-	3.82534E-06	5	5.88896E-07	2.8	up	sigma-54-dependent Fis family transcriptional regulator CDS	Pden_2365	PDEN_RS11750
cds-WP_011748735.1	tssI	3.57935E-09	8	3.4381E-10	2.8	up	type VI secretion system tip protein VgrG	Pden_2455	PDEN_RS12205
cds-WP_011748395.1	-	3.31588E-07	6	4.27786E-08	2.8	up	Crp/Fnr family transcriptional regulator CDS	Pden_2108	PDEN_RS10470
cds-WP_011750754.1	-	5.86663E-08	7	6.70363E-09	2.8	up	sodium:solute symporter family protein CDS	Pden_4529	PDEN_RS22575
cds-WP_011746794.1	-	3.60495E-20	19	9.37976E-22	2.8	up	hypothetical protein CDS	Pden_0447	PDEN_RS02225
cds-WP_011750770.1	dctP	1.08124E-18	18	3.16493E-20	2.8	up	dctP CDS	Pden_4546	PDEN_RS22645
cds-WP_164901615.1	-	6.64984E-08	7	7.65626E-09	2.8	up	hypothetical protein CDS	-	PDEN_RS27345
cds-WP_011750560.1	-	6.2623E-13	12	3.66614E-14	2.7	up	APC family permease CDS	Pden_4334	PDEN_RS21580
cds-WP_011750863.1	-	1.06349E-12	12	6.47964E-14	2.7	up	tyrosinase family protein CDS	Pden_4643	PDEN_RS23115
cds-WP_011749264.1	-	3.38897E-08	7	3.74756E-09	2.7	up	protein MoxZ CDS	Pden_2992	PDEN_RS14935
cds-WP_049792297.1	-	8.8447E-06	5	1.43832E-06	2.7	up	DNA/RNA non-specific endonuclease CDS	Pden_0949	PDEN_RS04715
cds-WP_011750773.1	-	1.26297E-13	13	6.54488E-15	2.6	up	iron-containing alcohol dehydrogenase CDS	Pden_4549	PDEN_RS22660
cds-WP_011749107.1	-	1.78847E-20	20	4.49832E-22	2.6	up	aromatic ring-hydroxylating dioxygenase subunit alpha CDS	Pden_2832	PDEN_RS14100
cds-WP_011746953.1	-	2.64213E-19	19	7.3329E-21	2.6	up	peptide ABC transporter substrate-binding protein CDS	Pden_0608	PDEN_RS03025
cds-WP_011750740.1	-	4.10865E-17	16	1.37193E-18	2.6	up	VOC family protein CDS	Pden_4515	PDEN_RS22505
cds-WP_011750633.1	-	2.99821E-05	5	5.35674E-06	2.6	up	allantoin permease CDS	Pden_4407	PDEN_RS21945

cds-WP_011746952.1	-	6.55491E-16	15	2.51565E-17	2.6	up	ABC transporter permease CDS	Pden_0607	PDEN_RS03020
cds-WP_011750487.1	xdhB	1.1606E-13	13	5.98923E-15	2.6	up	xanthine dehydrogenase molybdopterin binding subunit	Pden_4258	PDEN_RS21210
cds-WP_011750418.1	ugpA	4.02813E-19	18	1.13542E-20	2.6	up	sn-glycerol-3-phosphate ABC transporter permeaseUgpA	Pden_4189	PDEN_RS20870
cds-WP_011750978.1	-	2.46167E-09	9	2.30582E-10	2.6	up	alpha-ketoacid dehydrogenase subunit beta CDS	Pden_4758	PDEN_RS23685
cds-WP_011746738.1	-	4.50678E-05	4	8.2963E-06	2.6	up	hypothetical protein CDS	Pden_0391	PDEN_RS01930
cds-WP_011746796.1	-	1.38646E-13	13	7.27501E-15	2.6	up	DNA polymerase III subunit epsilon CDS	Pden_0449	PDEN_RS25930
cds-WP_011750417.1	ugpE	1.59096E-18	18	4.69147E-20	2.6	up	sn-glycerol-3-phosphate ABC transporter permeaseUgpE	Pden_4188	PDEN_RS20865
cds-WP_011746954.1	-	8.56217E-15	14	3.84295E-16	2.6	up	ABC transporter ATP-binding protein CDS	Pden_0609	PDEN_RS03030
cds-WP_128492982.1	-	5.46752E-08	7	6.20016E-09	2.6	up	hypothetical protein CDS	-	PDEN_RS04720
cds-WP_011747391.1	-	4.88201E-09	8	4.79521E-10	2.6	up	flavin reductase family protein CDS	Pden_1062	PDEN_RS05275
cds-WP_011750940.1	-	4.0844E-11	10	2.99334E-12	2.6	up	chaperone NapD CDS	Pden_4720	PDEN_RS23495
cds-WP_011750059.1	-	1.01888E-11	11	7.11358E-13	2.6	up	CoA-binding protein CDS	Pden_3824	PDEN_RS19025
cds-WP_011746951.1	-	7.02985E-07	6	9.63327E-08	2.6	up	ABC transporter permease CDS	Pden_0606	PDEN_RS03015
cds-WP_011746870.1	-	5.34176E-17	16	1.80684E-18	2.5	up	ABC transporter permease CDS	Pden_0525	PDEN_RS02615
cds-WP_041529929.1	-	7.64945E-10	9	6.71732E-11	2.5	up	hypothetical protein CDS	-	PDEN_RS10215
cds-WP_011749574.1	-	9.43538E-11	10	7.18087E-12	2.5	up	molybdopterin-dependent oxidoreductase CDS	Pden_3313	PDEN_RS16450
cds-WP_011747752.1	bioB	2.76344E-15	15	1.15643E-16	2.5	up	bioB CDS (part of biotin synthesis/import cluster)	Pden_1433	PDEN_RS07085
cds-WP_198140556.1	-	5.14456E-05	4	9.67116E-06	2.5	up	hydantoinase/oxoprolinase family protein CDS	Pden_4263	PDEN_RS21235
cds-WP_011751198.1	-	2.51754E-08	8	2.71296E-09	2.5	up	2,3-butanediol dehydrogenase CDS	Pden_4980	PDEN_RS24765
cds-WP_011746553.1	-	1.33024E-05	5	2.23821E-06	2.5	up	SDR family oxidoreductase CDS	Pden_0206	PDEN_RS00990
cds-WP_011748717.1	-	2.12119E-05	5	3.69783E-06	2.5	up	DUF4150 domain-containing protein CDS	Pden_2437	PDEN_RS25610
cds-WP_011748261.1	-	5.64885E-05	4	1.07008E-05	2.5	up	recombinase family protein CDS	Pden_1972	PDEN_RS26105
cds-WP_011750702.1	-	7.23386E-10	9	6.28963E-11	2.5	up	CBS domain-containing protein CDS	Pden_4477	PDEN_RS22310
cds-WP_011747298.1	-	1.31044E-39	39	1.10813E-41	2.5	up	hypothetical protein CDS	Pden_0959	PDEN_RS04770
cds-WP_041530327.1	-	1.54435E-05	5	2.63002E-06	2.5	up	hypothetical protein CDS	-	PDEN_RS15600
cds-WP_011747675.1	-	1.78372E-07	7	2.18517E-08	2.4	up	methionine synthase CDS	Pden_1355	PDEN_RS06690
cds-WP_011748716.1	-	6.6643E-12	11	4.43612E-13	2.4	up	hypothetical protein CDS	Pden_2436	PDEN_RS12110
cds-WP_011748294.1	-	1.52114E-08	8	1.56996E-09	2.4	up	acyl-CoA synthetase CDS	Pden_2005	PDEN_RS09970
cds-WP_011748341.1	-	2.10131E-07	7	2.60614E-08	2.4	up	hypothetical protein CDS	Pden_2053	PDEN_RS10205
cds-WP_041530076.1	-	8.93522E-22	21	2.03425E-23	2.4	up	ABC transporter permease CDS	Pden_0526	PDEN_RS02620
cds-WP_011748015.1	-	3.9757E-08	7	4.46534E-09	2.4	up	malonyl-CoA decarboxylase CDS	Pden_1720	PDEN_RS08455
cds-WP_011750419.1	ugpB	1.17588E-26	26	1.81022E-28	2.4	up	ugpB CDS (glycerol-3-p permease)	Pden_4190	PDEN_RS20875

cds-WP_011747674.1	-	3.06796E-07	7	3.93141E-08	2.4	up	DUF1852 domain-containing protein CDS	Pden_1354	PDEN_RS06685
cds-WP_128492935.1	-	2.92407E-12	12	1.864E-13	2.4	up	hypothetical protein CDS	Pden_1356	PDEN_RS26870
cds-WP_011747140.1	-	4.98541E-07	6	6.6155E-08	2.4	up	ABC transporter ATP-binding protein CDS	Pden_0800	PDEN_RS03980
cds-WP_011750862.1	-	3.99193E-18	17	1.21177E-19	2.4	up	hypothetical protein CDS	Pden_4642	PDEN_RS23110
cds-WP_011751042.1	-	8.26721E-07	6	1.14992E-07	2.4	up	SDR family oxidoreductase CDS	Pden_4822	PDEN_RS24005
cds-WP_011750489.1	guaD	5.69731E-12	11	3.74303E-13	2.4	up	guaD CDS	Pden_4260	PDEN_RS21220
cds-WP_011747600.1	-	5.66681E-23	22	1.16727E-24	2.4	up	purine permease CDS	Pden_1277	PDEN_RS06305
cds-WP_011750082.1	-	2.45053E-12	12	1.54619E-13	2.4	up	site-specific integrase CDS	Pden_3849	PDEN_RS19160
cds-WP_011750861.1	-	1.49889E-10	10	1.17649E-11	2.4	up	hypothetical protein CDS	Pden_4641	PDEN_RS23105
cds-WP_011751214.1	-	2.19471E-08	8	2.32224E-09	2.4	up	acetate--CoA ligase family protein CDS	Pden_4996	PDEN_RS24845
cds-WP_011749717.1	-	8.16135E-16	15	3.25605E-17	2.3	up	hypothetical protein CDS	Pden_3470	PDEN_RS17190
cds-WP_011750980.1	lpdA	3.72321E-06	5	5.7156E-07	2.3	up	lpdA CDS	Pden_4760	PDEN_RS23695
cds-WP_011748944.1	-	3.69179E-10	9	3.09784E-11	2.3	up	LysR family transcriptional regulator CDS	Pden_2664	PDEN_RS13260
cds-WP_011750771.1	-	9.48495E-12	11	6.49879E-13	2.3	up	glutamine synthetase CDS	Pden_4547	PDEN_RS22650
cds-WP_011749534.1	-	1.38238E-09	9	1.2439E-10	2.3	up	LysR family transcriptional regulator CDS	Pden_3271	PDEN_RS16245
cds-WP_011750772.1	-	6.89098E-08	7	7.97871E-09	2.3	up	aldehyde dehydrogenase family protein CDS	Pden_4548	PDEN_RS22655
cds-WP_011746947.1	-	4.88398E-14	13	2.35092E-15	2.3	up	hypothetical protein CDS	Pden_0602	PDEN_RS02995
cds-WP_041530454.1	-	3.6689E-08	7	4.10484E-09	2.3	up	glycosyltransferase family 2 protein CDS	Pden_4162	PDEN_RS20735
cds-WP_011747779.1	-	8.09818E-05	4	1.56275E-05	2.3	up	GNAT family N-acetyltransferase CDS	Pden_1461	PDEN_RS07200
cds-WP_011748633.1	-	5.56367E-05	4	1.05193E-05	2.3	up	hypothetical protein CDS	Pden_2350	PDEN_RS11670
cds-WP_011751039.1	-	9.28236E-10	9	8.21162E-11	2.3	up	acetyl-CoA acetyltransferase CDS	Pden_4819	PDEN_RS23990
cds-WP_011748185.1	msrB	1.28044E-05	5	2.14332E-06	2.3	up	msrB CDS	Pden_1893	PDEN_RS09355
cds-WP_128493090.1	-	2.5118E-06	6	3.74156E-07	2.3	up	hypothetical protein CDS	Pden_3848	PDEN_RS19155
cds-WP_011748543.1	-	9.43538E-11	10	7.16121E-12	2.2	up	NAD-dependent succinate-semialdehyde dehydrogenase CDS	Pden_2257	PDEN_RS11220
cds-WP_011750493.1	-	7.28019E-23	22	1.51539E-24	2.2	up	sigma-54-dependent Fis family transcriptional regulator CDS	Pden_4264	PDEN_RS21240
cds-WP_011749132.1	-	2.86647E-10	10	2.35558E-11	2.2	up	formate dehydrogenase beta subunit CDS	Pden_2857	PDEN_RS14225
cds-WP_041529877.1	-	2.15456E-10	10	1.73318E-11	2.2	up	LacI family DNA-binding transcriptional regulator CDS	Pden_1685	PDEN_RS08280
cds-WP_011749587.1	-	1.56436E-05	5	2.66945E-06	2.2	up	recombinase family protein CDS	Pden_0106	PDEN_RS00535
cds-WP_011749390.1	-	1.1514E-08	8	1.17337E-09	2.2	up	tyrosine-type recombinase/integrase CDS	Pden_3122	PDEN_RS15545
cds-WP_011750707.1	mmsB	1.76933E-11	11	1.26216E-12	2.2	up	3-hydroxyisobutyrate dehydrogenase	Pden_4482	PDEN_RS22335
cds-WP_011748636.1	-	3.39695E-08	7	3.76375E-09	2.2	up	FIST C-terminal domain-containing protein CDS	Pden_2353	PDEN_RS11685
cds-WP_074810797.1	-	5.71194E-13	12	3.31917E-14	2.2	up	hypothetical protein CDS	Pden_0973	PDEN_RS04850

cds-WP_128493044.1	-	2.07601E-05	5	3.60555E-06	2.2	up	hypothetical protein CDS	Pden_3322	PDEN_RS16495
cds-WP_011747100.1	-	4.53575E-10	9	3.84536E-11	2.2	up	hypothetical protein CDS	Pden_0757	PDEN_RS03760
cds-WP_157137424.1	-	1.35322E-20	20	3.37425E-22	2.2	up	hypothetical protein CDS		PDEN_RS26815
cds-WP_011747881.1	-	1.44805E-15	15	5.90274E-17	2.2	up	TRAP transporter substrate-binding protein CDS	Pden_1563	PDEN_RS07680
cds-WP_011747751.1	-	8.98662E-05	4	1.75757E-05	2.2	up	biotin transporter BioY CDS	Pden_1432	PDEN_RS07080
cds-WP_157137429.1	-	8.70516E-06	5	1.41374E-06	2.2	up	hypothetical protein CDS		PDEN_RS26875
cds-WP_011750416.1	-	1.88572E-09	9	1.73771E-10	2.2	up	sn-glycerol-3-phosphate import ATP-binding protein UgpC CDS	Pden_4187	PDEN_RS20860
cds-WP_011748634.1	-	4.83278E-06	5	7.54467E-07	2.2	up	hypothetical protein CDS	Pden_2351	PDEN_RS11675
cds-WP_011750486.1	xdhA	3.23361E-08	7	3.55473E-09	2.2	up	xanthine dehydrogenase small subunit	Pden_4257	PDEN_RS21205
cds-WP_011749823.1	-	8.16135E-16	15	3.25456E-17	2.2	up	transglutaminase domain-containing protein CDS	Pden_3586	PDEN_RS17770
cds-WP_011751037.1	-	9.94574E-12	11	6.92234E-13	2.2	up	TRAP transporter substrate-binding protein CDS	Pden_4817	PDEN_RS23980
cds-WP_011746571.1	-	1.80288E-21	21	4.22184E-23	2.2	up	sigma-54-dependent Fis family transcriptional regulator CDS	Pden_0224	PDEN_RS01080
cds-WP_011749101.1	fdhE	4.08026E-09	8	3.97233E-10	2.2	up	fdhE CDS	Pden_2826	PDEN_RS14070
cds-WP_198140519.1	-	3.56041E-12	11	2.29281E-13	2.1	up	Na/Pi symporter CDS	Pden_0816	PDEN_RS04055
cds-WP_011749131.1	fdhF	2.5938E-15	15	1.07981E-16	2.1	up	formate dehydrogenase subunit alpha	Pden_2856	PDEN_RS14220
cds-WP_011749201.1	-	3.42724E-17	16	1.13696E-18	2.1	up	L-lactate permease CDS	Pden_2927	PDEN_RS14580
cds-WP_011749696.1	-	3.18621E-23	22	6.494E-25	2.1	up	multidrug efflux RND transporter permease subunit CDS	Pden_3448	PDEN_RS17080
cds-WP_011746900.1	-	2.84316E-37	37	2.65082E-39	2.1	up	2-oxoglutarate dehydrogenase E1 component CDS	Pden_0555	PDEN_RS02770
cds-WP_011746873.1	-	2.76775E-14	14	1.30826E-15	2.1	up	BMP family ABC transporter substrate-binding protein CDS	Pden_0528	PDEN_RS02630
cds-WP_011748622.1	-	1.33414E-07	7	1.60548E-08	2.1	up	4-aminobutyrate--2-oxoglutarate transaminase CDS	Pden_2338	PDEN_RS11610
cds-WP_011749743.1	-	1.36678E-10	10	1.06687E-11	2.1	up	TRAP transporter substrate-binding protein CDS	Pden_3497	PDEN_RS17330
cds-WP_011751040.1	-	4.57072E-13	12	2.61637E-14	2.1	up	acyl-CoA synthetase CDS	Pden_4820	PDEN_RS23995
cds-WP_011749869.1	-	1.64513E-15	15	6.77741E-17	2.1	up	isovaleryl-CoA dehydrogenase CDS	Pden_3633	PDEN_RS18015
cds-WP_011750239.1	-	9.57349E-08	7	1.12715E-08	2.1	up	DUF2945 domain-containing protein CDS	Pden_4005	PDEN_RS19945
cds-WP_011747578.1	-	8.65655E-09	8	8.65279E-10	2.1	up	SDR family oxidoreductase CDS	Pden_1255	PDEN_RS06195
cds-WP_011746872.1	-	9.5675E-09	8	9.60484E-10	2.1	up	ABC transporter ATP-binding protein CDS	Pden_0527	PDEN_RS02625
cds-WP_041529795.1	-	9.51651E-07	6	1.33503E-07	2.1	up	hypothetical protein CDS	Pden_0978	PDEN_RS04875
cds-WP_011747142.1	-	6.56117E-05	4	1.25334E-05	2.1	up	ABC transporter permease CDS	Pden_0802	PDEN_RS03990
cds-WP_011750101.1	-	4.08146E-10	9	3.43366E-11	2.1	up	zinc metallopeptidase CDS	Pden_3868	PDEN_RS19245
cds-WP_041529728.1	-	4.24381E-08	7	4.78487E-09	2.0	up	hypothetical protein CDS	Pden_0347	PDEN_RS01705
cds-WP_011750741.1	-	3.14314E-10	10	2.58975E-11	2.0	up	VOC family protein CDS	Pden_4516	PDEN_RS22510
cds-WP_128492954.1	-	5.9106E-10	9	5.10065E-11	2.0	up	tyrosine-type recombinase/integrase CDS	Pden_2419	PDEN_RS12025

cds-WP_011746899.1	odhB	6.06734E-35	34	6.05156E-37	2.0	up	2-oxoglutarate dehydrogenase complex dihydrolipoyllysine-residue succinyltransferase	Pden_0554	PDEN_RS02765
cds-WP_104493368.1	-	9.22046E-12	11	6.26583E-13	2.0	up	hypothetical protein CDS	Pden_0393	PDEN_RS01940
cds-WP_011749712.1	-	2.10941E-05	5	3.66814E-06	2.0	up	Rieske 2Fe-2S domain-containing protein CDS	Pden_3465	PDEN_RS17165
cds-WP_011749575.1	-	3.78018E-07	6	4.94243E-08	2.0	up	hypothetical protein CDS	Pden_3314	PDEN_RS16455
cds-WP_081465042.1	-	3.96294E-06	5	6.11799E-07	2.0	up	rhomboid family intramembrane serine protease CDS	Pden_2337	PDEN_RS11605
cds-WP_041529953.1	-	1.12582E-09	9	1.0106E-10	2.0	up	Arc family DNA-binding protein CDS	Pden_2281	PDEN_RS26955
cds-WP_164901601.1	-	5.09035E-05	4	9.54717E-06	2.0	up	hypothetical protein CDS		PDEN_RS27300
cds-WP_011747299.1	phaR	2.14211E-21	21	5.1091E-23	2.0	up	polyhydroxyalkanoate synthesis repressor PhaR	Pden_0960	PDEN_RS04775
cds-WP_011748334.1	-	6.65088E-08	7	7.67188E-09	-2.0	down	TonB-dependent receptor CDS	Pden_2046	PDEN_RS10170
cds-WP_011747230.1	rpsF	1.62712E-26	26	2.54017E-28	-2.0	down	rpsF CDS	Pden_0891	PDEN_RS04425
cds-WP_011748873.1	-	1.56791E-13	13	8.2951E-15	-2.0	down	RNA-binding protein CDS	Pden_2593	PDEN_RS12885
cds-WP_011749934.1	-	3.25276E-07	6	4.18232E-08	-2.0	down	RNA methyltransferase CDS	Pden_3698	PDEN_RS18360
cds-WP_011748055.1	ilvC	2.75472E-10	10	2.25777E-11	-2.0	down	ketol-acid reductoisomerase	Pden_1760	PDEN_RS08665
cds-WP_011747229.1	-	7.58753E-13	12	4.53118E-14	-2.0	down	30S ribosomal protein S18 CDS	Pden_0890	PDEN_RS04420
cds-WP_041530668.1	-	2.35576E-06	6	3.48869E-07	-2.0	down	hypothetical protein CDS	Pden_4302	PDEN_RS21430
cds-WP_041530731.1	-	6.49124E-19	18	1.88601E-20	-2.0	down	altronate dehydratase CDS	Pden_4928	PDEN_RS24515
cds-WP_010400236.1	rpsS	2.86461E-07	7	3.64597E-08	-2.0	down	30S ribosomal protein S19	Pden_0763	PDEN_RS03790
cds-WP_011748577.1	-	8.03332E-05	4	1.54849E-05	-2.0	down	glycosyl transferase CDS	Pden_2293	PDEN_RS11390
cds-WP_011747088.1	rplK	5.48385E-17	16	1.86679E-18	-2.0	down	50S ribosomal protein L11	Pden_0743	PDEN_RS03695
cds-WP_011747028.1	tolQ	9.96023E-13	12	6.04698E-14	-2.0	down	tolQ CDS	Pden_0683	PDEN_RS03395
cds-WP_011747109.1	rpsQ	1.96741E-07	7	2.423E-08	-2.0	down	30S ribosomal protein S17	Pden_0768	PDEN_RS03815
cds-WP_011750311.1	-	6.36432E-18	17	1.97333E-19	-2.0	down	50S ribosomal protein L25/general stress proteinCtc CDS	Pden_4077	PDEN_RS20310
cds-WP_041530730.1	-	1.00529E-07	7	1.19099E-08	-2.0	down	amino acid ABC transporter permease CDS	Pden_4924	PDEN_RS24495
cds-WP_011750529.1	rpsD	7.40185E-13	12	4.39745E-14	-2.1	down	30S ribosomal protein S4	Pden_4303	PDEN_RS21435
cds-WP_011748890.1	-	2.60821E-06	6	3.89083E-07	-2.1	down	TonB-dependent receptor CDS	Pden_2610	PDEN_RS12975
cds-WP_104491135.1	-	5.30849E-09	8	5.23713E-10	-2.1	down	H-type lectin domain-containing protein CDS	Pden_3820	PDEN_RS19005
cds-WP_041529773.1	rpmC	7.36309E-13	12	4.35846E-14	-2.1	down	50S ribosomal protein L29	Pden_0767	PDEN_RS03810
cds-WP_011749035.1	rpsO	1.66471E-10	10	1.31387E-11	-2.1	down	30S ribosomal protein S15	Pden_2760	PDEN_RS13740
cds-WP_011750809.1	-	1.94114E-09	9	1.79299E-10	-2.1	down	co-chaperone GroES CDS	Pden_4586	PDEN_RS22840
cds-WP_011747105.1	rplV	3.39651E-10	9	2.82061E-11	-2.1	down	50S ribosomal protein L22	Pden_0764	PDEN_RS03795
cds-WP_011751150.1	-	1.12779E-05	5	1.86824E-06	-2.1	down	SDR family oxidoreductase CDS	Pden_4932	PDEN_RS24535
cds-WP_011747103.1	-	1.04265E-13	13	5.35793E-15	-2.1	down	50S ribosomal protein L23 CDS	Pden_0761	PDEN_RS03780

cds-WP_010400243.1	rplN	1.79749E-20	20	4.55998E-22	-2.1	down	rplN CDS	Pden_0769	PDEN_RS03820
cds-WP_011747115.1	rplR	1.77872E-14	14	8.3305E-16	-2.1	down	rplR CDS	Pden_0775	PDEN_RS03850
cds-WP_041529977.1	-	4.64011E-11	10	3.42072E-12	-2.1	down	non-ribosomal peptide synthetase CDS	Pden_2564	PDEN_RS12745
cds-WP_011748559.1	rplT	1.39224E-17	17	4.43754E-19	-2.1	down	50S ribosomal protein L20	Pden_2273	PDEN_RS11300
cds-WP_011748041.1	ndk	9.24805E-22	21	2.12553E-23	-2.1	down	nucleoside-diphosphate kinase	Pden_1746	PDEN_RS08590
cds-WP_041530417.1	-	3.39964E-06	5	5.17465E-07	-2.1	down	hypothetical protein CDS		PDEN_RS19080
cds-WP_041530427.1	-	1.52466E-09	9	1.37854E-10	-2.1	down	chorismate mutase CDS	Pden_3880	PDEN_RS19305
cds-WP_011747113.1	rpsH	1.50647E-19	19	4.08301E-21	-2.1	down	30S ribosomal protein S8	Pden_0773	PDEN_RS03840
cds-WP_011746353.1	mnmE	5.01848E-15	14	2.17627E-16	-2.1	down	tRNA uridine-5-carboxymethylaminomethyl(34) synthesis GTPase MnmE	Pden_0003	PDEN_RS00020
cds-WP_011747114.1	rplF	8.58302E-24	23	1.6377E-25	-2.1	down	50S ribosomal protein L6	Pden_0774	PDEN_RS03845
cds-WP_011750114.1	rpsP	1.87962E-27	27	2.64908E-29	-2.1	down	30S ribosomal protein S16	Pden_3881	PDEN_RS19310
cds-WP_011749243.1	rplM	7.8E-29	28	1.03166E-30	-2.1	down	50S ribosomal protein L13	Pden_2969	PDEN_RS14790
cds-WP_011750112.1	-	9.79608E-07	6	1.38063E-07	-2.1	down	GNAT family N-acetyltransferase CDS	Pden_3879	PDEN_RS19300
cds-WP_011749491.1	-	4.78384E-15	14	2.0434E-16	-2.1	down	enoyl-CoA hydratase/isomerase family protein CDS	Pden_3225	PDEN_RS16020
cds-WP_011747231.1	-	3.199E-10	9	2.64272E-11	-2.2	down	polyisoprenoid-binding protein CDS	Pden_0892	PDEN_RS04430
cds-WP_011749482.1	-	5.07436E-14	13	2.46998E-15	-2.2	down	NAD(P)-dependent oxidoreductase CDS	Pden_3256	PDEN_RS16165
cds-WP_011749481.1	-	4.4001E-16	15	1.62189E-17	-2.2	down	carboxymuconolactone decarboxylase family protein CDS	Pden_3257	PDEN_RS16170
cds-WP_011747030.1	tolA	1.28906E-12	12	7.88194E-14	-2.2	down	cell envelope integrity protein TolA	Pden_0685	PDEN_RS03405
cds-WP_011747029.1	-	9.12503E-11	10	6.90511E-12	-2.2	down	ExbD/TolR family protein CDS	Pden_0684	PDEN_RS03400
cds-WP_011750115.1	rimM	1.00562E-33	33	1.04661E-35	-2.2	down	16S rRNA processing protein RimM	Pden_3882	PDEN_RS19315
cds-WP_011751144.1	-	1.27925E-06	6	1.8279E-07	-2.2	down	amino acid ABC transporter ATP-binding protein CDS	Pden_4926	PDEN_RS24505
cds-WP_011748418.1	-	4.72334E-10	9	4.02488E-11	-2.2	down	GNAT family N-acetyltransferase CDS	Pden_2131	PDEN_RS10585
cds-WP_011749734.1	-	4.17521E-06	5	6.48189E-07	-2.2	down	FAD-dependent monooxygenase CDS	Pden_3488	PDEN_RS17285
cds-WP_011747112.1	rpsN	6.33318E-15	14	2.80132E-16	-2.2	down	30S ribosomal protein S14	Pden_0772	PDEN_RS03835
cds-WP_011749475.1	dctP	2.00951E-08	8	2.11756E-09	-2.2	down	TRAP transporter substrate-binding protein DctP	Pden_3209	PDEN_RS15945
cds-WP_011746516.1	-	7.18256E-13	12	4.23603E-14	-2.2	down	cupin domain-containing protein CDS	Pden_0167	PDEN_RS00805
cds-WP_011750335.1	-	4.7603E-27	26	6.91545E-29	-2.2	down	GNAT family N-acetyltransferase CDS	Pden_4101	PDEN_RS20440
cds-WP_011746938.1	-	1.06554E-09	9	9.51867E-11	-2.2	down	hypothetical protein CDS	Pden_0593	PDEN_RS02955
cds-WP_011747080.1	-	4.42051E-16	15	1.639E-17	-2.3	down	dienelactone hydrolase family protein CDS	Pden_0735	PDEN_RS03650
cds-WP_011747110.1	-	3.64938E-15	14	1.54299E-16	-2.3	down	50S ribosomal protein L24 CDS	Pden_0770	PDEN_RS03825
cds-WP_011750599.1	-	1.11461E-05	5	1.84275E-06	-2.3	down	TonB-dependent siderophore receptor CDS	Pden_4373	PDEN_RS21785
cds-WP_011747395.1	-	2.50982E-06	6	3.73317E-07	-2.3	down	hypothetical protein CDS	Pden_1066	PDEN_RS05295

cds-WP_011748329.1	-	1.05151E-31	31	1.20837E-33	-2.3	down	aspartate aminotransferase family protein CDS	Pden_2041	PDEN_RS10145
cds-WP_011749962.1	rpsB	2.85785E-26	26	4.58545E-28	-2.3	down	30S ribosomal protein S2	Pden_3726	PDEN_RS18490
cds-WP_011750900.1	-	3.40184E-07	6	4.4091E-08	-2.3	down	MaoC family dehydratase CDS	Pden_4680	PDEN_RS23300
cds-WP_011747117.1	rpmD	3.34279E-16	15	1.21042E-17	-2.3	down	50S ribosomal protein L30	Pden_0777	PDEN_RS03860
cds-WP_011750640.1	gabT	3.41155E-08	7	3.78733E-09	-2.3	down	4-aminobutyrate--2-oxoglutarate transaminase	Pden_4414	PDEN_RS21980
cds-WP_019353022.1	groES	3.56599E-10	9	2.97681E-11	-2.3	down	co-chaperone GroES		PDEN_RS18130
cds-WP_011749493.1	-	6.23656E-14	13	3.05608E-15	-2.4	down	CoA transferase CDS	Pden_3227	PDEN_RS16030
cds-WP_041530483.1	-	3.94797E-15	14	1.6778E-16	-2.4	down	DUF1775 domain-containing protein CDS	Pden_4444	PDEN_RS22135
cds-WP_011749303.1	-	6.3387E-06	5	1.00468E-06	-2.4	down	ABC transporter substrate-binding protein CDS	Pden_3033	PDEN_RS15130
cds-WP_011749492.1	-	2.61895E-16	16	9.31284E-18	-2.4	down	thiolase family protein CDS	Pden_3226	PDEN_RS16025
cds-WP_011747619.1	-	3.76874E-07	6	4.91931E-08	-2.4	down	DegT/DnrJ/EryC1/StrS family aminotransferase CDS	Pden_1296	PDEN_RS06400
cds-WP_011750312.1	trmFO	6.17576E-17	16	2.11572E-18	-2.4	down	methylenetetrahydrofolate--tRNA-(uracil(54)- C(5))-methyltransferase (FADH(2)-oxidizing) TrmFO	Pden_4078	PDEN_RS20315
cds-WP_011747084.1	-	6.95284E-27	26	1.04021E-28	-2.4	down	ABC transporter ATP-binding protein CDS	Pden_0739	PDEN_RS03670
cds-WP_011750569.1	cysT	2.98425E-06	6	4.48414E-07	-2.4	down	sulfate ABC transporter permease subunit CysT	Pden_4343	PDEN_RS21630
cds-WP_198140538.1	-	6.71859E-16	15	2.59304E-17	-2.4	down	AMP-binding protein CDS	Pden_3230	PDEN_RS16045
cds-WP_011751149.1	-	1.80674E-09	9	1.66101E-10	-2.4	down	zinc-binding alcohol dehydrogenase family protein CDS	Pden_4931	PDEN_RS24530
cds-WP_011749495.1	-	2.28546E-16	16	8.02786E-18	-2.4	down	MaoC family dehydratase N-terminal domain-containing protein CDS	Pden_3229	PDEN_RS16040
cds-WP_011747111.1	rplE	1.40972E-11	11	9.96462E-13	-2.5	down	rplE CDS	Pden_0771	PDEN_RS03830
cds-WP_011750669.1	-	3.24357E-15	14	1.36438E-16	-2.5	down	SCO family protein CDS	Pden_4443	PDEN_RS22130
cds-WP_011750945.1	-	5.97674E-07	6	8.06057E-08	-2.5	down	hypothetical protein CDS	Pden_4725	PDEN_RS23520
cds-WP_011749961.1	-	3.7282E-39	38	3.23348E-41	-2.5	down	elongation factor Ts CDS	Pden_3725	PDEN_RS18485
cds-WP_011746417.1	tnpB	2.53926E-08	8	2.74188E-09	-2.5	down	IS66 family insertion sequence element accessoryprotein TnpB	Pden_0067	PDEN_RS00375
cds-WP_011747189.1	-	4.2325E-25	24	7.43348E-27	-2.5	down	porin family protein CDS	Pden_0849	PDEN_RS04220
cds-WP_011746845.1	-	1.7296E-09	9	1.57884E-10	-2.5	down	VOC family protein CDS	Pden_0500	PDEN_RS02485
cds-PDEN_RS14835	-	9.02857E-06	5	1.47018E-06	-2.5	down	?	Pden_2973	PDEN_RS14835
cds-WP_011751143.1	-	2.50718E-07	7	3.14757E-08	-2.6	down	amino acid ABC transporter permease CDS	Pden_4925	PDEN_RS24500
cds-WP_011750484.1	-	1.07338E-05	5	1.76646E-06	-2.6	down	Hsp70 family protein CDS	Pden_4255	PDEN_RS21195
cds-WP_011747262.1	-	5.76323E-16	15	2.16184E-17	-2.6	down	hypothetical protein CDS	Pden_0923	PDEN_RS04585
cds-WP_011747154.1	-	2.90382E-19	19	8.12215E-21	-2.7	down	phosphoglycerate dehydrogenase CDS	Pden_0814	PDEN_RS04045
cds-WP_104494388.1	-	1.52458E-06	6	2.2115E-07	-2.7	down	TetR family transcriptional regulator CDS	Pden_2940	PDEN_RS14645
cds-WP_011749494.1	-	8.69252E-21	20	2.12978E-22	-2.7	down	aldehyde dehydrogenase CDS	Pden_3228	PDEN_RS16035

cds-WP_011749216.1	-	1.0367E-39	39	8.5418E-42	-2.8	down	multidrug efflux RND transporter permease subunit CDS	Pden_2942	PDEN_RS14655
cds-WP_011747531.1	ureC	3.40184E-07	6	4.41089E-08	-2.8	down	urease subunit alpha	Pden_1208	PDEN_RS05985
cds-WP_041529781.1	-	2.97041E-07	7	3.78992E-08	-2.8	down	hypothetical protein CDS		PDEN_RS04285
cds-WP_011748469.1	-	7.60771E-15	14	3.38157E-16	-2.9	down	DUF1800 domain-containing protein CDS	Pden_2182	PDEN_RS10840
cds-WP_011747118.1	-	1.8687E-08	8	1.95703E-09	-2.9	down	hypothetical protein CDS	Pden_0778	PDEN_RS03865
cds-WP_128492943.1	-	4.32341E-19	18	1.22803E-20	-2.9	down	ammonium transporter CDS	Pden_2032	PDEN_RS10105
cds-WP_011749215.1	-	1.18288E-07	7	1.41507E-08	-3.0	down	efflux RND transporter periplasmic adaptor subunit CDS	Pden_2941	PDEN_RS14650
cds-WP_011750899.1	-	1.09018E-23	23	2.10377E-25	-3.0	down	6,7-dimethyl-8-ribityllumazine synthase CDS	Pden_4679	PDEN_RS23295
cds-WP_011750642.1	-	1.61074E-38	38	1.46685E-40	-3.0	down	NAD-dependent succinate-semialdehyde dehydrogenase CDS	Pden_4416	PDEN_RS21990
cds-WP_011750125.1	pdhA	2.83234E-40	40	2.27226E-42	-3.2	down	pyruvate dehydrogenase (acetyl-transferring) E1 component subunit alpha	Pden_3892	PDEN_RS19370
cds-WP_011749301.1	-	2.84838E-06	6	4.26145E-07	-3.3	down	iron ABC transporter permease CDS	Pden_3031	PDEN_RS15120
cds-WP_011750124.1	-	3.9234E-44	43	2.63715E-46	-3.4	down	pyruvate dehydrogenase complex E1 component subunit beta CDS	Pden_3891	PDEN_RS19365
cds-WP_011750123.1	-	1.41783E-52	52	7.68553E-55	-3.5	down	pyruvate dehydrogenase complex dihydrolipoamide acetyltransferase CDS	Pden_3890	PDEN_RS19360
cds-WP_011749300.1	-	4.60306E-09	8	4.50125E-10	-3.5	down	class I SAM-dependent methyltransferase CDS	Pden_3030	PDEN_RS15115
cds-WP_011748558.1	-	3.00914E-05	5	5.38278E-06	-3.6	down	cytochrome P450 CDS	Pden_2272	PDEN_RS11295
cds-WP_011747493.1	-	1.13413E-05	5	1.88119E-06	-4.1	down	ABC transporter substrate-binding protein CDS	Pden_1168	PDEN_RS05785
cds-WP_011748511.1	-	5.21305E-57	56	2.48671E-59	-4.1	down	NADP-dependent malic enzyme CDS	Pden_2224	PDEN_RS11050
cds-WP_164901616.1	-	8.65261E-35	34	8.81771E-37	-4.4	down	TonB-dependent siderophore receptor CDS	Pden_3029	PDEN_RS15110
cds-WP_011750985.1	-	1.2001E-101	101	3.1225E-104	-9.6	down	dicarboxylate/amino acid:cation symporter CDS	Pden_4765	PDEN_RS23720

Supplementary Table 4: Top regulated genes KO_{Suc}/WT_{Suc}. Listed are all genes regulated above a threshold of log_2-fold 2.0 in Pd1222 *ΔramB* on succinate compared to the Pd1222 wild type on succinate.

gene_id	Gene	padj	neg. log10 (padjust)	pvalue	log2-Fold Change	regula-tion	CDS/product description	Old locus tag	New locus tag
cds-WP_011747683.1	*aceB*	3.44E-27	26.46	1.E-30	4.87	up	malate synthase	Pden_1364	PDEN_RS06730
cds-WP_086000156.1	*aceA*	5.82E-65	64.23	1.E-68	4.42	up	isocitrate lyase	Pden_1363	PDEN_RS06725